PREDICTING THE THERMOPHYSICAL PROPERTIES OF MOLECULES WITH ANISOTROPIC INTERACTION AND STRUCTURE USING THE STATISTICAL ASSOCIATING FLUID THEORY

By

Gaurav Das

Dissertation

Submitted to the Faculty of the

Graduate School of Vanderbilt University

in partial fulfillment of the requirements

for the degree of

DOCTOR OF PHILOSOPHY

in

Chemical Engineering

August, 2015

Nashville, Tennessee

Approved By

Clare McCabe, Ph.D.

Peter T. Cummings, Ph.D.

Kenneth A. Debelak, Ph.D.

Florence Sanchez, Ph.D.

Dedicated to my grandparents

ACKNOWLEDGEMENT

My graduate school experience has been one of my best years of my life and this would not have been possible without a lot of people. Here, I would sincerely like to express my gratitude and appreciation to them.

First, I would like to thank my Ph.D. advisor Prof. Dr. Clare McCabe, for giving me the opportunity to work under her mentorship. Her guidance, suggestions, and critiques have helped me to excel in my research, learnt how to write a paper and present at conferences. I would like to extend my appreciation to my committee members – Professors Peter Cummings, Ken Debelak and Florence Sanchez for their valuable comments and insights throughout my graduate study period. In particular, I am thankful to Dr. Cummings for his insight, comments and critiques on my research during group and personal meetings. I cherished each and every opportunity of exchanging thoughts and ideas on my research with him. A big thank you to the post-doctoral researchers whom I have worked with extensively - Dr. M. Carolina dos Ramos Goncalves, Dr. Stepan Hlushak, and to the collaborators - Prof. E. J. M. Filipe and Dr. P. J. R. Morgado. A special mention to Dr. dos Ramos, who helped me get started in this Ph.D. journey. My special thanks also goes to the past and present lab members of Dr. McCabe and Dr. Cummings groups, current graduate students and administrative assistants in the Department of Chemical and Bimolecular Engineering. In particular, I am thankful to Tim Moore, Jessica Haley, Will French, Neil Templeton, Carlos Escobar. A huge thanks also to my close friends Parikshit, Sandeepan, Tania, Siladitya, Aritra, Joyeeta, Anirban, Asish without whom, my years here would not been this enjoyable.

Lastly, I would like to express my gratitude and thanks to my family - my parents and sister Tina - you all have been an integral part of this journey and without your support and sacrifice it would have been impossible to achieve this dream. And, last but definitely not the least, a big thank you to my wife Aradhana for being there for me whenever I needed. Her constant support and love made this journey a memorable one. She lends me an ear to complain to and stood by me in my hard times.

TABLE OF CONTENTS

Page

DEDICATION…….....iii

ACKNOWLEDGMENT……..…….....iv

LIST OF TABLES……..….....viii

LIST OF FIGURES…….…….....x

Chapter 1: Introduction 1

Chapter 2: Background 9
2.1 Statistical associating fluid theory 9
2.2 SAFT-VR 16
2.2.1 Ideal contribution 17
2.2.2 Monomer contribution 17
2.2.3 Chain contribution 21
2.2.4 Association contribution 22
2.3 GC-SAFT-VR 23
2.3.1 Monomer contribution 25
2.3.2 Chain contribution 27
2.3.3 Association contribution 28

Chapter 3: Accurately modeling benzene and alkylbenzenes using a group contribution based SAFT approach 30
3.1 Introduction 30
3.2 Molecular model and theory 35
3.2.1 Chain contribution 36
3.3 Results and discussion 38
3.3.1 Pure compounds 38
3.3.2 Binary mixtures 42
3.4 Conclusion 51

Chapter 4: Predicting the thermodynamic properties and dielectric behavior of electrolyte solutions using the SAFT-VR+DE equation of state 53
4.1 Introduction 53
4.2 Molecular model and theory 65
4.3 Results and Discussion 71
4.3.1 Water 71
4.3.2 Electrolytes 74
4.3.3 Gibbs free energy of solvation 81
4.3.4 Effect of ions on the dielectric properties of water 84

4.3.5 Temperature effect on thermodynamic properties of electrolytes 87
4.3.6 Mean ionic activity coefficient at high salt concentrations and ion-association 91
4.4 Conclusion 98

Chapter 5: Development of a non primitive model based theoretical framework for mixed solvent electrolyte systems 101
5.1 Introduction 101
5.2 Molecular model and theory 109
5.3 Simulation 115
5.4 Results and discussion 119
5.5 Conclusion 134

Chapter 6: Studying the thermodynamic properties of mixed solvent electrolytes using the SAFT-VR+DE equation of State 136
6.1 Introduction 136
6.2 Molecular model and theory 146
6.3 Results and discussion 147
6.3.1 Pure fluids 147
6.3.2 Water-alcohol mixture 152
6.3.3 Mixed solvent electrolyte 155
6.4 Conclusion 170

Chapter 7: Conclusion and recommendation 172

REFERENCES 177

Appendix 205

LIST OF TABLES

Table **Page**

3.1 GC-SAFT-VR parameters for the segment number and size of each new functional group studied. 39

3.2 Segment–segment dispersion energy well depth parameters $\varepsilon_{ki,lj}/k_b$ (K) for each new functional group studied. 39

3.3 GC-SAFT-VR segment–segment dispersion energy range parameters $\lambda_{ki,lj}$ for each new functional group studied. 39

3.4: Average absolute deviation in vapor pressures and saturated liquid densities obtained between experimental data and theoretical results for pure benzene and alkylbenzenes 40

4.1. SAFT-VR+DE parameters for water and the % average absolute deviation (AAD) in vapor pressure and saturated liquid density as compared to experiment. 73

4.2.%AAD in $\gamma \pm$ for salts containing Li^+, Na^+, F^- using ionic radii proposed by Mähler et al. 76

4.3 Ion specific SAFT-VR+DE diameter (σion) and square-well dispersion range (λion) parameters for alkali and halide ions studied. 76

4.4. Salt specific dispersion range parameter between cations and the solvent (εcation-H_2O) for different electrolytes along with the %AAD for the SAFT-VR+DE EoS for as compared to the experimental data over the molality range specified. 78

4.5. Comparison between experimental and SAFT-VR+DE equation of state prediction for osmotic coefficient, water activity coefficient and solution densities of different electrolytes 79

4.6.Comparison between experimental and SAFT-VRE theoretical predictions for the Gibbs free energy of solvation for different aqueous electrolytes. 83

4.7 Comparison between experiment and the SAFT-VR+DE EoS predicts for the Gibbs free energy of hydration for different electrolyte solutions. 83

4.8. Experimental v/s theoretically obtained dielectric constant when different dipole moments are used across a range of temperature and pressure 89

4.9. Salt specific dispersion energy parameters between the anion and solvent ($\boldsymbol{\varepsilon}_{\text{anion-H2O}}$) and dispersive ion association energy parameter ($\varepsilon^{ion-assoc}$) obtained from the correlation of mean ionic activity coefficient data ($\gamma \pm$) at molality range > 6*m* using the SAFT-VR+DE equation of state. 97

4.10. Summary of the proposed modeling approaches considered in this work and the required adjustable parameters for each. 98

5.1 Model parameters for the electrolyte fluids studied. σ^*_{d1}, σ^*_{d2}, σ^{*+} and σ^{*-} are the reduced diameter of the solvent 1 (monomer), solvent 2 (dimer), cation and anion molecules respectively. μ^{*2}_{d1} and μ^{*2}_{d2} are the reduced squared dipole moments of solvent 1 and solvent 2, where $\mu^{*2} = \mu^2 / k_b T \sigma^3$, ε^* is the reduced depth of the square-well potential, λ the range of the potential, ψ^* the reduced association energy, r_c the reduced association cutoff radius, N_{ion} the number of ions, and $N_{solvent1}$, $N_{solvent2}$ the number of monomer and dimer solvent molecules. 120

5.2. NPT Monte Carlo simulation results for systems 1–8. The reduced temperature is given by $T^* = k_b T / \varepsilon$, reduced pressure by $P^* = P\sigma^3 / \varepsilon$ and reduced energy by $E^* = E / N\varepsilon$ 129

5.3 SAFT-VR+DE parameters for water, methanol, Na and Br 134

6.1. SAFT-VR+D parameters for alcohols and the % average absolute deviation (AAD) in vapor pressure and saturated liquid densities as compared to experiment 151

6.2. Salt specific dispersion energy parameters for the cation-alcohol ($\boldsymbol{\varepsilon}_{\text{cation-alcohol}}$) interaction for the different mixed solvent electrolytes studied and the % average absolute deviation (AAD) for the SAFT-VR+DE equation of state for as compared to experimental data at 298.15 K and 1.01325 bar 158

6.3. Comparison between experimental mean ionic activity coefficient ($\boldsymbol{\gamma}_{\pm}$) and theoretical predictions obtained by SAFT-VR+DE EOS for the different electrolytes 169

LIST OF FIGURES

Figure **Page**

2.1 Schematic picture of formation of SAFT chain associating fluids. A collection of hard spheres which interact through dispersion interaction, and those hard spheres tangibly bond together to form chain molecules, then those molecules interact through association interaction 9

2.2 Schematic picture of ethyl acetate formed by combining CH_3, OCH_2 and C=O groups. 25

2.3 Schematic picture of formation of hetero-segmented chain fluids, theoretically represented by GC-SAFT-VR. A collection of hard spheres of asymmetric sizes which interact through asymmetric dispersion interactions, and those hard spheres tangibly bond together to form a hetero-segmented chain molecules, then those molecules interact through association interaction. The sites can be placed upon the specific segment of a molecule as intended. 25

3.1 Theoretical results for liquid densities of alkylbenzenes obtained from (a) the GC-SAFT approach using parameters reported by Tamouza et al. for octylbenzene to ethylbenzene from left to right and (b) the GC-SAFT-VR approach using parameters reported by Peng et al. for octylbenzene to ethylbenzene from left to right. Symbols and solid lines represent the experimental and theoretical results respectively. 34

3.2 Schematic representation of benzene and ethylbenzene illustrating the new CH=(Bz) (blue) and CH=(aBz) (green) and C= (red) functional groups. 36

3.3. Comparison between theoretical results using GC-SAFT-VR and the experimental data for (a) vapor pressure and (b) saturated liquid density for benzene to octylbenzene from left to right. Symbols and solid lines represent the experimental data and theoretical results respectively. 41

3.4. Vapor–liquid equilibria for binary mixtures of benzene (a) / toluene (b) with Hexane (o), Heptane (▽), Octane (Δ), Decane (♦) at 313.15K. The solid lines represent the theoretical predictions and the symbols represent the experimental results 43

3.5.Vapor–liquid equilibria for binary mixtures of (a) benzene + toluene at 273.15K (♦), 283.15K (□), 293.15K(△) and 313.15K(O) and (b) benzene + ethylbenzene at 453.15K (□), 483.15K (△), 523.15K(O). The symbols represent experimental results..... 44

3.6. Vapor–liquid equilibria for binary mixture of benzene with propylbenzene at 1.01325 bar (●). The solid lines represent the theoretical predictions and the symbols represent the experimental results. 45

3.7. Vapor–liquid equilibria for binary mixtures of (a) benzene + dimethylether at 323.15K(O) and (b) benzene + dibutylether at 308.15K (O). The solid lines represent the theoretical predictions and the symbols represent the experimental results 46

3.8. Vapor–liquid equilibria for binary mixture of (a) toluene + diethylether at constant pressure of 1.01325 bar (O); (b) and (c) ethylbenzene + dipropylether at 323.15K (green ●), 333.15K (red ▲), 343.15K (blue ♦).The solid lines represent the theoretical predictions and the symbols represent the experimental results 48

3.9. Vapor–liquid equilibria for binary mixtures of (a) 1-butanol + benzene (O)/ toluene (◇) at 308.15K (b) ethanol + toluene at 303.15K (♦) and 328.15K (●). The solid lines represent the theoretical predictions and the symbols represent the experimental results..... 49

3.10. Vapor–liquid equilibria for binary mixtures of n-butylamine + benzene(◇)/ toluene (O)/ ethylbenzene (♦) at 298.15K. The solid lines represent the theoretical predictions and the symbols represent the experimental results 50

4.1. Schematic representation of the molecular model used in the SAFT-VR+DE approach to describe electrolyte solutions. The model shown considers ions in an associating dipolar solvent with the ionic species completely dissociated. 66

4.2. Change in the dielectric constant ε as a function of dipole moment μ for water as predicted by the SAFT-VR+D equation of state at room temperature (298.15 K) and pressure (0.101325 MPa). Dashed line represents the dielectric constant for water as reported in experimental studies 73

4.3. Comparison of vapor pressure (a) and vapor-liquid coexisting densities (b) for water from the SAFT-VR+D EoS and experiment. Symbols represent the experimental data and the theory is represented by the solid line 73

4.4. Mean ionic activity co-efficient of (a) LiCl (red ◆), LiBr (blue ●), LiI (green ▲) and (b) NaBr (orange ■), KBr (black ▼), RbBr (purple ▲) at 298.15 K and 0.101325 MPa from the SAFT-VR+DE EOS. Symbols represent the experimental data and solid lines the theoretical correlations. 78

4.5. Aqueous osmotic co-efficient of (a) LiCl (red ◆), LiBr (blue ●), LiI(green ▲) and (b) NaCl (brown ◆), KCl (blue ▼), RbCl (green ●), CsCl

(orange ▲) (c) NaF (brown ◇), KF (red ○), RbF (purple △), CsF (green □) at 298.15 K and 0.101325 MPa from the SAFT-VR+DE EOS. Symbols represent the experimental data and solid lines the theoretical predictions. 80

4.6. Water dielectric constant for different salt solutions (a) LiCl (grey ◇), KCl (red ○), NaCl (green □), RbCl (purple △), CsCl (orange ▽) and (b) KF (grey ◇), NaI (red ○) at 298.15K temperature and 0.101325 MPa pressure. Symbols represent the experimental data and solid lines the theoretical predictions. 86

4.7. Densities of aqueous solution of (a) KBr at 293.15K (grey ◇), 303.15K (red ○), 313.15K (green □) and (b) KCl at 313.15K (grey ◇), 333.15K (red ○), 348.15K (green □), 373.15K (purple △), 398.15K (black ◆), 423.15K (blue ▼). Theoretical predictions have been obtained by using SAFT-VR+DE EOS. Symbols represent the experimental data and solid lines theoretical results. 88

4.8. Comparison of the predicted and experimental (a) mean ionic activity and (b) osmotic co-efficient for NaCl at 298.15K/0.1MPa (grey, ◇), 373.15K/0.1MPa (red, ○), 473.15K/1.55MPa (green, □), 573.15K/8.6MPa (purple, △). The theoretical predictions from the SAFT-VR+DE EOS with a water dipole moment of 2.179D are represented btydashed lines while the solid lines correspond to the theoretical results using the modified dipole moments . The symbols represent the experimental data. 90

4.9. Comparison of the predicted and experimental (a) mean ionic activity and (b) osmotic co-efficient for NaBr at 298.15K/0.1MPa (grey ◇), 373.15K/0.1MPa (red ○), 473.15K/1.55MPa (green □), 573.15K/8.6MPa (purple △). The theoretical predictions from the SAFT-VR+DE EOS with a water dipole moment of 2.179D are represented by dashed lines while the solid lines correspond to the theoretical results using the modified dipole moments . The symbols represent the experimental data. 91

4.10. Mean ionic activity co-efficient of CsCl (green ○) , RbCl (blue □) and NaBr (red ◇) as predicted by the SAFT-VR+DE EOS (solid lines) compared to experimental data. 92

4.11. Association energy (dotted line) and dielectric decrement (solid line) as a function of ionic concentration for LiCl (blue) and KF (red). 94

4.12. Comaprison of the mean ionic activity coefficient (a) and osmotic coefficient (b) for LiCl (blue □) and KF (red ◇) from the SAFT-VR+DE EOS without ion association (solid lines) and with ion association (dashed lines) as compared to the experimental data (symbols) 95

4.13. Comparision of the mean ionic activity coefficient for (a) LiBr (red ◇) and (b) NaI (blue □) obtained from the SAFT-VR+DE EOS with (dashed lines)

and without (solid line) anion-water interaction with experimental data. Symbols represent the experimental data 97

5.1 Schematic representation of the molecular model used in the SAFT-VR+DE equation to describe mixed solvent electrolyte solutions containing ions and two types of associating dipolar solvent. 110

5.2 Schematic representation of one-fluid like approximation scheme adopted for the theoretical treatement of mixed solvent electrolyte solution using SAFT-VR+DE EoS. 111

5.3 Comparison of predictions from the SAFT-VR + DE equation and NPT Monte Carlo simulation results for symmetric electrolyte solutions with $\varepsilon^* = 1.0$, $\lambda = 1.5$, $\sigma^{*+} = \sigma^{*-} = \sigma^*_{d1} = \sigma^*_{d2} = 1.0$, $\psi^* = 5.0$, $r_c = 1.05$, charge q = 1, ion concentration of 8 / 256, and (a) dipole moment $\mu^{*2}_{d1} = 0.5$ and $\mu^{*2}_{d2} = 2.0$ at T* = 1.2, 1.4, 1.6 and 1.8 for system 1 and (b) dipole moment $\mu^{*2}_{d1} = 0.5$ and $\mu^{*2}_{d2} = 4.0$ at T* = 1.2, 1.4, 1.6, and 1.8 for system 2. The solid lines represent predictions from the modified SAFT-VR + DE equation and the squares the NPT Monte Carlo simulation data. 121

5.4. Comparison of predictions from the SAFT-VR + DE equation and NPT Monte Carlo simulation results for symmetric electrolyte solutions with $\varepsilon^* = 1.0$, $\lambda = 1.5$, $\sigma^*_{d1} = \sigma^*_{d2} = \sigma^{*+} = \sigma^{*-} = 1.0$, $\psi^* = 5.0$, $r_c = 1.05$, charge q = 1, dipole moment $\mu^{*2}_{d1} = 0.5$ and $\mu^{*2}_{d2} = 2.0$ at T* = 1.2, 1.4, 1.6 and 1.8 for ion concentration of (a) 4 / 256, and (b) 16 / 256. The solid lines represent predictions from the modified SAFT-VR + DE equation and the squares the NPT Monte Carlo simulation data. 122

5.5. Comparison of predictions from the SAFT-VR + DE equation and NPT Monte Carlo simulation results for symmetric electrolyte solutions with $\varepsilon^* = 1.0$, $\lambda = 1.5$, $\sigma^*_{d1} = \sigma^*_{d2} = \sigma^{*+} = \sigma^{*-} = 1.0$, $\varepsilon^* = 5.0$, $r_c = 1.05$, charge q = 1, dipole moment $\mu^{*2}_{d1} = 0.5$ and $\mu^{*2}_{d2} = 2.0$, ion concentration of 8/256 at T* = 1.2, 1.4, 1.6 and 1.8 for different solvent rations. (a) 200 particles of monomers and 48 of dimers; (b) 4 particles of monomers and 244 of dimers. The solid lines represent predictions from the modified SAFT-VR + DE equation and the squares the NPT Monte Carlo simulation data. 124

5.6. Comparison of predictions from the SAFT-VR + DE equation and NPT Monte Carlo simulation results for asymmetric electrolyte solutions with $\varepsilon^* = 1.0$, $\lambda = 1.5$, $\varepsilon^* = 5.0$, $r_c = 1.05$, charge q = 1, dipole moment $\mu^{*2}_{d1} = 0.5$ and $\mu^{*2}_{d2} = 2.0$, ion concentration of 8/256 at T* = 1.2, 1.4, 1.6 and 1.8 for different solvent and ion sizes. (a) $\sigma^{*+} = \sigma^{*-} = \sigma^*_{d1} = 1.0, \sigma^*_{d2} = 1.333$;

(b) σ^{*+}=0.667, σ^{*-}=1.667, σ^{*}_{d1}=1.0, σ^{*-}=1.333. The solid lines represent predictions from the modified SAFT-VR + DE equation and the squares the NPT Monte Carlo simulation data. 125

5.7 Comparison of the ion concentration and solvent composition dependent dielectric constant (solid line) with the solvent concentration dependent dielectric constant calculated predicted from the SAFT-VR+D equation (dotted line) for NaBr + water + (50 weight%) methanol mixed solvent electrolyte systems. The system parameters are given in table 5.3. 126

5.8. Comparison of predictions from the SAFT-VR + DE equation and NPT Monte Carlo simulation data for symmetric electrolyte solutions with ε^{*} = 1.0, λ = 1.5, $\sigma^{*}_{d1}=\sigma^{*}_{d2}=\sigma^{*+}=\sigma^{*-}$=1.0, ψ^{*} = 5.0, r_c=1.05, charge q=1, dipole moment μ^{*2}_{d1} = 0.5 and μ^{*2}_{d2}=2.0, and ion concentrations of 8/256 (124 monomers and 124 dimers) at T* = 1.8. The solid line represents predictions from the non-primitive model based SAFT-VR + DE, dotted line represents predictions from the primitive model + SAFT-VR using a solvent composition based (and salt concentration independent) dielectric constant, dash-dotted line represents predictions form the PM + SAFT-VR using a salt concentration and solvent composition dependent dielectric constant, and the squares are NPT Monte Carlo simulation results. 127

5.9. Comparison of predictions from the SAFT-VR + DE equation and NPT Monte Carlo simulation data for asymmetric electrolyte solutions with ε^{*} = 1.0, λ =1.5, σ^{*+}=0.667, σ^{*-}=1.667, σ^{*}_{d1}=1.0, μ^{*2}_{d2}=1.333, ψ^{*}=5.0, r=1.05, charge q = 1, dipole moment μ^{*2}_{d1} = 0.5 and μ^{*2}_{d2}=2.0, and ion concentrations of 8 / 256 (124 monomers and 124 dimers) at T* = 1.8. The solid line represents predictions from the non-primitive model based SAFT-VR + DE, dotted line represents predictions from the primitive model + SAFT-VR using a solvent composition based (and salt concentration independent) dielectric constant, dash-dotted line represents predictions form the PM + SAFT-VR using a salt concentration and solvent composition dependent dielectric constant, and the squares are NPT Monte Carlo simulation results. 128

6.1. Change in the dielectric constant ε as a function of dipole moment μ for alcohols as predicted by the SAFT-VR+D equation of state at room temperature (298.15 K) and pressure (0.101325 MPa). Solid line represents the dielectric constant for methanol (green) and ethanol (red) as reported in experimental studies 151

6.2. Comparison of vapor pressure (a) and vapor-liquid coexisting densities (b) for methanol (green) and ethanol (red) from the SAFT-VR+D EoS and experiment. Symbols represent the experimental data and the theory is represented by the solid line. 152

6.3. Vapor–liquid equilibria for binary mixtures of alcohol + water. Part (a) methanol + water binary mixture at 298.15 K (red), 313.15 K (blue), 323.15 K (green), 333.15 K (black). Part (b) ethanol + water at 298.15 K (red), 323.15 K (blue), 328.15 K (green), 333.15 K (black). The solid lines correspond to the theoretical predictions from the SAFT-VR+D approach and the symbols to the experimental data 154

6.4. Dielectric constant of salt free methanol+ water mixture at 293.15 K (black), 298.15 K (red), 303.15 K (blue), 313.15 K (green), 323.15 K (yellow), 333.15 K (orange),. The solid lines correspond to the theoretical predictions from the SAFT-VR+D approach and the symbols to the experimental data 154

6.5. Mean ionic activity coefficients of RbCl in water/ methanol mixtures at 298.15 K and 1.0125 bar with salt-free alcohol weight fractions at 20% (red), 40% (blue). The symbols represent experimental data and solid lines are theoretical correlations/ predictions by SAFT-VR+DE equation of state. 159

6.6. Mean ionic activity coefficients of CsCl in water + (a) methanol and (b) ethanol mixtures at 298.15 K and 1.01325 bar with salt-free alcohol weight fractions at 10% (red), 20% (blue), 30% (green), 40% (orange). The symbols represent experimental data[349] and solid lines are theoretical correlations/ predictions by SAFT-VR+DE. 1611

6.7. Mean ionic activity coefficients of KCl in water/ methanol mixtures at 298.15 K and 1.0125 bar with salt-free alcohol weight fractions at 20% (red), 40% (blue), 60% (green). The symbols represent experimental data and solid lines are theoretical correlations/ predictions by SAFT-VR+DE. 162

6.8. Mean ionic activity coefficients of NaF in water/ ethanol mixtures at 298.15 K and 1.0125 bar with salt-free alcohol weight fractions at 10% (red), 20% (blue), 30% (green), 40% (orange), 50% (purple), 60% (yellow), 70% (brown), 80% (black). The symbols represent experimental data and solid lines are theoretical correlations/ predictions by SAFT-VR+DE..... 163

6.9 Mean ionic activity coefficients of LiCl in water/ methanol mixtures at 298.15 K and 1.0125 bar with salt-free alcohol weight fractions at 10% (red), 20% (blue). The symbols represent experimental data[348] and solid lines are theoretical correlations/ predictions by SAFT-VR+DE..... 164

6.10. Mean ionic activity coefficients of NaCl in water/ methanol mixtures at 298.15 K and 1.0125 bar with salt-free alcohol weight fractions at 20% (blue), 40% (orange), 60% (yellow), 80% (green). The symbols represent experimental data and solid lines are theoretical correlations/ predictions by SAFT-VR+DE. 166

6.11. Mean ionic activity coefficients of NaBr in water/ (a) methanol and (b) ethanol mixtures at 298.15 K and 1.0125 bar with salt-free alcohol weight fractions at 10% (red), 20% (blue), 40% (green), 60% (orange), 80% (purple), 90% (yellow). The symbols represent experimental data and solid lines are theoretical correlations/ predictions by SAFT-VR+DE..... 167

6.12. Mean ionic activity coefficients of NaBr in water + methanol mixture (alcohol weight fractions 90%) at 298.15 K and 1.0125 bar. The symbols represent experimental data, solid and dashed line presents theoretical prediction and correlation with original and effective dipole moments respectively using of SAFT-VR+DE. 168

6.13. SAFT-VR+D equations of state prediction for dielectric constant ε as a function of ionic concentration using different dipole moments μ for methanol + water + NaBr mixture system. Solid line represents the dielectric constant corresponding to original dipole (2.45 D), dashed line gives dielectric constant corresponding to effective dipole moment (2.65 D) and dotted line represnts salt free mixed solvent (90 weight % methanol with water) dielectric constant 168

Chapter 1: Introduction

In the words of the famous chemical engineer and entrepreneur Bodo Linnhoff "Most chemical processes are network of different pieces of equipment. Usually, even the best pieces of equipment will give a poor overall process if linked up inappropriately in the network [1]." The fundamental concept behind process design is the selection of processing steps in the correct order and their integration into an operation unit. Since the 1970's, in the midst of the energy crisis, a new generation of process modeling tools and software were developed that led to the modernization of industrial chemical process design [1, 2]. The annual worldwide expenditure by the chemical industry on conceptual design, engineering, operation and maintenance of chemical, refining, polymer and power plants is estimated to be around $500 billion[3]. Process design decisions are therefore made with the aim of reducing unnecessary waste and reducing operating costs[4]. This calls for reliable theoretical frameworks, including equation of state or activity coefficient models, within process modeling tools that can accurately capture the thermo-physical properties and phase behavior of the systems under consideration.

Traditional theoretical methods, such as cubic equation of state and activity coefficient models, are still predominantly used in chemical process industries for thermophysical property and phase behavior calculations in fluid/solid systems. For example, the Soave-Redlich-Kwong[5] equation finds its application in air separation, gas processing, and petroleum refining processes. Similarly, the non-random two liquid (NRTL)[6] equation is often the model of choice in processes dealing with polymers/ oligomers while processes containing electrolyte solutions can be described using

electrolyte NRTL[3, 7]. Although, these activity coefficient models and cubic equation of state are intuitive and simple to apply, in practice there is considerable room for improvement. These approaches typically work as correlative tools able to correlate experimental data, with extrapolation outside the range of available experimental data often unreliable The key point is that there needs to be sufficient experimental data in order to make these highly parameterized theoretical frameworks work[3]. In cases where inadequate experimental data is available to develop parameters or validate the model, empirical methods show limitations. Although group contribution methods such as UNIFAC[8] have somewhat helped to eliminate this limitation, there are still voids as its application is limited only to low pressure systems, which need to be filled in terms of thermodynamic property predictions for complex systems such as polymers and ionic liquids. An extensive discussion on the advantages and disadvantages of currently-used activity coefficient models and cubic equation of state and their applicability can be found in the review articles of Chen et al.[3] and Valderrama[9]. To summarize these reviews, the primary limiting aspect of classical cubic equation of state and activity coefficient models is that they are reliant on fitted parameters that do not carry any physical meaning. As a result, classical methods often fail in the study of complex fluids and mixtures to provide accurate predictions, as several fitted interaction parameters are required.

Over the years, the systems of interest from a process modeling perspective increase in complexity. For example, compounds such as surfactants, polymers with multiple functional groups, mixed solvents and multiple salt electrolyte systems, ionic liquids and polyfunctional molecules such as amino acids, peptides, and fatty acids are

now commonly considered during process development. These compounds contain anisotropies: anisotropy in molecular level interactions (for example, hydrogen bonding, polar, ionic fluids) or structural anisotropy (for example, long chains, molecules with branches e.g. branched alkanes). Thus, there is a need to have a thermodynamic modeling framework, which explicitly captures these molecular level interactions through physically meaningful parameters. In recent years, the statistical associating fluid theory (SAFT)[10, 11] has provided a major advancement in thermodynamic modeling as a molecular based theoretical framework that contains physically meaningful parameters. Due to the molecular model basis and firm statistical mechanical roots, systematic improvement of the SAFT theory is possible with the approximations made able to be validated against computer simulation results for the same molecular model. This has allowed many different versions of SAFT to be proposed that have been used to correlate as well as predict the thermophysical properties and phase behavior of a wide range of pure fluids and their mixtures. These systems include low molecular weight alkanes to simple polymers[12, 13], perfluoroalkanes[14, 15], alcohols[16, 17], water[18, 19], refrigerant systems[20, 21], carbon dioxide [22, 23], amines[24, 25], electrolytes[26-29], ionic liquids[30], biomolecules[31], nanoparticles[32], polyhedral oligomeric silsesquioxanes (POSS)[33] and their binary mixtures[34, 35].

Initial versions of the SAFT equation were somewhat simplistic in nature, with the contributions due to the monomer and chain interactions being described by different levels of theory. Such inconstancies in the theoretical framework of so-called first-generation SAFT based equations of state were eliminated in subsequent versions, with both the monomer and chain terms typically being described by second order perturbation

theory[29, 36-38]. However more recently, in an effort to increase the predictive ability of SAFT-based equations of state, several group contribution schemes have been proposed[39-44], some of which are even capable of capturing structural anisotropy/ heterogeneity within the theoretical framework[41, 44]. In this work, a version of SAFT that describes molecules as chains of tangentially bonded spherical segments that interact through a potential of variable range - SAFT-VR[36]-is used to study two sets of unique systems: compounds with aromatic rings (i.e., benzene and alkylbenzenes) and electrolyte solutions (both aqueous and mixed solvents). In the chemical process industry, benzene is mainly used as a solvent for fats, waxes, resins, oils, inks, paints, plastics, rubber; also finds its application in the oil extraction from seeds and nuts. Alkylbenzenes find application in industry primarily as solvents. For example, methylbenzene (toluene) finds its application universally as a solvent and as industrial feedstock while ethylbenzene is applied as a solvent in inks, rubber adhesives, varnishes, and paints; it is also used as an intermediate reactant in styrene production. Due to their industrial importance, it is important to be able to capture the phase behavior of alkylbenzenes appropriately through theoretical an equation of state.

Electrolytes, more precisely aqueous electrolytes, are widely investigated systems due to their application in chemical processes such as osmosis and reverse osmosis, fertilizer production, water purification, geochemistry, electrochemistry, enhanced oil recovery, as well as in biological systems[45-49]. Although electrolyte solutions are simple in structure, significant anisotropies in the physical interactions are present[50-52]. Electrostatic charged and polar interactions make the electrolyte systems highly non-ideal. There are two ways available for modeling electrolyte solutions, one with implicit

solvent assumption also known as a primitive model[53] of electrolytes and another with explicit consideration of dipolar solvent molecules along with charged ions, known as non primitive model[54]. In the primitive model ions are considered to be in an implicit solvent represented by a dielectric continuum. The majority of the theoretical investigations into the thermophysical properties of electrolyte solutions to date utilize this implicit solvent model and therefore, are very limited in predictive ability. In primitive model, due to the consideration of implicit solvent ion-solvent interaction are not account appropriately, so the success of theoretical framework largely depends upon quality of input dielectric[26, 55]. Drawback in the theoretical formalism is compensated by the experiment dielectric constant. Since the dielectric constant is a property inputted to the problem, several key properties such as ionic concentration effect on the solvent dielectric,, solvation can never be accurately captured in existing primitive model based theoretical frameworks. Also, in general, electrolytes are modeled as fully dissociated species, and theoretical frameworks remain confined to a particular range of salt concentrations rather than the entire range from dilute solution up to the saturated salt limit. Using the recently developed, SAFT-VR+DE equation[29], a non primitive model based equation of state which explicitly considers the solvent within the molecular model, a range of thermodynamic properties across the range of temperature, pressure and salt concentrations have been studied and efforts have been made to overcome limitations of the existing theoretical frameworks available in the literature.

Although aqueous electrolyte systems have been widely investigated both experimentally as well as theoretically in the literature, studies of mixed solvent electrolytes are very limited. However, there is a great deal of interest from chemical

process industry point of view. The addition of salts alters the phase equilibrium behavior of systems containing more than one molecular solvents. One prime example is the alteration of relative volatilities (salting-in or salting-out) and liquid-phase stability for mixed-solvent electrolyte systems. Because of the salt effect can often shift phase equilibrium toward more effective separation of selective components, there is a potential for using salts to enhance separation processes. Although, there is actually a lack of experimental data from which to build a reliable and predictive model for mixed solvent electrolytes. All theoretical frameworks for mixed solvent electrolyte developed to date by only adopting primitive model of electrolyte and require knowledge of the appropriate dielectric constant. However, there is no experimental data for the dielectric constant available for mixed solvent electrolyte solutions. In this scenario, a non primitive model based equation of state provides an attractive alternative as no prior knowledge of solution dielectric constant is required, which instead is calculated within the theory from the solvent dipole moment. A non primitive model based theoretical framework can lead the way and predict thermodynamic properties, which may work as a forerunner for experimental studies. In this regard, SAFT-VR+DE equation of state have been extended for the study of mixed solvent electrolyte systems with a one-fluid like approximation for the mixed solvent. After the initial validation of the approximation within SAFT-VR+DE theoretical framework by computer simulation of model systems, SAFT-VR+DE has been applied for the study of thermodynamic property of real mixed solvent electrolyte systems.

In the remainder of this chapter, a summary of the thesis that indicates the content of each chapters is provided.

In chapter 2, a brief literature review of the statistical associating fluid theory (SAFT) based equation of state is presented. The development of the SAFT family of equation from basic SAFT theoretical framework is discussed, with particular focus on the SAFT-VR equation and it's group contribution scheme in the GC-SAFT-VR approach.

A novel-modeling scheme within group-contribution SAFT-VR approach for compounds with aromatic rings, in this case specifically for benzene and family of alkylbenzenes is presented in chapter 3. The structural asymmetry/ anisotropy has been treated explicitly with the previously developed GC-SAFT-VR equation of state. The correlated results of vapor pressure and saturated liquid densities for benzene to declybenzene are reported along with theoretical prediction of the same properties for undecylbenzene to octadecylbenzene. The study has been further extended to the binary phase behavior of mixtures of benzene/ alkylbenzenes, with both non-associating (alkane, ether) and associating fluids (alcohol, amines).

A molecular model for aqueous electrolyte systems along with a detailed description of the SAFT-VR+DE equation of state is presented in chapter 4. Non-primitive model based SAFT-VR+DE equation of state has been applied to study the mean ionic activity coefficient, osmotic coefficient, water activity coefficient, solution densities, Gibbs free energy of solvation, and dielectric decrement of nineteen different aqueous alkali halide electrolyte systems. Temperature and pressure effects on thermodynamic properties are also investigated. At higher salt concentrations, the proposed model has been improved with the inclusion of an ion-association term in salt specific cases to accurately capture the thermodynamic properties.

In chapter 5, the SAFT-VR+DE approach is extended to the study of mixed solvent electrolyte systems with a one-fluid like approximation for mixed solvents. The proposed approximation scheme within SAFT-VR+DE equation of state has been tested against *NPT* Monte Carlo simulation results for ionic salt and dipolar solvent particles of different sizes, polarity, ionic and solvent concentrations at different conditions (temperatures and pressures).

In chapter 6, the SAFT-VR+DE approach is applied to several water + alcohol mixed solvent alkali halide electrolyte systems. Solvent parameters are developed using the SAFT-VR+D approach and dielectric property of salt free mixed solvent systems are predicted. Thermodynamic property, mean ionic activity coefficients for mixed solvent electrolyte systems are predicted for a wide range of salt and solvent concentrations.

Finally, in chapter 7 concluding remarks are made and recommendations for future works are discussed in this chapter.

Chapter 2: Background

2.1 Statistical associating fluid theory

The statistical associating fluid theory (SAFT), developed by Gubbins and co-workers [10, 11] based on the thermodynamic perturbation theory (TPT) of Wertheim [56-59], has gained considerable popularity in both the academic and industrial communities over the last twenty-five years. In the SAFT framework a molecule is modeled as a chain of spherical segments tangentially bonded together that interact via repulsive and dispersive interactions and short ranged attractive (association) interactions when appropriate. A representative schematic diagram of a SAFT fluid is presented in the figure 2.1.

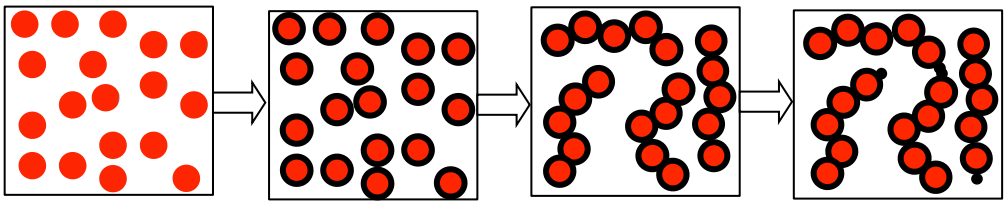

Figure 2.1 Schematic picture of formation of SAFT chain associating fluids. A collection of hard spheres which interact through dispersion interaction, and those hard spheres tangibly bond together to form chain molecules, then those molecules interact through association interaction.[60]

Within the SAFT formalism the Helmholtz free energy (A) for an associating chain fluid is expressed as a combination of four contributions:

$$\frac{A}{Nk_bT} = \frac{A^{ideal}}{Nk_bT} + \frac{A^{mono}}{Nk_bT} + \frac{A^{chain}}{Nk_bT} + \frac{A^{assoc}}{Nk_bT} \qquad (2.1)$$

where N is the number of chain molecules, k_B is Boltzmann's constant and T is the temperature. A^{ideal} is the ideal free energy, A^{mono} is the contribution to the free energy due to the monomer segments, A^{chain} is the contribution due to the formation of bonds

between monomer segments, and A^{assoc} is the contribution due to association. In the initial studies, Chapman et al. [11, 61] used the SAFT equation of state to model Lennerd-Jones (L-J) chain molecules with one or more hydrogen-bonding sites, where the L-J segment free energy contribution term was taken from the work of Twu et. al. [62] or Cotterman et. al. [63] in subsequent works (ref [11, 61]). However, the reference system in chain and association terms was described by a hard sphere fluid instead of the L-J fluid. In subsequent work, Johnson et. al.[64, 65] proposed a version of SAFT for chain composed of tangentially bonded Lennerd-Jones (L-J) spheres, where the free energy due to chain contribution and radial distribution function for LJ polymeric fluid was obtained by fitting to the molecular simulation data of internal energy and pressure at wide range of conditions ($0.005 \le \rho^* = \rho\sigma_{LJ}^3 \le 1.25$ and $0.7 \le T^* = k_b T/\varepsilon_{LJ} \le 6.0$). Later, Muller et. al.[49] further extended the approach to associating Lennard-Jones chains by including the association term.

Huang and Radosz developed a version of SAFT, referred as SAFT-HR[66, 67], using a similar approach as Chapman et al., with the expression for dispersive interaction taken from the work of Chen and Kreglewski[68], where the dispersive energy parameters for the dispersion term were obtained by fitting to the thermodynamic property data (pressure-volume-temperature (PVT) and internal energy) of argon. SAFT-HR has been mostly applied to the study of polymeric systems and able to successfully capture liquid-liquid and vapor-liquid phase behavior of a wide range of systems containing polymers[69-73], olefins[69], alkenes[71], CO_2[72] despite of its simple treatment.

In another extension of SAFT, SAFT-HS[74, 75] was proposed by Jackson et al.,

which can also be referred as the simplest version of SAFT. In SAFT-HS equation of state, monomers are modeled as dispersive hard spheres with Carnahan and Starling expression[76] is used to describe hard sphere interactions and van der Waals mean field attraction term for the representation of dispersive interaction. Whereas only hard sphere radial distribution function expression given by Carnahan and Starling are used to evaluate contact values within chain and association free energy contribution terms. Proposed equation of state was primarily used to study systems with strong associating forces and was successful in describing phase equilibrium and critical behaviors mixtures containing water with alkane[77], difluoromethane[78], 1,1,1,2-tetrafluoromethane[78], hydrogen fluoride, alkyl polyoxyethylene surfactants[79] and alcohol[78]. The theory was able correlate complex closed loop liquid-liquid equilibrium phase behavior of the water−alkylpolyoxyethylene surfactant mixtures systems[79] with relatively simpler SAFT-HS.

Blas and Vega[80] used the approach as proposed by Johnson et al. with a Lennerd-Jones reference fluid term and referred to the approach as soft-SAFT. Soft-SAFT has been successfully applied to study phase behavior, second derivative properties[81], excess properties[82] of wide variety of fluid and fluid mixtures including light and heavy n-alkanes[82-84], alkenes[85], 1-alcohols[85] and their binary and ternary mixtures[85], perfluoroalkanes[86, 87], carbon dioxide[88, 89], oligomers[90], room temperature ionic liquids[91], biodesels[92], N_2O[93].

In another development, SAFT has been extended to model monomer segments with attractive potentials of variable range (SAFT-VR) by Jackson et al.[36, 94] Variable range potential can be represented by square well, L-J, Mie, Yukawa. In this version of

the theory the dispersive interactions are treated via a second-order high-temperature perturbation expansion, providing a more rigorous description of the thermodynamics than found in simpler versions of the SAFT approach SAFT-VR EOS provides better description of the dispersion interactions than the SAFT-HS EOS and also has the advantage over other SAFT s in that it uses analytical expressions to describe the monomer fluids. In this way the theory can readily extended by using different approximations for the reference fluid. SAFT-VR has been successfully used to describe the fluid phase equilibrium of a wide range of industrially important systems; for example, alkanes[75, 95-97] of low molar mass through to simple polymers[96], and their binary mixtures, refrigerant systems: perfluoroalkanes[98, 99], alcohols[100, 101], water[19, 102], petroleum fluids[103], asphaltene[104] and carbon dioxide[88, 105, 106], have been studied.

In contrast with previously described versions of SAFT, PC-SAFT[107], another version of SAFT EoS, was developed by considering hard chain as reference model instead of a hard sphere. In PC-SAFT formalism, the expression for reference hard chain term is similar to original SAFT approach[74], where as the expression for the perturb chain term, representative of dispersive interactions, was obtained by integral expressions for the first- and second-order terms refitted to appropriate Taylor series expansions in density using pure n-alkane phase behavior data[108] and the association term was taken from the original work of Wertheim. The PC-SAFT equation of state has been successfully applied to the study of high-temperature and pressure vapor-liquid and liquid–liquid equilibrium of associating[24], non-associating, polar[109], non-polar fluids such as short-chain hydrocarbons[108], benzene[24], alkylbenzenes, CO_2, N_2,

polymers[110], water, ionic liquids[111], pharmaceuticals[112, 113], asphaltenes[114] with considerable accuracy. In cases PC-SAFT, gave improved performance compared to preliminary SAFT versions such as one due to Huang and Radosz but

Later, a simplified version of PC-SAFT EoS, (sPC-SAFT) was proposed in order to reduce the computational time and programming efforts. The main deference between sPC-SAFT and PC-SAFT lies in the hard sphere, radial distribution function in chain term and association term. It is in sPC-SAFT assumed that all segments have same diameter in mixture and as a result of that Carnahan-Starling expressions for the free energy and radial distribution function of a pure component hard sphere system are used and the association term becomes relatively simpler. The approach is mainly applied to the phase equilibrium modeling of polymer systems[110, 115, 116].

In recent works, several group-contribution based SAFT approaches have been proposed in an effort to develop a more predictive approach and enable the study of systems for which there is limited experimental data. In group-contribution approaches parameters for functional groups are developed rather than molecular parameters. This approach allows one to build up a molecule based upon the knowledge of the functional groups and predict the thermodynamic and phase behavior without fitting to any experimental data. Several group-contribution based SAFT EoS have been developed to date. For instance, the group-contribution based SAFT approach by Tobaly et al[39, 117-119], SAFT-γ approach[40, 120, 121], group-contribution SAFT-VR (GC-SAFT-VR) EoS[122-124], GC-PC-SAFT[42, 125], GC-sPC-SAFT[43], Hetero-segmented PC-SAFT EoS[44]. Amongst these approaches only GC-SAFT-VR and Hetero-segmented PC-SAFT EoS allow modeling of a molecule as heterogeneous chain.

Amongst several group-contribution versions of SAFT, the first real group-contribution based SAFT approach was proposed by Tobaly et al. [39, 117-119], a group contribution scheme that has been applied to the SAFT approach (referred as GC-SAFT) due to Huang and Radosz [11] (denoted as SAFT-0 in their work), the SAFT-VR equation[36] and the PC-SAFT equation[126] for the study of wide variety of compounds such as The phase behavior of a wide range of pure fluids such as linear alkanes[39], alkylbenzenes[39, 119], alkylcyclohexane[39], olefins[39], alcohols[39, 119], esters[127], ethers[128], aldehydes[128], ketones[128] and their various mixtures[117, 129-131] have all been studied using this group contribution method. In this GC approach parameters are determined for the different functional groups present in the molecule by fitting the GC-SAFT parameters to the vapor pressure and saturated liquid densities of the pure compounds. Although parameters for individual functional groups are determined, the molecular parameters are obtained by taking the geometric and arithmetic averages of the group parameters, thus converting the model into a homo-segmented chain molecule. The approach therefore requires no modifications to the original SAFT-0, SAFT-VR or PC-SAFT expressions. Therefore, the method can be outlined as GC-based mixing rule for molecular parameters implemented into several SAFT versions, which can explicitly capture thermodynamic behavior in terms of the different groups making up the molecules.

In another development, Tihic et al.[43] proposed a group contribution scheme based on a sPC-SAFT[132] and applied it to different systems consisting of hydrocarbons, polar compounds, and polymers[43, 133, 134]. It is again a homo nuclear model based GC method but the difference with the GC-SAFT approaches by Tobaly et

al. lies in the averaging scheme, how the group parameters are weighed based upon their impact on thermodynamics and structure. Furthermore, in the work of Tihic et al., a much greater number of functional groups are defined in order to build compounds with smaller building blocks.

The major shortcoming of the described homo-segmented group contribution methods is that they disregard connectivity between the groups and as a result structural anisotropy is completely ignored. Vijande et al.[42, 125] proposed another GC-methodology based upon PC-SAFT for modeling molecules, in which account of molecular topology was taken through mutual perturbation coefficients describing to what extent each group present in the molecule affects the others. The method was shown to be capable of accurately capture phase behavior for some small and long chain linear and branched hydrocarbons, ethers, and esters [42, 125] but again heterogeneity was not considered within the chain term.

Subsequently Lymperiadis *et al*.[40] proposed the SAFT-γ approach, also based upon the SAFT-VR equation, in which the SAFT monomer fluid is defined as a collection of heteronuclear segments of different types that in turn form homonuclear chains, as in the original SAFT-VR approach. A number of functional groups[40, 120] have been defined that allow the phase behavior of alkanes, alkylbenzenes, alcohols, ketones, amines, carboxylic acids and alcohols to be studied[40, 120, 121].

In another development, GC-SAFT-VR [122-124] was proposed in which formalism, a molecule is described as a chain formed of heteronuclear segments. For the first time heterogeneity was taken into account through the modification of chain term within GC framework. In subsequent work [124], association contribution was added

with in the model, which even gives the flexibility of placing an association site on a specific segment. Within GC-SAFT-VR approach a range of functional groups such as CH_3, CH_2, C=O, OH, NH_2 etc were defined for the study of wide variety of systems from simple alkanes to complex polymers, acid, ester, alcohol molecules.

In recent development, a hetero-segmented group contribution version of PC-SAFT EoS was proposed by Gross et al. [44] refered as hs-PC-SAFT. In hs-PC-SAFT theoretical framework, the chain term was modified to incorporate the connectivity between heterogeneous segments and hence heterogeneity was captured in the structure of molecule as in the case of GC-SAFT-VR. In the study, series of saturated hydrocarbons was studied using several simple functional groups defined within the hs-PC-SAFT framework. The investigated systems comprise pure n-alkanes, branched alkanes, alkyl-monosubstituted cyclohexanes, cyclopentanes and wide ranges of properties such as liquid and vapor density, vapor pressure, enthalpy of vaporization, surface tension, isobaric heat capacity, speed of sound, the Joule–Thomson coefficient, the Joule–Thomson inversion curve, and the second virial coefficient were studied with excellent accuracy.

. Since in this work as we apply GC-SAFT-VR and develop different versions of SAFT-VR equations of state, in following part of this chapter we provide a detailed overview both SAFT-VR and GC-SAFT-VR equations of state.

2.2 SAFT-VR

In the SAFT-VR formalism a molecule is comprised of a homonuclear chain formed from hard-core monomers with attractive potentials of variable range (square-well, LJ, Mie and Yukawa), typically a square-well potential[135]. The attractive spherical

monomeric segments of diameter (σ) interact through the intermolecular square well potential given by,

$$u_{ij}^{SW}(r) = \begin{cases} +\infty & \text{if} \quad r < \sigma_{ij} \\ -\varepsilon_{ij} & \text{if} \quad \sigma_{ij} \le r < \lambda_{ij}\sigma_{ij} \\ 0 & \text{if} \quad r \ge \lambda_{ij}\sigma_{ij} \end{cases} \tag{2.2}$$

where ε gives the depth and λ gives the range of square-well potential. Detailed expressions for each term of the equation 2.1 are presented in turn below.

2.2.1 Ideal contribution

The Helmholtz free energy contribution of an ideal gas is given by,

$$\frac{A^{ideal}}{Nk_bT} = \ln\left(\rho\Lambda^3\right) - 1 \tag{2.3}$$

where, $\rho = N/V$ is the molecular number density, and Λ is the thermal de Broglie wavelength which incorporates the kinetic (translational, rotational, and vibrational) contributions to the partition function of the molecular chain.

2.2.2 Monomer contribution

The monomer free energy of the pure fluid is given as,

$$\frac{A^{mono}}{Nk_BT} = m\frac{A^{mono}}{N_sk_BT} = ma^M \tag{2.4}$$

where, m is the number of square well dispersive spherical monomer segments in each chain, N_S is the number of spherical monomer segments and a^M is the excess Helmholtz free energy contribution due to the interactions of the square well monomer segments in this case.

Square-well Interactions:

From the Barker and Henderson perturbation theory[136, 137], originated from high temperature expansion approach of Zwanzig[138], the monomer-monomer square well dispersion free energy per segment can be obtained. The high temperature expansion of the Helmholtz free energy is obtained as a series taken up to the second-order of the inverse of the temperature, using hard-sphere system as reference fluid given by the following expression,

$$a^{M} = a^{HS} + \beta a_1^{SW} + \beta^2 a_2^{SW} \tag{2.5}$$

where $\beta = 1/k_b T$, a^{HS} is the free energy contribution due to reference hard sphere fluid, a_1^{SW} and a_2^{SW} are the first two perturbation terms associated with the attractive energy ε_{ij}, and in the SAFT-VR approach the series is truncated at second order. The free energy expression for the reference hard sphere is obtained from Carnahan and Starling equation of state[76] and given by,

$$a^{HS} = \frac{4\eta - 3\eta^2}{\left(1-\eta\right)^2} \tag{2.6}$$

where, η is the system packing fraction, related to the molecular number density ρ expressed as, $\eta = \frac{\pi}{6}\rho\sigma^3$.

First–order perturbation term:

The mean attractive energy a_1 corresponds to the average of the monomer-monomer interaction calculated with the hard sphere structure is given by[139],

$$a_1 = -2\pi\rho_s\varepsilon\int_{\sigma}^{\infty} r^2\phi\left(r\right)g^{HS}(r)\,dr \tag{2.7}$$

where, $\rho_s = N_s/V$ is the number density of spherical segments and $g^{HS}(r)$ is the pair radial distribution function of the hard-sphere reference system.

The van der Waals (VDW) mean field energy is calculated by taking $g^{HS}(r)=1$ for all inter-molecular distances. This corresponds to the assumption of random correlation between the position of the particles. Under this approximation, the a_1 corresponds to a_1^{VDW} is given by,

$$a_1^{VDW} = -2\pi\rho_s\varepsilon\int_{\sigma}^{\infty} r^2\phi(r)\,dr = -\rho_s\alpha^{VDW} \tag{2.8}$$

where, α^{VDW} is the van der Waals attractive parameter.

The pair radial distribution function of hard sphere systems g^{HS} is solved analytically by using mean value theorem, and correlates to the first perturbation term with van der Walls attractive energy constant in the following way[135],

$$a_1 = -\rho_s\alpha^{VDW}g^{HS}(\xi;\eta) = a_1^{VDW}g^{HS}(\xi;\eta) \tag{2.9}$$

where, ξ represents certain distance in the expression dependent upon the density and range. In case of square well variation of variable range potential, the van der Waals attractive parameter is given by,

$$a_1^{VDW} = -4\eta\varepsilon\left(\lambda^3-1\right) \tag{2.10}$$

In the work of Gil Villegas et al.[135], it has been discussed, that since the leading term of the Tayor expansion of g^{HS} around contact value, is $g^{HS}(1;\eta)$, it is reasonable to represent the full function of $g^{HS}(\xi;\eta)$ with leading term and the expression reduces to,

$$g^{HS}(\xi;\eta) \cong g^{HS} \tag{2.11}$$

where, $g^{HS}(1;\eta)$ evaluated with an effective packing fraction η_{eff} at contact. The final expression for a_1^{SW} term becomes,

$$a_1^{SW} = -4\eta\varepsilon\left(\lambda^3 - 1\right)g^{HS}\left(1;\eta_{eff}\right) \tag{2.12}$$

where the Carnahan and Starling equation of state is used to evaluate $g^{HS}(1;\eta_{eff})$.

$$g^{HS}\left(1;\eta_{eff}\right) = \frac{1-\eta_{eff}/2}{\left(1-\eta_{eff}\right)^3} \tag{2.13}$$

For range $1.1 \le \lambda \le 1.8$, the effective packing fraction η_{eff} is described by a function of η and λ, viz

$$\eta_{eff}\left(\eta,\lambda\right) = c_1\eta + c_2\eta^2 + c_3\eta^3 \tag{2.14}$$

where the coefficients c_n are given by

$$\begin{pmatrix} c_1 \\ c_2 \\ c_3 \end{pmatrix} = \begin{pmatrix} 2.25855 & -1.50349 & 0.249434 \\ -0.669270 & 1.40049 & -0.827739 \\ 10.1576 & -15.0427 & 5.30827 \end{pmatrix}\begin{pmatrix} 1 \\ \lambda \\ \lambda^2 \end{pmatrix} \tag{2.15}$$

In recent work, Patel et al.[140] examined other functional forms for η_{eff} in order to increase the applicable range of λ to 3. The Pade expression proposed by Patel et al., is given by,

$$\eta_{eff}\left(\eta,\lambda\right) = \frac{c_1\eta + c_2\eta^2}{\left(1+c_3\eta\right)^3} \tag{2.16}$$

$$\begin{pmatrix} c_1 \\ c_2 \\ c_3 \end{pmatrix} = \begin{pmatrix} -3.16492 & 13.35007 & -14.80567 & 5.07286 \\ 43.00422 & -191.66232 & 273.89683 & -128.93337 \\ 65.04194 & -266.46273 & 361.04309 & -162.69963 \end{pmatrix}\begin{pmatrix} 1/\lambda \\ 1/\lambda^2 \\ 1/\lambda^3 \\ 1/\lambda^4 \end{pmatrix} \tag{2.17}$$

Second–order perturbation term:

The second perturbation term a_2^{SW} is obtained from the first density derivative of a_1^{SW} within the local compressibility approximation

$$a_2^{SW} = \frac{1}{2} K^{HS} \varepsilon \eta \frac{\partial a_1^{SW}}{\partial \eta} \tag{2.18}$$

where K^{HS} is the hard-sphere isothermal compressibility of Percus-Yevick (PY)

$$K^{HS} = \frac{\left(1-\eta\right)^4}{1+4\eta+\eta^2} \tag{2.19}$$

2.2.3 Chain contribution

The contribution to the free energy due to chain formation from the monomer segments is given in terms of the contact value of the pair background distribution function of the monomers,

$$\frac{A^{chain}}{Nk_BT} = -(m-1)\ln\left(y^{SW}\left(\sigma\right)\right) \tag{2.20}$$

where, $y^{SW}\left(r\right)$ is the background correlation function and obtained from the high-temperature expansion of the pair radial distribution function $g^{SW}\left(r\right)$. The expression of the background correlation function is given by,

$$y^{SW}\left(\sigma\right) = \exp\left[\beta u^{SW}(\sigma)\right] g^{SW}\left(\sigma\right) = \exp\left[-\beta\varepsilon\right] g^{SW}\left(\sigma\right) \tag{2.21}$$

The $g^{SW}\left(\sigma\right)$ is obtained from the high-temperature expansion for the radial distribution function. In the expansion for the radial distribution function, the (n-1) th order expansion for the structure corresponds to the n-th order for the thermodynamics. Since the monomer free energy is described by a second order expansion, for the structure it is

truncated at first-order term g_1. So, for the square-well fluid the radial distribution function is given by

$$g^{SW}(\sigma) = g^{HS}(\sigma) + \beta\varepsilon g_1(\sigma) \tag{2.22}$$

where, $g^{HS}(\sigma)$ is obtained from the equation evaluated at η. The expression for $g_1(\sigma)$ is derived from a self-consistent method for the pressure using Clausius virial theorem and the density derivative of the Helmholtz free energy and given by,

$$g_1(\sigma) = \frac{1}{4\varepsilon}\left[\frac{\partial a_1}{\partial \eta} - \frac{\lambda}{3\eta}\frac{\partial a_1}{\partial \lambda}\right] \tag{2.23}$$

2.2.4 Association contribution

The excess free energy contribution due to the association of *s* sites on a chain molecule is given by[74],

$$\frac{A^{assoc}}{Nk_bT} = \sum_{i=1}^{n} x_i \left[\sum_{a=1}^{s}\left(\ln X_{a,i} - \frac{X_{a,i}}{2}\right) + \frac{s_i}{2}\right] \tag{2.24}$$

where, the first sum is over all s sites of type a in a molecule, and X_a is the fraction of molecules not bonded at site a

$$X_a = \frac{1}{1 + \sum_{b=1}^{s} \rho X_b \Delta_{a,b}} \tag{2.25}$$

where, $\Delta_{a,b}$ is the association strength between sites of kind a and kind b; given by,

$$\Delta_{a,b} = K_{a,b} f_{a,b} g^M(\sigma) \tag{2.26}$$

$f_{a,b}$ is the Mayer *f* function for the *a-b* site-site interaction with bonding energy $\varepsilon_{a,b,i,j}$ and volume $K_{a,b}$ available for bonding. g^M is the monomer-monomer radial distribution,

which for water association is mediated by four dispersive SW association sites. The expressions for $f_{a,b}$ and $K_{a,b}$ are given by,

$$f_{a,b} = \exp\left(-\psi_{a,b}/k_bT\right) - 1 \tag{2.27}$$

$$\begin{aligned} K_{a,b} = 4\pi\frac{\sigma^2}{72r_d^2}\Bigg[\ln\left(\frac{r_c + 2r_d}{\sigma}\right)\left(6r_c^3 + 18r_c^2 r_d - 24r_d^3\right) + \ldots \\ \left(r_c + 2r_d - \sigma\right)\left(22r_d^2 - 5r_c r_d - 7r_d\sigma - 8r_c^2 + r_c\sigma + \sigma^2\right)\Bigg] \end{aligned} \tag{2.28}$$

where, r_d is the position of the site within the molecule and r_c represents range of association site. Although in most studies, $K_{a,b}$ is obtained directly by fitting to the experimental phase behavior data rather than fitting for r_d and r_c .

.

2.3 GC-SAFT-VR

SAFT-VR equation of state forms the basis behind the development of two group contribution based equations of state, viz. GC-SAFT-VR and SAFT-γ. GC-SAFT-VR explicitly captures the heterogeneity within the molecular structure (hetero-segmented chain) as opposed to SAFT-γ, which considers molecules to be homonuclear chains. In the GC-SAFT-VR formalism a molecule is described as a chain formed of heteronuclear segments, which interact through square well dispersive interactions, where specific groups can have short ranged square well associating sites. GC-SAFT-VR equation of state defines a molecule through a combination of different segments and connectivity, which provides an appropriate framework to accurately capture the nature of the molecular structure, including branching and location of functional groups within a

molecule. This hetero-segmented approach also provides the liberty of explicitly defining different functional groups such as CH_3, CH_2, C=O, OH etc. Once parameters have been determined for a wide range of functional groups, within the GC-SAFT-VR approach, a number of different molecules, which were not included in the fitting procedure, can then be modeled by connecting appropriate functional groups and thus enhances predictive nature of the theoretical model in the study of thermodynamic properties and phase behavior. For example, in figure 2.2, an ethyl acetate molecule has been presented. The molecule is formed by functional groups CH_3, OCH_2, C=O. The GC-SAFT-VR parameters, segment diameter σ, well depth ε, potential range λ and number of segments *m*, of these function groups are obtained by fitting to the experimental data for members of alkane, ether and ketone families respectively and functional group parameters can be used in a transferable manner to compute vapor pressure and saturated liquid densities of ethyl acetate. The cross interaction between simple function groups are obtained by using Lorentz-Berthelot combining rule[141] in the following way,

$$\varepsilon_{ij} = \sqrt{\varepsilon_{ii}\varepsilon_{jj}} \tag{2.29}$$

$$\lambda_{ij} = \frac{\lambda_{ii}\sigma_{ii} + \lambda_{jj}\sigma_{jj}}{\sigma_{ii} + \sigma_{jj}} \tag{2.30}$$

Where as interactions involving polar groups are expected to show some deviations from Lorentz-Berthelot combining rule and hence the unlike interactions between those functional groups are obtained by fitting to the pure experimental data of compound consists of both the groups.

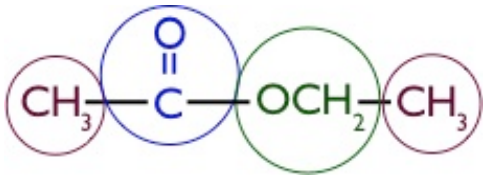

Figure 2.2: Schematic picture of ethyl acetate formed by combining CH_3, OCH_2 and C=O groups.

Similar to the SAFT VR EoS, repulsive and attractive interactions between segments that represent the functional groups are treated by a square-well (SW) potential. In this framework GC-SAFT-VR[122] Helmholtz free energy is represented as a combination of four contributions ideal, monomer, chain and association. A schematic representation of different contributions for model hetero segmented chain associating fluid has been provided in figure 2.3.

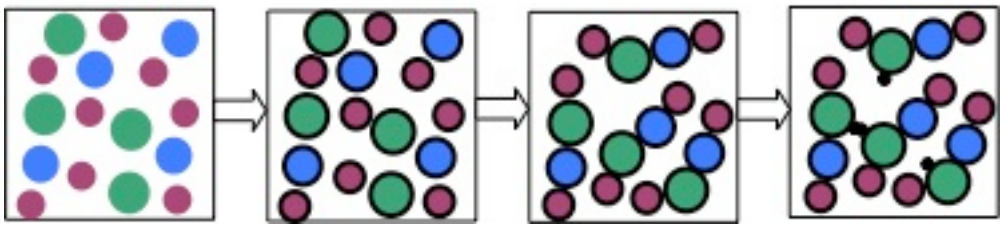

Figure 2.3: Schematic picture of formation of hetero-segmented chain fluids, theoretically represented by GC-SAFT-VR. A collection of hard spheres of asymmetric sizes which interact through asymmetric dispersion interactions, and those hard spheres tangibly bond together to form a hetero-segmented chain molecules, then those molecules interact through association interaction. The sites can be placed upon the specific segment of a molecule as intended.

2.3.1 Monomer contribution

The monomer free energy term in the GC-SAFT-VR framework for a *n*-component mixture is given by,

$$\frac{A^{mono}}{Nk_BT} = \sum_{k=1}^{n}\sum_{i=1}^{n_k'} x_k m_{k,i} a^{SW} \tag{2.31}$$

The first sum is over all the different segments and the second one is over number of

compounds present in the mixture. $n_k^{'}$ represents number of types of functional group present and m_{ki} represents the chain length of functional group of type *i*. The free energy of the reference hard sphere (HS) a^{HS} mixture is derived from the expression of Boublik [142] and Mansoori [143] as

$$a^{HS} = \frac{6}{\pi\rho_s}\left[\left(\frac{\zeta_2^3}{\zeta_3^2} - \zeta_0\right)\ln\left(1-\zeta_3\right) + \frac{3\zeta_1\zeta_2}{1-\zeta_3} + \frac{\zeta_2^3}{\zeta_3\left(1-\zeta_3\right)^2}\right] \tag{2.32}$$

where, ζ_l is the reduced density given by a sum over all segments given by following expression,

$$\zeta_l = \frac{\pi}{6}\rho_s\left[\sum_{k=1}^{n}\sum_{i=1}^{n_k^{'}} x_{s,ki}\left(\sigma_{ki,ki}\right)^l\right],\ l = \quad 0,\quad 1,\quad 2,\quad 3 \tag{2.33}$$

where , $\sigma_{ki,ki}$ is the diameter of segments of type *i* in chain k and $x_{s,ki}$ the segment fraction of type i in chain k, expressed as

$$x_{s,ki} = \frac{x_k m_{ki}}{\sum_{k=1}^{n} x_k m_{ki}} \tag{2.34}$$

The first perturbation term (a_1) describing the mean-attractive energy is obtained from the sum of all pair interactions for mixtures of different kinds of segments and are given by following sets of equation,

$$a_1 = \sum_{l=1}^{n}\sum_{j=1}^{n_l^{'}}\sum_{k=1}^{n}\sum_{i=1}^{n_k^{'}} x_{s,ki}x_{s,lj}\left(a_1\right)_{ki,lj} \tag{2.35}$$

$$\left(a_1\right)_{ki,lj} = -\rho_s \frac{2\pi}{3}\sigma^3_{ki,lj}\varepsilon_{ki,lj}\left(\lambda^3_{ki,lj}-1\right)g_0^{HS}\left[\sigma_x;\zeta_x^{eff}\left(\lambda_{ki,lj}\right)\right] \tag{2.36}$$

The hard sphere radial distribution function g^{HS} is calculated from the Carnahan and Starling equation of state evaluated at ζ^{eff} using the Padé expression proposed by Patel et al. given by equation 2.18 and 2.19.

$$g_0^{HS}\left[\sigma_x;\zeta_x^{eff}\left(\lambda_{ki,lj}\right)\right] = \frac{1-\zeta_x^{eff}/2}{\left(1-\zeta_x^{eff}\right)^3} \tag{2.37}$$

where,

$$\zeta_x = \frac{\pi}{6}\rho_s\sigma_x^3 = \frac{\pi}{6}\rho_s\sum_{l=1}^{n}\sum_{j=1}^{n_l'}\sum_{k=1}^{n}\sum_{i=1}^{n_k'}x_{s,ki}x_{s,lj}\sigma^3_{ki,lj} \tag{2.38}$$

The second-order monomer perturbation term a_2 for the mixture of molecules made up of heterogeneous segments is given by,

$$a_2 = \sum_{l=1}^{n}\sum_{j=1}^{n_l'}\sum_{k=1}^{n}\sum_{i=1}^{n_k'}x_{s,ki}x_{s,lj}\left(a_2\right)_{ki,lj} \tag{2.39}$$

$$\left(a_2\right)_{ki,lj} = \frac{1}{2}K^{HS}\varepsilon_{ki,lj}\rho_s\frac{\partial\left(a_1\right)_{ki,lj}}{\partial\rho_s} \tag{2.40}$$

$$K^{HS} = \frac{\zeta_0\left(1-\zeta_3\right)^4}{\zeta_0\left(1-\zeta_3\right)^2+6\zeta_1\zeta_2\left(1-\zeta_3\right)+9\zeta_2^3} \tag{2.41}$$

2.3.2 Chain contribution

The free energy term for chain interactions between a functional group of type *i* present in molecule *k* with a functional group of type *j* in molecule *k* for a *n*-component mixture

is given by,

$$\frac{A^{chain}}{Nk_BT} = -\sum_{k=1}^{n} x_k \sum_{ij} \ln y_{ki,kj}^{SW}\left(\sigma_{ki,kj}\right) \tag{2.42}$$

where the first sum is over all components in the mixture and the second sum considers the chain formation and connectivity of the segments within a given chain k. The background correlation function is in turn given by,

$$y_{ki,kj}^{SW}\left(\sigma_{ki,kj}\right) = \exp\left(\frac{-\varepsilon_{ki,kj}}{k_BT}\right) g_{ki,kj}^{SW}\left(\sigma_{ki,kj}\right) \tag{2.43}$$

where $g_{ki,kj}^{SW}\left(\sigma_{ki,kj}\right)$ is the radial distribution function for the SW monomers at the contact distance $\sigma_{ki,kj}$ and is approximated by a first-order high-temperature perturbation expansion[135]. The exact form of the above mentioned equation depends on the number of different types of segments and connectivity of the molecules being studied.

2.3.3 Association contribution

The association contribution between sites on different functional groups forming the molecules is expressed as follows[124],

$$\frac{A^{assoc}}{Nk_BT} = \sum_{k=1}^{n} x_k \sum_{i=1}^{n_k^{'}} v_{ki} \sum_{a=1}^{ns_i^{'}} n_{ia}\left(\ln X_{kia} + \frac{1 - X_{kia}}{2}\right) \tag{2.44}$$

where, the first sum is over the number of components n ,the second sum corresponds to a sum over all the types of functional groups in a molecule k ($n_k^{'}$), and the third sum is over the total number of site types in a functional group i ($ns_i^{'}$); n_{ia} is the number of associating sites of type a on each functional group of type i , and X_{kia} is the fraction of

component k not bonded at site a on functional group i. The fractions X_{kia} are obtained from the solution of the mass-action equation expressed as

$$X_{kia} = \frac{1}{1 + \rho \sum_{l=1}^{n} x_l \sum_{j=1}^{n_l'} v_{lj} \sum_{b=1}^{n_s'} n_{jb} X_{ljb} \Delta_{kia,ljb}} \tag{2.45}$$

One should note that GC-SAFT-VR is only SAFT based equations of state, which presents the opportunity of placing the associating sites to a specific functional group.

Chapter 3: Accurately modeling benzene and alkylbenzenes using a group contribution based SAFT approach

3.1 Introduction

Knowledge of the phase behavior of multi-component mixtures is essential for separation and purification techniques in the chemical process industry. Design and analysis of such operations requires the quantitative knowledge of the equilibrium composition of co-existing vapor and liquid phases. One way of catering to this need is by performing experimental measurements; however, increasingly theoretical tools that can predict phase behavior are being sought as an alternative means of generating "pseudo" experimental data. Classical equations of state (EoS), such as the Peng-Robinson and Soave-Redlich-Kwong[5] equations, and activity coefficient models[144, 145], have long been used to study phase behavior; however, their role tends to be as a more correlative, rather than predictive, tool for all but the simplest of systems and typically rely heavily on adjustable parameters fitted to experimental data in order to obtain accurate results, thus limiting their predictive ability[9, 146].

Over the past two decades significant advances have been made in the development of theoretical approaches based upon molecular-based models that can be used for the prediction of thermodynamic properties and phase behavior. The statistical associating fluid theory (SAFT)[10, 11, 147] is one such approach that has been successful in describing the phase behavior of a wide range of industrially important complex fluid systems. Based on Wertheim's first-order perturbation theory (TPT1)[56-59], in the SAFT framework molecules are described as chains of tangentially bonded homonuclear spherical segments that can interact through short ranged dispersion and association interactions. Since the introduction of the original SAFT EoS by Gubbins and

co-workers[10] many modifications have been made to the original equations and different versions of SAFT proposed (see for example the recent review by McCabe and Galindo[38]), which has resulted in the application of SAFT to a wide range of fluid systems[148]. Typically the SAFT parameters for a pure fluid are fitted to vapor pressure and saturated liquid and vapor density data, and when mixtures are studied, cross interactions determined either from Lorentz-Berthelot combining rules or by fitting to experimental mixture data. The cross interaction parameters are generally found to be transferable in that they can be used to accurately predict the phase behavior over a wide range of temperatures and pressures and predict the phase behavior of similar systems, such as within a homologous series[14, 75, 149, 150].

In recent works, several group-contribution based SAFT approaches have been proposed in an effort to develop a predictive approach that can be used for systems where experimental data is limited; the idea being that parameters can be developed based on functional groups, rather than molecular parameters. In the first real group-contribution based SAFT approach Tobaly *et al.*[39, 117-119] proposed a group contribution scheme (GC-SAFT) that could be applied to the SAFT approach due to Huang and Radosz[11], the SAFT-VR equation[36] and the PC-SAFT equation[126]. In their approach parameters are determined for the different functional groups present in the molecule by fitting the GC-SAFT parameters to the vapor pressure and saturated liquid densities of the pure compounds. Although parameters for individual functional groups are determined, the molecular parameters are obtained by taking the geometric and arithmetic averages of the group parameters, thus converting the model into a homo-segmented chain molecule. The approach therefore requires no modifications to the original SAFT-

0, SAFT-VR or PC-SAFT expressions. The phase behavior of a wide range of pure fluids such as linear alkanes[39], alkylbenzenes[39, 119], alkylcyclohexane[39], olefins[39], alcohols[39, 119], esters[127], ethers[128], aldehydes[128], ketones[128] and their various mixtures[117, 129-131] have all been studied using this group contribution method.

Subsequently Lymperiadis *et al*.[40] proposed the SAFT-γ approach, also based upon the SAFT-VR equation, in which the SAFT monomer fluid is defined as a collection of heteronuclear segments of different types that in turn form homonuclear chains, as in the original SAFT-VR approach. A number of functional groups[40, 120] have been defined that allow the phase behavior of alkanes, alkylbenzenes, alcohols, ketones, amines, carboxylic acids and alcohols to be studied.[40, 120, 121] In similar work, the group-contribution SAFT-VR (GC-SAFT-VR)[41, 123, 124] EoS based on the SAFT-VR equation has also been proposed. In the GC-SAFT-VR approach a collection of heteronuclear segments representing the different functional groups in a given molecule are considered to form the model chain. The GC-SAFT-VR EoS therefore allows the location of functional groups and association sites within a molecule, to be specified by retaining the identity of the functional groups in the model chain and defining the connectivity of the segments within the chain. Using this hetero-segmented approach GC-SAFT-VR parameters have been developed for a wide range of organic functional groups that allow the phase behavior of compounds such as alkanes linear and branched[41], alkenes[41], alkylbenzenes[41], ketones[41], acetates[41], esters[41], alcohols[124], aldehydes[124], amines[124], carboxylic acids[124] and polymers[123] containing these functional groups to be studied.

While these group-contribution based SAFT approaches have been shown to be successful in predicting fluid phase behavior for most systems, all three approaches appear to struggle with the description of alkylbenzene molecules using a group contribution scheme. To model alkylbenzenes Tamouza *et al.*[39] introduced the $(C=)_{Bz}$ group to describe the benzene ring and obtained both SAFT-VR[36] and SAFT-0[11] parameters by fitting to the vapor pressure and saturated liquid density data of ethyl to decylbenzene. While the correlated results show low deviations from the experimental results, due to the exclusion of experimental data at temperatures higher than 453K from the correlation, this is somewhat misleading as can be seen from Figure 3.1a. With the SAFT-γ approach Lymperiadis et al.[40] introduced two functional groups $ACCH_2$ and ACH (where A stands for aromatic) to model alkylbenzene molecules that also fails to predict the correct curvature seen in the experimental liquid density data of alkylbenzenes (as shown in figure 8 of Lymperiadis et al[40]). In the GC-SAFT-VR approach both benzene and alkylbenzenes were studied[41] by describing, the benzene ring as a single functional group. Similar to the GC-SAFT and SAFT-γ approaches, the theory was not able to accurately correlate the alkylbenzene liquid densities as shown in Figure 3.1b. While in both the GC-SAFT and SAFT-γ approaches the alkylbenzene molecule is treated as a homonuclear linear chain, the heteronuclear treatment provided by the GC-SAFT-VR approach, in which the benzene segment has different parameters from the alkyl chain, does not appear to address the problem.

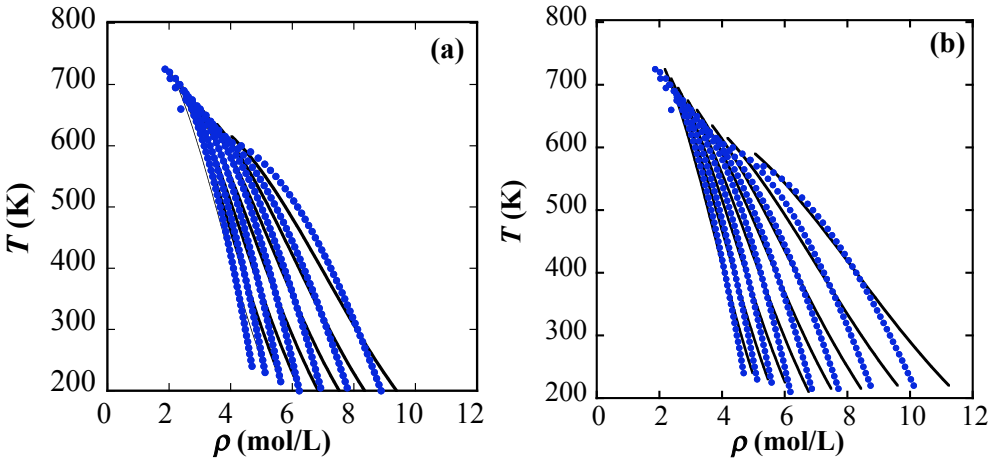

Figure 3.1: Theoretical results for liquid densities of alkylbenzenes obtained from (a) the GC-SAFT approach using parameters reported by Tamouza *et al.*[39] for octylbenzene to ethylbenzene from left to right and (b) the GC-SAFT-VR approach using parameters reported by Peng *et al.*[41] for octylbenzene to ethylbenzene from left to right. Symbols and solid lines represent the experimental and theoretical results[151] respectively.

Perhaps in recognition of this problem, subsequently NguyenHuynh *et al*[119] introduced a quadrupolar term into the GC-SAFT approach and two new functional groups ((CH)AB in the benzene ring and (C)BR to describe the connection between the benzene ring and the alkyl chain) were defined to model alkylbenzene molecules. Parameters for the new functional groups were obtained for use in the SAFT-0[11], SAFT-VR[36], and PC-SAFT[126] frameworks by fitting to the experimental coexistence data for pure benzene to decylbenzene and benzene + hexadecane, benzene + toluene, and ethylbenzene + octane mixtures. The quadrupolar moments of benzene and the alkylbenzenes were included in the fitting procedure as adjustable parameters. Inclusion of polarity into the model did not improve the theory in terms of obtaining the correct curvature in the saturated liquid densities of the alkylbenzene molecules[152].

From these prior studies it is clear that a modeling scheme that captures the π-π electronic interactions[153] between benzene molecules is needed in order to accurately describe the phase behavior of these molecules. In order to achieve this, the benzene ring

has been broken into several smaller segments, which introduces three new functional groups, CH=(Bz) for the CH groups in benzene, CH=(aBz) for the CH groups in alkylbenzenes, and C= for the connection point in alkylbenzenes, and explicitly form a ring by considering the appropriate number of bonds amongst these segments. After demonstrating that a more accurate theoretical description of the phase behavior of the pure compounds can be obtained, then the study has been extended to mixtures. The binary phase behavior of benzene and alkylbenzenes with alkanes through to strongly associating molecules, such as amines and alcohols have been studied and the results compared with experimental data.

3.2 Molecular model and theory

In the proposed model of benzene and alkylbenzene molecules the aromatic ring is broken down into several smaller segments (Figure 3.2). In the case of benzene, the ring is divided into six CH= segments with six bonds between the segments forming a closed ring. In the case of alkylbenzene molecules, the ring is modeled as a combination of CH= and C= segments; five CH= segments in the alkylbenzene molecule are connected together with four bonds, with one C= segment bonded to two CH= segments, to form a closed ring. In the benzene molecule the six π electrons in the benzene ring occupy the lower energy bonding orbitals; this arrangement accounts for the stability of benzene. Attachment of an electron donating alkyl group to the benzene ring effects the electron cloud above and below the ring (the alkyl group donates electrons making the ring more electron rich[154, 155]), which in turn affects the orientation of the electron cloud. To take this behavior into account, two different set of parameters for the CH= functional group have been considered for the benzene and alkylbenzene molecules. The CH=

groups in alkylbenzenes are denoted by CH=(aBz) and those associated with benzene, denoted as CH=(Bz). So, for example, if ethylbenzene is considered, as shown in Figure 3.2, five CH=(aBz) groups and one C= group form the benzyl ring and are connected to an alkyl chain containing one CH_2 and one CH_3 functional groups.

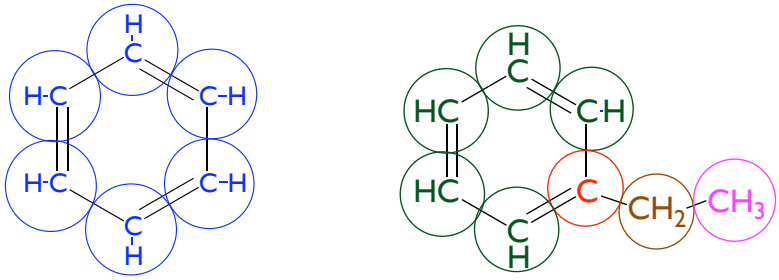

Figure 3.2 Schematic representation of benzene and ethylbenzene illustrating the new CH=(Bz) (blue) and CH=(aBz) (green) and C= (red) functional groups.

In what follows, a short overview of the chain contribution of GC-SAFT-VR theoretical framework has been provided that has been used to treat the model and refer the reader to the background chapter in the thesis or to the original work for additional details[41, 124, 156].

3.2.1 Chain contribution

The Helmholtz free energy contribution due to the formation of a chain containing heterogeneous SW segments is given by,

$$\frac{A^{chain}}{Nk_BT} = -\sum_{k=1}^{n} x_k \sum_{ij} \ln y_{ki,kj}^{sw}\left(\sigma_{ki,kj}\right) \tag{3.1}$$

where, the first sum is over all compounds in the mixture and the second sum considers the chain formation and connectivity between the segments of type i and j within a molecule of compound k. The background correlation function $y_{ki,kj}^{sw}$ is in turn given by,

$$y_{ki,kj}^{sw}\left(\sigma_{ki,kj}\right)=\exp\left(\frac{-\varepsilon_{ki,kj}}{k_bT}\right)g_{ki,kj}^{sw}\left(\sigma_{ki,kj}\right) \tag{3.2}$$

where $g_{ki,kj}^{sw}(\sigma_{ki,kj})$ is the radial distribution function for the SW monomers evaluated at the contact distance $\sigma_{ki,kj}$ and is approximated by a first-order high-temperature perturbation expansion[135]. The exact form of equation (8) depends upon the number of monomer segments and the connectivity between them. For example for a pure benzene molecule where six CH=(Bz) segments are bonded with six bonds between them the equation reduces to the following one.

$$\frac{A^{chain}}{Nk_bT}=-6m_{CH=(Bz)}\ln y_{CH=(Bz),CH=(Bz)}^{sw}\left(\sigma_{CH=(Bz),CH=(Bz)}\right) \tag{3.3}$$

In case of alkylbenzenes, such as ethylbenzene, where the molecule contains five CH=(aBz) segments, one C= segment and CH_2 and CH_3 segments the expression becomes,

$$\begin{aligned}\frac{A^{chain}}{Nk_bT}=-\Big[&(5m_{CH=(aBz)}-1)\ln y_{CH=(aBz),CH=(aBz)}^{sw}(\sigma_{CH=(aBz),CH=(aBz)})+(m_{C=}-1)\ln y_{C=,C=}^{sw}(\sigma_{C=,C=})\\&+2\ln y_{CH=(aBz),C=}^{sw}(\sigma_{CH=(aBz),C=})+(m_{CH_2}-1)\ln y_{CH_2,CH_2}^{sw}(\sigma_{CH_2,CH_2})\\&+\ln y_{C=,CH_2}^{sw}(\sigma_{C=,CH_2})+(m_{CH_3}-1)\ln y_{CH_3,CH_3}^{sw}(\sigma_{CH_3,CH_3})+\ln y_{CH_2,CH_3}^{sw}(\sigma_{CH_2,CH_3})\Big]\end{aligned} \tag{3.4}$$

In equation (11) the first term represents the four bonds between the five CH=(aBz) segments, the second term describes the contribution from the single C= segment in the molecule, and the two bonds between C= and the CH=(aBz) segments are represented by the third term. The remaining terms describe the bonding between C= , CH_2 and CH_3 groups in an analagous way.

3.3 Results and discussion

3.3.1 Pure compounds

Three new functional groups, CH= (aBz), CH= (Bz), and C=, have been defined in this work to model the benzene and alkylbenzene molecules in conjunction with the CH_2 and CH_3 segments developed in an earlier work[41]. The GC-SAFT-VR parameters for the CH=(Bz) group in benzene were obtained by fitting to experimental vapor pressure and saturated liquid density data for pure benzene[151] using a simulated annealing (SA) technique.[157, 158], Experimental data close to the critical region (around 10%) have been excluded from the fitting procedure, as GC-SAFT-VR like other analytical EoS exhibits classical critical behavior and over predicts the critical point. Additionally data points near the triple point have also been excluded since it has been shown that inclusion of the experimental data close to triple point can distort the results[159, 160]. In the same manner the parameters for CH= (aBz) and C= in alkylbenzenes were obtained by fitting to the saturated liquid density and vapor pressure data of toluene to decylbenzene[151]. In tables 3.1-3.3 the GC-SAFT-VR parameters $\sigma_{ki,ki}$, $\lambda_{ki,lj}$, $\varepsilon_{ki,lj}/k_b$, m_{ki} are reported for the new functional groups obtained using the SA optimization procedure. The use of SA is intended to find the global optimum parameters; the values reported in tables 3.1-3.3 are the optimal parameters found from multiple applications of the SA method using different initial guesses. Tables 3.2 and 3.3 also provide the molecular parameters that describe the interactions between and with the new functional groups studied herein. In all cases Lorentz-Berthelot combining rules have been used to determine the cross interactions between the functional groups.

Table 3.1 GC-SAFT-VR parameters for the segment number and size of each new functional group studied.

Group	$\sigma_{ki,ki}$ (Å)	m_{ki}
CH=(Bz)	3.028	0.619
CH=(aBz)	3.928	0.350
C=	2.112	0.382

Table 3.2 Segment–segment dispersion energy well depth parameters $\varepsilon_{ki,lj}/k_b$ (K) for each new functional group studied.

	CH_3	**CH_2**	**OCH_2**	**OCH_3**	**NH_2**	**OH(Linear)**	**CH=(Bz)**	**CH=(aBz)**	**C=**
CH_3	234.25	235.74	205.49	232.31	239.09	353.95	185.24	293.44	153.87
CH_2	235.74	237.23	206.80	233.78	240.61	356.19	186.41	295.30	154.84
OCH_2(ether)	205.49	206.80	180.27	203.79	209.74	310.50	162.50	257.42	134.97
OCH_3(ether)	232.31	233.78	203.79	230.39	237.11	351.01	183.70	291.01	152.59
NH_2	239.09	240.61	209.74	237.11	244.03	430.16	189.07	299.51	157.04
OH(Linear)	353.95	356.20	310.50	351.01	430.16	534.81	279.89	443.39	232.48
CH=(Bz)	185.24	186.41	162.50	183.70	189.07	279.89	146.48	232.05	121.66
CH=(aBz)	293.44	295.30	257.42	291.01	299.51	443.39	232.05	367.59	192.74
C=	153.86	154.84	134.97	152.59	157.04	232.48	121.67	192.74	101.06

Table 3.3 GC-SAFT-VR segment–segment dispersion energy range parameters $\lambda_{ki,lj}$ for each new functional group studied.

	CH_3	**CH_2**	**OCH_2**	**OCH_3**	**NH_2**	**OH(Linear)**	**CH=(Bz)**	**CH=(aBz)**	**C=**
CH_3	1.49200	1.58292	1.58282	1.52742	1.51986	1.49376	1.60989	1.49148	1.38398
CH_2	1.58292	1.66700	1.67694	1.56836	1.61951	1.56942	1.70485	1.58024	1.50425
OCH_2(ether)	1.58282	1.67694	1.68957	1.62915	1.62393	1.56716	1.67117	1.60917	1.53905
OCH_3(ether)	1.52742	1.56836	1.62915	1.56980	1.56260	1.52305	1.66032	1.52625	1.41935
NH_2	1.51986	1.61951	1.62393	1.56260	1.55490	1.51652	1.65610	1.51851	1.40445
OH(Linear)	1.49376	1.56942	1.56716	1.52305	1.51652	1.49500	1.58969	1.49329	1.40889
CH=(Bz)	1.60989	1.70485	1.67117	1.66032	1.65610	1.58969	1.75536	1.66292	1.55866
CH=(aBz)	1.49148	1.58024	1.60917	1.52625	1.51851	1.49329	1.60608	1.49099	1.38674
C=	1.38398	1.50425	1.53905	1.41935	1.40445	1.40889	1.55866	1.38674	1.19284

Table 3.4: Average absolute deviation in vapor pressures and saturated liquid densities obtained between experimental data and theoretical results for pure benzene and alkylbenzenes.**[151]**

	T (K)	Npt	AAD P (%)	T (K)	Npt	AAD ρliq (%)
Correlated						
Benzene	284-550	42	0.63	284-550	42	2.19
Methylbenzene	220–590	38	9.81	220–590	38	1.66
Ethylbenzene	240–615	39	12.94	220-615	41	0.97
Propylbenzene	255–635	39	3.58	215-235	43	1.82
Butylbenzene	265–660	41	2.53	215-660	46	2.16
Pentylbenzene	290–675	40	3.82	210-675	48	1.73
Hexylbenzene	295–695	41	3.70	225-695	48	1.78
Heptylbenzene	310–710	41	6.44	230-710	49	1.77
Octylbenzene	320–725	42	6.03	240-725	50	2.00
Nonylbenzene	340–740	41	6.04	250-740	50	2.22
Decylbenzene	350–750	41	8.78	260-750	50	2.11
Predicted						
Undecylbenzene	360–760	41	10.69	280–780	50	2.13
Dodecylbenzene	370–780	41	12.51	280–780	51	2.80
Tridecylbenzene	385–790	42	13.44	285–790	52	2.99
Tetradecylbenzene	390–800	42	16.73	290–800	52	2.82
Pentadecylbenzene	400–805	42	18.14	300–805	52	2.34
Hexadecylbenzene	405–815	43	19.06	305–815	53	2.53
Heptadecylbenzene	415–825	42	22.81	295–825	54	2.54
Octadecylbenzene	420–830	42	24.92	310–830	53	2.73

The percentage average absolute deviation in vapor pressure (%AADP) and saturated liquid density (%AADρ_{liq}) from the experimental data for benzene and the alkylbenzene molecules is reported in Table 3.4. The average absolute deviations in pressure and liquid density expressed using *AAD P* (%) and *AAD* ρ_{liq} (%) are given by following equations,

$$AAD\ P\ (\%) = \frac{1}{N_{pt}} \sum_{i=1}^{N_{pt}} \left| \frac{P_i^{theo} - P_i^{\exp}}{P_i^{\exp}} \right| \times 100\% \tag{3.5}$$

$$AAD\ \rho_{liq}\ (\%) = \frac{1}{N_{pt}} \sum_{i=1}^{N_{pt}} \left| \frac{\rho_i^{theo} - \rho_i^{\exp}}{\rho_i^{\exp}} \right| \times 100\% \tag{3.6}$$

where N_{pt} is the number of experimental points being evaluated, $P_i^{\exp}$ and P_i^{theo} are the experimental and calculated pressure; $\rho_i^{\exp}$ and ρ_i^{theo} are the experimental and calculated saturated liquid density, respectively.

In Figure 3.3, pure phase behavior of benzene and alkylbenzenes from toluene up to octylbenzene has been presented. Although these are correlated systems and so a good agreement between the theory and the experimental saturated liquid density and vapor pressure data is expected, from the figure it can be clearly observed that theory is now able to capture the correct trend in the curve of the alkylbenzene saturated liquid densities, which is a significant improvement over current group-contribution predictions for these molecules.[39-41] This is also reflected in the lower % average absolute deviation (AAD) in the saturated liquid densities (1.82 compared to 3.53 obtained in previous work)[41].

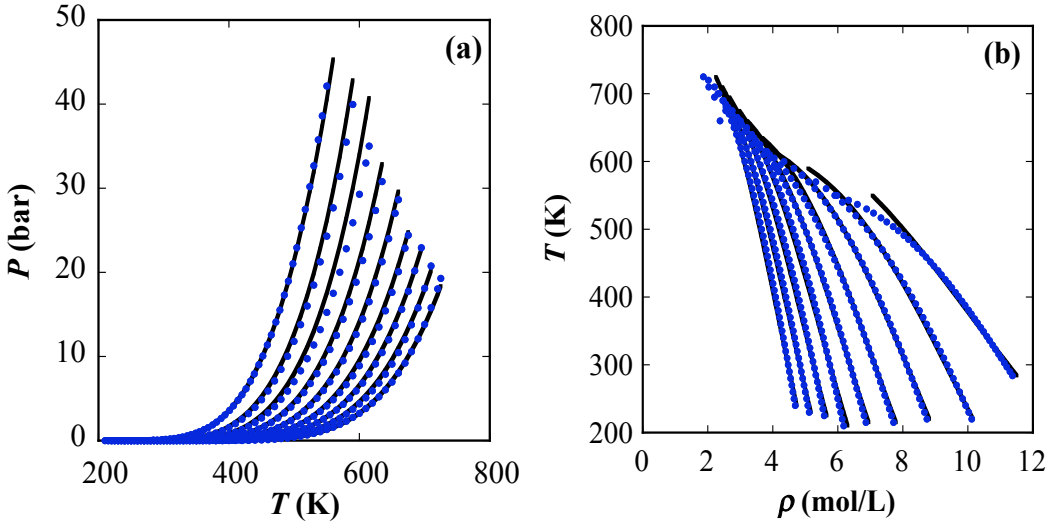

Figure 3.3. Comparison between theoretical results using GC-SAFT-VR and the experimental data for (a) vapor pressure and (b) saturated liquid density for benzene to octylbenzene from left to right. Symbols and solid lines represent the experimental data[151] and theoretical results respectively.

After determining the optimal parameters for the newly defined functional groups, the phase behavior of higher members of the homogeneous series were then predicted as a means of testing and validating the new parameters. The percentage average absolute deviations from the experimental data are again reported in Table 3.4. One should note that the GC-SAFT-VR equation is accurately predicting the saturated liquid density for the alkylbenzenes studied, though higher deviations are seen for the vapor pressures, which is typical from a group contribution method as the vapor pressure is a more sensitive property. Remembering that the main focus of the work was to obtain a more accurate model for the saturated liquid density of the alkylbenzenes, it can be considered that the model to be in good agreement with the experimental data and examine the influence of the more accurate model in the study of the phase behavior of mixtures of benzene and alkylbenzenes. Here the focus remains primarily on presenting results for new binary mixtures and only reconsider systems previously studied when differences are observed in the predicted results with the new ring based model compared to the earlier work[123, 124].

3.3.2 Binary mixtures

Benzene / alkylbenzenes + n-alkanes

Initially binary mixtures of benzene and alkylbenzenes with linear alkanes are considered. In figure 3.4, results for binary mixtures of benzene and toluene (methylbenzene) with alkanes from n-hexane to n-decane at a temperature of 313.15K are presented. As stated earlier, for these binary systems three functional groups are used to represent the toluene molecule (CH_3, CH=(aBz) and C=), two functional groups are used to represent the alkane molecules (CH_3 and CH_2) and only one type of group CH=(Bz) is

used to describe benzene. As can be seen from the figure, the theoretical predictions for the constant temperature P-x-y slices of the phase diagrams are in good agreement with the experimental data, except for the case of the benzene + n-hexane and + n-heptane binary mixtures where significant deviations from experiment are observed. Although the use of a fitted cross interaction parameter between the CH=(Bz) group of benzene ring and the CH_2 group in the alkane chain could significantly reduce this deviation, focus here remains on the predictive capability of the theory using only Lorentz-Berthelot combining rules. In figure 3.4b, it also can be noted that the theory accurately captures the changes in phase behavior with the increase in the number of CH_2 groups in the linear alkane.

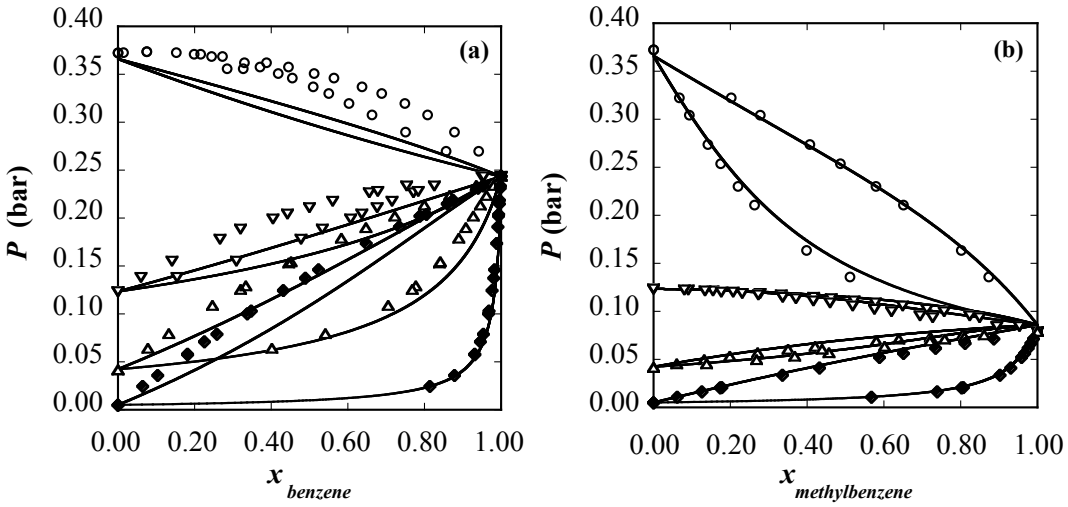

Figure 3.4. Vapor–liquid equilibria for binary mixtures of benzene (a) / toluene (b) with Hexane (o), Heptane (∇), Octane (Δ), Decane (♦) at 313.15K. The solid lines represent the theoretical predictions and the symbols represent the experimental results[161].

Benzene + alkylbenzene mixtures

Now constant temperature and pressure slices of the phase diagrams for binary mixtures

of benzene with methylbenzene, ethylbenzene and propylbenzene has been considered in this phase of the study. These systems being chosen as experimental data is available in the literature for comparison. In Figure 3.5 constant temperature P-x-y slices of the benzene + toluene[162] and benzene + ethylbenzene[163] phase diagrams are presented. As can be seen from the figures, the proposed model is able to capture the changes in phase behavior as a function of temperature without fitting any of the cross interactions to the experimental mixture data, though some deviation for the toluene + benzene mixture can be observed, which is due to the over prediction of the vapor pressure of pure toluene (table 3.4).

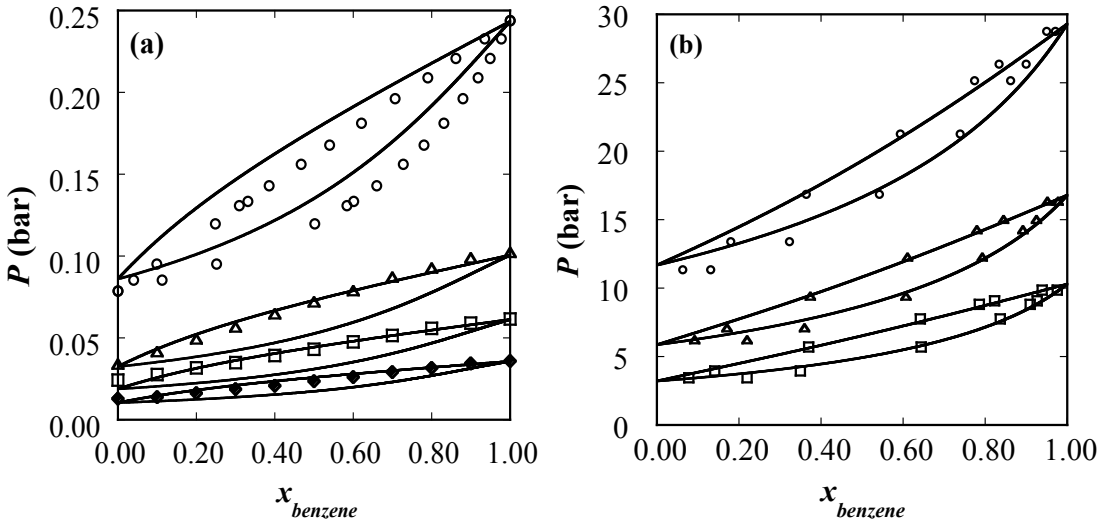

Figure 3.5. Vapor–liquid equilibria for binary mixtures of (a) benzene + toluene at 273.15K (♦), 283.15K (□), 293.15K(△) and 313.15K(O) and (b) benzene + ethylbenzene at 453.15K (□), 483.15K (△), 523.15K(O). The symbols represent experimental results[162, 163].

In Figure 3.6, a constant pressure T-x-y slice of the benzene + propylbenzene phase diagram is presented at 1.01325 bar for which excellent agreement with the experimental data is obtained. Unfortunately additional experimental data against which I can compare

the theory to is to the best of our knowledge unavailable for benzene + alkylbenzene systems.

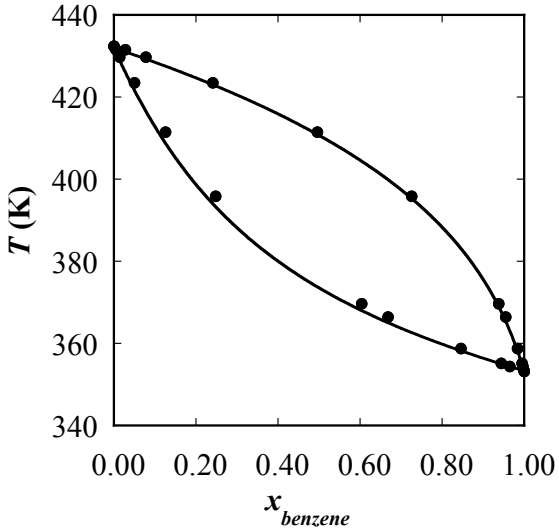

Figure 3.6. Vapor–liquid equilibria for binary mixture of benzene with propylbenzene at 1.01325 bar (●). The solid lines represent the theoretical predictions and the symbols represent the experimental results.[164]

Benzene, alkylbenzene + ether mixtures

Ethers are slightly polar molecules due to the presence of a lone pair of electrons on the oxygen atom, which can interact with the delocalized electrons in the benzene ring and so represent a good test of the new functional groups in terms of capturing the unlike interactions. In figure 3.7 the binary phase behavior of dimethylether and dibutylether with benzene is presented. Here two functional groups (OCH_3(ether) and CH_3) are used to form the dimethylether molecule and three functional groups (OCH_2(ether), CH_2 and CH_3) are used to form dibutylether, the parameters for which are all taken from earlier work[41, 123]. As discussed in the introduction, in previous work[123] benzene was

described as a single C_6H_6 group in the GC-SAFT-VR approach; using this model benzene + ether phase behavior was studied and a cross-interaction parameter between the C_6H_6 group and the OCH_3(ether) group was used to capture the non-ideal nature of their mixtures. Here I find that using a different kind of modeling scheme for benzene, the GC-SAFT-VR approach can predict the correct phase behavior for the binary benzene + ether mixtures using Lorentz-Berthelot combining rules, except for the methoxybutane + benzene binary mixture. In contrast to earlier work[123] we therefore do not use a fitted cross-interaction parameter between the OCH_3 (ether) and CH=(Bz) groups. In this regard, it appears that the explicit modeling of the benzene ring improves the predictive capability of the EOS, though we again note that there is limited experimental data against which to test the broader applicability of the theoretical approach.

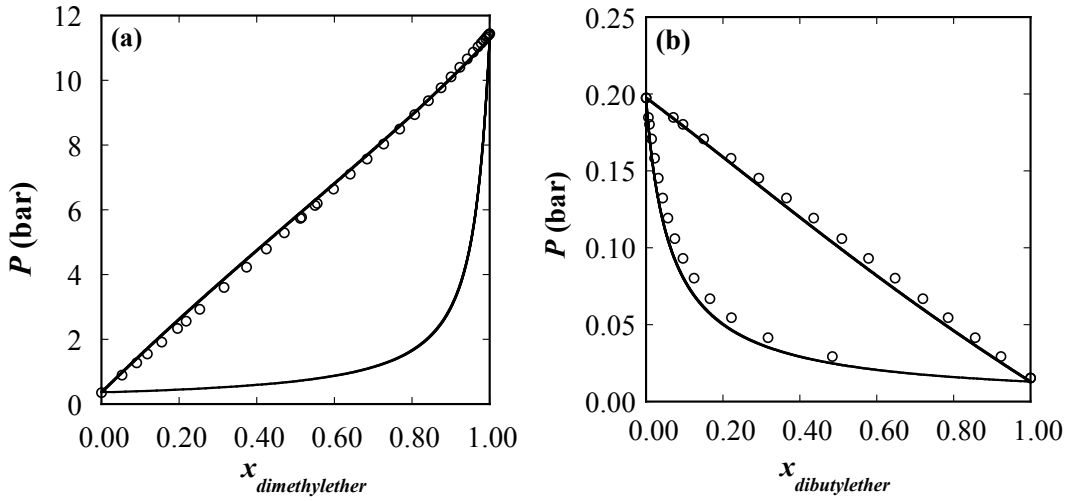

Figure 3.7. Vapor–liquid equilibria for binary mixtures of (a) benzene + dimethylether at 323.15K(O) and (b) benzene + dibutylether at 308.15K (O). The solid lines represent the theoretical predictions and the symbols represent the experimental results[165, 166].

In figure 3.8a the phase behavior of methylbenzene + diethylether has been studied at a constant pressure of 1.01325 bar and in figure 3.8b constant *P-x-y* slices of the ethylbenzene + dipropylether binary mixture is presented. Again we do not use any fitted cross-interaction parameters between the CH=(aBz) and OCH_2 groups and so the results presented are true predictions. Although at higher pressures, and close to the pure limit of ethylbenzene, the theory under predicts the pressure due to the fact that we under predict the vapor pressure of pure dipropylether, a good description of the equilibrium phase composition is obtained as presented by x,y phase diagram figure 3.8c[167].

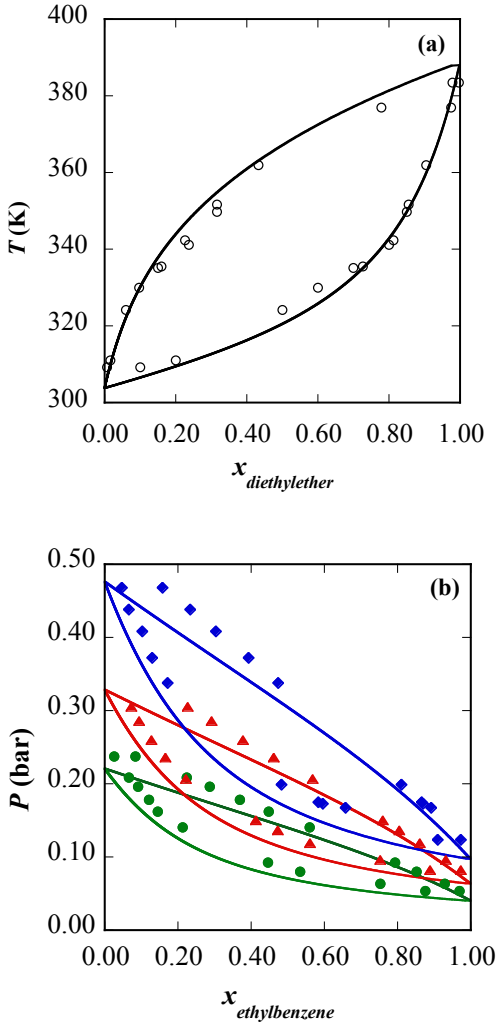

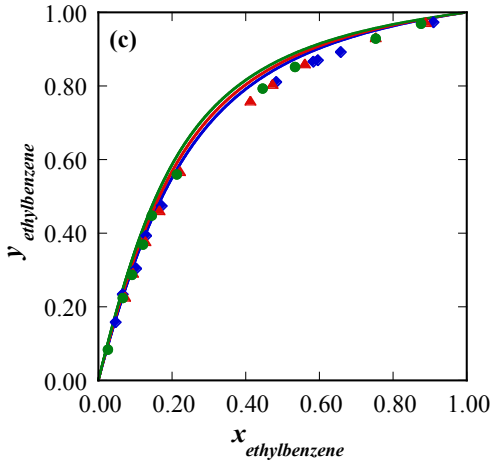

Figure 3.8. Vapor–liquid equilibria for binary mixture of (a) toluene + diethylether at constant pressure of 1.01325 bar (O); (b) and (c) ethylbenzene + dipropylether at 323.15K (green ●), 333.15K (red ▲), 343.15K (blue ♦).The solid lines represent the theoretical predictions and the symbols represent the experimental results[167, 168].

Benzene, alkylbenzene + associating fluids

In Figure 3.9 we consider mixtures of benzene and alkylbenzenes with ethanol and 1-butanol. It is interesting to study the mixtures of strongly associating fluids with compounds containing a benzene ring to test whether the theory can capture the complex interactions between the lone pair of electrons present on the alcohol oxygen atom and the π electrons of the ring. 1-butanol is formed from the CH_3, CH_2 and OH (terminal) functional groups, and the hydrogen bonding interactions are described by three association sites on the OH (terminal) group, the parameters for which are taken from previous studies.[41, 124] From figure 3.9a we find that the theory shows good agreement with experimental results[169] at 308K, with the prediction being more accurate for toluene than benzene. We also note that the GC-SAFT-VR approach correctly predicts the azeotropic nature of the mixtures studied, again without fitting any binary interaction parameters. Though one could argue that a cross-interaction parameter

between the CH=(Bz)/ CH=(aBz) groups and the OH (terminal) group could be warranted due to the non-ideal nature of the mixture. In the figure 3.9b we present the phase behavior of ethanol and toluene at two different temperatures 303.15K and 328.15K. It can again be observed that the GC-SAFT-VR approach has been able to successfully predict the isotropic behavior observed in the alcohol + alkylbenzene systems. We note that higher deviations are seen for ethanol due to the fact that smaller members of a family of chemical compounds typically fail to exhibit group additivity and hence show higher pure component deviations[124].

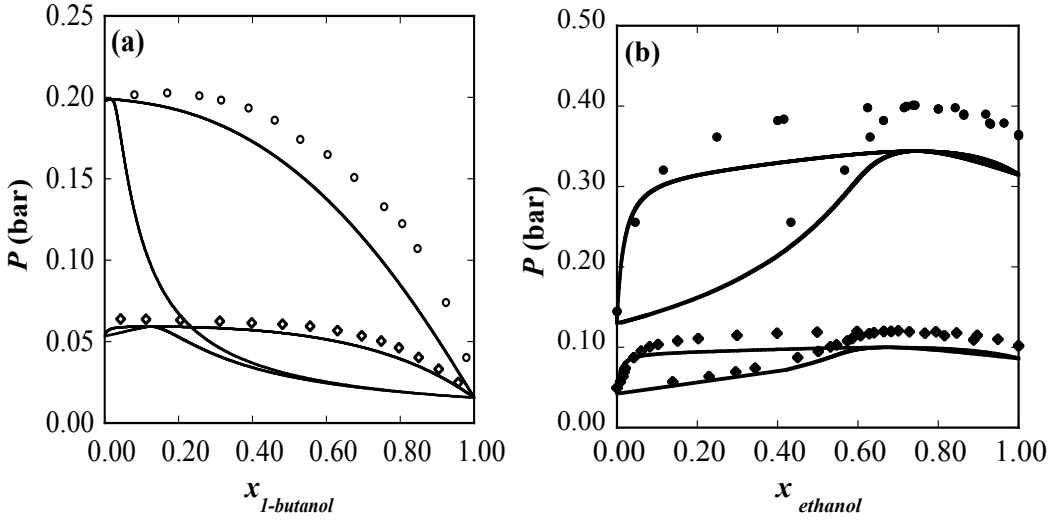

Figure 3.9. Vapor–liquid equilibria for binary mixtures of (a) 1-butanol + benzene (O)/ toluene (◇) at 308.15K (b) ethanol + toluene at 303.15K (♦) and 328.15K (●). The solid lines represent the theoretical predictions and the symbols represent the experimental results[169, 170].

Finally, we consider the mixture of benzene and alkylbenzenes with amines, which are associating fluids. In figure 3.10 we present results for the binary mixture of benzene, toluene and ethylbenzene with n-butylamine. n-butylamine is described using the CH_3, CH_2 and NH_2 functional groups determined in earlier work[124]. As can be seen from the

figure, using these group parameters and without fitting to mixture experimental data we can accurately capture the phase behavior of the binary mixtures of alkylbenzenes with amines at 298.15K[171, 172]. We also note that the theory correctly predicts the transformation from a non-azeotropic phase behavior for alkylbenzene + amine binary mixtures to an azeotropic system for mixtures containing benzene. Compared to earlier work by dos Ramos *et al* (figure 7a)[124], in which the alkylbenzene and benzene rings were modeled as a single group, we note a definite improvement in the predictive ability of the theory for amine + alkylbenzene systems. In particular, at lower temperatures (below 325 K) the new modeling scheme improves the saturated liquid densities of pure alkylbenzenes which results in better agreement between experimental and predicted phase behavior for alkylbenzene + amine systems. However for the benzene + amine system studied the azeotropic pressure maximum is over predicted compared to dos Ramos *et al.,* which could be attributed to the fact that when benzene is treated as a single group the predicted pure component vapor pressure is lower than that reported in this study.

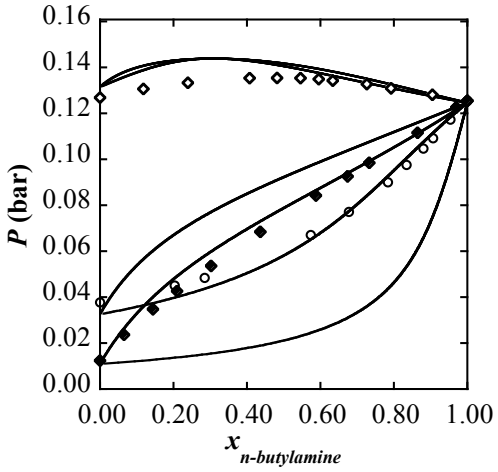

Figure 3.10. Vapor–liquid equilibria for binary mixtures of n-butylamine + benzene(◇)/ toluene (O)/ ethylbenzene (♦) at 298.15K. The solid lines represent the theoretical predictions and the symbols represent the experimental results[171, 172].

3.4 Conclusion

The correct curvature in the experimental saturated liquid densities of pure alkylbenzenes has been captured in a group-contribution SAFT based approach by explicit consideration of the benzene ring in the theoretical framework. Typically alkylbenzenes are described in group contribution SAFT approaches as linear chain molecules and fail to describe the correct trend in the curvature of the saturated liquid densities that is seen experimentally for alkylbenzenes. To our knowledge this is the first time ring molecules have been explicitly described in a group contribution SAFT approach. In this work we propose three new functional groups CH=(Bz), CH=(aBz), C= to describe benzene and the alkybenzene family. The parameters for these groups were obtained by fitting to experimental vapor pressure and saturated liquid density data for benzene and the lower members of the alkylbenzene (methylbenzene to decylbenzene) family. These parameters were then used to predict the phase behavior of longer members of the alkylbenzene family and study the phase behavior of binary mixtures of benzene and alkylbenzenes with alkanes, ethers, amines and alcohols. If we draw a comparison between the earlier heteronuclear chain model for alkylbenzenes with the current ring based model we find improvement in the theoretical representation of the saturated liquid densities, particularly at lower temperatures. For mixture systems, the results obtained from the two models are generally comparable, though we do obtain better predictive ability for the mixture of alklybenzene (toluene/ ethylbenzene) and n-butylamine. Additionally by more accurately capturing the intermolecular forces between unlike groups using the ring based

model we are able to predict the correct phase behavior using simple Lorentz-Berthelot combining rules.

Chapter 4: Predicting the thermodynamic properties and dielectric behavior of electrolyte solutions using the SAFT-VR+DE equation of state

4.1 Introduction

From natural biological systems to industrial chemical processes such as osmosis and reverse osmosis, fertilizer production, water purification, geochemistry, electrochemistry, and enhanced oil recovery, the ubiquitous presence of electrolytes has made the thermodynamic study of these fluids an active area of research both experimentally and theoretically[45-49]. These are however challenging fluids to study since the presence of long-range coulombic interactions between the ionic species makes electrolyte solutions highly non-ideal[50]. In any theoretical investigation of electrolyte solutions, describing the complex nature of the electrostatic interactions present between the ionic species and the ions and the aqueous solution is key[51, 52].

One approach to address the thermodynamics of electrolyte solutions is through the use of an implicit solvent model, that is by approximating the dipolar water solvent by a constant dielectric continuum, which presents a simplistic view of the complexity of the interactions involved in these systems. Often, Debye-Hückel (DH) theory, which considers point charges in a dielectric medium, is used to represent the electrostatic behavior in equations of state used to model electrolyte solutions. Several semi-empirical equations of state and modified versions of activity coefficient models rooted in DH theory have also been proposed, such as the Pitzer equations [51, 173, 174] and the electrolyte nonrandom two-liquid (eNRTL) model[175], amongst others[176-186]. This kind of implicit treatment of the solvent is also known as a McMillan-Mayer (MM) level[187] model and is more generally referred to as a primitive model[53]. Implicit

treatment of the solvent, although widely used to describe thermophysical properties of electrolyte solutions, has limitations in terms of capturing the effects of the solvent-ion interactions as they are solely described through the solvent dielectric constant.

A step towards a more accurate description of ionic species in dipolar solvents is introduced at the Born-Oppenheimer (BO) level[54], in which the solvent species appear explicitly in the model and is also referred to as a non-primitive model. In the simplest case a BO level model can be conceptualized as a mixture of charged hard spheres in a solvent of hard spherical molecules with a point dipole embedded in the center. For further complex cases, higher order multipole moments or discrete charges at a specified position within the ion can be included.

Analytical expressions to calculate the free energy and thermodynamic properties have been derived for both MM and BO level of models. Broadly, two kinds of statistical mechanics based approaches are used, perturbation theory and integral equation theory. Stell and Lebowitz[188] were the first to derive a perturbation term for the Helmholtz free energy for the ion-ion interaction from DH theory. Henderson[189] later proposed a restricted perturbation theory (i.e., an equimolar mixture of equal-diameter hard spheres are assumed in a dielectric continuum) in which the ion-ion interaction is treated as a perturbation term. In a subsequent effort Henderson[190] extended the approach for ion-dipole interactions and Jin and Donohue[191-193] further refined the theory by combining, the perturbed-anisotropic-chain theory (expressions for short- range interactions) with Henderson's primitive model expressions for the ion-ion interactions. With integral equation theory, generally the hypernetted chain (HNC)[194] or the mean spherical approximation (MSA) are used to solve the relation between the direct

correlation function and the pair correlation function given by the Ornstein-Zernike (OZ) equation. Although the HNC approximation is more accurate, it is mathematically more complex and unlike the MSA, does not provide analytical solutions to the OZ equation. The MSA approach, introduced by Percus, Yevick and Lebowitz[195, 196] to solve the OZ equation, has been analytically solved for a wide range of important model systems such as the hard-sphere,[197] Yukawa,[198] and dipolar hard-sphere fluids,[199] electro-neutral mixtures of hard charges[197] and plasma[200] (charges in neutralizing background), mixtures of hard dipoles[201, 202] and hard ions with dipoles.[203-205] The MSA was first applied in the primitive model by Waisman and Lebowitz[197] and Blum[206] and analytical expressions for the thermodynamic properties of both the restricted and unrestricted primitive MSA models were obtained. In the primitive model expressions for the MSA (PMSA) the effect of the volume of the ions is taken into account explicitly and when the diameters of the ions is reduced to zero the MSA expressions reduce to point charges and the DH equation. Later Blum[207] and Adelman and Deutch[202] developed analytic solutions for the non-primitive MSA (NPMSA) by explicitly including the effect of the solvent, yielding expressions for the thermodynamic properties of a mixture of equal sized ions and dipolar hard spheres. In subsequent work Blum and Wei[204] extended the solutions to a system of arbitrary sizes of charged and dipolar hard spheres. The solution of the NPMSA includes three types of interactions: ion-ion, ion-dipole, and dipole-dipole. Explicit forms for the ion-ion, ion-dipole, and dipole-dipole pair distribution functions was later developed by Hoye and Stell[208] using the approach proposed by Blum and Wei[204]. For a comprehensive review of theories developed for aqueous electrolyte fluids, the reader is directed to the excellent

reviews of Loehe and Donohue[52], Anderko *et al*.[49], and McCabe and Galindo[209]. Since the focus of this work is on the further development and application of the SAFT based approach of Zhao *et al.*[210] to experimental electrolyte systems, we will limit the remaining discussion to SAFT-based approaches to describe electrolyte solutions.

The statistical associating fluid theory (SAFT)[11, 61, 211], based upon Wertheim's first-order thermodynamic perturbation theory (TPT1)[212-215], is a statistical mechanics based equations of state that in various forms has been used to describe the phase behavior of a wide range of industrially important complex fluid systems.[148, 209, 216, 217] Among the many variations of SAFT are several approaches to describe electrolyte systems.[210, 218-220] The study of electrolytes with SAFT-derived equations of state can be broadly divided into two categories: those based on the primitive and non-primitive models. In one of the first developments Galindo *et al.*[218] applied a modified version of SAFT, termed SAFT-VRE, to describe strong-real electrolyte solutions. The MSA was used at the level of the RPM to account for the charged interactions, while the water-water and ion-water attractive interactions were described via square-well dispersive interactions. The results from the SAFT-VRE approach using ion-specific (rather than salt-specific) parameters were found to be in good agreement with experimental vapor pressure and solution density data for electrolytes up to concentrations of 10 *mol/L* between 273*K* and 373*K*. However, although a wide range of temperatures were studied, the ability of the theory to describe more sensitive thermodynamic properties such as the osmotic co-efficient and mean ionic activity coefficient were not considered and hydration effects were not discussed. In more recent work, Schreckenberg *et al*.,[27] proposed an improved formulation of SAFT-VRE

that incorporates a Born term that describes the contribution due to the solvation of ions at infinite dilution. While this improves the theoretical treatment of solvation effects by partially addressing the poor solvation behavior that results from using a primitive model, ion-polar and polar-polar interactions are still not explicitly described. The implicit solvent within the PM framework of SAFT-VRE was represented through a empirical solution dielectric constant model, following the work of Uematsu and Franck,[221] which takes into account the temperature, density and composition of the solvent and in turn makes the dielectric constant a differentiable variable. The electrolytes were described using a fully dissociated model and ion-specific interaction parameters, with the effective ionic diameter, ion-solvent and ion-ion dispersive energy parameters fitted to vapor pressure, solution density, and mean ionic activity coefficient data for fifteen different alkali halide salts at temperatures below 523 K. The cross ion-ion dispersive interaction energy was estimated using a procedure proposed by Hudson and McCoubrey.[222] Although the theory was shown to provide a good representation of correlated properties (<5% in most cases) and predicted properties such as osmotic coefficients (<5% in most cases) and freezing temperature depression (for NaCl, LiCl) at 1 bar pressure, an accurate quantitative prediction of the free energy of solvation (average error ~35%) was not possible. The study was subsequently extended to predict the vapour pressures and solution densities of multi salt systems over a range of temperature (298.12 - 397.97 K) and pressure (0.92–68.42 MPa) without fitting any additional parameters. Mixed solvent electrolytes (methanol /*n*-butanol and water + salt systems) were also studied with the alcohol-ion unlike dispersion energy parameter obtained by fitting to experimental water + alkanol + salt VLE/ LLE data and good agreement with the

experimental results were obtained. In related work Tan *et. al.*[219] combined the RPM with the SAFT1 (a variant of SAFT-VR) equation of state to treat electrolyte solutions. Ions were described as hard charged spheres and hence only water-ion and water-water dispersive interactions were considered. To parameterize the model a hydrated ion diameter (salt specific property) along with ion specific volumes and ion-water dispersion (hydration) energies, were obtained by fitting to experimental data for the mean ionic activity coefficient and salt densities for individual salt solutions. In order to accurately correlate the experimental data all model parameters and the water dielectric constant, which was determined from an empirical equation, were made temperature dependent. The approach was then used to predict the osmotic coefficient and vapor pressures for Cl^-, Br^-, I^- salts of Na^+, K^+ and Li^+ at 298.15 to 373.15 K with very low deviations (<1% for most cases) from experimental data. Ji *et. al.*[55, 223] later extended the approach to study mixed salt solutions and introduced a mixing rule for the hydrated ion diameter with a binary adjustable parameter for each pair of salts studied. The binary adjustable parameters (referred to as l_{ij} in their work) were obtained from fitting to the osmotic coefficient for ternary salt solutions (i.e., two salts + water) and then used to predict the solution densities and osmotic coefficient of quaternary solutions (i.e., three different salts + water). One should note that the use of an additional adjustable parameter (i.e., l_{ij} along with the ionic volume and ion-water dispersion energy) further reduces the predictive ability of the theory. Behzadi *et al.*[220] used a version of the SAFT-VR equation of state with a Yukawa potential and the non restricted MSA as extended by Blum[224, 225] to study the vapor pressure, solution densities and activity coefficients of electrolyte solutions. Long-range Coulombic interactions between ionic species were

taken into account using the non-restricted MSA, while solvent-solvent and solvent-ion dispersion interactions were described through the Yukawa potential. Twenty-three salts in seven different solvents (water and alcohols) were studied using three different parameterization schemes: ion-specific, cation-specific, and salt-specific. In each case the dispersion interaction was optimized by fitting to experimental vapor pressures and liquid volumes while the cross-interaction range parameter was fixed at 1.2. The ionic radii was taken to be the Pauling radii or thermochemical radii whichever was available for a specific ion. To test the thermodynamics of the model the mean ionic activity of LiCl and NaCl were predicted and the salt-specific parameters were found to give more accurate predictions compared to the ion-specific and cation-specific ones. Also, in this work results with the Yukawa based approach were compared with the more commonly used square-well potential and the Yukawa model found to give slightly better results.

Focusing on DH approaches, Cameretti[226] *et al.* extended the perturbed chain SAFT (PC-SAFT) equation to electrolyte systems by taking into account the electrostatic interactions in ionic solutions using a simple DH term. The resulting ePC-SAFT equation of state was found to be able to accurately correlate and predict the vapor pressures of single- and mixed-salt (NaCl-KBr, NaBr-KCl) solution densities up to high salt concentrations (>6 *m* for some salts, including 12.7 *m* for LiCl and 13.8 *m* LiBr). Only two salt-specific parameters, the hydrated ion diameter and water-ion dispersion energy (for both cations and anions), were required and obtained by fitting to experimental vapor pressure and density data. In an extension of this work, Held *et al.*[227, 228] subsequently studied both VLE and the mean ionic activity coefficient of both weak and strong aqueous electrolyte solutions. The previously developed ion-specific diameter and

dispersive energy parameters of Cameretti *et al*, which were obtained by only fitting to vapor pressure and solution densities, were found to be inaccurate in describing the mean ionic activity coefficient and so ion-specific diameters and dispersive energies were determined by fitting to the mean ionic activity coefficient and salt solution density data. The water model was also revised to include a temperature dependent diameter. With these modifications, the ePC-SAFT equation was found to provide an accurate description of the thermodynamics of 115 aqueous electrolyte solutions at 298.15K. Subsequently, the equation of state was successfully extended to mixed solvent electrolyte systems by representing the solvent with an effective dielectric constant, again in a primitive model[229]. The dielectric constant was calculated from empirical equation dependent upon temperature and the mixture solvent composition. Solution densities and mean ionic activities of KCl, NaBr, NaCl, NaI, LiCl in ethanol + water, methanol + water and methanol + ethanol + water mixed solvents were studied across different weight fractions of solvent and found to represent the experimental data accurately.

In an alternative approach, Liu *et. al.*[230] combined the original SAFT approach (in which the dispersion term is given by the expression of Cotterman[63]) with the PM expressions obtained from the MSA and Henderson-Blum-Tani[190] perturbation theory expansion for the ion-dipole and dipole-dipole terms to study aqueous single salt and mixed salt systems at 298.15 K. Salts were modeled as LJ spheres using the Pauling diameter for the anion and the cation diameter as an adjustable parameter that was obtained by correlating experimental mean ionic activity coefficient data. The Mavroyannis-Stephen equation,[231] which calculates dispersion energy for individual ions based upon the ionic radii, number of electrons and polarizibility, was used to obtain

the dispersive interaction parameters for the ions. Thirty single and thirteen-mixed salt electrolyte systems were studied with good accuracy (%AAD for the mean ionic activity coefficient and density was < 3% for concentrations up to 6 *m*). In subsequent work, Liu *et. al.*[232] modified the approach to include the low-density expansion[233] of the solution of the primitive MSA to describe ion-dipole interactions. We note that although the theory is described as a non-primitive approach, when the solvent volume is neglected, as is done by the authors, the expression for the ion-solvent term reduces to the Born expression in the PM. The ions were again described as charged LJ spheres with the Pauling ionic radii used for the ion-ion, dispersive and associative SAFT terms and an effective average ion radii (representing a Born type ionic radii) used for the ion-solvent term. The ion dispersive energy parameters were again obtained using the Mavroyannis-Stephen equation. To effectively capture the ion-solvent interactions, a SAFT association term was considered between the ions and solvent with several association sites (7-12) being placed on the ions. The effective average ion radii and SAFT association energy between the ions and solvent was obtained by fitting to experimental mean ionic activity coefficient data. Both salt dependent and salt independent parameters were investigated, with salt dependent parameters found to provide lower deviations. Furthermore, if the anion-solvent association was removed from the model, and only cation-solvent association considered, there was little to no impact observed on the correlated results. Using the fitted parameters, the density, osmotic coefficient and water activity were then predicted for fifteen different aqueous electrolyte salts with <2% average absolute deviations. The predicted water activity and osmotic coefficient was compared with those from Jin and Donohue,[191] Myers *et al*.,[234] and Fürst *et al.*[235] and the proposed

approach found to be superior in terms of the % average absolute deviations with experiment.

More recently, Rozmus *et al*.[236] developed the ePPC-SAFT equation of state by combining the polar perturbed chain (PPC)-SAFT equation of state with the MSA for a primitive model of electrolyte solutions. Association sites between the ions and solvent were considered to describe the ion-solvent interactions and a Born term was included in addition to the MSA term for electrostatics to describe the change in the dielectric constant resulting from the solvation of the ionic species. The dielectric constant of the water solvent was made temperature and solution density dependent using an empirical equation proposed by Schimdt.[237] Ion specific diameters and association energies were obtained by fitting to mean ionic activity coefficient and apparent molar volume data for nineteen alkali-halide aqueous solutions. The performance of the approach was then tested through the prediction of the mean ionic activity coefficient, density, and vapor pressure of the aqueous solutions over a wide range of temperatures and molalities (298− 573 K and 0− 8 m). We note that, salting out of carbon dioxide and methane in saline water was also accurately predicted.

All of the approaches discussed thus far combine the SAFT framework with the PM to describe the ionic species. A more accurate, but more complex, approach is to explicitly include ion-dipole interactions in the model by describing the solvent as a dipolar fluid. In this approach, the solvent dielectric is not required as an input to the calculations as it is calculated from the dipole moment within the theory. In his seminal work, Zhao *et al.* developed an electrolyte version of the SAFT-VR equation - SAFT-VR+DE[29] - based on the fully non-primitive model of electrolytes. The SAFT-VR+DE

approach allows the explicit description of the ion-solvent and solvent-solvent interactions between asymmetric ions and the dipolar solvent. During its development, SAFT-VR+DE was tested against isothermal-isobaric ensemble Monte Carlo simulations and the effect of different ion concentrations and different ratios of the cation, anion, and solvent segment diameters on PVT behavior studied. The simulations highlighted the importance of accounting for the size of the ions and accurate values for the solvent dielectric constant. As such, it was shown that the NPM provides a more accurate prediction of the PVT behavior of model electrolyte solutions compared to the more commonly used Debye-Hückel theory and primitive models. In closely related work, Herzog *et al.*[238] later combined the PC-SAFT equation of state with the non-primitive model of electrolytes, with the ions considered to be a mixture of charged hard spheres of the same diameter (i.e., a semi-restricted non-primitive model (SNPM)). The accuracy of the approach, and specifically the ion-dipole interaction term, was validated by predicting the Gibbs free energy of solvation at infinite dilution. The Pauling crystal diameters were used to determine the ion radii and the ion/water dispersion interaction was calculated using the relationship of Mavroyannis and Stephen; no ion-ion dispersive interactions and fitted parameters were used. Excellent agreement for the Gibbs free energy of solvation with experimental data was obtained for some (particularly similar anionic and cationic sizes such as KF, RbF, CsCl) alkali halide salt solutions whilst pronounced deviations were observed for most of the others. The authors suggested that the use of the SNPM, as opposed to the full NPM could be one reason for the observed deviations from experimental data. To achieve a better representation of the macroscopic thermodynamic properties a salt specific fitted ion diameter and cation-water interaction was included via

a SAFT-association term. The ion diameter and association energy parameters were obtained by fitting to the mean ionic activity coefficient and osmotic coefficient of different aqueous electrolyte solutions; however, one should note, that the fitted radii exhibit a reverse size trend in that, for example, LiCl has a larger radii than CsCl. Systematically increasing deviations in the correlated properties were observed as the size of the ions increased, which may be due to the inappropriate ion sizes. Using this approach vapor pressure and salt densities were predicted and found to be in good agreement with experimental data.

Irrespective of the adopted molecular model, a common aspect of almost all SAFT based studies of electrolyte solutions is the use of multiple fitted parameters, which overshadows the predictive ability of the approach. Furthermore, with few exceptions[27, 236] these approaches concentrate on determining the mean ionic activities, osmotic coefficients and solution densities at room temperature and pressure, with no effort made to cover broader arrays of thermodynamic properties such as solvation and dielectric decrement. In an effort to develop a more accurate approach, here the non-primitive model based SAFT-VR+DE equation of state is used to study nineteen different 1:1 electrolyte solutions. Emphasis is placed on developing a predictive equation of state that is capable of capturing a wide range (i.e., mean ionic activity, osmotic coefficient to dielectric decrement, solvation) of thermodynamic properties and at temperatures beyond standard conditions. Therefore the number of fitted parameters is minimized and those parameters that are essential to capture the physical interactions identified. The remainder of the chapter is organized as follows: in section 2 the molecular model and theory are discussed, in the section 3 we report the parameters determined for water and

the salts studied and a discussion of results of range of thermodynamic properties and conclusions of this work is provided in section 4.

4.2 Molecular model and theory

In this work we have used the SAFT-VR+DE equation[29] to study the thermodynamic properties of electrolyte solutions. In the SAFT-VR+DE approach the solvent is explicitly taken into account as a dipolar associating fluid. The electrolyte solution is therefore described by a mixture of charged ions of arbitrary sizes and dipolar associating molecules, as shown in figure 4.1. We first consider only weak electrolyte systems and so a completely dissociated model for the ions is adopted following the work of Zhao *et al.*.[210] In this case, the ions are described as a mixture of positively and negatively charged hard spheres that interact via Coulombic attraction and hard-sphere repulsion terms. The water molecules are modeled as dipolar associating hard spheres with an embedded dipole and four association sites to capture the H-bonding nature of the water molecule. In addition to the ion-dipole, dipole-dipole and associative interactions between the solvent-solvent molecules, a dispersive interaction representing induced dipolar-charge interactions between the cation and solvent has been considered through a square-well potential.

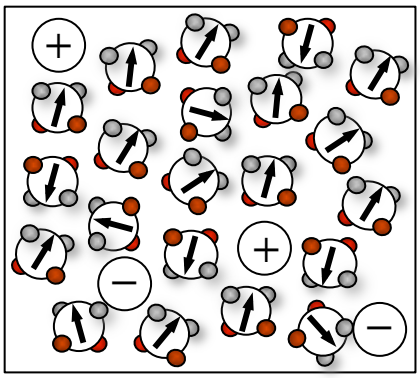

Figure 4.1. Schematic representation of the molecular model used in the SAFT-VR+DE approach to describe electrolyte solutions. The model shown considers ions in an associating dipolar solvent with the ionic species completely dissociated.

The potential model for the interaction of the solvent and ionic species is therefore given by,

$$u(r) = u^{SW}(r) + u^{CC}(r) + u^{CD}(r) + u^{DD}(r) \tag{4.1}$$

where

$$u_{ij}^{SW}(r) = \begin{cases} +\infty & r < \sigma_{ij} \\ -\varepsilon_{ij} & \sigma_{ij} \le r < \lambda_{ij}\sigma_{ij} \\ 0 & r > \lambda_{ij}\sigma_{ij} \end{cases} \tag{4.2}$$

$$u_{ij}^{CC}(r) = \begin{cases} +\infty & if \quad r \le \sigma_{ij} \\ \dfrac{z_i z_j e^2}{4\pi\varepsilon r} & if \quad r > \sigma_{ij} \end{cases} \tag{4.3}$$

$$u_{ij}^{CD}(r) = \begin{cases} +\infty & if \quad r \le \sigma_{ij} \\ \dfrac{z_i e\mu}{4\pi\varepsilon r^2}\left(\hat{r}.\hat{n}\right) & if \quad r > \sigma_{ij} \end{cases} \tag{4.4}$$

and

$$u_{ij}^{DD}(r)=\begin{cases} +\infty & if \quad r\le\sigma_{ij} \\ -\dfrac{\mu^2}{4\pi\varepsilon r^3}D\left(\mathbf{n_1 n_2 \hat{r}}\right) & if \quad r>\sigma_{ij} \end{cases} \tag{4.5}$$

where,

$$D(\mathbf{n_1 n_2 \hat{r}})=3\left(\mathbf{n_1}.\hat{\mathbf{r}}\right)\left(\mathbf{n_2}.\hat{\mathbf{r}}\right)-\mathbf{n_1}.\mathbf{n_2} \tag{4.6}$$

Here ε_{ij} and λ_{ij} are the depth and width of the square-well dispersive pair potential between molecules i and j and $\sigma_{ij}=\left(\sigma_i+\sigma_j\right)/2$ with σ_i and σ_i being the hard core diameter of molecules i and j. In the above expressions, $\hat{r}$ is the unit vector in the direction of r joining the center of the segments and n_i is a unit vector parallel to the dipole moment of segment i , the index n denotes the dipolar solvent molecule and $\mathbf{z}_i$ and μ are the charge of ion i and dipole moment of the solvent molecule, respectively. The model outlined above is used to describe electrolyte solutions at low and moderate salt concentrations (from 0 to 6 *mol/l*). Of particular interest in our work is the study of mixed solvent electrolytes for which most experimental data lies below the concentrations of 6 *m*. The model parameters have therefore been developed with the goal of providing a good representation of electrolyte solutions up to concentrations of 6 *m.* At higher concentrations (>6*m*), the model parameters have been used to predict the thermodynamic properties and if needed ion association is also considered. As the ionic concentration increases, the dielectric of the solvent media decreases, allowing more interaction between ionic species and the formation of ion pairs[239-241]. Thus including ion association at higher salt concentrations provides a more realistic model of these systems and a better theoretical representation of the experimental results.

In the SAFT-VR+DE theoretical framework the Helmholtz free energy [202] of an electrolyte solution is given by

$$\frac{A}{Nk_bT} = \frac{A^{ideal}}{Nk_bT} + \frac{A^{mono}}{Nk_bT} + \frac{A^{assoc}}{Nk_bT} + \frac{A^{ion-assoc}}{Nk_bT} \tag{4.7}$$

where, N is a total number of molecules, k_B is a Boltzmann constant, T is temperature, and A^{ideal} , A^{mono} and A^{assoc} are the free energy contributions due to the ideal, monomer, and association interactions respectively. For concentrated electrolyte solutions, the free energy contribution due to the presence of association between the ions, $A^{ion-assoc}$, is also included. Since all of the molecules considered in this work are monomeric species, we omit the free energy contribution due to chain formation.

The ideal Helmholtz free energy of a mixture of *n* components is given by,

$$\frac{A^{ideal}}{Nk_bT} = \sum_{i=1}^{n} x_i \left[ln(\rho x_i \Lambda_i^3) - 1 \right] \tag{4.8}$$

where ρ is the molecular number density, x_i is the mole fraction and Λ the thermal de Broglie wavelength of species i, which incorporates the kinetic (translational, rotational, and vibrational) contributions to the partition function of the molecule.

The contribution to the Helmholtz free energy due to the interactions between monomer segments is given as

$$\frac{A^{mono}}{Nk_bT} = \frac{A^{mono}}{Nk_bT} + \frac{A^{el}}{Nk_bT} \tag{4.9}$$

where, A^{sw} and A^{el} are the free energy contribution due to the square-well dispersion and electrostatic interactions respectively.

$$\frac{A^{sw}}{Nk_bT}=\left(\sum_{i=1}^{n}x_im_i\right)\frac{A^{sw}}{N_sk_bT}=\left(\sum_{i=1}^{n}x_im_i\right)a^{sw} \tag{4.9}$$

a^{sw} is the contribution to the free energy due to the attractive square well interactions. The monomer free energy per segment of a mixture is obtained as in the original SAFT-VR approach from a second order high temperature perturbation expansion[36],

$$a^{sw}=a^{hs}+\beta a_1+\beta^2 a_2 \tag{4.10}$$

where $\beta=\left(1/k_bT\right)$, a^{hs} is the free energy contribution due to the reference hard sphere system and a_1 and a_2 are the first two perturbation terms associated with the attractive energy.

A^{el} is determined using the MSA for mixtures of ions and dipoles developed by Blum and Wei[204, 242]. Within the MSA, the expression for the electrostatic free energy is given by

$$\frac{A^{el}}{Vk_bT}=\frac{E^{el}}{Vk_bT}-J-J' \tag{4.11}$$

where, V is a total volume of the solution, and E^{el}/Vk_bT is an internal energy per unit of volume. Details of these terms can be found in appendix 1.

The contribution to the free energy due to the associative (short-ranged attractive) nature of the molecules is given by [147],

$$\frac{A^{assoc}}{Nk_bT}=\sum x_i\left[\sum\left(\ln X_{a,i}-\frac{X_{a,i}}{2}\right)+\frac{s_i}{2}\right] \tag{4.12}$$

where, the first sum is over the number of species present in the system and the second sum is over all sites s_i of type *a* in a molecule corresponding to species *i*. $X_{a,i}$ represents

the fraction of molecules of species *i* that are not bonded at site *a* and satisfies the mass action law,

$$X_{a,i} = \frac{1}{1 + \sum\sum \rho x_j X_{b,j} \Delta_{a,b,i,j}} \tag{4.13}$$

where,

$$\Delta_{a,b,i,j} = K_{a,b,i,j} f_{a,b,i,j} g_{ij}^{M}\left(\sigma_{ij}\right) \tag{4.13}$$

$$f_{a,b,i,j} = \exp(-\varepsilon_{a,b,i,j} / kT) - 1 \tag{4.14}$$

The function $\Delta_{a,b,i,j}$ characterizes the association between site *a* on molecule *i* and site *b* molecule *j*; $f_{a,b,i,j}$ is the Mayer *f* function for the *a*-*b* site-site interaction with bonding energy $\varepsilon_{a,b,i,j}$ and volume $K_{a,b,i,j}$ available for bonding. g^{M} is the monomer-monomer radial distribution, which for water association is mediated by four dispersive SW association sites and is given by,

$$g^{M} = g_{ij}^{SW} = g^{hs}\left(\sigma_{ij}\right) + \beta\varepsilon_{ij} g_1\left(\sigma_{ij}\right) \tag{4.15}$$

as in the original SAFT-VR approach.[36] Ions are regarded as having one association (charged SW dispersive) site and so the monomer-monomer radial distribution becomes,

$$g^{M} = g^{csw} = g^{sw}\left(\sigma_{ij}\right)\left(1 + g_{ij}^{el}\left(\sigma_{ij}\right)\right) \tag{4.15}$$

where, the contact value for the radial distribution function for columbic charged interactions, g_{ij}^{el}, is obtained from the MSA as[242],

$$g_{ij}^{el}(\sigma_{ij}) = \frac{-D_i^F D_j^F}{4\pi\sigma_{ij}} \left\{ \frac{\rho_n \sigma_n^2 V_\eta^2}{D\beta_6^2\left(\sigma_n + \lambda\sigma_i\right)\left(\sigma_n + \lambda\sigma_j\right)} + \frac{4\Gamma_i^s \Gamma_j^s}{DD_{ac}} \right\} \tag{4.16}$$

and ρ_n is a density of dipolar solvent particles.

4.3 Results and Discussion

4.3.1 Water

Water molecules are modeled as SW dispersive hard spheres with a dipole moment embedded in the center of the sphere and four short-range attractive square-well sites to describe association interactions that mimic hydrogen bonding, as in earlier work.[243] Although it is well known that the value of the water dipole moment varies significantly from the gas to a liquid phase and the gas phase dipole moment for water[244] is well characterized, the liquid phase moment is not as well defined. A wide range of values have been reported in the literature from both experimental and theoretical studies, with the most commonly accepted value being 2.6D due to Coulson and Eisenberg[245]. However, far-IR vibration-rotation-tunneling spectroscopy along with accurate *ab initio* calculations have shown that the liquid phase dipole moment depends upon the cluster size and can have a value as high as 2.7D[246]. Since a variable dipole moment cannot be used in the theory, and in the study of electrolyte solutions we are primarily concerned with liquid water, we have re-parameterized the original SAFT-VR+D water model that was fitted with a dipole moment of 1.8 D. As can be seen from figure 4.2, when a dipole moment of 2.18 D is used the theory provides a good representation of the water liquid phase dielectric at room temperature and pressure. Hence an effective dipole moment of 2.18 D that takes into account the actual dipole moment of an isolated water molecule (1.80D) and the effect of polarizibility induced by neighboring water molecules was chosen. We note that the dipole moment used is lower than the typically reported values for the liquid phase due to the fact that dispersion energy parameters also partially take

account induced polarizibility effects. The remaining model parameters (i.e., the hard-core diameter (σ), square-well potential depth (ε) and range (λ), association energy (ε^{HB}) and bonding volume (κ^{HB})) were obtained by fitting to experimental vapor pressure and saturated liquid density data between 290-595 K[247]. Experimental data close to the critical region (around 10%) have been excluded from the fitting procedure, as SAFT-VR+D like other analytical equations of state exhibits classical critical behavior in the critical region and so over predicts the critical point[248]. Additionally data points near the triple point have also been excluded since it has been shown that inclusion of such data can distort the results[160]. Simulated annealing[157, 158] is used to the fit the model parameters with an objective function defined as a function of vapor pressure and saturated liquid density as given in appendix A. The resulting parameters are presented in table 4.1, and as can be seen from figure 4.2, the theory provides a good representation of the dielectric constant of water at room temperature and pressure whilst also capturing the phase behavior (Figure 4.3). The average absolute deviation (AAD) over the whole phase diagram is 1.49% for the vapor pressures and 2.43% for saturated liquid densities using the SAFT-VR + D equation of state. We note that the %AADs are comparable to our previous work (%AADP 0.92 and %AADρ 2.87)[243], in which a dipole moment of 1.8 D was used, whilst giving us a more accurate description of the saturated liquid densities that are essential for liquid phase characterization. As expected, and can be seen from figure 13, SAFT-VR+D over predicts the critical region of the phase diagram[159, 249] and does not capture the experimentally observed density maximum of water at lower temperature since a temperature dependent segment diameter is not used[250].

Table 4.1. SAFT-VR+DE parameters for water and the % average absolute deviation (AAD) in vapor pressure and saturated liquid density as compared to experiment[247].

	μ (D)	σ (Å)	ε/k_b (K)	λ	m	ε^{HB}/k_b (K)	K^{HB} (Å^3)	%AAD p	%AAD ρ_{liq}
H_2O	2.179	3.003	312.3598	1.5296	1	758.55	1.5	1.49	2.43

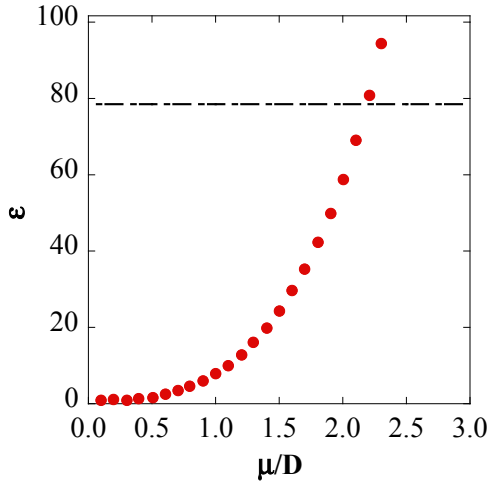

Figure 4.2. Change in the dielectric constant ε as a function of dipole moment μ for water as predicted by the SAFT-VR+D equation of state at room temperature (298.15 K) and pressure (0.101325 MPa). Dashed line represents the dielectric constant for water as reported in experimental studies[221].

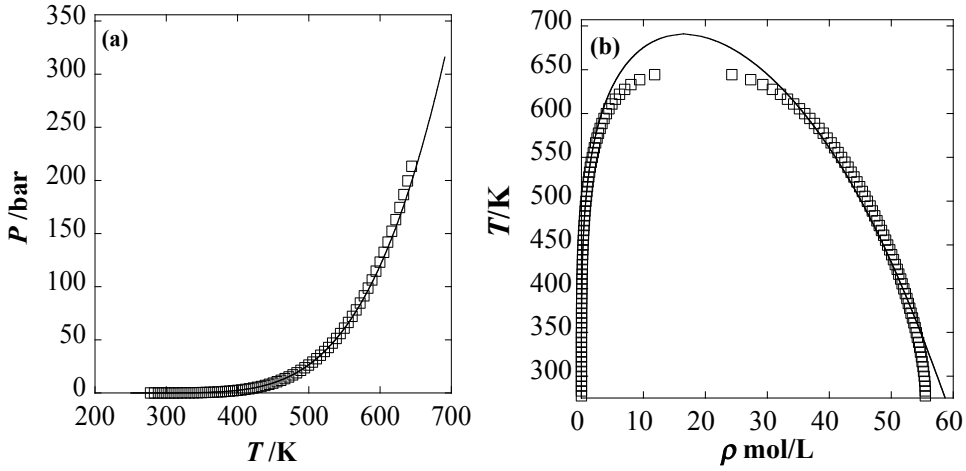

Figure 4.3. Comparison of vapor pressure (a) and vapor-liquid coexisting densities (b) for water from the SAFT-VR+D EoS and experiment. Symbols represent the experimental data and the theory is represented by the solid line[247].

4.3.2 Electrolytes

In this work, several 1:1 alkali halide salts have been studied. The salts are modeled as charged hard spheres of asymmetric size. In any study of electrolytes the concept of "ionic radius," which depends upon the valence, electronic spin state, and coordination number of the ions, is a central one[251]. Goldschmidt[252] was the first to propose a limited set of crystal ionic radii on the basis of interatomic distances. Subsequently, Pauling[253] recommended sets of radii for monoatomic ions, measured from the spatial proportion occupied by the ions within the salt crystal based upon assuming a coordination number of six. Later, Shannon [254, 255] proposed a list of revised effective ionic radii and crystal ionic radii to include more unusual oxidation states and coordinations using a more extensive set of experimental data on intermolecular distances, empirical bond length-bond strength relations etc. These Pauling-type ionic radii, although common and widely used, are not the only ones that have been proposed. For example, Gourary and Adrian[256] and Levy and Danford[257] recommended new sets of ionic radii by redefining the cation-anion distances. More recently, Mähler *et al.*[258] studied the hydrated structures of several different alkali metals using large angle X-ray scattering (LAXS) and double difference infrared spectroscopy and proposed a new set of ionic radii for Li, Na, K, Rb and Cs ions in aqueous solution that corresponded to newly determined coordination numbers. The radial distribution functions (RDFs) obtained from the LAXS experiments indicated coordination numbers of 6, 7 and 8 for Na, K, and Cs ions respectively. A coordination number of 8 was suggested for Rb and 4 for lithium. In this study the cationic radii have been taken from the work of Mähler *et*

al.[258] and for anions, the effective ionic radii proposed by Shannon,[254, 255] which correspond to a coordination number of six[259], have been used.

Ionic species in the electrolyte solution interact via charge-charge and charge-dipole interactions with the ion/solvent molecules. Additionally, a salt-specific dispersion interaction between the cation and the solvent is considered to capture the non-electrostatic induced dispersive effect. Initially, no dispersion interaction between the anion and solvent is included in the model. The unlike cross dispersion interaction energy ($\varepsilon_{cation-H_2O}$) between the cation and solvent is obtained by fitting to the mean ionic activity coefficient data at 298.15 K and 0.101325 MPa using the Levenberg-Marquardt[260] algorithm. The dispersive square-well interaction range (λ) for the cations is fixed at 1.2[27, 261]. The Lorentz-Bethelot combining rule has been used to determine the cross-interaction range parameters between the cations and solvent molecules.

$$\lambda_{H_2O-cation} = \frac{\sigma_{H_2O}\lambda_{H_2O} + \sigma_{cation}\lambda_{cation}}{\sigma_{H_2O} + \sigma_{cation}} \tag{4.17}$$

It was observed during the fitting process that a reasonable theoretical representation of the experimental mean ionic activity coefficient data could not be obtained for several of the salts containing Li^+, Na^+ and F^- ions using the ionic radii proposed by Mähler *et al*. (the % average absolute deviation obtained is reported in table 4.2). The smaller ions Li^+, Na^+, F^- are considered to be net structure makers, which implies these ions distort the water structure around them over to multiple water shells[262, 263]. As a result, the use of a larger diameter for Li^+, Na^+ and F^- ions, better captures the induced effect on water molecules. The diameters for these ions were therefore obtained from the fitting process alongside the dispersion energy between the cations-water. The approach therefore

requires summary, two fitted parameters for ten of the aqueous salt solutions studied and only one for the other nine. We note, that although the radii of some of the ions is now fitted, this does not disrupt the trend in the values for the ionic radii, i.e., Li<Na and F< other anions. The final values of the ionic radii used in this study are reported in table 4.3. We also note that the proposed radii for Li and Na fall between the ionic radii proposed by Mähler *et al*. and the van-der-Waals radii, which corresponds to the dispersive interactions.

Table 4.2.%AAD in $\gamma\pm$ for salts containing Li^+, Na^+, F^- using ionic radii proposed by Mähler *et al*.

Salt	% AAD $\gamma\pm$	*Molality*
LiCl	33.65	0.1-6.0
LiBr	29.08	0.1-6.0
LiI	23.84	0.1-3.0
NaF	4.93	0.1-1.0
NaCl	20.94	0.1-6.0
NaBr	8.80	0.1-4.0
NaI	12.99	0.1-3.5
KF	13.64	0.1-4.0
RbF	15.25	0.1-3.5
CsF	6.96	0.1-3.5

Table 4.3 Ion specific SAFT-VR+DE diameter (σion) and square-well dispersion range (λion) parameters for alkali and halide ions studied.

	Li	**Na**	**K**	**Rb**	**Cs**	**F**	**Cl**	**Br**	**I**
σ_{ion}	2.65	2.8	2.92	3.28	3.46	3.32	3.62	3.92	4.4
λ_{ion}	1.2	1.2	1.2	1.2	1.2	-	-	-	-

In table 4.4 we report the binary salt-specific cation-H_2O dispersion interaction parameters obtained from fitting to experimental mean ionic activity coefficient data at 298.15 K and 0.101325 MPa and the corresponding average absolute deviations from the experimental data over a specified molality range. In the figure 4.4, selected results for

the mean ionic activity coefficient of different salts are presented. As can be seen from the figure we have been able to obtain a good representation of the experimental data up to 6 *m* salt concentration. It can be noted that as the anion size increases for a specific alkali cation, larger deviations are seen compared to the smaller anions studied, particularly at higher salt concentrations. This may be due to the exclusion of dispersion interactions between the anions and water molecules, which plays a greater role with increasing ion concentration and will be further discussed later.

Using the parameters determined, other thermodynamic properties of the aqueous electrolyte solutions studied, such as osmotic co-efficient, water activity co-efficient and density, were then predicted at 298.15 K. The predicted osmotic coefficients for the 19 different salts studied were found to be in good agreement with the experimental data (%AADs are reported in the table 4.5), especially considering the approach uses only a single fitted salt specific parameter. We also note that the predicted results for the osmotic coefficients are well with in the range of %AAD reported by Herzog *et al*.[238], who correlated the osmotic coefficient, although in our case a smaller molality range has been studied. In figure 4.5, the predicted osmotic coefficient (Φ) for different salts from 0-6 *m* are presented. Good agreement for different Li salts in comparison with experimental data is found as shown in Figure 4.5a. As can be seen from figure 4.5b, for some of the salts studied, such as NaCl, the theory overpredicts the osmotic coefficient at high salt concentrations. We believe this is due to the presence of ion association[264] and an effort has been made to incorporate this behavior into the theory through the inclusion of an association term, as discussed further below.

Table 4.4. Salt specific dispersion range parameter between cations and the solvent (ε$_{cation-H_2O}$) for different electrolytes along with the %AAD for the SAFT-VR+DE EoS for $\gamma\pm$ as compared to the experimental data over the molality range specified.

Salts	$\varepsilon_{cation-H2O}$ (K)	% AAD $\gamma\pm$	*molality*
LiCl	1770.968	8.51	0.1-6.0
LiBr	1606.255	5.86	0.1-6.0
LiI	1444.732	9.18	0.1-3.0
NaF	1732.250	0.93	0.1-1.0
NaCl	1382.396	8.03	0.1-6.0
NaBr	1274.406	3.53	0.1-4.0
NaI	1209.249	9.78	0.1-3.5
KF	1478.095	8.64	0.1-4.0
KCl	1189.358	4.60	0.1-4.5
KBr	1087.631	3.10	0.1-5.5
KI	1067.243	9.09	0.1-4.5
RbF	1043.135	4.95	0.1-3.5
RbCl	863.759	2.42	0.1-5.0
RbBr	826.077	5.66	0.1-5.0
RbI	858.326	12.1	0.1-5.0
CsF	919.569	1.69	0.1-3.5
CsCl	749.444	5.70	0.1-6.0
CsBr	734.455	9.11	0.1-5.0
CsI	760.645	8.55	0.1-3.0

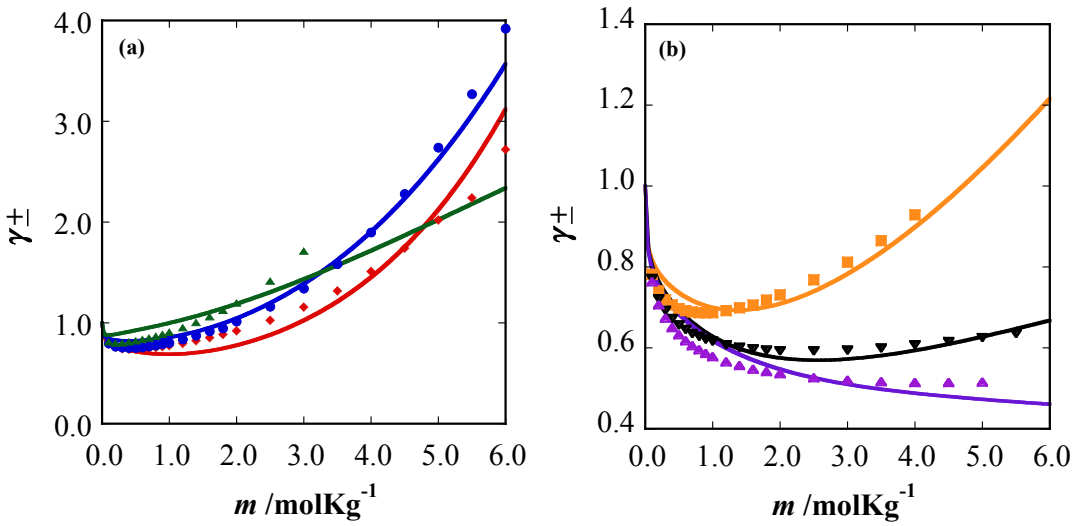

Figure 4.4. Mean ionic activity co-efficient of (a) LiCl (red ◆), LiBr (blue ●), LiI (green ▲) and (b) NaBr (orange ■), KBr (black ▼), RbBr (purple ▲) at 298.15 K and 0.101325 MPa from the SAFT-VR+DE EOS. Symbols represent the experimental data[265] and solid lines the theoretical correlations.

Table 4.5. Comparison between experimental[265] and SAFT-VR+DE equation of state prediction for osmotic coefficient (Φ), water activity coefficient (γ_w) and solution densities (ρ) of different electrolytes

Salts	**%AAD Φ**	**% AAD γ_w**	**%AAD ρ**	***molality***
LiCl	4.92	6.72	2.66	0.1-6.0
LiBr	2.53	7.50	3.19	0.1-6.0
LiI	4.64	4.11	2.83	0.1-3.0
NaF	0.57	1.99	NA	0.1-1.0
NaCl	5.58	6.81	1.09	0.1-6.0
NaBr	1.53	5.05	2.16	0.1-4.0
NaI	4.79	4.70	2.09	0.1-3.5
KF	5.84	4.80	2.80	0.1-4.0
KCl	3.79	5.41	1.74	0.1-4.5
KBr	2.02	6.74	1.77	0.1-5.5
KI	4.90	5.88	2.61	0.1-4.5
RbF	3.69	4.43	2.77	0.1-3.5
RbCl	1.85	6.25	3.71	0.1-5.0
RbBr	3.36	6.47	NA	0.1-5.0
RbI	7.13	6.82	2.57	0.1-5.0
CsF	1.34	4.49	4.50	0.1-3.5
CsCl	3.73	7.86	3.05	0.1-6.0
CsBr	5.63	6.69	2.47	0.1-5.0
CsI	5.72	4.29	3.03	0.1-3.0

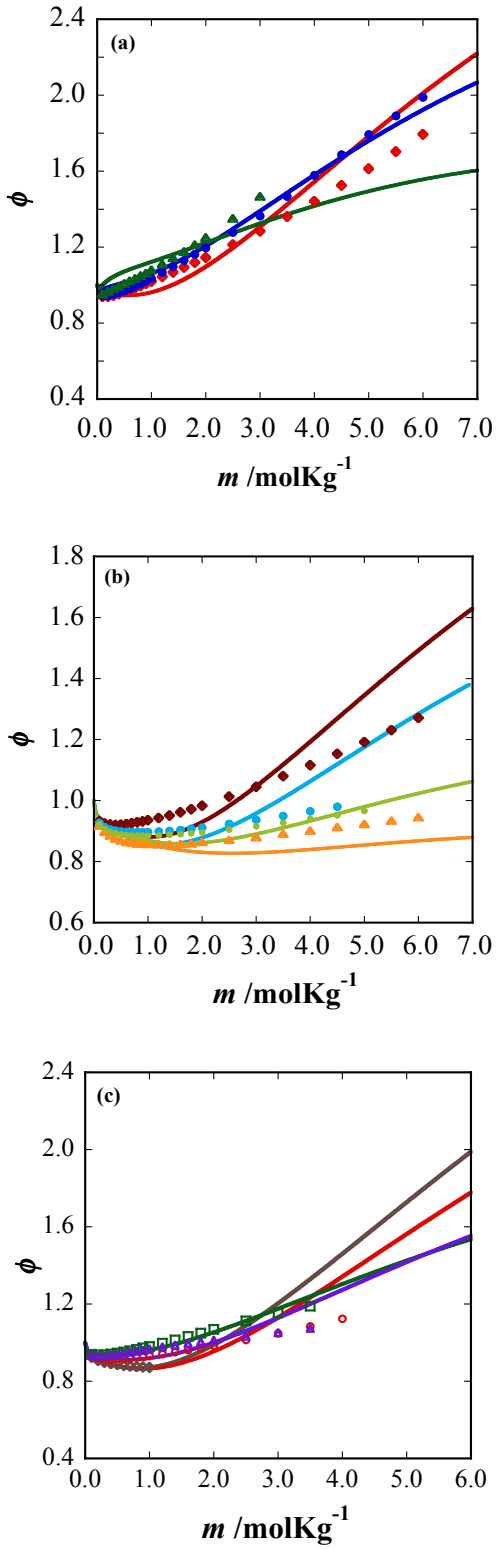

Figure 4.5. Aqueous osmotic co-efficient of (a) LiCl (red ◆), LiBr (blue ●), LiI(green ▲) and (b) NaCl (brown ◆), KCl (blue ▼), RbCl (green ●), CsCl (orange ▲) (c) NaF (brown ◇), KF (red ○), RbF (purple △), CsF (green □) at 298.15 K and 0.101325 MPa from the SAFT-VR+DE EOS. Symbols represent the experimental data[265] and solid lines the theoretical predictions.

4.3.3 Gibbs free energy of solvation

Upon dissolving a salt in water, the ions are surrounded by the water and form a hydrogen-bonded network with neighboring water molecules; the energy released during this process is termed the free energy of solvation. As one might expect, an implicit treatment of the solvent at the PM level fails to capture this phenomena. For example, using the salt parameters proposed in the SAFT-VRE approach[266], the predicted Gibbs free energy of hydration ($\triangle G^{hyd}$) shows large deviations from experimental data as presented in table 4.6. We note that while the recently modified SAFT-VRE by Schreckenberg *et al*.[27] improves the trend in the free energy of solvation, significant deviations from the experimental values are still observed. With the solvent treated as a dielectric continuum, it is difficult to obtain even qualitative agreement with experimental results. In the non-primitive model, as used in this study, the solvent molecules are explicitly included and so the ion-solvent interactions are described by an explicit ion-solvent term. This provides a theoretical advantage in terms of capturing the solvation behavior compared to the implicit solvent models frequently adopted in SAFT-based equations of state for electrolyte solutions. In table 4.7, $\triangle G^{hyd}$ as calculated from the SAFT-VR+DE equation of state for individual ions (cations and anions) and salts are presented and compared with experimental data[265]. Note that $\triangle G^{hyd}$ for the cations varies with the salts due to the use of salt specific water-cation dispersion energy parameters. From the table it can be seen that, while the theory provides a very good representation of the hydration energy for cations, deviations are seen in the predictions for the anions. This can be explained by the fact that at infinite dilution ionic concentrations the number of water molecules surrounding the anions increases

considerably compared to moderate or high concentration. In this scenario the anions will experience dispersion interactions with solvent, the neglect of which could be one reason behind the observed deviations.

As discussed previously, Herzog *et al.* investigated the Gibbs free energy of hydration using the semi non-primitive model[238]. Along with the dipolar and ionic interactions, dispersive interactions between both the cation and anion and water were considered. Although, higher deviations were observed from the experimental results for some of the cations, most of the anions were in good agreement. They also, commented that the use of fully non-primitive model, which captures individual sizes of cations and anions, might bring improvement in the predictions. Here we report that, significant improvements are achieved for cations Na, K, Rb and Cs in terms of the Gibbs free energy of hydration but some deviations have been observed for the anions, which again we believe is due to not considering the anion-solvent dispersive interactions. Irrespective of the deviations observed, we can however conclude, that the results predicted using the non-primitive or semi non-primitive models are still more accurate than any result obtained using a primitive model approach (as demonstrated in in table A3 in the supplemental material)[209].

Table 4.6.Comparison between experimental and SAFT-VRE theoretical predictions for the Gibbs free energy of solvation for different aqueous electrolytes.

Salt	$\triangle G^{hyd}$ (KJ/mol)	$\triangle G^{hyd}$ *Expt.* (KJ/mol)
LiCl	29.85	-833.4
LiBr	51.88	-807.1
LiI	65.17	-772
NaCl	-21.26	-727.7
NaBr	0.77	-701.4
NaI	11.61	-666.3
KCl	59.11	-655.9
KBr	81.13	-629.6
KI	94.43	-594.5

Table 4.7 Comparison between experiment**[265]** and the SAFT-VR+DE EoS predicts for the Gibbs free energy of hydration for different electrolyte solutions.

Salt	$\triangle G^{hyd}$ cation (KJ/mol)	$\triangle G^{hyd}$ *Expt.* cation (KJ/mol)	$\triangle G^{hyd}$ anion (KJ/mol)	$\triangle G^{hyd}$ *Expt.* anion (KJ/mol)	$\triangle G^{hyd}$ salt (KJ/mol)	$\triangle G^{hyd}$ *Expt.* salt (KJ/mol)	%AAD$\triangle G^{hyd}$ salt
LiCl	-464.72	-529.4	-228.35	-304	-693.08	-833.4	16.73
LiBr	-451.43	-529.4	-200.78	-277.7	-652.21	-807.1	19.12
LiI	-438.51	-529.4	-157.66	-242.6	-596.17	-772	22.86
NaF	-455.83	-423.7	-256.97	-429.1	-712.79	-852.8	16.38
NaCl	-425.42	-423.7	-228.35	-304	-653.77	-727.7	10.21
NaBr	-416.14	-423.7	-200.78	-277.7	-616.92	-701.4	12.14
NaI	-410.58	-423.7	-157.66	-242.6	-568.23	-666.3	15.02
KF	-428.63	-351.9	-256.97	-429.1	-685.59	-781	12.62
KCl	-402.20	-351.9	-228.35	-304	-630.55	-655.9	4.50

KBr	-392.99	-351.9	-200.78	-277.7	-593.77	-629.6	6.39
KI	-391.15	-351.9	-157.66	-242.6	-548.81	-594.5	8.66
RbF	-370.34	-329.3	-256.97	-429.1	-627.31	-758.4	17.4
RbCl	-343.03	-329.3	-228.35	-304	-579.39	-633.3	8.78
RbBr	-339.00	-329.3	-200.78	-277.7	-547.79	-607	10.08
RbI	-342.44	-329.3	-157.66	-242.6	-508.11	-571.9	11.74
CsF	-348.36	-306.1	-256.97	-429.1	-605.33	-735.2	17.24
CsCl	-328.52	-306.1	-228.35	-304	-556.87	-610.1	8.27
CsBr	-326.78	-306.1	-200.78	-277.7	-527.55	-583.8	9.22
CsI	-329.82	-306.1	-157.66	-242.6	-487.47	-548.7	10.98

4.3.4 Effect of ions on the dielectric properties of water

The interactions between charged ions and dipolar solvent molecules play an important role in determining the thermo-physical properties of electrolyte solutions. Over the years, although many SAFT-based equations of state based on the primitive model [218, 220, 226, 227] for electrolyte solutions have been proposed and found to be able to capture the essential thermodynamic properties of these systems, such as the mean ionic activity co-efficient, osmotic co-efficient and density, they are unable to capture the variation of the dielectric constant of the solvent with salt concentration. Generally, in primitive models the dielectric constant is fixed over the whole salt concentration range studied, whereas the dielectric constant of the solvent is experimentally a function of the salt concentration (i.e., the dielectric properties are reduced as the salt concentration increases, due to ionic polarizibility, as is the modification of the water structure due to the formation of hydration shells which restricts the rotation of free water

molecules)[188, 267, 268]. Implementation of a more advanced level of theory, such as a non primitive model that can capture the underlying physics of these complex phenomena, should provide an approach that is better equipped to capture this dielectric decrement phenomena. We note that although Herzog *et al*.[238] applied the SNPM in their study they do not examine the ability of the theory to capture the correct dielectric behavior. In this study we report for the first time the decrement of the dielectric constant in the presence of ions using a SAFT based equations of state.

The dielectric constant of the solution has been obtained following the work of Wei *et al*.[242] as

$$\varepsilon_A = 1 + \frac{\rho_n \alpha_2^2 \beta_6^2 \left(1+\lambda\right)^4}{16} \tag{4.17}$$

where $\alpha_2^2 = 4\pi\beta\mu^2/3$, $\lambda = \beta_3 \big/ \beta_6$, $\beta_3 = 1 + b_2/3$ and $\beta_6 = 1 - b_2/6$. α_2^2 and b_2 are the dipole-dipole strength parameters obtained when solving the MSA equations (see Appendix 2). In figure 4.6, we compare the experimental and predicted dielectric constant for different electrolyte solutions. From Figure 4.6a, which reports the dielectric constant for five salts with different cations (Li, Na, K, Rb and Cs) and the same chloride anion, we find that both the theory and experimental values do not show any dependence on the size of the cation and that a decreasing asymptotic trend in the dielectric permittivity is observed that is well captured by the theory. This is consistent with other work indicating dielectric decrement is more dependent on cationic charge than size[269]. In figure 4.6b a comparison between the theoretical predictions and experimental dielectric constant for KF and NaI is presented. As the size asymmetry

between the anion and cation increases with larger anion size, the dielectric depression increases, with the trend in the experimental data again well captured by the theory.

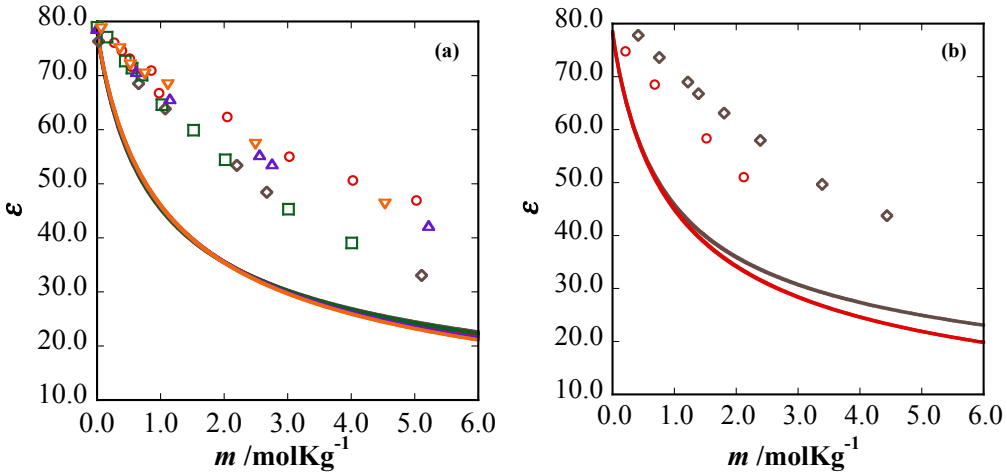

Figure 4.6. Water dielectric constant for different salt solutions (a) LiCl (grey ◇), KCl (red ○), NaCl (green □), RbCl (purple △), CsCl (orange ▽) and (b) KF (grey ◇), NaI (red ○) at 298.15K temperature and 0.101325 MPa pressure. Symbols represent the experimental data[270, 271] and solid lines the theoretical predictions.

In both cases the theory is only in qualitative agreement with experiment, in that it captures the correct trends, but deviates from the experimental values. Some inaccuracy in the theoretical predictions could be due to the approximations adopted when the expressions for the pair correlation functions and thermodynamics were developed by Wei and Blum[242]. Specifically, the proposed solution of the MSA is stated to be only valid for ions of similar size and at low ionic concentration (<3m), with several of the expressions, including pair correlation functions, only tested at low ionic concentrations (i.e., 0.1 and 1 m). Deviations are therefore perhaps to be expected when dealing with ions of asymmetric sizes and the higher ionic concentrations considered in this work. A further issue is the orientation of the water molecules in the hydration shell and the presence of ion-pairs. For salts such as NaCl and CsCl experiments and simulations confirm the existence of both contact and solvent separated ion pairs (CIP and SSIP respectively)[240, 241]. The existence of solvent separated ion pairs at low ion

concentrations effectively reduces the number of ions in the solution, which in turn behave more like dipolar molecules and hence increase the dielectric constant of the solvent. This effect is not well captured by the theory since a fully dissociated model is being used and inclusion of the ion-association term discussed below would not improve the situation since the dielectric is calculated from the ion-dipole and dipole-dipole free energy contribution expressions, which are not affected by ion association. We also note however, that the experimentally measured static permittivity of polar conducting fluids such as aqueous electrolytes is known to contain systematic errors due to dielectric saturation and kinetic depolarization and can result in a 25–75% decrease in the measured static permittivity.[272] Such a decrease in the experimental static permittivity would increase the accuracy of the theoretical predictions considerably.

4.3.5 Temperature effect on thermodynamic properties of electrolytes

In this section, the effect of temperature on the thermodynamic properties of the electrolyte solutions studied is considered. In figure 4.7 the predicted solution densities for KBr and KCl are presented over a wide range of temperatures. From the figure we can see that the theory accurately captures the behavior of the solution density as a function of temperature. In figure 4.7b we observe a slight (less than 5%) deviation of the theoretical predictions from the experimental data for KCl. We note that the density is a predicted property and that similar deviations in density are commonly seen with SAFT based equations of states for electrolytes, even though in most cases the density was included in the fitting process. At low temperatures in the pure limit the observed deviations from experimental results (apparent from figure 4.7b), are due to the over prediction of the saturated liquid density of pure water. Overall, we can conclude that the

SAFT-VR+DE approach with a single fitted parameter at 298.15 K and 1 bar for KCl and KBr salts, it describes the solution densities well over a range of temperatures (293.15 K to 423.15 K).

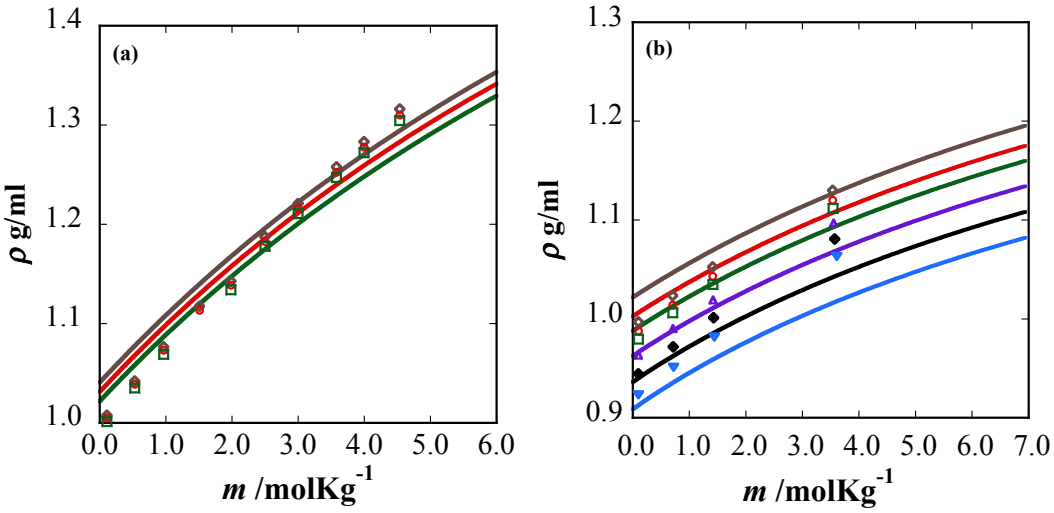

Figure 4.7. Densities of aqueous solution of (a) KBr at 293.15K (grey ◇), 303.15K (red ○), 313.15K (green □) and (b) KCl at 313.15K (grey ◇), 333.15K (red ○), 348.15K (green □), 373.15K (purple △), 398.15K (black ◆), 423.15K (blue ▼). Theoretical predictions have been obtained by using SAFT-VR+DE EOS. Symbols represent the experimental data and solid lines theoretical results.

We now consider the temperature and pressure dependence of the mean ionic activity coefficient and osmotic coefficient which are more temperature sensitive properties. In figure 4.8 and 4.9 respectively the predicted mean ionic activity coefficient and osmotic coefficient for NaCl and NaBr over a temperature range from 298.15K to 573.15K at saturation pressures are presented. As can be seen from the figures, while the SAFT-VR+DE equation of state is able to capture the correct trend in the mean ionic activity coefficient and osmotic coefficient a function of temperature, the predictions are not in quantitative agreement. As previously discussed, the dipole moment for water used in the calculations is one that accurately captures the dielectric constant of water at room temperature and pressure. If we consider the behavior of the pure solvent dielectric as a

function of dipole moment, as shown in table 4.8, it can be observed that although a dipole of 2.18 D works well at room temperature, it under predicts the dielectric constant at higher temperatures and pressures. In this scenario, if we use a higher dipole moment in the theoretical calculations, without altering/ refitting the SAFT-VR+D water parameters, the theory more accurately captures the dielectric of water at higher temperatures and pressures. In the subsequent rows of the table the value of the dipole moment that predicts a dielectric constant that most closely matches the experimental dielectric data is reported. We note that the dipole moment increases with temperature and pressure due to the fact that the theory under predicts the dielectric and so a larger effective dipole moment is needed to compensate.

Table 4.8. Experimental v/s theoretically obtained dielectric constant when different dipole moments are used across a range of temperature and pressure

T/K **(p/MPa)** **μ (D)**	298.15 /0.1	373.15 /0.1	473.15 /1.55	573.15 /8.6
Expt.	78.58	55.56	34.82	20.10
2.179	78.58	49.93	28.99	16.59
2.250	87.15	55.41	32.28	18.66
2.300	93.57	59.52	34.75	20.23

To determine the effect of capturing the correct solvent dielectric on the prediction of the thermodynamic properties the appropriate values of the dipole moment from table 4.8 have also been used in the calculations. As can be seen in figures 4.8 and 4.9, the use of the higher temperature and pressure dipole moments has a significant effect on the thermodynamic properties and the accuracy of the theoretical predictions.

While deviations between the theoretical predictions and experimental data are still observed, we note that the improvement is achieved simply by changing the dipole moment and without refitting other model parameters. We also note that further deviations are likely due to the fact that the theory under predicts the solvent dielectric at high salt concentrations, as previously discussed.

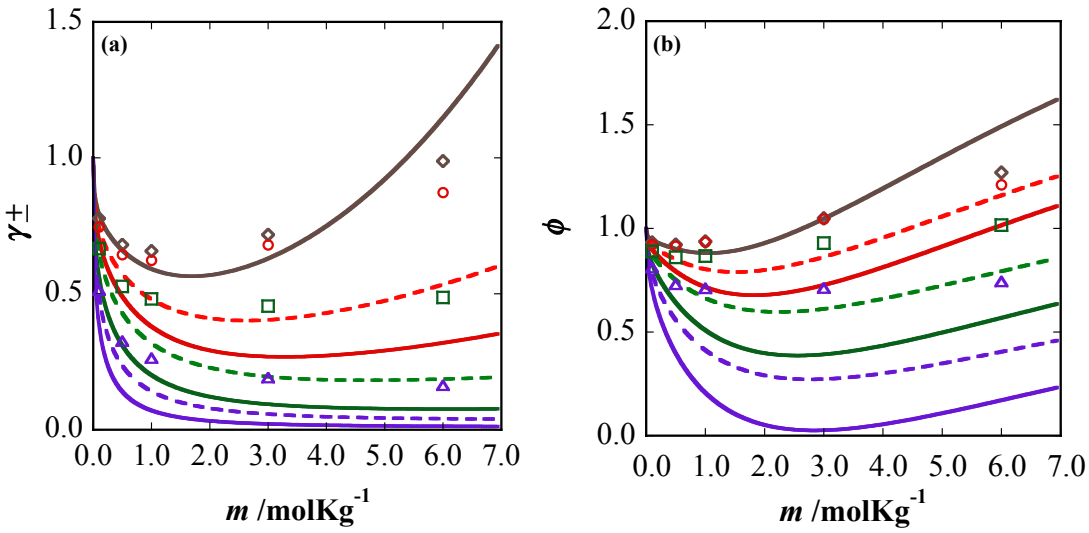

Figure 4.8. Comparison of the predicted and experimental (a) mean ionic activity and (b) osmotic coefficient for NaCl at 298.15K/0.1MPa (grey, ◇), 373.15K/0.1MPa (red, ○), 473.15K/1.55MPa (green, □), 573.15K/8.6MPa (purple, △). The theoretical predictions from the SAFT-VR+DE EOS with a water dipole moment of 2.179D are represented btydashed lines while the solid lines correspond to the theoretical results using the modified dipole moments . The symbols represent the experimental data.[273]

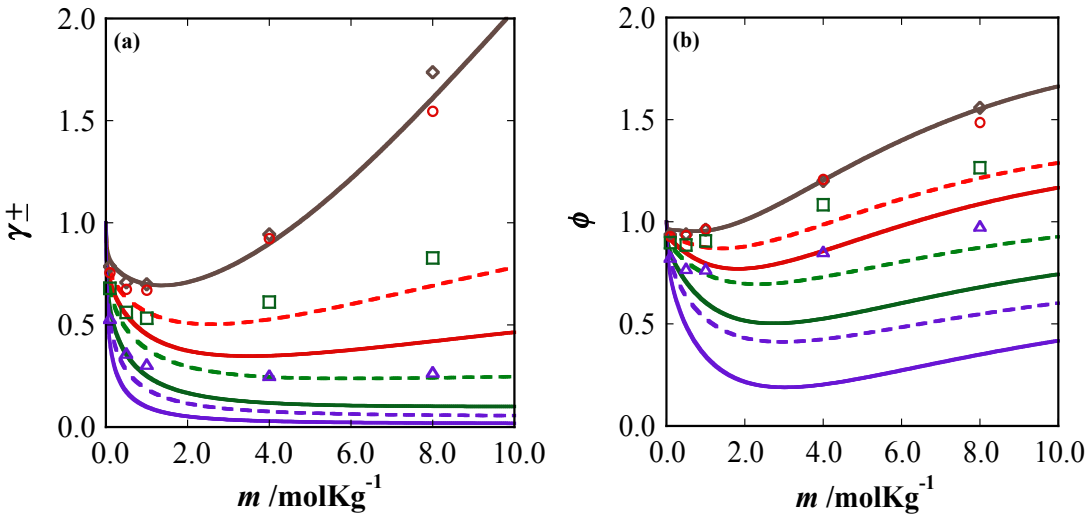

Figure 4.9. Comparison of the predicted and experimental (a) mean ionic activity and (b) osmotic co-efficient for NaBr at 298.15K/0.1MPa (grey ◇), 373.15K/0.1MPa (red ○), 473.15K/1.55MPa (green □), 573.15K/8.6MPa (purple △). The theoretical predictions from the SAFT-VR+DE EOS with a water dipole moment of 2.179D are represented by dashed lines while the solid lines correspond to the theoretical results using the modified dipole moments . The symbols represent the experimental data[273].

4.3.6 Mean ionic activity coefficient at high salt concentrations and ion-association

As the molality in a salt solution increases the solution dielectric constant decreases considerably due to ion pairing. While ion pairing is not significant in aqueous solutions of strong electrolytes at ambient temperatures and low salt molality, as the high dielectric constant of water very effectively screens the charge-charge coulombic interactions, as the salt molality increases change-charge interactions between the ions become more significant. The average distance between the ions decreases and the ions can form clusters of contact or solvent separated ion pairs in solution[239-241, 274, 275].

For seven of the nineteen salts studied herein, namely NaBr, RbCl, CsCl, KF, LiBr, LiCl, NaI mean ionic activity coefficient data is available at concentrations higher than 6 *m*. If the previously determined parameters are used to predict the mean ionic activity coefficient at these higher concentrations as can be seen from figure 4.10,

accurate results are obtained for NaBr, RbCl, and CsCl. The dissociated model can therefore be considered to describe the thermodynamic properties of these four salt solutions well. This is consistent with the molecular simulation study of Fennell *et al.*[240] which showed that size symmetric ions compared to size asymmetric ions more readily associate and form contact ion pairs. NaBr, RbCl, CsCl being asymmetric in size are less prone to ion-pair formation. This is also supported by the conductmetric study of Fuoss[276] who provides further evidence that Rb halide salts are less associative.

If we consider LiCl, LiBr, KF and NaI, significant deviations from the experimental data are seen in Figure 20 at higher concentrations (>6 *m*). This can be attributed due to other factors such as ion-association or increased ion-solvent interactions, including anion-solvent dispersive interactions, which so far have not been considered in the model but are discussed further below.

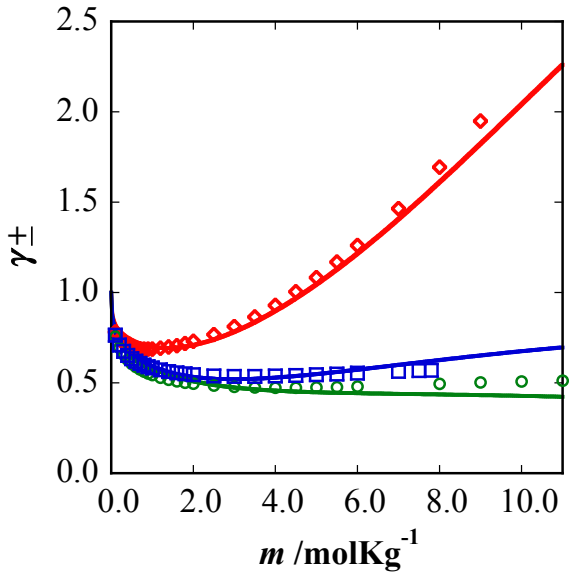

Figure 4.10. Mean ionic activity co-efficient of CsCl (green ○) , RbCl (blue □) and NaBr (red ◇) as predicted by the SAFT-VR+DE EOS (solid lines) compared to experimental data**[277].**

In order to better capture the molecular level interactions at higher salt concentrations ion pairing has been included in the model through the addition of an ion-association term to equation 4.19. Although several SAFT-based equations of state [232, 266] have been proposed that considered ion association, they failed to obtain (correlate [232] or predict [266]) the correct trends with increasing ionic concentrations for properties such as the mean ionic activity coefficient and solution vapor pressure when compared to experimental data. We note however that the more recent work of Rozmus *et al*.[236], included ion-association within the molecular model with the association energy parameter obtained by fitting to experimental mean ionic activity coefficient data at 298.15 K and 1 bar for salt concentrations up to 6 m. Although the theory was able to provide a good correlation of the mean ionic activity coefficient at 298.15 K an over prediction was observed at higher temperatures. In this study we investigate whether the inclusion of ion-association in the model improves the theoretical correlations or predictions of the thermodynamic properties at higher salt concentrations.

As discussed above, ion association has been included in the model through a sticky site placed on the charged spherical ions that interact via charged and associative dispersive interactions. In order to capture the increase in ion interaction and ion-association with the decrease in the dielectric of the medium, the association energy $\varepsilon^{ion-assoc}$ for ions is made dependent upon the solution dielectric constant using the following relation,

$$\varepsilon^{ion-assoc} = a - b\varepsilon_w^2 \tag{4.17}$$

where a is obtained by fitting to the experimental mean ionic activity coefficient data at higher concentration (> 6 m) and b is treated as a constant irrespective of the system.

These parameters for the specific solutions studied are given in table 6 and a graphical representation of equation 4.22 for LiCl and KF are provided in Figure 4.11.

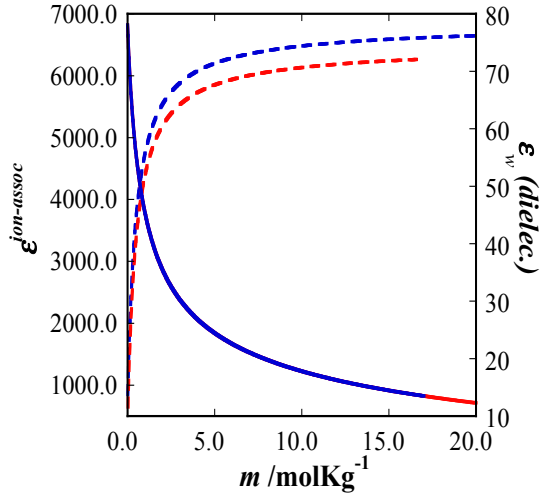

Figure 4.11. Association energy (dotted line) and dielectric decrement (solid line) as a function of ionic concentration for LiCl (blue) and KF (red).

In figure 4.12, the mean ionic activity and osmotic coefficient of LiCl and KF both with and without considering ion association are presented. From figure 4.12a, it can be seen that the inclusion of ion-association enables the theory to provide a better theoretical representation of the mean ionic activity data by reducing the mean ionic activity coefficient. In figure 4.12b, prediction of the osmotic coefficient is reported. For LiCl the inclusion of ion association into the model reduces the osmotic coefficient bringing it into closer agreement with the experimental data at higher concentrations (> 6 *m*). For KF, although the theory with ion association provides an improved prediction for the osmotic coefficient by bringing it closer to experimental data, the trend in the experimental data is still not correctly captured.

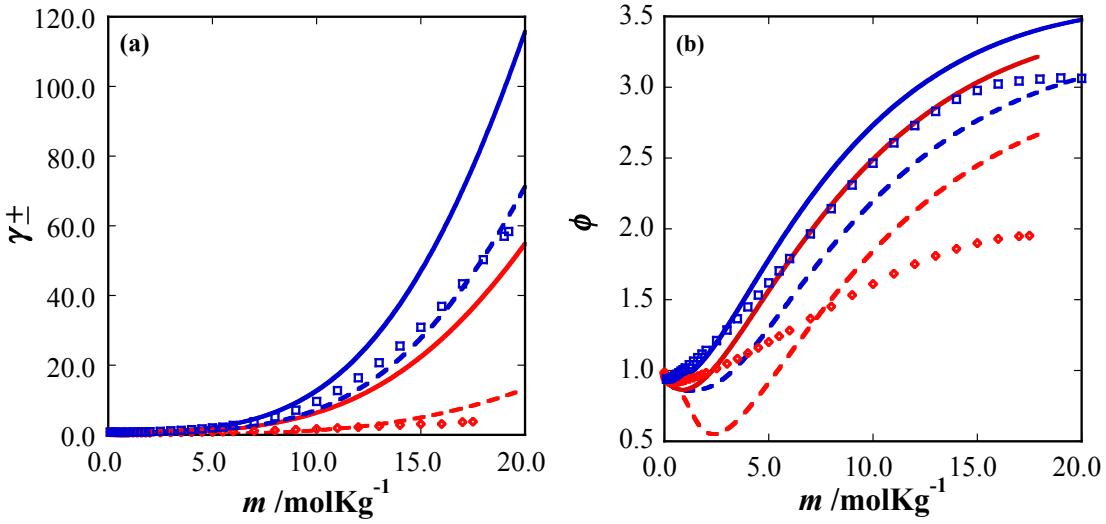

Figure 4.12. Comaprison of the mean ionic activity coefficient (a) and osmotic coefficient (b) for LiCl (blue □) and KF (red ◇) from the SAFT-VR+DE EOS without ion association (solid lines) and with ion association (dashed lines) as compared to the experimental data (symbols)**[277].**

While the inclusion of ion association improves the theoretical treatment of LiCl and KF, for salts such as NaI and LiBr, no improvement is seen even for the correlated mean ionic activity coefficient data, as the inclusion of ion-association decreases the mean ionic activity coefficient of the solution (as the ions form ion pairs the number of free ions decreases and the mean ionic activity coefficient decreases). Hence, inclusion of ion association only works in cases where the mean ionic activity coefficient is over estimated by the completely dissociated model. For NaI and LiBr, the completely dissociated SAFT-VR+DE model already under estimates the mean ionic activity coefficient at higher concentrations and so no further improvement can be achieved be with the inclusion of ion association. However, we would not expect NaI and LiBr to form ion pairs and so this behavior is consistent with the observations of others. For example, as discussed previously studies in the literature report that ions with symmetrical sizes more readily form ion pairs compared to ions of asymmetrical sizes[240]. Therefore we would expect NaI and LiBr, which are more asymmetric in size

than LiCl or KF to not significantly associate but increase their interaction with water molecules. Although, the SAFT-VR+DE approach describes the cation-solvent dispersion interaction and so would be expected to capture this behavior, anion-solvent interactions have been neglected. The need to include anion-water dispersion interactions is further supported by recent molecular dynamics simulations that investigated the effects of ion pairing in bulk water and showed that LiCl forms ion-pairs while LiBr remains completely dissociated at higher concentrations (~12 m) with the Br ion strongly interacting with the water molecules[278]. Hence anion-water interactions are more significant when dealing with higher ionic concentration regimes and should not be ignored in any theoretical treatment. In the SAFT-VR+DE approach the anion-solvent dispersive interaction parameter was initially not considered as it was found at lower concentrations (> 6 m) to not have a significant effect on the correlated results and enabled the number of fitted parameters to be reduced. Since at higher concentrations, anion-solvent interactions appear to be significant, for NaI and LiBr anion-solvent cross-dispersive interaction parameters have been determined by fitting to the mean ionic activity co-efficient data at higher molalities (> 6m) whilst keeping all other parameters unchanged. The dispersive square-well interaction range (λ) is again set to 1.2 and the Lorentz-Bethelot combining rule is used to obtain the cross-interaction range parameters between the anions and solvent molecules. As, we need to parameterize anion-solvent dispersive interaction parameter; the appropriate choice of ionic radii was also considered. As discussed previously, at lower concentrations ionic radii for several ions (Li^+, Na^+, F^-) were fitted and effective radii obtained in order to enable the theory to capture the structure making effect of the ionic interaction with water; however, at higher

ionic concentrations for dissociated salts, the ion-water interactions will not impact multiple water shells due to the more concentrated salt solution and lack of free water molecules. Therefore, in this scenario, the Shannon effective ionic radii is used for Li^+ (0.076 nm) and Na^+ (0.102 nm), rather than the previously obtained fitted one. The new parameters determined for NaI and LiBr are reported in table 4.9, with the other parameters remaining unchanged.

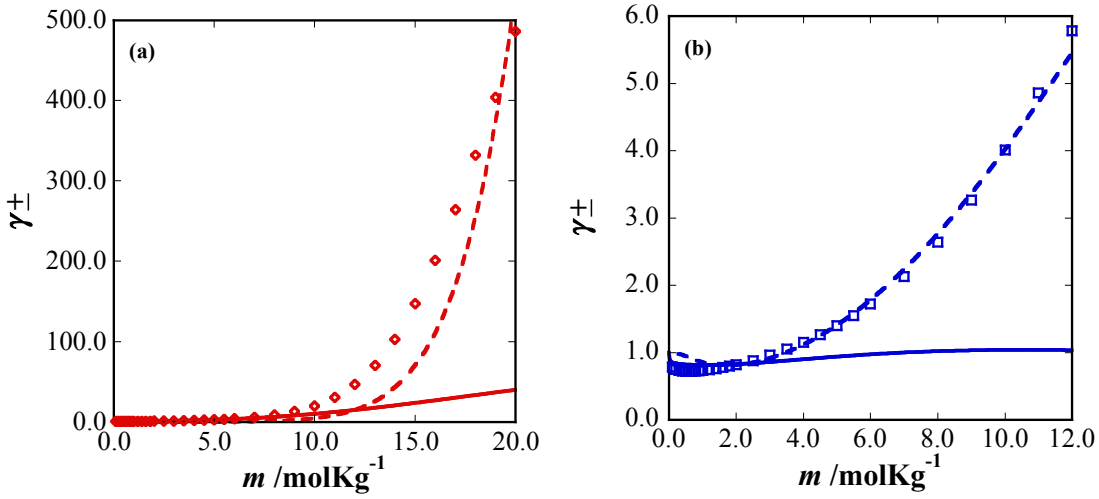

Figure 4.13. Comparision of the mean ionic activity coefficient for (a) LiBr (red ◇) and (b) NaI (blue □) obtained from the SAFT-VR+DE EOS with (dashed lines) and without (solid line) anion-water interaction with experimental data. Symbols represent the experimental data**[277].**

Table 4.9. Salt specific dispersion energy parameters between the anion and solvent ($\varepsilon_{\text{anion-H2O}}$) and dispersive ion association energy parameter (b) obtained from the correlation of mean ionic activity coefficient data ($\gamma\pm$) at molality range > 6*m* using the SAFT-VR+DE equation of state.

	$\varepsilon_{\text{anion-H2O}}/k_b$ (K)	$b/k_b(K)$	$a/k_b(K)$	K^{HB} (Å ^{3})
LiCl	-	1.0	6797.672	1.5
KF	-	1.0	7549.883	**1.5**
LiBr	1182.599	-	-	-
NaI	399.581	-	-	-

As can be seen from figure 4.13 inclusion of the anion-solvent dispersive energy significantly improves the theoretical representation of mean ionic activity coefficient for both LiBr and NaI. Overall, we can conclude that ion association phenomenon is salt dependent and therefore the addition of ion association and anion-solvent dispersion terms will be beneficial for only some systems. For the salts studied herein, the description of LiCl and KF is improved through the incorporation of ion association in to the model but for NaI and LiBr the inclusion of anion-solvent dispersive interactions are the key to a better theoretical description. Typically, salts containing symmetric sized ions will be more inclined to form ion-pairs at high ionic concentrations as compared to a salt formed from asymmetric ions where anion solvent interactions will be more significant.

Table 4.10. Summary of the proposed modeling approaches considered in this work and the required adjustable parameters for each.

Electrolytes	Molality range (m)	Model	Adjustable parameters
All	0-6	Fully dissociated	$\boldsymbol{\varepsilon_{\text{cation}-\text{H}_2\text{O}}}$ for all electrolytes, σ_{ion} for Li, Na and F ions
LiCl, KF	>6	partially associated	$\boldsymbol{\varepsilon^{\text{HB}}}$, $\boldsymbol{\varepsilon_{\text{cation}-\text{H}_2\text{O}}}$[1]
NaI, LiBr	>6	dissociated	$\boldsymbol{\varepsilon_{\text{anion-H2O}}}$

[1]Parameters for all electrolytes same as for 0-6 m range

4.4 Conclusion

In this work we have applied the SAFT-VR+DE equation of state, developed in earlier work, to study nineteen different 1:1 electrolyte solutions. A comprehensive study that evaluates a range of thermodynamic properties including the mean ionic activity

coefficient, osmotic coefficient, water activity coefficient, density, Gibbs free energy of hydration, and the dielectric decrement, has been performed. For electrolyte solutions in the concentration range up to 6m a fully dissociated model is considered that uses a salt specific cation-solvent dispersive energy parameter fitted to mean ionic activity coefficient data. For some systems (salts of Li, Na and F) the ionic radii are also fitted. In comparison to other SAFT-based approaches, the use of the full non-primitive model in the SAFT-VR+DE equation of state enables improved predictions for the Gibbs free energy of hydration, especially for cations, and the prediction of the dielectric decrement with increasing ionic concentration. The results for the dielectric decrement for different electrolyte solutions are qualitatively consistent with experimental observations but deviate quantitatively due to the approximations adopted within the theory. We also, report the effect of temperature on thermodynamic properties such as solution densities, mean ionic activity coefficients and osmotic coefficients for K and Na halide salts. Although the theory provides quantitatively accurate predictions of the solution densities over a range of temperatures (298.15 K - 473.15 K), the mean ionic activities and osmotic coefficients are only in qualitative agreement. The under prediction of the dielectric constant at higher temperatures and pressures, has been identified as the key reason behind the divergence of the SAFT-V+DE predictions from the experimental data. At higher ionic concentrations (> 6m) the theory has been extended to include ion association and shown to improve the correlation and prediction of the thermodynamic properties of LiCl and KF salts. For LiBr and NaI, due to the higher asymmetry between the ions, instead of ion association, consideration of anion-solvent (water) dispersion interactions is found to improve the theoretical description of the mean ionic activity

coefficient. The results demonstrate that when developing a predictive equation of state for a family of electrolyte solutions, a uniform model is not appropriate and the nature of the salt and the concentration range being studied should be taken into account and the model tailored to capture the correct interactions, as summarized in Table 7. Specifically when studying electrolyte solutions from infinite dilution to the fused salt limit, while a fully dissociated model of electrolytes can be expected to capture the thermodynamic behavior at low to moderate concentrations at higher concentrations, with the changes in intermolecular/ ionic interactions, the underlying theoretical considerations should also change. Depending upon the nature of the ions, ion association or enhanced anion-solvent interactions should be considered.

Chapter 5 : Development of a non primitive model based theoretical framework for mixed solvent electrolyte systems

5.1 Introduction

Mixed solvent electrolyte solutions are of significant industrial interest due to their application in several chemical processes such as wastewater treatment, crystallization, liquid-liquid extraction, extractive distillation, and seawater desalination [49]; however, only limited experimental data on the thermodynamic properties of these fluids are available. An attractive approach to explore such systems is therefore to develop theoretical tools that can predict the phase behavior and thermodynamic properties of mixed solvent electrolytes as a means of generating "pseudo" experimental data. Though this is made more difficult by the fact that these fluids are highly non-ideal systems because of the dominant long-range electrostatic interactions, which makes their theoretical study challenging.

Theoretical developments for electrolyte solutions can be broadly divided into two approaches: those in which the solvent is described implicitly by a dielectric constant (known as primitive models) [53] and those in which the ions and solvent species are both treated explicitly (known as non-primitive models). The primitive model is a McMillan-Mayer level of theory [187], developed with the notion that an explicit representation of the solvent is not necessary and can be treated implicitly within the theory. This approximation is likely to be valid at low ionic concentrations. In contrast, the non-primitive model allows the explicit description of solvent species within the theoretical framework and is in the general class of Born-Oppenheimer models [187]. In the simplest Born-Oppenheimer models of electrolytes, the electrolyte solution is described as a mixture of charged hard spheres in a solvent of spherical hard dipolar

molecules. We note that to date, only the primitive model has been applied to the study of mixed solvent electrolytes.

In the context of the development of theoretical approaches for the calculation of the thermodynamic properties of mixed solvent electrolytes, the primitive-model-based semi-empirical Debye–Hückel (DH) theory is the simplest. The DH theory, in which ions are treated as point charges in a dielectric media, is in general perhaps the most widely adopted approach for the treatment of electrostatic interactions because of its simplicity. However, the applicability of DH theory is limited to the very dilute regime of electrolyte solutions. Since its advent the most significant contribution to improving the DH approach was made by Pitzer. In the Pitzer-Debye–Hückel (PDH) [51] formalism the short ranged effect of electrostatics were accounted for by including ionic strength dependence in the second virial coefficient and thus the DH theory became applicable to higher ionic concentrations. Subsequently a number of theoretical approaches for mixed solvent electrolyte solutions have been developed that combine DH or PDH theory with activity coefficient models such as NRTL, UNIFAC, and UNIQUAC to describe the short ranged dispersive interactions [279-286]. These approaches correspond to the so-called Lewis–Randall [287] framework in which temperature, pressure and mole fraction of all species are independent variables. In other studies [282, 284], DH/ PDH theory and activity coefficient models, have been further combined with second virial coefficient[8] or Born contributions in order to provide an improved theoretical representation of the interactions present within mixed solvent electrolytes.

In general, the approaches for mixed solvent electrolytes discussed above typically work as correlative tools with very little or no predictive ability. Furthermore,

we note that in some cases there lies a significant inconsistency in the proposed theoretical framework [279, 284]. For example, in the work of Liu et al. [284], the NRTL model is derived from the Lewis–Randall framework, while DH theory is derived from the McMillan-Mayer framework in which the independent variables are temperature, volume, mole fraction of solute and the chemical potential of the solvents. For simplicity the rigorous conversion required between the Lewis–Randall and McMillan-Mayer frameworks are typically ignored [282, 284, 288]; however, the inconsistent treatment of the solvent chemical potential (i.e., as an independent variable in McMillan-Mayer framework and a dependent variable in the Lewis–Randall framework) gives rise to thermodynamic inconsistencies and introduces errors [289]. In order to rectify this inconsistency, several authors [281-283, 289-292] have developed an extended DH formalism that is suitable for use in the Lewis–Randall framework.

A more comprehensive approach to the development of equation of state can be adopted through the use of classical statistical mechanics, which relates intermolecular forces to the thermodynamic functions of fluids. In this regard statistical-mechanics-based perturbation theories and integral equation theory have both been applied to derive analytical expressions for the Helmholtz free energy due to charged Columbic interactions. Some integral equations (based on the mean spherical approximation closure) provide the advantage of yielding analytical expressions for both the structure and the thermodynamics of the fluid and have been widely utilized in the development of equation of state. In the context of charged fluids, Waisman and Lebowitz [197] and Blum [206] solved analytically the relation between the direct correlation function and the pair correlation function given by the Ornstein-Zernike equation with mean spherical

(MSA) closure for the restricted (i.e., an equimolar mixture of equal-diameter hard spheres are assumed) and unrestricted primitive models respectively, to derive analytical expressions for Columbic contribution to the thermodynamic properties and Helmholtz free energy. We note that DH is the limiting case of the primitive model expressions for the MSA i.e., the effect of the volume of the ions is reduced to zero. These analytical expressions of ion-ion interaction free energies were instrumental in the development of statistical associating fluid theory (SAFT) based electrolyte equations of state. SAFT [10, 11, 147] is a state-of-the-art molecular based equations of state, founded on Wertheim's first-order thermodynamic perturbation theory (TPT1) [212, 214, 215] that in its many variations has been applied to study the thermodynamic properties of a wide range of industrially important complex fluid systems (see for example [148, 209, 216, 217]). A MSA term combined with different versions of SAFT has been used by several authors to develop SAFT-based approaches for electrolyte solutions. For example, the SAFT-VRE [218, 226] equation was developed by combining the SAFT approach for potentials of variable attractive range (SAFT-VR) [36] with the MSA expressions for the restrictive primitive model (i.e., an equimolar mixture of equal-diameter hard spheres in a dielectric continuum). In related work, Tan et al. [219] proposed a version of SAFT1 (a variant of SAFT-VR) for electrolyte solutions that also uses the restrictive primitive model. In other examples, the perturbed chain SAFT (PC-SAFT) [24] equation was combined with a simple DH term to develop the ePC-SAFT [226] equation and the polar perturbed chain (PPC)-SAFT equation was combined with the MSA to develop a primitive model of electrolyte solutions in the ePPC-SAFT equation [236]. In these studies we note that the focus was typically on describing the thermodynamic properties and phase equilibrium of

single solvent and sometimes mixed salt electrolyte systems; only the SAFT-VRE [218] and ePC-SAFT equations have been applied to the study of mixed (i.e., water/ alcohol and water/ alkane) solvent electrolytes.

In the area of mixed solvent electrolyte systems, the SAFT-VRE [218] equation was applied to study the phase behavior of alkane + water + salt solutions [293]. The dielectric constant, required in this primitive model approach, was calculated using a temperature dependent correlation equation obtained by fitting to the pure water experimental dielectric data from 273 to 623 K. The effect of the second solvent or ions on the dielectric behavior of the solution is therefore not accounted for. In the ePC-SAFT equation of state [294], which was applied to study the thermodynamic properties of water + alcohol + salt systems (salts composed of Na^+, Li^+, K^+, $NH4^+$, Cl^-, Br^-, I^- ions in ethanol or methanol and water), the solvent composition and temperature dependent dielectric constant data were again obtained from an empirical correlation and required as an input to the equation of state. We note that more recently, a modified version of the SAFT-VRE equation [218] in which a Born solvation energy contribution was incorporated into the theory has been proposed and applied to study the VLE/ LLE of four mixed solvent electrolyte solutions. Although the inclusion of the Born term provides a better representation of solvation effects at the infinite dilution limit than in the original SAFT-VRE formalism, the explicit representation of long-ranged ion-dipole and dipole-dipole interactions are still absent from the theoretical framework. In this work, the dielectric constant was obtained following the empirical approach of Uematsu and Franck [221], which takes into account the temperature, density and composition of

the solvent and in turn makes the dielectric constant differentiable with respect to these same variables.

A common feature of these SAFT-based approaches and the previously mentioned activity-coefficient-based models is the implicit treatment of the solvent. A more comprehensive approach is to consider solvent molecules explicitly within the electrolyte solution, using a Born-Oppenheimer level model [187]. Analytical expressions to calculate the free energy and thermodynamic properties of a mixture of dipolar and charged hard spheres of arbitrary sizes was derived by Blum and Wei [204] using integral equation theory in which the Ornstein-Zernike equation was solved within the non-primitive MSA (NPMSA) closure. The solution provides mathematical expressions for the contribution to the free energy and pair correlation function for the ion-ion, ion-dipole, and dipole-dipole interactions. Recently, Zhao et al. [210] combined the SAFT-VR equation of state and the generalized mean spherical approximation (GMSA) using the non-primitive model to describe the long-range ion-ion, ion-dipole, and dipole-dipole interactions to develop the SAFT-VR+DE equation, a non-primitive-model-based electrolyte version of the SAFT-VR equation. The predictions of PVT behavior for several model electrolyte fluids were compared against NPT Monte Carlo simulation data for systems of different ionic concentrations and different ratio of the cation, anion, and solvent segment diameters to test the accuracy of the approach. Comparisons were also made with the DH and primitive models, illustrating that the full non-primitive model better captures the electrostatic interactions due to the explicit consideration of solvent. The importance of properly accounting for the difference in size between the ions and solvent and providing an accurate description of the dielectric

constant was also shown. In subsequent work, the SAFT-VR+DE equation of state was applied to study nineteen aqueous alkali halide electrolyte systems and evaluate a range of thermodynamic properties, including the mean ionic activity coefficient, osmotic coefficient, water activity coefficient, density, Gibbs free energy of hydration, and the dielectric decay [295]. The results demonstrate that when developing a predictive equation of state for a family of electrolyte solutions, a uniform model is not appropriate and the nature of the salt and the concentration range being studied should be taken into account and the model tailored to capture the correct interactions. Specifically when studying electrolyte solutions from infinite dilution to the fused salt limit, while a fully dissociated model of electrolytes can be expected to capture the thermodynamic behavior at low to moderate concentrations at higher concentrations, with the changes in intermolecular/ ionic interactions, the underlying theoretical considerations should also change and depending upon the nature of the ions, ion association or enhanced anion-solvent interactions should be considered.

Since statistical-mechanics-based equations of state like SAFT are formulated upon a well-defined molecular model, they have an inherent advantage over more empirical approaches as the approximations made in the development of the theory can be rigorously tested through comparison with computer simulation results for the exact same model. This allows the accuracy of the theory to be determined before comparison with experimental data and parameters are fitted [216]. This approach has been used heavily in the development and testing of new versions of the SAFT equation of state. For example, in the development of the SAFT-VR+D approach, which describes dipolar associating fluids and explicitly considers the effect of dipolar interactions on both the

thermodynamics and structure of the fluid, the theoretical framework was extensively tested against isothermal-isobaric (NPT) and Gibbs ensemble Monte Carlo simulation data for the thermodynamic properties and phase behavior of several model dipolar square-well monomer and chain fluids before application to experimental fluids. Similarly, as described above the SAFT-VR+DE equation was first validated using computer simulation results [210] before being applied to study experimental systems [295]. Through such studies systematic improvements to the theory can be made that allows the accuracy of the SAFT-based equations to continually evolve.

In this work, the SAFT-VR+DE equation of state has been applied to the study of mixed dipolar solvent electrolyte systems, i.e., ions solvated by at least two distinct dipolar solvent species. Computer simulations have been performed for a series of different molecular models to test the theory before experimental mixed dipolar solvent electrolyte systems are studied. Specifically simulations have been performed in which, the size of the cation, anion, and solvents are assumed to be equal (known as the semi-non-primitive model), the ions and solvents are of different sizes while the cation and anion have equal and also different diameters (known as the unrestricted non-primitive model). The effect of the dipole moment of each solvent and ion concentration is also investigated and a comparison with the primitive model of electrolytes included to examine the effect of using a salt-concentration-dependent dielectric constant on the theoretical predictions.

The remainder of the chapter is organized as follows: In chapter 5, I present the SAFT-VR+DE model as applied to mixed dipolar solvent electrolyte solutions, along with the primitive model approach. In section 3, details of the molecular simulations

performed are presented. A comparison of the theoretical predictions and simulation results are presented in section 4 and concluding remarks made in section 5.

5.2 Molecular model and theory

Mixed dipolar solvent electrolyte solutions are modeled as a mixture of charged ions of arbitrary size within a dipolar associating solvent composed of molecules of arbitrary size and polarity as illustrated in figure 5.1. The ions are described as hard spheres, half with charge $+q$ and diameter σ^+, and half with charge $-q$ and diameter σ^-. Two types of dipolar solvent molecules are considered: a monomer fluid that mimics water molecules and a dimer fluid that represents a second solvent such as an alcohol. The monomer solvent is described by diameter σ_{d1} and dipole moment μ_{d1} and contains four association sites, two each of different kinds that represent hydrogen bonding sites (i.e., mimicking H and O atoms in water). The dimer solvent molecules are described by segments of diameter σ_{d2} and embedded dipole moment of μ_{d2} with two association sites.

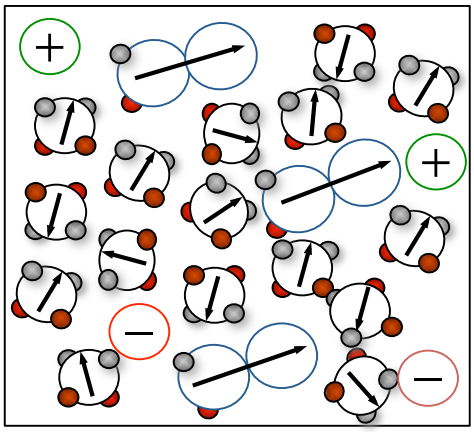

Figure 5.1 Schematic representation of the molecular model used in the SAFT-VR+DE equation to describe mixed solvent electrolyte solutions containing ions and two types of associating dipolar solvent.

The potential model for interaction between solvent and ionic species is given by,

$$u(r) = u^{SW}(r) + u^{CC}(r) + u^{CD}(r) + u^{DD}(r) \tag{5.1}$$

where the square-well, coulombic charge-charge, charge dipole, and dipole-dipole interactions are represented by u^{SW}, u^{CC}, u^{CD}, and u^{DD} potentials, respectively.

The solution of the Ornstein-Zernike with the NPMSA closure proposed by Blum et al. [296] was for ions of arbitrary sizes in a dipolar solvent with a separate segment diameter. No solution of the NPMSA has been developed to date for ions of arbitrary size in a solvent composed of more than one type of dipolar species. This limitation to the application of the NPMSA to the study of mixed dipolar solvent electrolytes has been circumvented in this work by using a one-fluid type approximation in the ion-dipole and dipole-dipole terms within the SAFT-VR+DE equation of state. It is therefore assumed that the properties of the solvent can be described by those of a hypothetical fluid that is represented through an effective segment diameter (σ_{eff}) and dipole moment (μ_{eff})

whose parameters are determined via [297, 298] (a representative diagram has been provided in figure 5.2):

$$\sigma_{eff}^3 = \sum_{i=1}^{n_{solvent}} \sum_{i=1}^{n_{solvent}} x_{s,i} x_{x,j} \sigma_{ij}^3 \tag{5.2}$$

and the dipole moment per segment of effective fluid given by [299],

$$\mu_{eff} = \frac{\sum_{i=1}^{n_{polar}} \sum_{j=1}^{n_{polar}} x_i x_j m_i m_j \left(\frac{\mu_i}{m_i} \frac{\mu_j}{m_j} \right)^{\frac{1}{2}}}{\left(\sum_{i=1}^{n_{polar}} x_i m_i \right)^2} \tag{5.3}$$

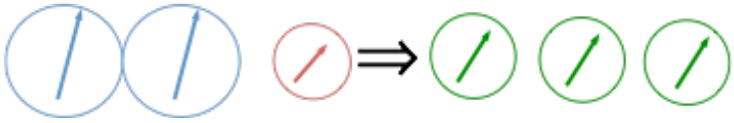

Figure 5.2 Schematic representation of one-fluid like approximation scheme adopted for the theoretical treatement of mixed solvent electrolyte solution using SAFT-VR+DE EoS.

In this work the reference fluid is a mixture of dipolar-charged square well monomer segments and within SAFT-VR+DE theoretical framework the Helmholtz free energy per molecule is given by

$$\frac{A}{Nk_bT} = \frac{A^{ideal}}{Nk_bT} + \frac{A^{mono}}{Nk_bT} + \frac{A^{chain}}{Nk_bT} + \frac{A^{assoc}}{Nk_bT} \tag{5.4}$$

where N is a total number of molecules, k_B is the Boltzmann constant, T is temperature, and A^{ideal}, A^{mono}, A^{chain} and A^{assoc} are the free energy contributions due to the ideal, monomer, and association interactions, respectively. Here only free energy contribution due to chain formation has been described, since all the other free energy contribution terms have already been discussed in previous chapter.

The Helmholtz free energy contribution due to the formation of a chain containing homogeneous monomeric segments is given by,

$$\frac{A^{chain}}{Nk_bT} = \sum_{i=1}^{n_{solvent}} x_i \left(1-m_i\right) \ln g_{ii}^{M}\left(\sigma_{ii}\right) \tag{5.5}$$

where, the sum is over all solvent compounds in the mixture and g^M represents the contact value of the radial distribution function (RDF) of monomer segments. Since solvent molecules are described as dipolar SW molecules, the required g^M is that of the dipolar square well fluid, i.e., g^{DSW} and is obtained from the linearized version of the exponential (LEXP) approximation [37]. As shown in previous work [37], the LEXP approximation for the RDF is more accurate than the MSA, as it provides a better description of PVT and VLE properties of dipolar dispersive square well chain fluids, while comparing against NPT and GEMC computer simulation data. The RDF at contact value due to square-well dispersive interaction is given by,

$$g^{DSW}\left(r\omega_1\omega_2;\rho,T\right) = g^{SW}\left(r;\rho,T\right)\left(1+g^{D}\left(\omega_1\omega_2;\rho,T\right)\right) \tag{5.6}$$

where $\left(g^{SW}\right)$ and $\left(g^{D}\right)$ are square well and dipolar RDF at contact values

$$g_{ij}^{sw}(\sigma_{ij}) = g^{hs}(\sigma_{ij}) + \beta\varepsilon_{ij} g_1(\sigma_{ij}) \tag{5.7}$$

$$g_1(\sigma_{ij}) = \frac{1}{2\pi\varepsilon_{ij}\sigma_{ij}^3}\left[3\left(\frac{\partial a_1^{ij}}{\partial\rho_s}\right) - \frac{\lambda_{ij}}{\rho_s}\frac{\partial a_1^{ij}}{\partial\lambda_{ij}}\right] \tag{5.8}$$

Contact value of RDF due to dipolar interactions is given by,[296, 300]

$$\begin{aligned} g_{nn}^{D}\left(\sigma_n\right) = g_{nn}^{000}\left(\sigma_n\right)\phi_{00}^{000}\left(\Omega_1,\Omega_2,\Omega_r\right) + g_{nn}^{110}\left(\sigma_n\right)\phi_{00}^{110}\left(\Omega_1,\Omega_2,\Omega_r\right) \\ + g_{nn}^{112}\left(\sigma_n\right)\phi_{00}^{112}\left(\Omega_1,\Omega_2,\Omega_r\right) \end{aligned} \tag{5.9}$$

where, $\phi_{00}^{mnl}(\Omega_1,\Omega_1,\Omega_r)$ denote rotational invariant and $g_{nn}^{mnl}(\sigma_{nn})$ are the coefficients of rotational invariant expansion of the contact value. It reads[301],

$$g_{nn}^{000} = \frac{1}{\Delta} + \frac{\pi\zeta_2\sigma_n}{4\Delta^2} \tag{5.10}$$

$$g_{nn}^{110} = \frac{\left(Q_{nn}^{'11} + \frac{2q^{'}}{\rho_n\sigma_n^2}\right)}{2\sqrt{3}\pi\sigma_n} \tag{5.11}$$

$$g_{nn}^{112} = \sqrt{10}\frac{\left(Q_{nn}^{'11} - \frac{2q^{'}}{\rho_n\sigma_n^2}\right)}{2\sqrt{3}\pi\sigma_n} \tag{5.12}$$

with,

$$q^{'} = \frac{-b_2(1-\lambda)(\lambda+3)}{(1+\lambda)^2} \tag{5.13}$$

and,

$$Q_{nn}^{'11} = \frac{2\lambda}{D\rho_n\sigma_n^2}\left[\lambda + \frac{\rho_n\sigma_n^2\Omega^{10}a_n^1}{2\beta_6^2}\right] + \frac{a_nB^{10}a_n^1}{2\beta_6} - \frac{2}{\rho_n\sigma_n^2} \tag{5.14}$$

where, $\Delta = 1 - \frac{\pi}{6}\sum_{i=1}^{n}\rho_i\sigma_i^3$ and $\zeta_2 = \sum_{i=1}^{n}\rho_i\sigma_i^2$ with ρ_i and σ_i representing density and segment diameter of individual species in the solution. ρ_n and σ_n are the density and segment diameter of the dipolar solvent species present in the solution. The parameters B^{10} and b_2 corresponds to the ion-dipole and dipole-dipole interactions respectively, and are obtained from the solution of Ornstein-Zernike equation given by Wei and Blum. The

quantities β_6, λ are related to dipolar strength parameters and expressions are given by,

$\beta_6 = 1 - \frac{1}{6} b_2$, $\beta_3 = 1 + \frac{1}{3} b_2$ and $\lambda = \frac{\beta_3}{\beta_6}$.

The expression for a_n^1 is given by, $a_n^1 = \frac{D\beta_6}{2D_{ac}} \left[\frac{\sigma_n B_{10}}{2} + \frac{\Omega^{10} \lambda}{D\beta_6} \right]$ with the quantities D, Ω^{10}, D_{ac} are obtained from following expressions,

$$D = 1 + \upsilon_\eta^2 \rho_n \sigma_n^2 \sum_{i=1}^{n-1} \frac{\rho_i \sigma_i^2 \left(D_i^F \right)^2}{\left[2\beta_6 \left(\sigma_n + \lambda \sigma_i \right) \right]^2}$$

$$D_{ac} = \sum_{i=1}^{n-1} \rho_i \left(D_i^F \right)^2, \; D_i^F = \frac{z_i \beta_6}{2\left(1 + \sigma_i \Gamma - \Delta\Gamma_i \right)}$$

$$\Omega_{10} = \upsilon_\eta \sum_{i=1}^{n-1} \frac{\rho_i \sigma_i \left(D_i^F \right)^2}{\left(\sigma_n + \lambda \sigma_i \right)}$$

where, z_i is the charge of individual ions, Γ is the ionic screening parameter and υ_η is related to ion-dipole and dipole-dipole strength parameters B^{10} and β_6.

The coefficients of rotational invariant g_{nn}^{mnl} is only dependent upon center-to-center distance r_{ij}, while the angular dependence of the correlations is given by the rotational invariant which is expressed as [302],

$$\hat{\phi}_{00}^{mnl}(\Omega_1, \Omega_2, \Omega_r) = \sqrt{(2m+1)(2n+1)} \sum_{\mu=-m}^{m} \sum_{\nu=-n}^{n} \sum_{\lambda=-l}^{l} \begin{pmatrix} m & n & l \\ \mu & \nu & \lambda \end{pmatrix} D_{0,\mu}^m(\Omega_1) D_{0,\nu}^n(\Omega_2) D_{0,\lambda}^l(\Omega_3) \quad (5.15)$$

Where, $\begin{pmatrix} m & n & l \\ \mu & \nu & \lambda \end{pmatrix}$ is a 3j-symbol, and, $D_{0n}^l(\Omega \equiv \phi\varphi\chi) = (-1)^n \left(\frac{4\pi}{2l+1} \right)^{\frac{1}{2}} Y_n^l(\phi\chi)$ denotes rotation matrix[302], where $Y_n^l(\phi\chi)$ is a spherical harmonic function.

$$Y_n^l(\theta\phi) = (-1)^n \left(\frac{2l+1}{4\pi}\right)^{1/2} \left(\frac{(l-n)!}{(l+n)!}\right)^{1/2} P_{ln}(\cos\theta) e^{in\phi}$$

with $i = \sqrt{-1}$ and P_{ln} is associated Legendre function.

$$P_{ln}(x) = (1-x^2)^{n/2} \left(\frac{d}{dx}\right)^n P_l(x)$$

where $P_l(x)$ is Legendre polynomial defined for x in the range $(-1,1)$.

5.3 Simulation

Monte Carlo simulations in the isothermal-isobaric (*NPT*) ensemble have been performed to study the PVT behavior of several model mixed dipolar solvent electrolyte systems. Each simulation was started from an initial configuration in which 256 molecules were placed in random orientations on the sites of a face centered cubic lattice in a simulation box with periodic boundary conditions. The long-range charge-charge, charge-dipole, and dipole-dipole interactions between polar solvents and charged ions were captured through the reaction field method [303-306]. The reaction field method has shown to be as accurate as the Ewald sum for calculating long-range dipolar and electrostatic forces [307-310]. In the reaction field method, the long-range interactions are truncated at a finite cut-off distance from each ion and dipolar molecule, and replaced by a dielectric continuum. The effect of the dielectric continuum is taken into account by including an additional term into the long-range charge-charge, charge-dipole, and dipole-dipole interaction potentials. viz.,

$$u^{CC} = \begin{cases} q_i q_j \left[1/r + \left((\varepsilon_{RF}-1)/(2\varepsilon_{RF}+1)\right)\left(r^2/r_c^3\right)\right], & r < r_c \\ 0 & r \geq r_c \end{cases} \qquad (5.16)$$

$$u^{CD} = \begin{cases} \left[\left(2\left(\varepsilon_{RF}-1\right)/\left(\varepsilon_{RF}+1\right)\right)\left(r/r_c\right)q.u\right] & r < r_c \\ 0 & r \geq r_c \end{cases} \tag{5.17}$$

$$u^{CD} = \begin{cases} \left[-\left(\mu_1\mu_2/r^3\right)D-\left(2\left(\varepsilon_{RF}-1\right)/\left(2\varepsilon_{RF}+1\right)\right)\left(\mu_1\mu_2/r_c^3\right)\right], & r < r_c \\ 0, & r \geq r_c \end{cases} \tag{5.18}$$

where, r_c is the cut-off distance beyond which the pair potential is set to zero and ε_{RF} is the dielectric constant of the continuum. In our simulations, the value of r_c is set to 3.0 and ε_{RF} to ∞.

In the systems included in this study, the solvent molecules are highly associative. This kind of strong association interaction between molecules can promote the formation of stable clusters, making the complete sampling of phase space challenging [311-313]. To avoid poor sampling, several biasing schemes have been proposed in the literature [311, 312, 314-316]. For example, the association-biased Monte Carlo (ABMC) [317] method, which strategically biases the configuration site where association is likely to occur, was the first biasing scheme to be proposed however it requires the determination of bonding regions, making the algorithm rather complex. Subsequently, Tsangaris et al. developed the bond bias Monte Carlo method for the sampling of dimer clusters [311] and Visco et al. [312] proposed the monomer-addition-subtraction algorithm for the study of linear and ring aggregates. More recently, Chen et al. [313] proposed the aggregation volume bias Monte Carlo (AVBMC) biasing scheme, which can be applied to any cluster

architecture (i.e., it is not restricted to the sampling of dimers, chains or rings) and is computationally more efficient as the identification of clusters is not required. In the simulations reported here, although systems with low association energy (i.e., $\varepsilon^{HB} < 10\varepsilon$) are studied and so are outside of range in which regular GEMC simulations are expected to fail [311], we have used the AVBMC biasing scheme developed by Chen et. al. [313] to avoid potential issues of poor sampling and increase the reliability of the PVT data

The AVBMC biasing scheme enhances the efficiency of the sampling by targeted sampling for the formation and destruction of clusters. It works as an intrabox swap move where four kinds of moves are allowed. (1) Placing a randomly selected particle within the bonded region (where association takes place) of another randomly selected target particle (termed as out-in move); (2) displacing a random particle from a bonded region to non-bonded region (termed as in-out move); (3) placing a particle from bonded region to another bonded region (termed as in-in move); (4) placing a particle from non-bonded region to another non-bonded region (termed as out-out move). The first two kinds of swap move carried out with a bias in probability of P_{bias}. The acceptance criteria for accepting the moves in-out and out-in (1 and 2) are given with the following set of acceptance probabilitie

$$acc(A_{out} \to B_{in}) = \min\left[1, \frac{(1-P_{bias}) \times V_{in} \times \exp\left(-\Delta E / k_b T\right)}{P_{bias} \times V_{out}}\right] \tag{5.19}$$

$$acc(A_{in} \to B_{out}) = \min\left[1, \frac{P_{bias} \times V_{out} \times \exp\left(-\Delta E / k_b T\right)}{(1-P_{bias}) \times V_{in}}\right] \tag{5.20}$$

For the next two cases (move type 3 and 4) in which particle follow *out- out* or *in- in* moves, the standard Metropolis acceptance rule is used. Each of the in-moves and out-moves outlined is selected with equal probability (this corresponds to the $P_{\text{bias}} = 0.5$). In

the above equations, V_{in} and V_{out} denotes the in and out volumes of the bonded regions, respectively where V_{in} is given by bonding volume per particle represented as,

$$V_{in} = \frac{\pi\left(1-\cos\theta\right)^2 \sigma^3 \left(\lambda^3 - 1\right)}{3} \tag{5.21}$$

$$\text{and} \quad V_{out} = V_{box} - V_{in}$$

where V_{box} is the volume of the simulation box.

The potential model for the associative interactions is given by,

$$u(r_{12};\theta_i,\theta_j) = \begin{cases} \varepsilon^{HB}, & \sigma \le r_{ij} < r_{12} \quad and \quad \left|\theta_i\right| < \theta_c \quad and \quad \left|\pi - \left|\theta_j\right|\right| < \theta_c \\ 0 & otherwise, \end{cases} \tag{5.22}$$

where, θ_i and θ_j are the angles between the direction vectors and the center-to-center vector of atoms *i* and *j* respectively. Different association sites residing upon the same or different molecules can interact with a short-ranged associating energy of magnitude ε^{HB}. Although, in Wertheim's theory, bonding is limited at each association site to dimers, higher order cluster formation is possible depending upon the size of the association site, strength of the site-site interactions, and the state conditions as illustrated by Docherty and Galindo [318]. In this work, the angular cut-off θ_c is set to 27° in order to restrict bonding to dimer formation [147].

The AVBMC move has been used in conjunction with traditional Monte Carlo displacement, rotation and volume moves. In a single simulation cycle, N trial displacement, rotations, and AVBMC moves along with one volume change move has been employed. The extent of displacement, reorientation, AVBMC and volume trial

moves has been adjusted so that individual acceptance probabilities are between 20-30%. An initial simulation of 500000–1000000 cycles was performed to equilibrate the system before averaging for between 1000000 and 2000000 cycles. In order to examine whether equilibrium had been reached or not, several simulations from different initial configurations were performed and results for the thermodynamic properties compared. For each system studied, the packing fraction and system energy at a given reduced pressure are reported and were obtained as ensemble averages and the errors estimated by taking the standard deviation.

5.4 Results and discussion

A complete list of systems studied by Monte Carlo simulation is provided in Table 5.1. In systems 1 and 2, the effect of solvent polarity on the PVT behavior is evaluated while systems 1, 3 and 4 enable the effect of different ionic concentrations on the PVT behavior to be examined. In order to take that into account the effect of solvent composition, in systems 1, 5 and 6 we consider different ratios of monomer and dimer solvent molecules. We note that systems 1-6 are symmetric in nature as all the ions and molecules have the same segment diameter; however, in experimental mixed solvent electrolyte systems the ions and solvent molecules are of different sizes. Therefore the effect of ion and solvent molecule size on the thermodynamics of the fluid has been tested in systems 7 and 8. The results of the NPT Monte Carlo simulations are provided in Table 5.2.

Table 5.1 Model parameters for the electrolyte fluids studied. σ_{d1}, σ_{d2}, σ^{*+} and σ^{*-} are the reduced diameter of the solvent 1 (monomer), solvent 2 (dimer), cation and anion molecules respectively. μ_{d1}^{*2} and μ_{d2}^{*2} are the reduced squared dipole moments of solvent 1 and solvent 2, where $\mu^{*2} = \mu^2 / k_b T \sigma^3$, ε^* is the reduced depth of the square-well potential, λ the range of the potential, ψ^* the reduced association energy, r_c^* the reduced association cutoff radius, N_{ion} the number of ions, and $N_{solvent1}$, $N_{solvent2}$ the number of monomer and dimer solvent molecules.

System	σ_{d1}^*	σ_{d2}^*	σ_+^*	σ_-^*	μ_{d1}^{*2}	μ_{d2}^{*2}	ε^*	λ	ψ^*	r_c^*	N_{ion}	$N_{solvent1}$	$N_{solvent2}$
1	1	1	1	1	1	2	1	1.5	5	1.05	8	124	124
2	1	1	1	1	1	4	1	1.5	5	1.05	8	124	124
3	1	1	1	1	1	2	1	1.5	5	1.05	4	126	126
4	1	1	1	1	1	2	1	1.5	5	1.05	16	120	120
5	1	1	1	1	1	2	1	1.5	5	1.05	8	200	48
6	1	1	1	1	1	2	1	1.5	5	1.05	8	4	244
7	1	4/3	1	1	1	2	1	1.5	5	1.05	8	124	124
8	1	4/3	2/3	5/3	1	2	1	1.5	5	1.05	8	124	124

In Figure 5.3, a comparison has been made between SAFT-VR+DE theoretical predictions and Monte Carlo NPT ensemble simulation results for the PVT behavior of systems 1 and 2. From the figure we can see that over the range of temperatures studied (T^*=1.2, 1.4, 1.6, 1.8), the theory is found to be in good agreement with the simulation results. In system 2, compared to system 1, the polarity of dimer molecules increases (from μ_{d2}^{*2} = 2 to 4), which results in increased attractive interactions between the solvent molecules and an increase in the density at a fixed pressure. Although the theory correctly captures this trend, we note that at higher temperatures for system 2 the theory

under predicts the density as shown in figure 5.3b; however, the deviations are well within the errors as reported in table 5.2.

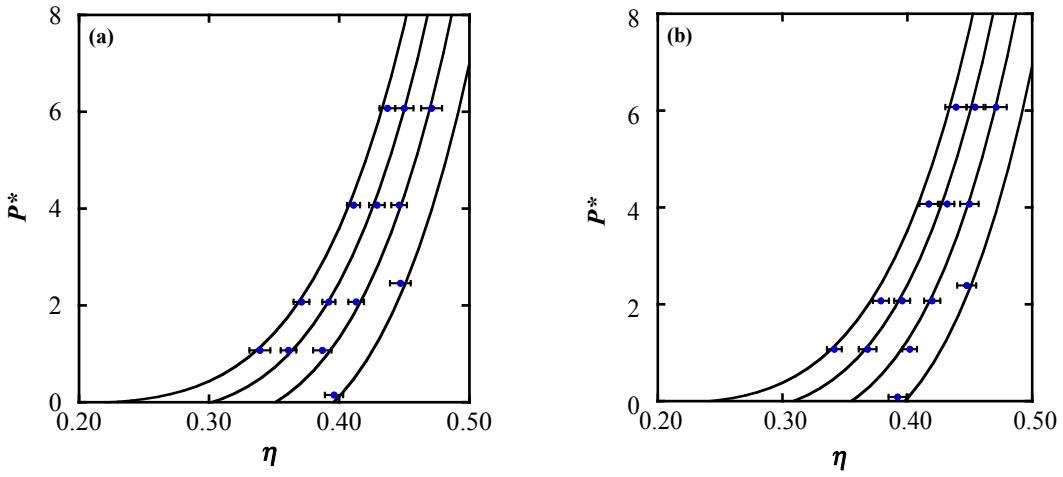

Figure 5.3 Comparison of predictions from the SAFT-VR + DE equation and *NPT* Monte Carlo simulation results for symmetric electrolyte solutions with $\varepsilon^* = 1.0$, $\lambda = 1.5$, $\sigma^{+*} = \sigma^{-*} = \sigma^*_{d1} = \sigma^*_{d2} = 1.0$, $\psi^* = 5.0$, $r_c^* = 1.05$, charge $q = 1$, ion concentration of 8 / 256, and (a) dipole moment $\mu^{*2}_{d1} = 0.5$ and $\mu^{*2}_{d2} = 2.0$ at T* = 1.2, 1.4, 1.6 and 1.8 for system 1 and (b) dipole moment $\mu^{*2}_{d1} = 0.5$ and $\mu^{*2}_{d2} = 4.0$ at T* = 1.2, 1.4, 1.6, and 1.8 for system 2. The solid lines represent predictions from the modified SAFT-VR + DE equation and the squares the NPT Monte Carlo simulation data.

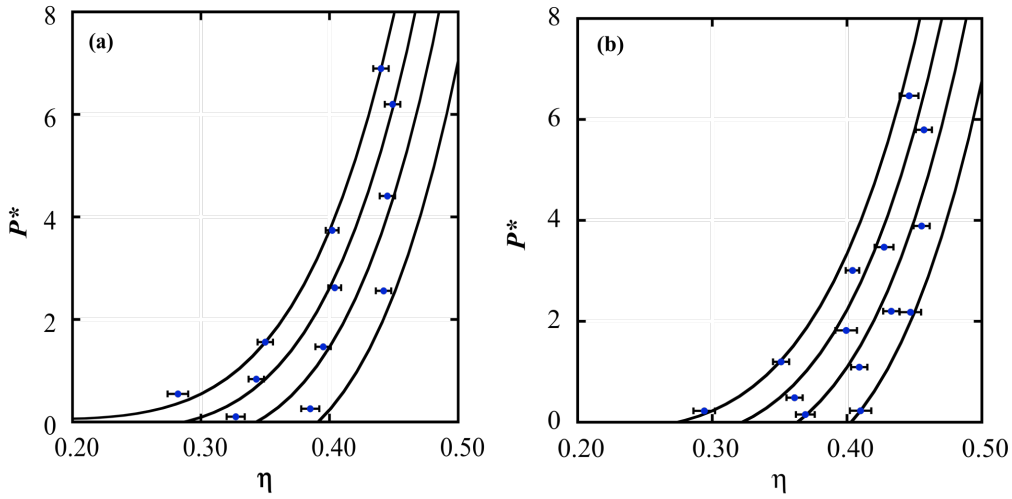

Figure 5.4. Comparison of predictions from the SAFT-VR + DE equation and *NPT* Monte Carlo simulation results for symmetric electrolyte solutions with $\varepsilon^* = 1.0$, $\lambda = 1.5$, $\sigma^{+*} = \sigma^{-*} = \sigma^*_{d1} = \sigma^*_{d2} = 1.0$, $\psi^* = 5.0$, $r_c^* = 1.05$, charge $q = 1$, dipole moment $\mu^{*2}_{d1} = 0.5$ and $\mu^{*2}_{d2} = 2.0$ at T* = 1.2, 1.4, 1.6 and 1.8 for ion concentration of (a) 4 / 256, and (b) 16 / 256. The solid lines represent predictions from the modified SAFT-VR + DE equation and the squares the NPT Monte Carlo simulation data.

Systems 1 and 2 contain 8 ions (4 cations and 4 anions) along with 248 solvent (both monomer and dimer) molecules. In experimental electrolyte systems, thermodynamic properties vary as a function of ion concentration. In order to test whether the proposed approach can capture the effect of changes in ion concentration systems 3 and 4 are studied in which the ion concentrations are 0.79% (4/256) and 3.2% (16/256) mol % of salt respectively. We note for comparison that 0.79% and 3.2% corresponds to 0.344 and 1.446 *m*, respectively for a methanol + water + NaCl solution. The highest tested molality of 1.446 *m* is comparable to experimental mixed solvent electrolyte systems as the majority of the available experimental data is below 1.5 m. The results for systems 3 and 4 are presented in figure. 5.4, from which we can see that the

theoretical predictions and Monte Carlo simulation results are in good agreement for both systems. As the concentration of the ions increases, the density at a given pressure and temperature increases, due to the increased attractive interaction. However, at higher ionic concentrations, the SAFT-VR+DE equation slightly over predicts the pressure, perhaps due to approximating the ion-dipolar interactions through those of an effective fluid.

In addition to the concentration of ions in electrolyte solutions, the composition of the solvent in mixed solvent electrolyte systems can play an important role in determining the thermodynamic properties [319]. For example, in the measurement of mean ionic activity coefficients for NaBr + ethanol + water the ionic activity was found to change from 0.6643 to 0.2951 at 0.31 salt molality (m) with a change in the solvent ratio between water and ethanol from 9:1 to 1:9 [319]. To examine this effect. in systems 5 and 6 the ratio of the dimer and monomer solvent is varied from the 50:50 mixture used in systems 1 – 4 (i.e., in systems 1-4, the solvent molecules are divided equally between the monomer and dimers molecule). In system 5 200/248 and in system 6 4/248 particles are considered monomers, whereas the number of ions is maintained at 8 in both cases. The polarity of the systems studied also increases as the number of dimers in the system increases, due to the higher dipole moment in the dimer molecules compared to the monomer molecules. As a result, as shown in figure 5.5, the density of system 6 is higher at a given temperature and pressure than for system 5. For system 1 with a 50:50 mixture of dimer and monomer solvent species the solution density lies as expected in between system 5 and 6 at a specific temperature and pressure. From figure 5.5, it can also be seen that the theory is able to capture this change in the PVT behavior and is in good

agreement with the simulation results.

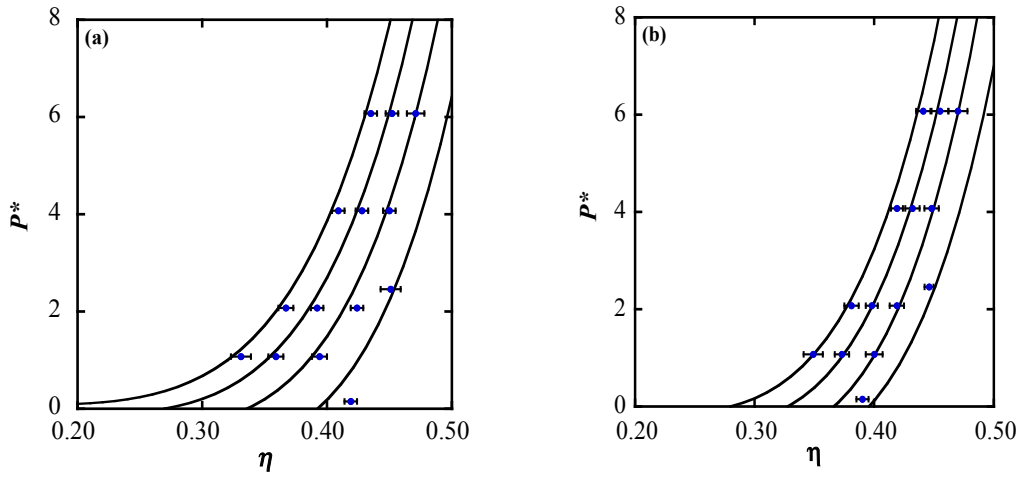

Figure 5.5. Comparison of predictions from the SAFT-VR + DE equation and *NPT* Monte Carlo simulation results for symmetric electrolyte solutions with $\varepsilon^* = 1.0$, $\lambda = 1.5$, $\sigma^{+*} = \sigma^{-*} = \sigma^*_{d1} = \sigma^*_{d2} = 1.0$, $\psi^* = 5.0$, $r_c^* = 1.05$, charge $q = 1$, dipole moment $\mu^{*2}_{d1} = 0.5$ and $\mu^{*2}_{d2} = 2.0$, ion concentration of 8/256 at T* = 1.2, 1.4, 1.6 and 1.8 for different solvent rations. (a) 200 particles of monomers and 48 of dimers; (b) 4 particles of monomers and 244 of dimers. The solid lines represent predictions from the modified SAFT-VR + DE equation and the squares the NPT Monte Carlo simulation data.

To more closely mimic experimental systems, we now consider systems (7 and 8) in which the ions and dipolar solvent molecules have different diameters. Experimentally, electrolyte solutions often contain highly asymmetric species, for example the LiBr + ethanol + water mixture in which Li^+ has an ionic diameter of 1.2 compared to Br^- having an ionic diameter of 3.92 and solvents water and ethanol are of different sizes and polarities. It is therefore desirable to be able to capture the effect of asymmetry on the PVT behavior. In system 7, while the ions have the same diameter, the solvent molecules are asymmetric in nature, with a ratio of 3:4 between the monomer and dimer molecules.

System 8 is composed of completely asymmetric species, with the ratio of monomer, dimer, cation and anion diameters being 3:4:2:5. The results for both systems are presented in figure 5.6, where again we see that the SAFT-VR+DE approach is in good agreement with the simulation data. From a comparison of systems 1, 7, and 8 (Figs. 5.3a, 5.6a, and 5.6b) we note that the asymmetric system (system 8) exhibits the highest density at a given pressure and temperature, while the symmetric system (system1) has the lowest density.

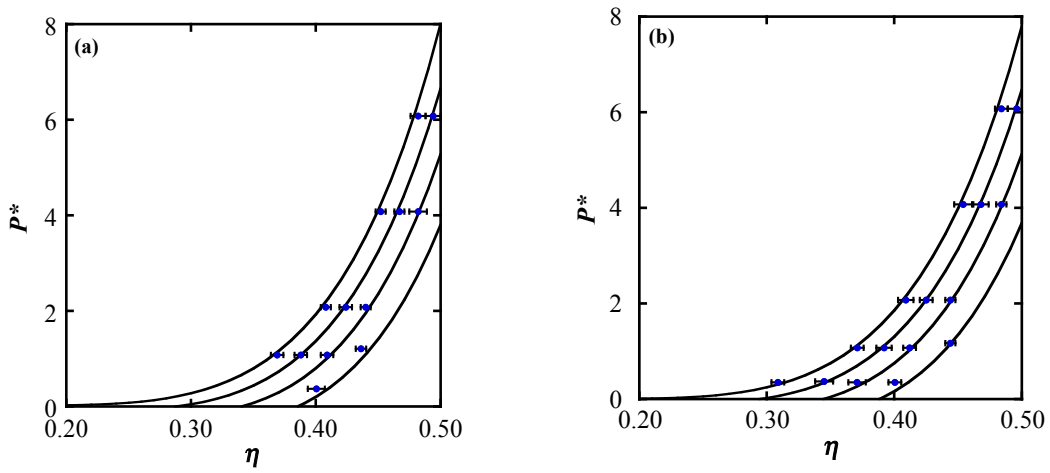

Figure 5.6. Comparison of predictions from the SAFT-VR + DE equation and *NPT* Monte Carlo simulation results for asymmetric electrolyte solutions with $\varepsilon^* = 1.0$, $\lambda = 1.5$, $\psi^* = 5.0$, $r_c^* = 1.05$, charge $q = 1$, dipole moment $\mu_{d1}^{*2} = 0.5$ and $\mu_{d2}^{*2} = 2.0$, ion concentration of 8/256 at T* = 1.2, 1.4, 1.6 and 1.8 for different solvent and ion sizes. (a) $\sigma^{+*} = \sigma^{-*} = \sigma_{d1}^* = 1.0$, $\sigma_{d2}^* = 1.333$; (b) $\sigma^{+*} = 0.667$ $\sigma^{-*} = 1.667$ $\sigma_{d1}^* = 1.0$ $\sigma_{d2}^* = 1.333$. The solid lines represent predictions from the modified SAFT-VR + DE equation and the squares the NPT Monte Carlo simulation data.

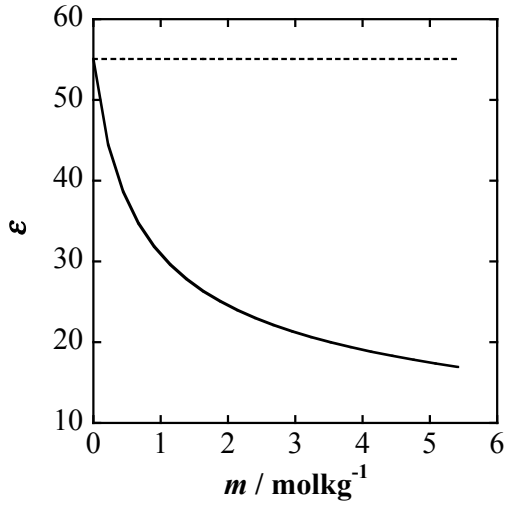

Figure 5.7 Comparison of the ion concentration and solvent composition dependent dielectric constant (solid line) with the solvent concentration dependent dielectric constant calculated predicted from the SAFT-VR+D equation (dotted line) for NaBr + water + (50 weight%) methanol mixed solvent electrolyte systems. The system parameters are given in table 5.3.

Having seen that the non primitive model based SAFT-VR+DE equation of state is able to accurately predict the effect of long-range electrostatic interactions on the thermodynamics of mixed dipolar solvent electrolyte solutions for both symmetric (semi-non primitive model) and asymmetric (unrestricted-non primitive model) model systems, a comparison is now made with the primitive model of electrolytes to highlight the improved accuracy obtained through an implicit representation of solvent species as in the SAFT-VR+DE equation. Since the primitive model employs an implicit solvent the dielectric constant is an input to the calculations and therefore dependent on available experimental data. Although ion concentration in the solution is known to have a significant influence on the solution dielectric [272], with the dielectric constant decreasing as the salt concentration increases, experimental dielectric data as a function of ion concentration is not available for mixed solvent electrolyte systems and so

primitive model approaches must use solvent composition based experimental dielectric constant data that is independent of salt concentration. In the figure 5.7, the SAFT-VR+DE prediction for the influence of the ion concentration on the dielectric constant for the NaBr + methanol + water system is presented. As can be seen from the figure, the theory predicts a significant reduction in the dielectric constant with increasing salt molality at 50 weight % composition of methanol-water. Although no experimental data is available for verification, the trend predicted by the SAFT-VR+DE equation is consistent with that observed in experimental studies of aqueous (i.e., single solvent) electrolyte systems [272].

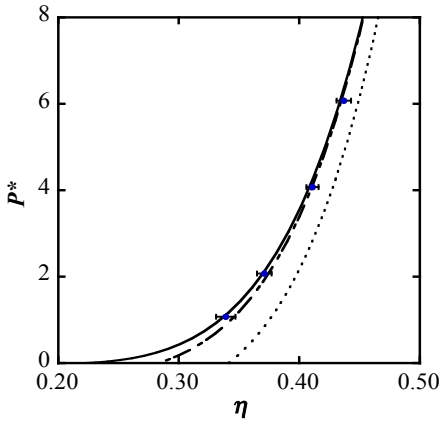

Figure 5.8. Comparison of predictions from the SAFT-VR + DE equation and *NPT* Monte Carlo simulation data for symmetric electrolyte solutions with $\varepsilon^* = 1.0$, $\lambda = 1.5$, $\sigma^{+*} = \sigma^{-*} = \sigma^*_{d1} = \sigma^*_{d2} = 1.0$, $\psi^* = 5.0$, $r_c^* = 1.05$, charge $q = 1$, dipole moment $\mu^{*2}_{d1} = 0.5$ and $\mu^{*2}_{d2} = 2.0$, and ion concentrations of 8 / 256 (124 monomers and 124 dimers) at $T^* = 1.8$. The solid line represents predictions from the non-primitive model based SAFT-VR + DE, dotted line represents predictions from the primitive model + SAFT-VR using a solvent composition based (and salt concentration independent) dielectric constant, dash-dotted line represents predictions form the PM + SAFT-VR using a salt concentration and solvent composition dependent dielectric constant, and the squares are NPT Monte Carlo simulation results.

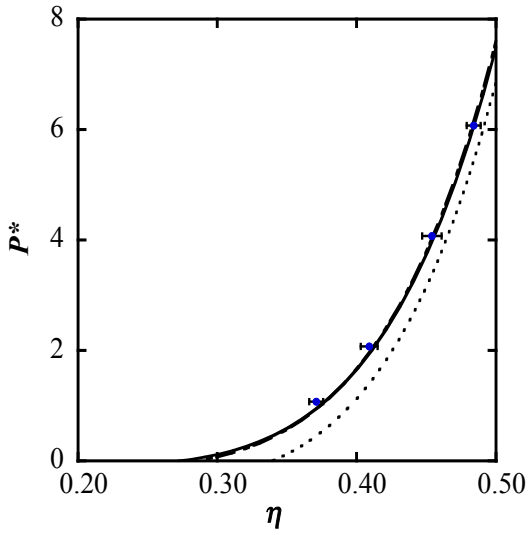

Figure 5.9. Comparison of predictions from the SAFT-VR + DE equation and *NPT* Monte Carlo simulation data for asymmetric electrolyte solutions with ε^* = 1.0, λ = 1.5, σ^{+*} =0.667, σ^{-*} = 1.667, σ^*_{d1} = 1.0, σ^*_{d2} = 1.333, ψ^* = 5.0, r_c^* = 1.05, charge q = 1, dipole moment μ^{*2}_{d1} = 0.5 and μ^{*2}_{d2} = 2.0, and ion concentrations of 8 / 256 (124 monomers and 124 dimers) at T^* = 1.8. The solid line represents predictions from the non-primitive model based SAFT-VR + DE, dotted line represents predictions from the primitive model + SAFT-VR using a solvent composition based (and salt concentration independent) dielectric constant, dash-dotted line represents predictions form the PM + SAFT-VR using a salt concentration and solvent composition dependent dielectric constant, and the squares are NPT Monte Carlo simulation results.

To quantify the effect of an ionic concentration based dielectric constant on the predictive ability of an equation of state a comparison has been made between the non-primitive and primitive models, both with and with out the salt concentration dependent dielectric constant in figure. 5.8 for system 1 at T*=1.8. From the figure we can see that the primitive model with a salt concentration independent dielectric constant shows

significant deviations from the simulated PVT results, whereas the non-primitive model provides an accurate prediction. We note that, when the input dielectric constant of the primitive model is changed to a salt concentration dependent one (obtained as an output from the non-primitive model), the primitive model shows immediate improvement in predictive ability and the result is comparable in accuracy with the non-primitive model. Similar trends are observed for the asymmetric system (system 8) as presented in the figure 5.9, i.e., the theoretical predictions of the PVT behavior from the primitive model significantly improve with the use of a salt concentration dependent dielectric constant, with the resulting accuracy being comparable to that of the non-primitive model. The use of the non-primitive model in the development of equation of state for mixed solvent electrolytes is therefore advantageous as it requires no prior knowledge of the appropriate dielectric constant in order to capture changes in the dielectric constant with salt concentration; such information can be hard to obtain for mixed solvent electrolyte systems.

Table 5.2. NPT Monte Carlo simulation results for systems 1–8. The reduced temperature is given by $T^* = k_B T/\varepsilon$, reduced pressure by $P^* = P\sigma^3/\varepsilon$ and reduced energy by $E^* = E/N\varepsilon$.

System	***T****	***P****	η	**Error**	***E****	Error
1	1.2	0.15	0.396	0.007	-12.029	0.513
		2.46	0.447	0.008	-12.841	0.537
	1.4	1.0733	0.387	0.007	-11.711	0.387
		2.0733	0.413	0.006	-12.008	0.373
		4.0733	0.446	0.006	-12.282	0.313
		6.0733	0.471	0.008	-12.655	0.393

	1.6	1.0733	0.361	0.006	-11.003	0.502
		2.0733	0.392	0.005	-11.618	0.409
		4.0733	0.429	0.006	-11.931	0.446
		6.0733	0.450	0.007	-12.662	0.317
	1.8	1.0733	0.339	0.008	-9.926	0.294
		2.0733	0.371	0.006	-11.118	0.520
		4.0733	0.411	0.005	-11.738	0.345
		6.0733	0.437	0.006	-11.950	0.305
2	1.2	0.086	0.392	0.007	-12.588	0.609
		2.3900	0.448	0.008	-13.860	0.559
	1.4	1.0733	0.402	0.006	-12.593	0.368
		2.0733	0.420	0.006	-12.725	0.387
		4.0733	0.450	0.007	-13.051	0.367
		6.0733	0.471	0.009	-14.002	0.601
	1.6	1.0733	0.368	0.007	-11.472	0.557
		2.0733	0.396	0.006	-12.301	0.559
		4.0733	0.432	0.006	-13.205	0.427
		6.0733	0.454	0.007	-13.279	0.481
	1.8	1.0733	0.341	0.007	-10.860	0.359
		2.0733	0.379	0.006	-11.560	0.292
		4.0733	0.417	0.005	-12.461	0.389
		6.0733	0.439	0.006	-12.665	0.279
3	1.2	0.260	0.385	0.007	-8.537	0.242
		2.560	0.442	0.006	-9.516	0.259
	1.4	0.105	0.327	0.009	-7.178	0.245
		1.467	0.395	0.005	-8.139	0.318
		4.410	0.445	0.006	-9.094	0.302

	1.6	0.838	0.343	0.007	-7.168	0.237
		2.619	0.404	0.005	-8.247	0.244
		6.200	0.449	0.006	-8.939	0.273
	1.8	0.549	0.282	0.008	-6.154	0.192
		1.558	0.350	0.006	-7.185	0.196
		3.740	0.402	0.005	-8.038	0.201
		6.895	0.440	0.006	-8.645	0.244
4	1.2	0.23	0.410	0.008	-19.677	0.961
		2.183	0.447	0.008	-20.440	0.840
	1.4	0.154	0.369	0.008	-19.116	0.935
		1.094	0.413	0.007	-20.307	0.900
		4.02	0.456	0.008	-21.267	0.899
	1.6	0.486	0.367	0.009	-18.451	1.081
		1.82	0.401	0.006	-19.821	0.844
		3.47	**0.427**	0.006	-20.523	0.831
		5.794	0.458	0.008	-21.725	1.076
	1.8	0.228	0.303	0.007	-17.269	1.017
		1.198	0.357	0.007	-18.240	0.715
		3.35	0.419	0.006	-20.066	0.721
		6.47	0.447	0.006	-20.126	0.717
5	1.2	0.15	0.419	0.005	-16.477	0.264
		2.46	0.451	0.008	-17.323	0.194
	1.4	1.0733	0.394	0.006	-14.590	0.194
		2.0733	0.424	0.005	-15.218	0.174
		4.0733	0.450	0.005	-15.798	0.183
		6.0733	0.471	0.007	-16.117	0.198
	1.6	1.0733	0.359	1.0733	-13.074	0.175

		2.0733	0.392	2.0733	-14.087	0.165
		4.0733	0.428	4.0733	-15.034	0.255
		6.0733	0.452	6.0733	-15.660	0.169
	1.8	1.0733	0.331	0.008	-12.871	0.191
		2.0733	0.367	0.006	-13.626	0.169
		4.0733	0.409	0.005	-14.105	0.161
		6.0733	0.435	0.005	-14.977	0.157
6	1.2	0.151	0.390	0.005	-10.036	0.182
		2.46	0.446	0.003	-10.861	0.344
	1.4	1.0733	0.400	0.007	-9.803	0.276
		2.0733	0.419	0.006	-10.287	0.199
		4.0733	0.448	0.006	-10.464	0.528
		6.0733	0.470	0.008	-10.626	0.165
	1.6	1.0733	0.373	0.006	-9.081	0.188
		2.0733	0.398	0.005	-9.778	0.255
		4.0733	0.432	0.006	-10.104	0.889
		6.0733	0.455	0.007	-10.246	0.192
	1.8	1.0733	0.349	0.008	-8.678	0.369
		2.0733	0.381	0.006	-9.362	0.161
		4.0733	0.419	0.005	-9.908	0.851
		6.0733	0.441	0.006	-10.063	0.115
7	1.2	0.37	0.404	0.005	-11.371	0.183
		1.21	0.436	0.004	-11.871	0.119
	1.4	1.0773	0.409	0.005	-10.930	0.190
		2.0773	0.441	0.004	-11.532	0.109
		4.0773	0.482	0.011	-11.870	0.728
	1.6	1.0773	0.388	0.005	-10.797	0.117

		2.0773	0.424	0.009	-10.619	0.682
		4.0773	0.467	0.011	-11.458	0.392
		6.0773	0.494	0.011	-12.015	0.277
	1.8	1.0773	0.369	0.009	-9.679	0.159
		2.0773	0.408	0.008	-10.392	0.347
		4.0773	0.452	0.009	-10.869	0.689
		6.0773	0.482	0.011	-10.963	0.531
8	1.2	0.35	0.401	0.005	-10.858	0.125
		1.17	0.435	0.004	-11.096	0.172
	1.4	0.35	0.371	0.006	-10.217	0.189
		1.0733	0.412	0.005	-10.638	0.118
		2.0733	0.443	0.004	-11.060	0.146
		4.0733	0.483	0.003	-12.357	0.298
	1.6	0.35	0.345	0.007	-9.653	0.162
		1.0733	0.392	0.005	-10.338	0.161
		2.0733	0.425	0.008	-10.644	0.468
		4.0733	0.468	0.009	-11.188	0.501
	1.8	0.35	0.309	0.010	-8.799	0.480
		1.0733	0.371	0.008	-9.318	0.469
		2.0733	0.409	0.008	-10.13	0.537
		4.0733	0.454	0.008	-10.85	0.485

Table 5.3 SAFT-VR+DE parameters for water, methanol, Na and Br

	μ(D)	σ (Å)	ε/k_b (K)	λ	m	ε^{HB}/k_b (K)	K^{HB} (Å^3)	ε_{ion-H_2O}	ε_{ion-CH_3OH}
H_2O	2.179	3.003	312.36	1.52956	1	758.5521	1.5		
CH_3OH	2.730	3.539	162.17	1.72229	1.2	1800.945	0.81		
Na		2.8			1			1274.406	1915.47
Br		3.92			1				

5.5 Conclusion

In this work the SAFT-VR+DE approach, which was developed by combining the SAFT-VR equation of state with the solution of the MSA within the non-primitive model, to provide an accurate representation of the free energy contribution due to electrostatic interactions in mixtures of ions and dipolar species, has been extended to the study of mixed dipolar solvent electrolytes. This is achieved using a one-fluid-like approximation in the ion-dipole and dipole-dipole terms. The approach has been extensively tested against PVT data obtained from NPT Monte Carlo simulations for a wide range of model mixed dipolar solvent electrolyte systems that vary in terms of the size of the ions and solvent molecules, polarity of solvent molecules, and salt and solvent composition. The theoretical approach is found to be in general in excellent agreement with the simulated PVT data illustrating that the effects of solvent and ionic size, polarity and composition on the thermodynamics of electrolyte solution are well captured by the theory. Comparisons were also made to predictions from the non primitive model to demonstrate that capturing the salt concentration dependence of the solvent dielectric is important in

order to accurately predict the PVT behavior of mixed solvent electrolyte solutions.

Chapter 6 : Studying the thermodynamic properties of mixed solvent electrolytes using the SAFT-VR+DE equation of State

6.1 Introduction

Over the years development of process modeling and product design tools is aided by advances in thermodynamic modeling[2]. Specifically, advances in equations of state and activity coefficient models enable a quantitative representation of thermophysical properties and phase behavior of mixtures, which serve as a foundation for process modeling and process and product design tools[2]. For example, Peng-Robinson, Soave-Redlich-Kwong are being used as the primary equation of state of choice for the thermodynamic property and phase behavior calculations (e.g. vapor liquid equilibrium (VLE)) in the air separation, gas processing units of petrochemical industries. Polymer non-random two liquid model (NRTL) serves as a model for systems consisting polymers and oligomers. Without these advances in thermodynamics modeling, it would not have been possible to develop these high fidelity process models that are instrumental for process and product design and optimization. Thus, it is essential to continue the development of the thermodynamic modeling framework and in one such effort, based upon Wertheim's seminal work on thermodynamic perturbation theory (TPT1)[199, 213-215], statistical associating fluid theory (SAFT)[11, 61, 211] was proposed. As a molecular model-based equation of state, it accounts for structural and physical anisotropies, which exist in complex chemical systems. In return, SAFT based equations of state have become more predictive compared to classical cubic equations of state. Thus

far, SAFT has been applied to a wide range of important systems from low molecular weight alkanes to simple polymers[12, 13], perfluoroalkanes[14, 15], alcohols[16, 17], water[18, 19], refrigerant systems[20, 21], carbon dioxide[22, 23], biomolecules[31], ionic liquids[320, 321] and their binary mixtures[34, 35]. The success of SAFT as a predictive tool for these systems, has allowed theoretical investigations into more complex systems, where in general cubic equation of state and activity coefficient models are not so efficient in predictive ability. One such system is mixed solvent electrolyte solutions.

Mixed solvent electrolyte solutions find applications in several industrial and natural biological processes. Examples include extractive distillation with salt, solution crystallization, waste and drinking water purification, fertilizer synthesis among many others[45-49]. Often these processes involve electrolyte systems over wide ranges of composition (e.g. aqueous, organic or mixed-solvent, dilute or concentrated solutions) and state conditions (e.g. from ambient temperatures to supercritical conditions). Thus the design of such processes (e.g. extractive distillation with salt or solution crystallization) requires a precise quantitative description of relevant thermodynamic properties such as salt solubility and mean ionic activity coefficient. There are two means of addressing this need; one is by performing experimental measurements and the other through theoretical predictions. As experimental studies on the thermodynamic properties of mixed solvent electrolyte systems are limited[229], theoretical approaches provide an alternate means to studying such systems for the sake of generating “pseudo” experimental data.

The development of a theoretical framework for the calculation of the thermodynamic properties and phase behavior of mixed-solvent electrolyte systems dates

back to the 1960's. In the first such study, Johnson and Furter[322] proposed a quantitative correlative equation, based upon the relation between relative volatility of solvents and salt concentration, for calculating the vapor-liquid equilibrium (VLE) of eighteen different alcohol (methanol/ ethanol/ 1-propanol)/water + salt mixed solvent electrolyte systems. However, the model parameters were dependent upon the salt and solvent compositions and the approach limited to cases where the solubility of salt was low and caused an insignificant increase in the boiling point of the solvent. Ohe[323] later proposed an empirical model for water-alcohol-$CaCl_2$ VLE calculations. The approach, based upon solvation number (ratio of the number of solvent molecules to salt molecules in the preferential solvate) assumed that no solvated salt molecules take part in vaporization. Rousseau et al.[324, 325] were the first to apply activity coefficient models (i.e., van Laar, Wilson, and UNIQUAC) to mixed solvent electrolyte systems and studied ternary mixtures of salt + two solvents as a binary mixture of two pseudo components; one salted-out component (non-preferential solvent component) and one salted-in component (preferential solvent component + salt). The approach was found to accurately correlate (~ 2% deviations in mole fractions) the vapor phase mole fraction data for methanol/ ethanol/ 1-propanol + water + NaBr/ KCl/ NaF/ LiCl/ $HgCl_2$ systems. Jaques and Furter[326] proposed a similar approach for the correlation of the VLE data for 23 water + ethanol + salt systems. Activity coefficient models are representative of local short ranged interactions governed only by local composition and correspond to the so-called Lewis–Randall (LR)[287] framework, where temperature, pressure and mole fractions of all species are independent variables. Subsequently, others combined activity coefficient models with approaches for the incorporation of electrolytes within the

theoretical framework, that is modeling the salt as a fully associated third component. For example, Mock et al.[327] and Kolker et al.[328, 329] with NRTL and Dahl and Macedo[330] with UNIFAC, studied mixed solvent electrolyte systems, however, only the short-ranged dispersive effects of the electrolytes were captured through these models with the negation of long-ranged electrostatic interactions. These approaches were able to correlate experimental vapor pressure depression, vapor-liquid composition of solvents (vapor liquid equilibrium data), and boiling point data for several water-alcohol-salt systems, though some deviations were observed due to the neglect of electrostatics from the model.

While the approaches discussed above capture the thermodynamics of electrolyte solutions through short-ranged dispersive forces, they completely ignore any long-range electrostatic forces, which play a central role in determining the properties of electrolyte solutions.[51, 52, 283] Thus, in later studies, a number of models, were proposed that combined the Gibbs free energy due to long-range electrostatic interactions with activity coefficient models[49]. The Debye–Hückel (DH) theory proved to be the most influential and forms the basis of several equations for mixed solvent electrolytes[279-286]. In the DH approach, ions are considered to be point charges in a dielectric continuum, thus the solvent is considered implicitly. The approach of treating solvent molecules implicitly using a representative dielectric constant in an electrolyte solution is in the McMillan-Mayer (MM) framework[187], also known as a primitive model (PM) of electrolyte solutions. DH theory was used to derive the Gibbs free energy contribution for long range interactions and then combined with activity coefficient models, such as NRTL, UNIFAC[279, 280], UNIQUAC[282] for the short-ranged dispersive interactions. For

example, Sander et al.[279] combined a DH term with the UNIQUAC equation to correlate the VLE and activity coefficients of 54 ternary alcohol-water-salt systems using concentration dependent ion-specific UNIQUAC interaction parameters. Although the correlations are in good agreement for the vapor phase composition data (1.2% deviation in mole fractions), significant deviations for temperature, pressure and solvent activity coefficient (about 10%) were observed. We also note that the UNIQUAC model, which is derived from the LR framework, and DH theory, which is derived from MM framework, were combined without correcting for the conversion between the two frameworks. In the LR framework temperature, pressure and mole fraction of all species are independent variables where as, in the MM framework, the independent variables are temperature, volume, mole fraction of solute and the chemical potential of the solvents. Due to this inconsistency, a conversion is required from the MM to the LR framework. Cardoso et al.[290], was one of the first to propose an extended DH formalism which is suitable for use in the LR framework. Later, Macedo et al[280], combined this extended DH formalism with UNIQUAC to correlate the VLE data for alcohol + water + salt systems using the same dataset as Sander et al.; however, a similar level of agreement as reported by Sander et al. was still obtained. Several other approaches, which further improved the theoretical representation of mixed solvent electrolyte solutions by including free energy terms representative of extended intermolecular dispersive interactions between species in solution along with traditional DH and activity coefficient (NRTL/ UNIQUAC/ UNIFAC) terms, were subsequently proposed. For example, Li et al.[282], combined UNIQUAC and the DH term with a so-called hard-core term, which depends on the ionic strength of the solution. The hard-core term, representative of

indirect effects, which arise as a consequence of introducing charge into a non-electrolyte solution, mainly captures the solvent and ion middle-ranged interactions. Proposed theoretical approach was used to correlate vapor-liquid equilibrium (salt free mole fraction of alcohol in vapor and liquid phase; T-x-y diagram at ~101.325 KPa pressure) of 185 data sets made out of 10 different solvents, 18 different cations and 10 different anions with good agreement (0.018 fraction average deviation in mole fraction, 1.04 K average deviation in temperature and 0.79 KPa in pressure). In another development, Liu et al.,[284] initially combined NRTL with Pitzer- Debye–Hückel (PDH)[51], excess Gibbs free energy and Born free energy term to study liquid-liquid equilibrium (LLE) of NaCl/ water/ alcohol systems. Born free energy term was added to account for the free energy required to move ions from reference mixed solvent state to aqueous state. However, in this work, a correction from MM to LR framework for long-range electrostatic PDH term was ignored. This theoretical approach failed to give a good correlation with the experimental data. Later, to improve upon the correlation of experimental LLE data, an empirical Brønsted-Guggenheim (BG)[331] term generalized to mixed solvent systems was introduced in the model. BG is an empirical ion interaction term which provides good estimation of ionic activity, which is essential to get a good estimation of LLE. Inclusion of BG term provided an improved correlation of LLE data of NaCl/ water/ alcohol systems. The problem with these kinds of activity coefficient model-based approaches is in predictive ability. In most cases, the applicability of the equations remain limited, to the infinite dilution limit in water dominated mixed solvent systems.

In an effort to improve the predictive ability of equation of state for the study of

electrolytes, recently SAFT based equations of state have been applied to study of mixed solvent electrolyte systems. In perhaps the first such study, the SAFT-VRE[34] equation developed by combining SAFT-VR with an electrostatic interaction contribution to the free energy obtained by using mean spherical approximation (MSA) at the level of the restrictive primitive model (i.e., an equimolar mixture of equal-diameter hard spheres are assumed in a dielectric continuum), was the first SAFT based equation of state to be applied for the study of mixed solvent electrolyte solution and water+ alkane+ salt system was studied[332]. Water molecule was model as an associative square well hard sphere with four association sites; alkanes (methane, n-hexane, n-decane) as a square well chain; and electrolytes as charged dispersive square well hard sphere. Water + electrolyte model parameters were used as transferable manner from previous SAFT-VRE study of aqueous electrolyte systems[218] and the alkane parameters were taken from the work of McCabe et al. In the calculation of phase behavior of ternary mixture, electrolyte ions were restricted only in the water rich phase. Although, the predictive approach of using parameters in a transferrable manner from previous studies provided good qualitative agreement with experimental data for phase behavior (Coexistence compositions of the liquid water-rich and n-alkane-rich phases, salting out property, solution densities of water rich phase) of water + n-alkane + salt systems (MX, M = Li^+, Na^+, K^+, and X= Cl^-, Br^-, I^-), unlike cross interaction energy range and depth parameters were introduced between water and alkanes, which was obtained by fitting to ternary phase behavior data, to improve quantitative agreement between theory and experimental data. In more recent developments, other SAFT based equation of states have also been developed for the study of mixed solvent electrolyte solutions. Held *et al*.[229], applied the previously

developed primitive model of electrolyte-based ePC-SAFT[226] equation of state for the study of mixed solvent electrolyte systems. The ePC-SAFT equation of state is an extension of the PC-SAFT[294] equation of state, with an electrostatic interaction contribution to the free energy, which is represented through a simple DH term. Both water and co-solvents (methanol and ethanol) were modeled as dispersive chain molecules with two associating sites. The pure solvent compound SAFT parameters: number of segments, segment diameter, dispersive energy, association energy and volume parameters were obtained by fitting to the vapor pressure and saturated liquid densities of pure fluids; the binary unlike cross dispersive interaction energy (for both methanol-water and ethanol-water systems) and association energy (only for ethanol-water system) parameters were obtained by fitting to the binary mixture vapor-liquid equilibrium data at 298.15 K. Two salt-independent but solvent-dependent parameters were used to describe the ions: the solvated ion diameter and the ionic dispersion energy parameter. Two alcohol based ion parameters were determined by simultaneous fitting to experimental solution densities and osmotic coefficients of various electrolyte solutions composed of Na^+, Li^+, K^+, $NH4^+$, Cl^-, Br^-, I^- ions in ethanol or methanol. The water based ionic parameters were taken from a previous study. For the ternary salt + water + alcohol systems, no ion-ion dispersion interactions were considered; only ion-solvent dispersion interactions were considered and obtained by using Lorenz-Berthelot combining rules. Ionic radii in mixed solvent were obtained by using an averaging scheme based upon salt free solvent compositions in solution. The relative permittivity of the salt free solvent mixtures was modeled by an empirical formula obtained by fitting to the experimental dielectric constant values. Using the parameters developed for binary systems, solution

densities and mean ionic activities of KCl, NaBr, NaCl, NaI, LiCl in ethanol + water, methanol + water and methanol + ethanol + water mixed solvents were predicted across different weight fractions of solvent with considerable accuracy (~1% for solution densities and < 5% in most cases for mean ionic activity coefficient). However, one should note that for most systems solution densities data are limited to only very dilute limit (< 1 m). In more recent work, Schreckenberg et al.[27], proposed an improved formulation of SAFT-VRE[218] that incorporates a Born contribution in order to better capture solvation effects. The implicit solvent within the PM framework of SAFT-VRE[218] was represented through an empirical solution dielectric constant model, following the work of Uematsu and Franck[221], which takes into account the temperature, density and composition of the solvent, and in, turn makes the dielectric constant a differentiable variable. The study contained VLE and LLE of mixed solvent electrolyte systems (methanol /n-butanol and water + salt systems) along with single and multi-salt aqueous electrolyte systems. The electrolytes were described using a fully dissociated model with ion-specific interaction parameters, where the effective ionic diameter, ion-water and ion-ion dispersive energy parameters were obtained by fitting to vapor pressure, solution density, and mean ionic activity coefficient data for fifteen different aqueous alkali halide salts at temperatures below 523 K (critical region). The cross ion-ion dispersive interaction energy was estimated using a procedure proposed by Hudson and McCoubrey[222]. For mixed solvent systems, the alcohol-ion unlike dispersion energy was obtained by fitting to experimental water + alcohol + salt VLE/ LLE data and was able to give good agreement with the experimental results.

In this study, recently developed non-primitive model based SAFT-VR+DE

equation of state[29], with one-fluid like approximation has been applied for the thermodynamic property study of mixed solvent electrolyte systems. Non-primitive model of electrolyte solution explicitly considers solvent species as oppose to primitive model; it is a Born-Oppenheimer (BO)[187] level of theoretical approach. For simplest of cases BO model is conceptualized as a mixture of charged hard spheres in a solvent of hard spherical molecules with a point dipole embedded in the center. While development, the SAFT-VR+DE equation of state, with one-fluid like approximation was extensively tested against PVT data obtained from NPT monte carlo (MC) simulation results for model mixed solvent electrolyte systems. Theoretical predictions of PVT data for model systems with different solvent polarities, ionic and solvent compositions and sizes were compared against NPT MC simulation results and excellent agreement were obtained.

The use of SAFT-VR+DE is a novel approach in the sense that for the first time in literature a non primitive model based EoS has been used to study mixed solvent electrolyte systems. Due to the explicit consideration of the solvent species within solution, the dielectric constant no longer remains an input instead gets calculated with in the theory from input dipole moment and it is a function of ionic concentration and solvent composition. Explicit treatment of solvent species certainly advantageous compared to the primitive model based implicit treatment, as it also eliminates any dependence upon empirical correlative equation for the calculation of dielectric constant, which give rise to the number of model parameters within proposed equations of state. In the previous work, it was observed while comparing against primitive model, an ion concentration and solvent composition dependent dielectric constant is essential to obtain an accurate prediction for PVT data. There is no study in literature till date to report salt

concentration dependent dielectric constant for mixed solvent electrolyte systems. Also, a non primitive model based approach allows to have contribution to the chemical potential and pressure from ion-dipole and dipole-dipole interactions, which is otherwise impossible from primitive model barring a few cases such as modified SAFT-VRE[27].

Focus of this study remains in accurate capture of the mean ionic activity coefficient, which is an equilibrium property and a measure of non-ideality of the system. Mean ionic activity coefficients of the salts have pronounced effect in many applications. One of the key areas of application for mixed solvent electrolyte is extractive distillation process where the salt separates two miscible compounds in an azeotropic mixture into two liquid phases. In liquid-liquid equilibrium the mean ionic activity coefficient plays a dominating role to produce salting in/ salting out behavior[284, 333]. So, it is essential to capture the mean ionic activity coefficients accurately and in this regard, SAFT-VR+DE has been used in predictive manner to study the mean ionic activity coefficients of several mixed solvent electrolyte systems ranging across salt and solvent compositions. The remainder of the chapter is organized as follows: in section 2 the molecular model and theory are discussed, in the section 3 we report the parameters considered for alcohols, water and electrolytes and a discussion of results and conclusions from this work is provided in section 4.

6.2 Molecular model and theory

In the SAFT-VR+DE[29] approach, mixed solvent electrolyte systems are described as a mixture of positively and negatively charged ions of arbitrary size in a dipolar solvent of associative chain molecules. Figure 1, provides a schematic representation of the model

system. The ions are represented by hard spheres, half with charge $+q$ and diameter σ^+ and half with charge $-q$ and diameter σ^-. Two kinds of solvent molecules are considered with arbitrary sizes and polarity and different associating sites.

Key forces of interactions within mixed solvent electrolyte systems between ionic species are coulombic charged interactions; between ionic-dipolar solvent species are dipolar-charge and dispersive interactions; and between solvent species dipolar, associative and dispersive interactions. The potential model for the interactions between species in solution is therefore given by,

$$u(r) = u^{SW}(r) + u^{CC}(r) + u^{CD}(r) + u^{CD}(r) \tag{5.22}$$

In the modified SAFT-VR+DE theoretical framework[334] the Helmholtz free energy per molecule in a mixed solvent electrolyte solution is given by,

$$\frac{A}{Nk_bT} = \frac{A^{ideal}}{Nk_bT} + \frac{A^{mono}}{Nk_bT} + \frac{A^{chain}}{Nk_bT} + \frac{A^{assoc}}{Nk_bT} \tag{5.23}$$

where N is a total number of molecules, k_b is the Boltzmann constant, T is temperature, and A^{ideal}, A^{mono}, A^{chain}, and A^{assoc} are free energy contributions due to the ideal, monomer, chain, and association interactions, respectively. Since the general development of the theory and mathematical expressions are elaborately described in previous chapters, in the following paragraphs the discussion is limited to the results.

6.3 Results and discussion

6.3.1 Pure fluids

Water molecules are modeled as dipolar square-well dispersive hard spheres with four short-range attractive square-well associating sites describing association interactions,

which mimic hydrogen bonding. The four association sites are of two distinctly different types, where two representing hydrogen sites and other two representing lone pair of electrons on oxygen atom. Intermolecular SAFT-VR+D[243] parameters were developed in the previous study[335]; hard-core diameter (σ), square-well potential depth (ε), range (λ), association energy (ε^{HB}), bonding volume (κ^{HB}) of water; were obtained by fitting to experimental vapor pressure and saturated liquid densities using a condensed phase effective dipole moment of 2.18 D. A condensed phase dipole moment for water corresponds to a higher value compared to isolated water monomer dipole moment of 1.855 D due to the polarization effect of the environment[336]. So, the effective dipole moment of 2.18 D captures the effect of bare water molecule dipole moment along with the polarization. SAFT-VR+D approach found to provide an excellent correlation for the pure water vapor pressure and saturated liquid densities[335]. The previously developed SAFT-VR+D parameters along with % average absolute deviations (AAD) in vapor pressure and saturated liquid densities of water has been reported in table 1.

The alcohol molecules, are described as dipolar square-well chain fluids with association sites to capture H-bonding. The H-bonding sites of 1-alcohols can be described with both 2-site (2B) and 3-site (3B) association schemes. Gross and Sadowski[24] described 1-alcohols with a 2B association scheme and commented that use of either 2B or 3B model provide similar results for phase behavior property. Karakatsani and Economou[299] treated 1-alcohols with 2B scheme and mentioned such association scheme effectively captures the experimentally observed linear oligomer formation of heavier alcohols. Kontogeorgis et al.[337] compared three EoSs: cubic-plus-association (CPA)[338], simplified-PC-SAFT (sPC-SAFT)[132] and non-random

hydrogen bonding (NRHB)[339] for study on association behavior of alcohols. It was commented that, methanol is best represented by a 3B association scheme; while for ethanol and heavier alcohols there is small difference between 2B and 3B schemes, with the former (2B) being possibly the best choice. Since the objective of this study is to capture condensed or liquid phase property, a 2B-associating model for ethanol has been employed as it better captures the liquid phase structure. However, for methanol a 3B association scheme has been used as proposed by other studies.

Dipole moment can be considered as an important physical property for polar fluids such as alcohol due to its effect on thermodynamic property and phase behavior. Similar to the treatment with water in our previous study[334], a condensed phase effective dipole moment for methanol and ethanol has been used, rather than the gas phase dipole moment of these alcohols (~ 1.7 D). In condensed phase the dipole moment for polar fluids is in general higher than gas phase isolated molecule dipole moment[340]. The effective dipole moment for methanol and ethanol are obtained by varying the dipole moment as a model parameter and fitting the calculated dielectric constant to the experimental dielectric constant at room temperature and pressure as presented in figure 6.1. It can be observed in the figure 6.1, the dipole moment of methanol and ethanol correspond to 2.73 D and 3.35D respectively, provides a good representation of the liquid phase dielectric constant at room temperature and pressure for respective alcohols. In SAFT-VR+D framework, an associating dipolar chain molecule like alcohol is characterized by model parameters: hard-core diameter (σ), square-well potential depth (ε) and range (λ), number of segments per chain (m), association energy (εHB) and bonding volume (κHB)). The number of segments per chain (m) for each alcohol, has

been calculated using the previously developed empirical relationship proposed by Garcia-Lisbona *et al.,*[341] for which $m = 0.33(C-1)+1.2$. The rest of the SAFT-VR+D parameters were obtained by fitting to experimental vapor pressure and saturated liquid density data between 220-475 K for methanol and 215-465 for ethanol[247]. Experimental data close to the critical region (around 10%) have been excluded from the fitting procedure, as SAFT-VR+D like other analytical EoS exhibits classical critical behavior in the critical region and so over predicts the critical point[248]. Additionally data points near the triple point have also been excluded since it has been shown that inclusion of such data can distort the results[160]. Simulated annealing[157, 158] is used to the fit the model parameters with an objective function defined as a function of vapor pressure and saturated liquid density as given in appendix A. The resulting parameters along with %AAD in pressure and saturate liquid densities are reported in table 6.1, and as can be seen from figure 6.2, the theory provides a good representation of the experimental phase behavior data for pure methanol and ethanol. The percent average absolute deviation (%AAD) over the whole phase diagram is 1.305 (methanol)/ 0.474 (ethanol) for the vapor pressures and 0.082 (methanol)/ 0.298 (ethanol) for saturated liquid densities using the SAFT-VR + D EoS

Table 6.1. SAFT-VR+D parameters for alcohols and the % average absolute deviation (AAD) in vapor pressure and saturated liquid densities as compared to experiment**[247]**

	μ (D)	σ (Å)	ε /k_b (K)	λ	m	ε^{HB}/k_b (K)	K^{HB} (Å^3)	%AAD p	%AAD ρ_{liq}
CH_3OH	2.730	3.5396	162.17	1.72229	1.2	1800.945	0.81	1.305	0.082
C_2H_5OH	3.370	3.728	252.71	1.445	1.5333	2030.0	2.0561	0.474	0.298

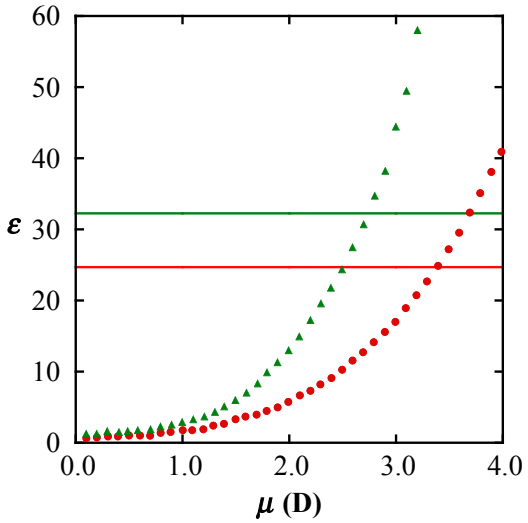

Figure 6.1. Change in the dielectric constant ε as a function of dipole moment μ for alcohols as predicted by the SAFT-VR+D equation of state at room temperature (298.15 K) and pressure (0.101325 MPa). Solid line represents the dielectric constant for methanol (green) and ethanol (red) as reported in experimental studies[342, 343].

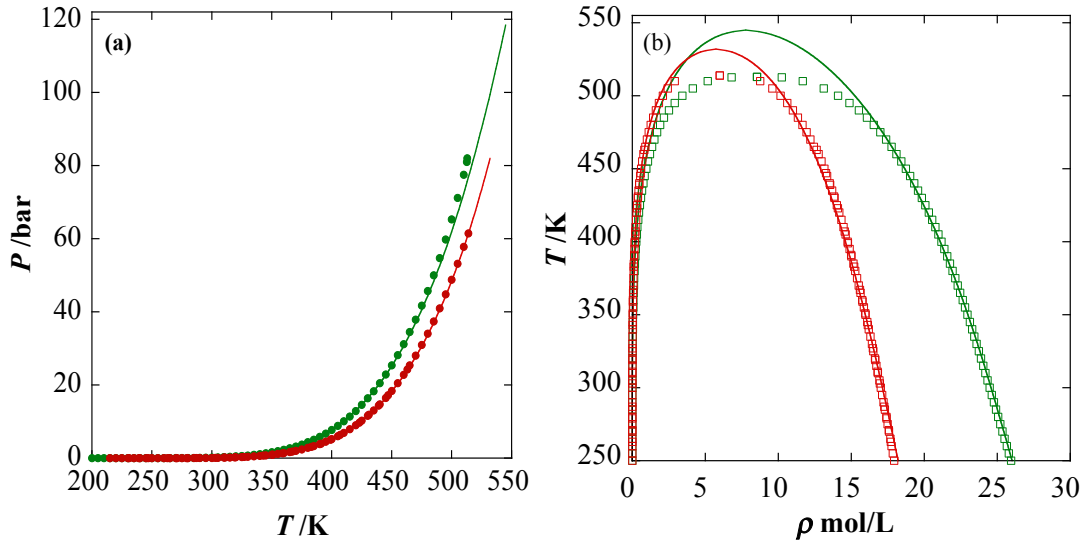

Figure 6.2. Comparison of vapor pressure (a) and vapor-liquid coexisting densities (b) for methanol (green) and ethanol (red) from the SAFT-VR+D EoS and experiment. Symbols represent the experimental data[247] and the theory is represented by the solid line.

6.3.2 Water-alcohol mixture

We first consider the phase behavior of the binary methanol/ ethanol + H_2O mixtures to test the transferability of the alcohol parameters before studying salt containing systems. Figure 6.3 presents the SAFT-VR+D predictions for the P-x projection of the PTx surface for the alcohol-water mixtures over a range of different temperatures. As can be seen from figure 6.3a, the predictions using Lorentz-Berthelot combining rules for methanol-water system are in excellent agreement with the experimental phase behavior data[344] at room temperature (298.15 K) as well as elevated temperatures of 313.15, 323.15 and 333.15 K. However, in case of ethanol-water system, the Lorentz-Berthelot combining rules fail to predict the constant temperature P-x phase envelope. This may be due to inaccurate estimation of polarization with the theoretical framework. The unlike cross-dispersion energy parameter (ξ=1.2) obtained by fitting to the experimental binary phase

equilibrium P-x data[345] at 298.15 K is found to correct this behavior and is transferrable to the higher temperatures studied. In figure 6.3b, Pxy phase diagrams of water-ethanol mixture correlated at 298.15 K and predicted at higher temperatures using SAFT-VR+D has been presented along with experimental data.

As shown in figure 6.4, the theory accurately predicts the dielectric behavior of the water/alcohol mixtures over the entire salt free solvent mixture composition. A comparison has been made with the theoretical prediction of dielectric property of the salt free alcohol-water mixture using the gas phase dipole moment value for water (1.84 D) and methanol (1.7 D) and as can be seen from the figure 6.4, it fails to capture the experimental dielectric property of the mixture accurately. In our previous study, it was discussed, how important it to capture the dielectric property of the solution in order to obtain an accurate estimation of thermodynamic properties of the electrolyte solutions. With the use of condensed phase dipole moments for constituting compounds, which gives an accurate description of the solution dielectric property, we look to accurately capture the thermodynamic property of the mixed solvent electrolyte systems.

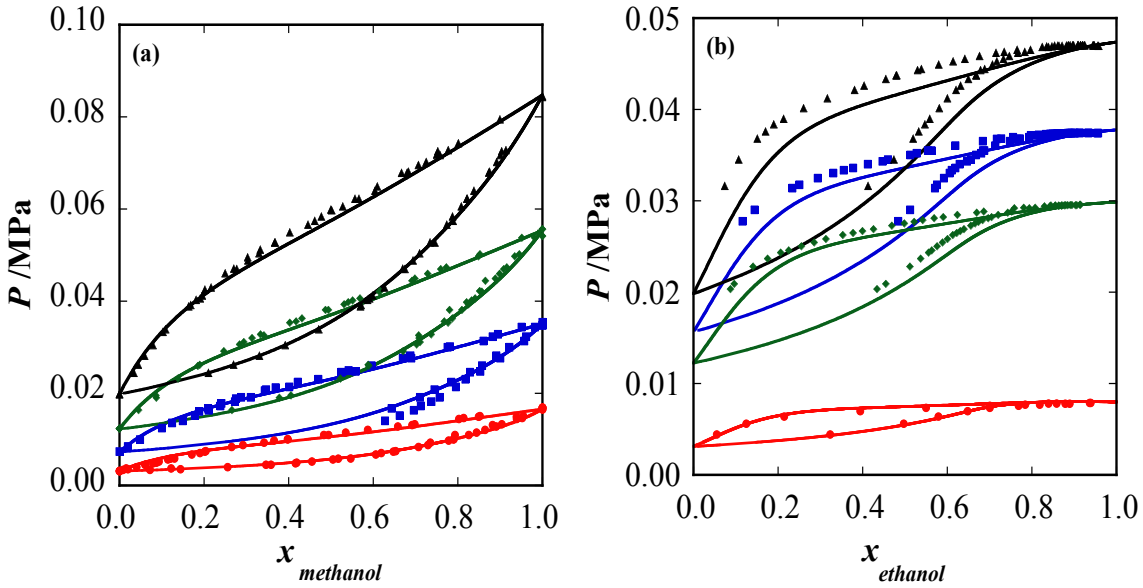

Figure 6.3. Vapor–liquid equilibria for binary mixtures of alcohol + water. Part (a) methanol + water binary mixture at 298.15 K (red), 313.15 K (blue), 323.15 K (green), 333.15 K (black). Part (b) ethanol + water at 298.15 K (red), 323.15 K (blue), 328.15 K (green), 333.15 K (black). The solid lines correspond to the theoretical predictions from the SAFT-VR+D approach and the symbols to the experimental data[344, 345].

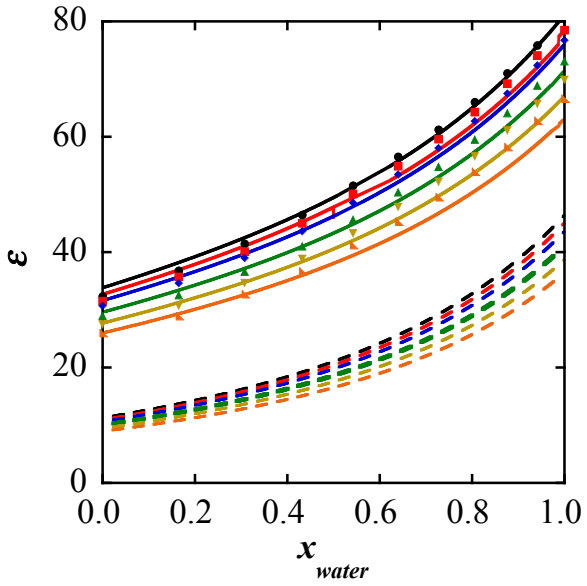

Figure 6.4. Dielectric constant of salt free methanol+ water mixture at 293.15 K (black), 298.15 K (red), 303.15 K (blue), 313.15 K (green), 323.15 K (yellow), 333.15 K (orange),. The solid lines correspond to the theoretical predictions from the SAFT-VR+D approach and the symbols to the experimental data[342].

6.3.3 Mixed solvent electrolyte

In the previous work, two sets of ion parameters were developed to represent binary mixtures of aqueous alkali halide solution: salt independent ionic radii and salt dependent cation-water dispersion interaction energy parameter. For cations such as K^+, Cs^+, Rb^+ the ionic radii were taken from the work of Mähler et al.[258] corresponding to the appropriate coordination number and ionic radii for anions (Cl^-, Br^-, I^-) were taken from the work of Shannon.[254, 255] Ions with smaller radii and higher charge densities, such as Li^+, Na^+, F^- are termed net structure makers, as these ions distort the water structure beyond the first water shell[262, 263]. The greater solvation influence of such ions on surrounding water molecules which is spread across multiple shell were not well captured by the theoretical framework of SAFT-VR+DE equation of state as salts containing Li^+, Na^+, F^- ions failed to give an accurate description of the mean ionic activity coefficient experimental data at 298.15 K and 1.01325 bar. Hence salt independent ionic radii of Li^+, Na^+, F^- were obtained by fitting to the mean ionic activity coefficient experimental data at 298.15 K and 1.01325 bar. The set of ionic radii for both cations and anions reported in the earlier study has been used in this work.

Apart from the ion specific ionic radii parameter, the cation–solvent (water) binary dispersion interaction energy ($\varepsilon^{cation-H_2O}$) parameter were obtain in the previous work fitting to the experimental mean ionic activity coefficient data of nineteen different alkali-halide aqueous solution at 298.15 K and 1 bar. The dispersive square-well interaction range (λ) for the cations was fixed at 1.2 and Lorentz-Bethelot combining rule was used to determine the cross-interaction range parameters between the cations and solvent water molecules.

In the mixed solvent electrolyte solution, the dispersive interaction acts between three kinds of compounds: water, alcohol and salt. Among which the salt (cation)-water, water-alcohol cross-dispersive interaction energy parameters have already been obtained from the binary data of aqueous electrolytes and water-alcohol mixtures respectively. Now a salt (cation/ anion)-alcohol cross energy parameter is needed to capture the dispersive nature of interactions. This cross-interaction energy parameter between alcohol-salt (cation/ anion) can be obtained in two ways: fitting to the alcohol-salt binary mean ionic activity coefficient data or fitting to the ternary mean ionic activity coefficient data from mixed solvent electrolyte solution. Unfortunately, the mean ionic activity coefficient data for binary mixture of alcohol-salt are available for only few systems. So, the only choice remain is of using ternary mixed solvent electrolyte mean ionic activity coefficient data. In experimental studies a range of mean ionic activity coefficient data with the variation in composition of water –alcohol solvents and salt concentration have been reported. To decide upon the set of data to use (water-rich region or alcohol rich-region) and set of dispersion energy parameters to fit (cation-alcohol or anion-alcohol) understanding of the relative interactions of electrolytes with solvents is necessary. Experimental NMR studies[346] and molecular dynamics (MD) computer simulation studies[347] on alkali halides /methanol−water systems have indicated preferential solvation of ions within mixed solvent. Preferential solvation is defined in terms of local composition of solvent species around the solute electrolytes. Studies concluded that cations of alkali halide salts show preferential hydration even in water-deficit solution where as anions are selectively solvated by alcohol molecule. Based upon this fact, the cation-alcohol dispersive interaction will be screened by water molecules, present at the

hydration shell of cation even at alcohol rich region. Since one-fluid approximation within the proposed theoretical approach for mixed solvent electrolyte presents solvent as an average entity, this fact (reduced interaction between cation-alcohol) cannot be captured well by cation-alcohol cross dispersive energy parameter if the experimental data from alcohol rich region is chosen. So, the cation-alcohol cross dispersive energy parameters ($\varepsilon_{cation-H_2O}$) are obtained by fitting to experimental mean ionic activity coefficient data corresponding to the highest available weight fraction of water within mixed solvent electrolyte solution. It was observed during fitting procedure that anion-solvent dispersion energy has lesser influence on mean ionic activity coefficient data, which is consistent with other SAFT study and hence no anion-solvent dispersion interactions are considered. The dispersive square-well interaction range (λ) for the cations has been fixed at 1.2 and Lorentz-Bethelot combining rule has been used to determine the cross-interaction range parameters between the cations and solvent water molecules.

$$\lambda_{cation-alcohol} = \frac{\sigma_{cation}\lambda_{cation} + \sigma_{alcohol}\lambda_{alcohol}}{\sigma_{cation} + \sigma_{alcohol}} \tag{5.24}$$

The binary salt-specific cation-alcohol dispersion interaction parameters obtained from fitting to experimental mean ionic activity coefficient data of different mixed solvent electrolyte solutions at 298.15 K and 1.01325 bar along with % average absolute deviations (AAD) has been reported in table 6.2. Simulated annealing[157, 158] is used in the fitting process. Table also contains average absolute deviations from the experimental data, corresponding to the specific systems,

Table 6.2. Salt specific dispersion energy parameters for the cation-alcohol ($\varepsilon_{\text{cation-alcohol}}$) interaction for the different mixed solvent electrolytes studied and the % average absolute deviation (AAD) for the SAFT-VR+DE equation of state for $\gamma \pm$ as compared to experimental data at 298.15 K and 1.01325 bar

System	Alcohol weight fraction	$\varepsilon_{\text{cation-H2O}}$	% AAD $\gamma\pm$
CsCl/ water/ ethanol	10	344.39	2.95
NaBr/ water/ ethanol	10	2512.74	4.53
NaF/ water/ ethanol	10	1923.89	2.77
CsCl/ water/ methanol	10	894.87	1.40
KCl/ water/ methanol	20	2052.31	1.65
LiCl/ water/ methanol	10	2349.11	5.37
NaBr/ water/ methanol	10	1915.47	3.11
NaCl/ water/ methanol	20	2359.89	4.29
RbCl/ water/ methanol	20	1080.15	2.92

The mean ionic activity coefficient of several mixed solvent electrolyte systems over the wider ranges of ionic and solvent compositions has been predicted using set of fitted cation-alcohol dispersive energy parameters. A comprehensive discussion on correlated results as well as theoretical predictions is given in following paragraphs.

RbCl/ Water/ Methanol

The SAFT-VR+DE approach with the one fluid like approximation gives a good correlation of mean ionic activity coefficient experimental data[348] with 2.92% AAD for the ternary mixture of RbCl +water +methanol (weight fraction of alcohol 20%) at

298.15 K and 1 bar. Theory captures the experimental trend well, especially at lower ionic concentrations where the bulk of the experimental data is available as can be seen in figure 6.5. Using the fitted cation-alcohol dispersive interaction energy parameter, the mean ionic activity coefficient of the ternary solution has been predicted at a higher alcohol concentration (weight fraction of alcohol 40%) and presented in figure 6.5. Experimental results show a gradual decrease in mean ionic activity coefficient with the increase in alcohol concentration due to the decrease in salt solubility, and the theoretical prediction captures the trend at 40-weight % of alcohol. The increase in alcohol concentration decreases the overall solution dielectric constant and subsequently ions move into the water rich phase of the solution, causing decrease in salt solubility. Theory captures this phenomenon well and predicts with 7.49 % in AAD as reported in table 6.3 of appendix. The deviation in theoretical prediction from experimental result at higher salt concentrations perhaps due to the failure of theory in accurately capturing the ion-dipole interaction.

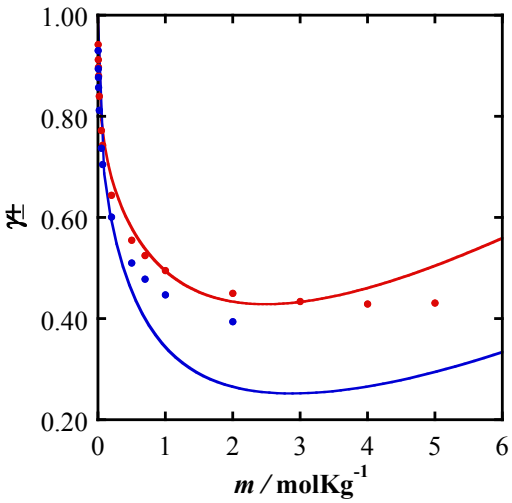

Figure 6.5. Mean ionic activity coefficients of RbCl in water/ methanol mixtures at 298.15 K and 1.0125 bar with salt-free alcohol weight fractions at 20% (red), 40% (blue). The symbols represent experimental data[348] and solid lines are theoretical correlations/ predictions by SAFT-VR+DE equation of state.

CsCl/ Water/ Alcohol system

Next focus is shifted to systems containing CsCl, water, and alcohol (ethanol/ methanol). In both cases: CsCl+water+ methanol and CsCl+ water+ ethanol the theory gives a good correlation of experimental data[349] (1.40 and 2.95 % AAD respectively) at 298.15 K, 1 bar and 10 weight % of alcohol, as can be seen in figure 6.6. Using the fitted cation-alcohol unlike dispersive energy parameter, mean ionic activity coefficients at higher weight fractions up to 40% of alcohol have been predicted. The theory gives an excellent qualitative as well as quantitative representation of experimental data for most weight fractions of alcohol. With increasing alcohol weight fraction in solution, the experimental mean ionic activity coefficient decreases, this effect has been captured by the theoretical predictions. The SAFT-VR+DE prediction deviations in average within ~7% AAD of the experimental data up to 30 weight % of alcohol as presented in figure 6.6 and reported in table A1. At 40% weight fraction of alcohol, theory over predicts the mean ionic activity coefficient for both methanol and ethanol based mixed solvent electrolyte systems, although in general for other systems SAFT-VR+DE tends to under predict the experimental results. This inconsistency may be due to some errors present in experimental result.

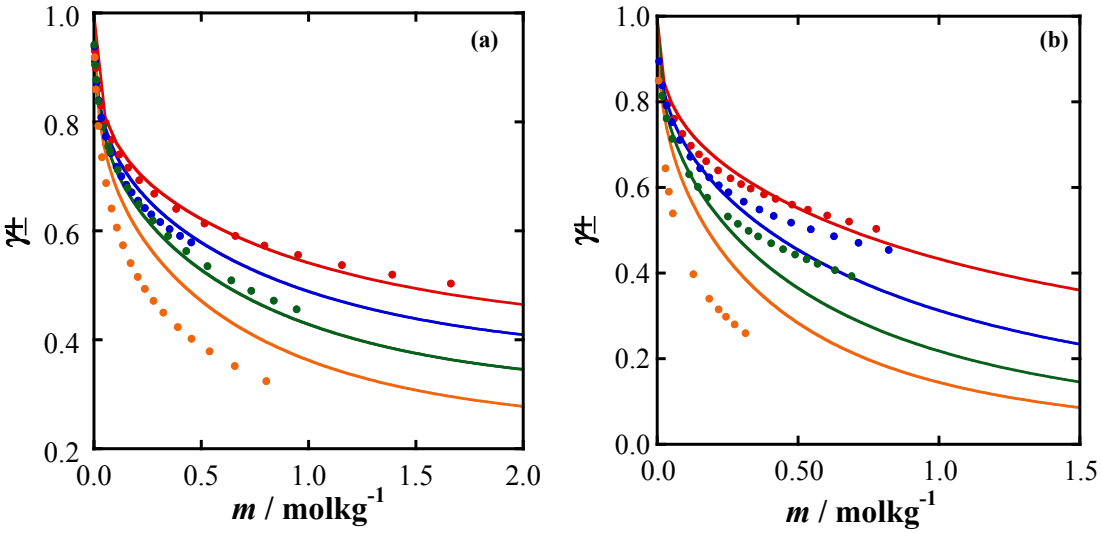

Figure 6.6. Mean ionic activity coefficients of CsCl in water + (a) methanol and (b) ethanol mixtures at 298.15 K and 1.01325 bar with salt-free alcohol weight fractions at 10% (red), 20% (blue), 30% (green), 40% (orange). The symbols represent experimental data[349] and solid lines are theoretical correlations/ predictions by SAFT-VR+DE.

KCl /Water/ Methanol

Experimental data[348] of mean ionic activity coefficient data for KCl mixed solvent systems are available for three alcohol weight fractions: 20%, 40% and 60%. Theoretical approach of SAFT-VR+DE gives a good correlation of mean ionic activity for KCl+ water+ methanol system at 298.15 K, 1 bar and 20 weight % of the alcohol with 1.65 %AAD as can be seen in figure 6.7. At higher alcohol weight fractions the SAFT-VR+DE approach gives good prediction and more so at dilute salt concentrations where most of the experimental data exists. The theoretical predictions for 40% and 60% weight fractions of alcohol gives an average deviations of 3.4 and 7.6% respectively. The predicted results have been presented in figure 6.7 and %AADs are reported in table 6.3 of appendix. Some deviations in prediction can be observed at higher salt concentrations, this is due to higher coulombic interaction predicted by the theory with decreasing

dielectric constant of the solution. A detailed discussion on correcting this under prediction has been made at the end of this section..

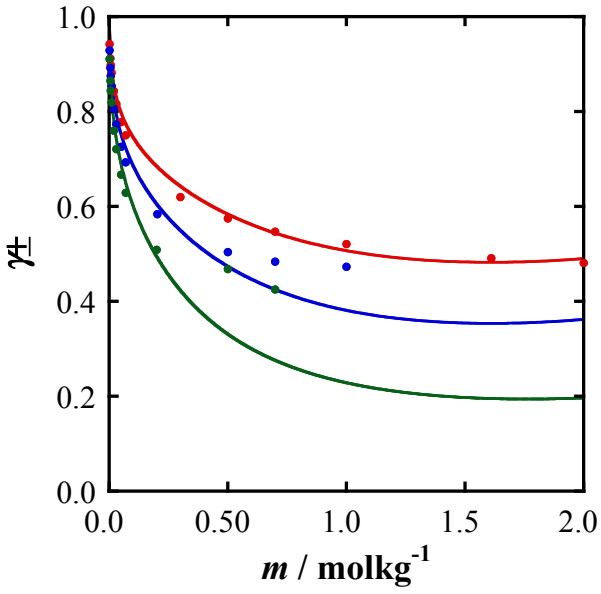

Figure 6.7. Mean ionic activity coefficients of KCl in water/ methanol mixtures at 298.15 K and 1.0125 bar with salt-free alcohol weight fractions at 20% (red), 40% (blue), 60% (green). The symbols represent experimental data[348] and solid lines are theoretical correlations/ predictions by SAFT-VR+DE.

NaF/ Water/ Ethanol

One of our systems of interest is NaF mixed solvent solution. The main difference between this system with previously studied ones is the nature of ionic radii used for Na^+ and F^- ions. While developing the ionic radii of Na^+ and F^- ions for the binary aqueous electrolyte systems, an effective radii was proposed which affects multiple water shells. It will be interesting to observe, how this effective ionic radii works in mixed solvent electrolyte system, where some amount of alcohol is present along with water molecules. As can be seen from figure 6.8, the theory has been able to give a good correlation (10 weight % of alcohol) with average deviation of 2.85% as well as prediction for

experimental[350] mean ionic activity coefficients data of the NaF +water +methanol system ranging from 20-80% weight fraction of ethanol. Even at higher alcohol concentration (80 weight % of alcohol), the parameters show good transferability and theory gives accurate prediction with %AAD of 4.2. In case of NaF, the experimental data is available only for dilute salt concentrations where even at high alcohol concentrations enough water molecules are present to form multiple shells to solvate Na^+ and F^- ions. This allows the effective ionic radii of Na developed by fitting to the experimental binary aqueous electrolyte solution data to work well. Now, lets see what happens for LiCl system, which also contains an ion (Li^+) with effective ionic radii.

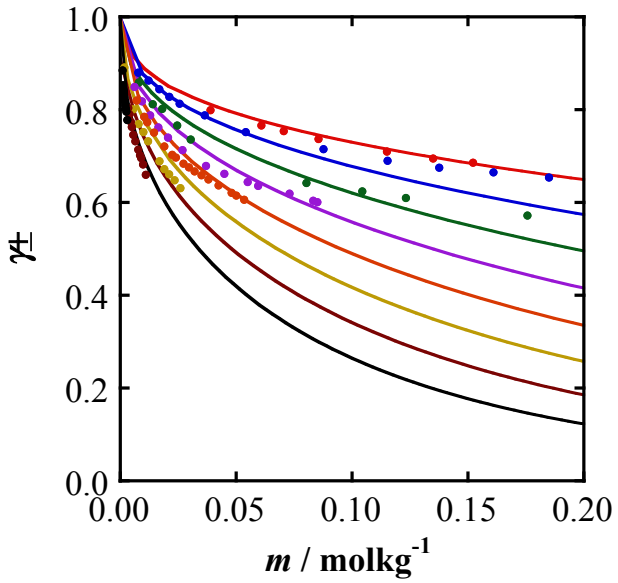

Figure 6.8. Mean ionic activity coefficients of NaF in water/ ethanol mixtures at 298.15 K and 1.0125 bar with salt-free alcohol weight fractions at 10% (red), 20% (blue), 30% (green), 40% (orange), 50% (purple), 60% (yellow), 70% (brown), 80% (black). The symbols represent experimental data[350] and solid lines are theoretical correlations/ predictions by SAFT-VR+DE.

LiCl/ Water/ methanol

In case of LiCl, an effective ionic radii for Li^+ ion was defined in previous study as it is a

structure making/ breaking ion. SAFT-VR+DE theoretical approach has been able to give a good correlation of mean ionic activity coefficient at 10 weight% of alcohol with 5.3% average deviation as can be seen from figure 6.9. In predicting the mean ionic activity coefficients at higher weight fraction of alcohol in solution, theory shows the correct experimental trend as mean ionic activity coefficient decreases with increasing alcohol fraction in solution. Along with good qualitative trend, good quantitative agreement has been achieved as well, theory predicts the mean ionic activity coefficient with an average deviation of ~8% at 20 weight % of alcohol in ambient condition. The fitted cation-alcohol unlike dispersive energy parameter demonstrates good predictive ability as it gives a good theoretical representation of activity coefficient even at high (8 m) ionic concentration. Use of the effective ionic radii for Li^+ ion works fine as experimental data is only available for water rich phase and enough water molecules are present to form multiple shells around the Li cation.

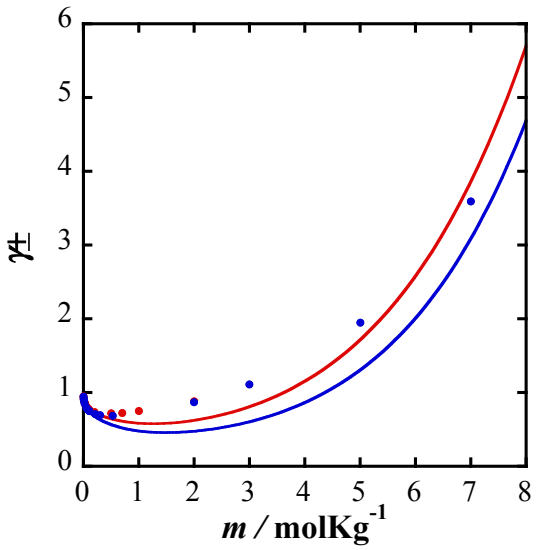

Figure 6.9 Mean ionic activity coefficients of LiCl in water/ methanol mixtures at 298.15 K and 1.0125 bar with salt-free alcohol weight fractions at 10% (red), 20% (blue). The symbols represent experimental data[348] and solid lines are theoretical correlations/ predictions by SAFT-VR+DE.

NaCl/ Water/ methanol

Now, mean ionic activity coefficient of NaCl +water + methanol mixture has been investigated using SAFT-VR+DE approach. From figure 6.10, it can be observed that although theory gives a good correlation of experimental mean ionic activity coefficient data[351] at 20% weight fraction of alcohol with average deviation of 4.3% but fails to give an accurate quantitative prediction and more so at higher weight fractions of alcohol and ionic concentrations. It is due to the use of effective ionic radii for Na^+, which considers a greater influence of cation on solvent species. Although Na^+ is a structure making ion in aqueous conditions, it shows no structure making effect on alcohol rich solvent media. Even at higher weight fraction of alcohol in solution Na^+ is preferencially solvated by water molecules. However, theory captures a greater interaction between cation-solvent species even at higher alcohol concentrations and influences more decrement in dielectric constant of the solution than actually exists. This kind of influence of effective radii on mean ionic activity coefficient was not observed in previously discussed LiCl and NaF salt systems. Compared to LiCl and NaF systems, NaCl shows a higher solubility in alcohol rich phase and experimental data are available for higher salt and alcohol concentrations. At a higher salt concentrations and higher alcohol fraction for NaCl solution, there is lesser (in some cases only trace amount) number of water molecules available to form multiple shells around the cation. Other Na ion containing systems are investigated in the following paragraphs to find whether this trend of under predicting mean ionic activity coefficient with increasing salt and alcohol fraction in solution exists for all the other systems or not.

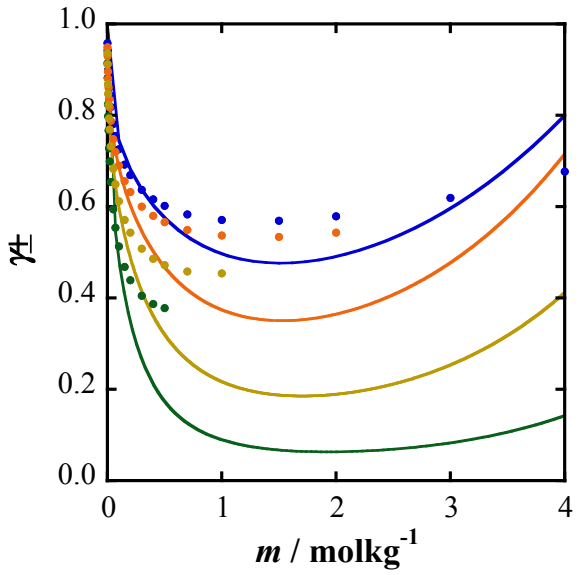

Figure 6.10. Mean ionic activity coefficients of NaCl in water/ methanol mixtures at 298.15 K and 1.0125 bar with salt-free alcohol weight fractions at 20% (blue), 40% (orange), 60% (yellow), 80% (green). The symbols represent experimental data[351] and solid lines are theoretical correlations/ predictions by SAFT-VR+DE.

NaBr/ Water/ alcohol

In the study of NaBr + water + alcohol (methanol/ ethanol) mixture system although theory gives an good correlation at 10 weight % of alcohol (average deviations of 4.53% and 3.11% for ethanol and methanol containing systems respectively) but fails to give an accurate quantitative prediction of mean ionic activity coefficient at higher concentrations of alcohol in solution as can be observed from figures 6.11a and 6.11b for methanol and ethanol systems respectively. Again theory predicts greater influence of ionic effect on alcohol molecules, which results in a greater dielectric decrement than actually exists and hence under predicts the mean ionic activity coefficient. To substantiate this fact, an effective dipole moment of 2.65 D for the hypothetical one-fluid representative of mixed solvent solution (methanol + water) has been considered instead of the originally used 2.45 D (comes from average of water dipole 2.179 and methanol 2.73) for improvement

of theoretical representation of mean ionic activity coefficient of NaBr + methanol (90 weight %)+ water system as can be seen in figure 6.12. Use of a higher value of effective dipole moment compared to original one essentially improves the dielectric decrement as presented in figure 6.13. Although, there is no experimental dielectric decrement data available to get the actual measure of decrement, it can always be postulated the dielectric property of alcohol rich solution will be less affected by electrolytes than water due to lesser interactions of ions with alcohol molecules and in case of aqueous electrolyte solution SAFT-VR+DE does under predict the dielectric decrement as discussed in precious study. So, it is expected to get some under prediction of dielectric decrement for alcohol rich mixed solvent electrolyte systems. In figure 6.12, the effective dipole moment over estimates the mean ionic activity coefficient at lower ionic concentrations; this is due to the fact the dipole moment is not fitted to the pure fluids and over predicts the pure fluid dielectric constant as presented in figure 6.13.\

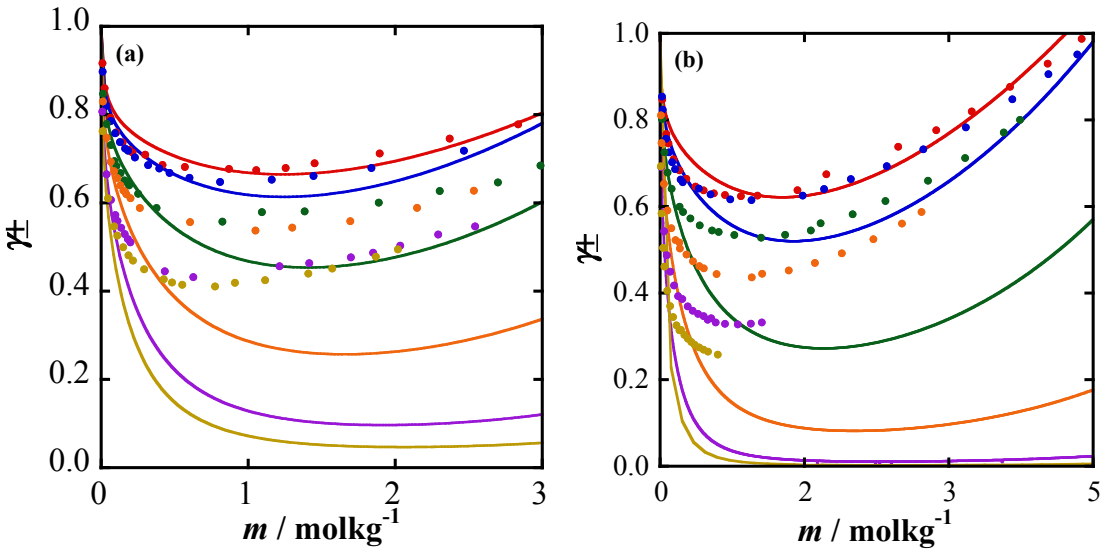

Figure 6.11. Mean ionic activity coefficients of NaBr in water/ (a) methanol and (b) ethanol mixtures at 298.15 K and 1.0125 bar with salt-free alcohol weight fractions at 10% (red), 20% (blue), 40% (green), 60% (orange), 80% (purple), 90% (yellow). The symbols represent experimental data[319] and solid lines are theoretical correlations/ predictions by SAFT-VR+DE.

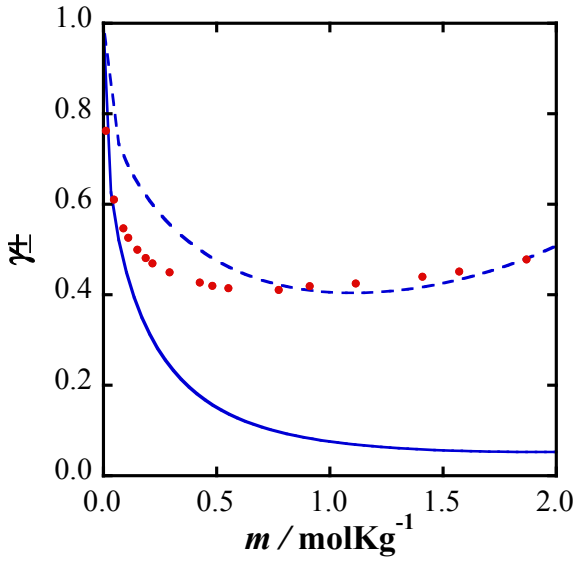

Figure 6.12. Mean ionic activity coefficients of NaBr in water + methanol mixture (alcohol weight fractions 90%) at 298.15 K and 1.0125 bar. The symbols represent experimental data,[319] solid and dashed line presents theoretical prediction and correlation with original and effective dipole moments respectively using of SAFT-VR+DE.

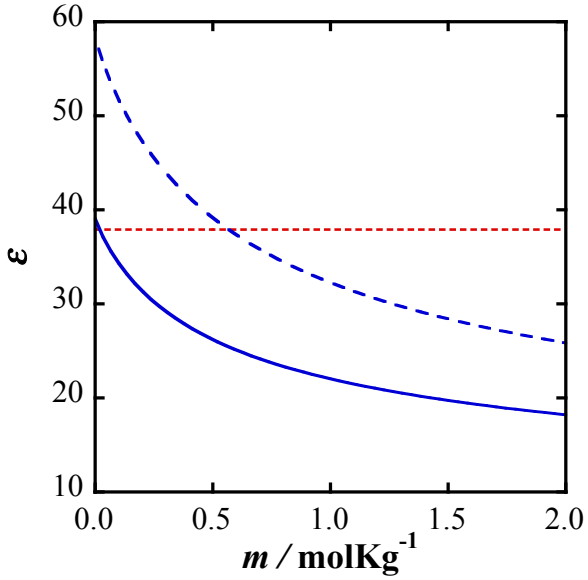

Figure 6.13. SAFT-VR+D equation of state prediction for dielectric constant ε as a function of ionic concentration using different dipole moments μ for methanol + water + NaBr mixture system. Solid line represents the dielectric constant corresponding to original dipole (2.45 D), dashed line gives dielectric constant corresponding to effective dipole moment (2.65 D) and dotted line represnts salt free mixed solvent (90 weight % methanol with water) dielectric constant .[343]

Table 6.3. Comparison between experimental mean ionic activity coefficient ($\gamma_{\pm}$) and theoretical predictions obtained by SAFT-VR+DE EOS for the different electrolytes

System	Alcohol weight fraction	% AAD $\gamma_{\pm}$
RbCl + Methanol + Water	40%	7.49
CsCl + Methanol + Water	20%	2.23
	30%	5.55
	40%	15.29
CsCl + Ethanol + Water	20%	6.13
	30%	9.92
	40%	34.36
KCl + Methanol + Water	40%	3.44
	60%	7.63
NaF + Methanol + Water	20%	2.85
	30%	3.29
	40%	3.00
	50%	2.13
	60%	4.19
	70%	7.43
	80%	4.22

LiCl + Methanol + Water	20%	9.43
NaCl + Methanol + Water	40%	8.71
	60%	10.97
	80%	12.02
NaBr + Methanol + Water	20%	2.89
	40%	8.64
	60%	5.42
	80%	31.24
	90%	53.97
NaBr + Ethanol + Water	20%	8.02
	40%	30.54
	60%	48.39
	80%	50.46
	90%	52.59

6.4 Conclusion

SAFT-VR+DE with one fluid approximation has been used to study experimental mixed solvent electrolyte systems ranging across different ionic concentrations and solvent compositions. A non-primitive model based equation of state has been use for the first

time in literature to study mixed solvent electrolyte systems. The solvent alcohol molecules are modeled as a dipolar square-well dispersive chain with association sites. 2-site association scheme has been used for ethanol where as a 3-site scheme of methanol. The SAFT-VR+D parameters for alcohols are obtained by fitting to experimental vapor pressure and liquid densities data with an effective dipole moment representative of dielectric constant at ambient condition, where as the water parameters are taken from a previous study. The fitted parameters show excellent transferability as vapor-liquid equilibrium of methanol-water system ranging from ambient to 333.15 K temperature along with the composition dependent dielectric constants are predicted without fitting to the mixture data. However, for ethanol-water system a binary unlike dispersive interaction energy parameter is needed for accurate representation of phase behavior at room temperature. For, experimental alcohol-water-salt systems, a predictive approach has been taken; based upon a single alcohol-salt fitted parameter obtained from ternary mean ionic activity coefficient data, mean ionic activity coefficients of nine different electrolyte systems have been predicted. Theory in general shows excellent qualitative as well as quantitative agreement with experimental data for most of the systems. In case of NaCl, NaBr systems, as use of effective ionic radii for Na cation influences a greater amount of dielectric decrement, an improvement can be made with the use of a higher effective dipole moment, which produces less dielectric decrement at higher ionic concentrations.

Chapter 7 : Conclusion and recommendation

The development of a theoretical framework for the accurate prediction of thermodynamics and phase behavior of complex industrially relevant system is of great practical importance to chemical process design. Over last 20 years, advancement in chemical process design can be attributed to the development and improvements in thermodynamic modeling tools such as the SAFT equation of state. The family of SAFT equations has received significant attention due to their ability to rigorously incorporate the effect of anisotropic interactions, such as polar and electrostatic interactions, and structure on the thermodynamics properties of fluids through modification of the reference fluid within the SAFT framework. Building on earlier work, we have taken advantage of this feature of the SAFT family of equations to propose new approaches to model ring containing molecules, like benzene and alkylbenzenes, and electrolytes.

In chapter 3 the main aim of the study was to capture the correct curvature in the experimental saturated liquid densities of pure alkylbenzenes. In this work, an improved modeling scheme for aromatic ring has been adopted, which able to accurately capture $\pi - \pi$ interactions present within benzene/ alkylbenzene rings and thus improves the theoretical representation of saturated liquid densities of pure alkylbenzenes. In future, the novel modeling scheme which has been proposed in this work, can be applied to the study of polymeric compounds with aromatic rings, where phase behavior and thermodynamic properties can be predicted with greater accuracy. In petroleum industry asphaltenes appear as a problem to oil refining, deposits plugs in wellbore tubing and valves, thus possess a hurdle in oil production. Aromatic rings in asphaltene can be modeled using the newly developed modeling scheme and, solubility, phase behavior of

those compounds in hydrocarbons can be accurately predicted. Another possible field of application can be ionic liquids. Using the novel modeling scheme, charge present in the cation can be explicitly positioned at a specific location of the ring.

In chapter 4, the recently developed non primitive model based SAFT-VR+DE approach was used to describe nineteen 1:1 aqueous electrolyte solutions with both a fully dissociated model (as in the original work of Zhao) and a partially dissociated model, considered in order to capture ion association at high salt concentrations. The approach was found to predict thermodynamic properties such as the osmotic coefficient, water activity coefficient and solution density, across different salt concentrations at room temperature and pressure in good agreement with experiment and using only one or two fitted parameters. Although the theory is able to capture the qualitative trend in dielectric decrement of aqueous electrolyte solutions it fails to give quantitative agreement. However one should note, there are also inconsistencies lie within experimental observations due to dielectric saturation and kinetic depolarization and can result in a 25–75% decrease in the measured static permittivity.

In this study, ion-association has been considered via a free energy contribution term similar to SAFT association. In future, ion association can be considered within non primitive model closure while solving Ornstein-Zernike equation for greater consistency. This study only considers nineteen different aqueous electrolyte solution systems of 1:1 alkali halide salts. SAFT-VR+DE can be used for the study of more complex systems, such as salts containing divalent/ trivatent cations and anions in future. Study can also be extended by including systems containing mixed salts as the theory allows the treatment of arbitrary number of ions within the solution. The non primitive model based equation

of state also can be applied for the phase behavior study of complex mixtures such as ionic liquid + alcohol, ionic liquid + CO_2. However, for the study of compounds with quadrupole such as CO_2, it is also necessary to extend the theory to the mixture of ions and quadrupole.

In chapter 5, SAFT-VR+DE approach has been extended to mixed solvent electrolyte systems. In this section, the theory is applied to study several model mixed solvent electrolytes in order to validate a simple one-fluid-like approximation that is proposed in order to describe the interactions between ions and dipolar solvents of arbitrary size and dipole moment within SAFT-VR+DE framework as solution of non primitive model proposed by Blum and Wei only allows one kind of dipolar solvent particle. Before application to real fluids the approach is extensively tested through comparison with isothermal-isobaric ensemble (NPT) Monte Carlo simulations for a number of model mixed solvent electrolyte systems. Simulations have been performed for different ionic concentrations, solvent compositions, cation, anion, and solvent segment diameters, and solvent polarity. The results show that the SAFT-VR+DE equation provides a good description of the PVT behavior of the model mixed solvent electrolyte systems studied, with some over-prediction of the PVT behavior observed at higher ionic concentrations. Additionally, comparisons are made between predictions from the non-primitive and primitive models for electrolytes and the importance of capturing the effect of the ions on the solvent dielectric demonstrated. Subsequently, upon validation the theory has been applied to the study of experimental mixed dipolar solvent electrolyte systems in chapter 6.

In this study, ions are considered to be fully dissociated within the solvent and the

solvent molecules are explicitly treated within the model as well as the theoretical framework. Typically in the study of electrolyte systems the simpler primitive model is used, which requires as input values for the experimental dielectric constant. With the non-primitive model the dielectric is calculated as part of the theory, which is a particularly attractive feature when mixed solvent electrolyte systems are being studied as for those systems experimental dielectric behavior is more scarce. Here for the first time a non-primitive based equations of state has been used for the study of real mixed solvent electrolytes. The solvents considered, water, methanol and ethanol are modeled using the SAFT-VR+D approach in the contribution of the dipole to the thermodynamics and structure of the fluid are explicitly accounted for. The theory is found to accurately predict the vapor-liquid equilibrium, as well as dielectric properties of the salt free alcohol-water mixtures both at room and elevated temperatures. The ternary mixture of salt/water/alcohol was then studied using the SAFT-VR+DE parameters for the salts determined in earlier work containing binary systems and the cation-alcohol unlike dispersive energy parameter obtained by fitting to mean ionic activity coefficient data at room temperature and pressure. Thus, with only one adjustable parameter, a predictive approach is developed. The SAFT-VR+DE predictions are found to be in good quantitative agreement with mean ionic activity coefficient data for several mixed solvent electrolyte systems over a wide range of molalities and solvent weight fractions. In cases where only qualitative agreement is obtained, the theoretical predictions can be improved at higher salt concentrations near the pure alcoholic limits by considering an adjustable effective dipole moment for the mixed solvent, which captures the dielectric decay more accurately.

Mixed solvent electrolyte systems are of industrial interest due to their application in liquid-liquid and vapor-liquid separation processes. Application of salt within miscible mixture of dipolar solvents, phase separates the solvents and helps to recover compounds. In future, SAFT-VR+DE can be used for the prediction of properties such as osmotic coefficients, activity coefficient of the solvents in mixed solvent electrolyte systems for which experimental data is scarce. Using solvent activity coefficient one can determine change in relative volatility of solvent species in the solution, which is a very useful property for the design of separation process. SAFT-VR+DE for mixed solvent electrolyte is an approximated approach as no solution of non primitive mean spherical approximation has been derived to date for mixture composed of arbitrary kinds of ions and dipolar particles, which is useful for the study of system containing multiple kinds of solvent species. In future analytical expression for Helmholtz free energy can be developed for systems composed of arbitrary number of ions along with dipolar particles.

REFERENCES

[1] B. Linnhoff, New Concepts in Thermodynamics for Better Chemical Process Design, in: J. Lewins (Ed.) Teaching Thermodynamics, Springer US, 1985, pp. 297-339.

[2] C.C. Chen, Toward development of activity coefficient models for process and product design of complex chemical systems, Fluid Phase Equilibria, 241 (2006) 103-112.

[3] C.C. Chen, P.M. Mathias, Applied thermodynamics for process modeling, Aiche J, 48 (2002) 194-200.

[4] D. Sama, The use of the second law of thermodynamics in process design, Journal of energy resources technology, 117 (1995) 179-185.

[5] G. Soave, Equilibrium Constants from a Modified Redlich-Kwong Equation of State, Chem Eng Sci, 27 (1972) 1197.

[6] C.C. Chen, A Segment-Based Local Composition Model for the Gibbs Energy of Polymer-Solutions, Fluid Phase Equilibria, 83 (1993) 301-312.

[7] C.C. Chen, L.B. Evans, A Local Composition Model for the Excess Gibbs Energy of Aqueous-Electrolyte Systems, Aiche J, 32 (1986) 444-454.

[8] A. Fredenslund, R.L. Jones, J.M. Prausnitz, Group-Contribution Estimation of Activity-Coefficients in Nonideal Liquid-Mixtures, Aiche J, 21 (1975) 1086-1099.

[9] J.O. Valderrama, The state of the cubic equations of state, Ind. Eng. Chem. Res., 42 (2003) 1603-1618.

[10] W.G. Chapman, K.E. Gubbins, G. Jackson, M. Radosz, Saft - Equation-of-State Solution Model for Associating Fluids, Fluid Phase Equilibr, 52 (1989) 31-38.

[11] W.G. Chapman, K.E. Gubbins, G. Jackson, M. Radosz, New reference equation of state for associating liquids, Industrial & Engineering Chemistry Research, 29 (1990) 1709-1721.

[12] G. Jackson, A. Galindo, A. Gil-Villegas, P.J. Whitehead, A.N. Burgess, Prediction of phase equilibria for refrigerant mixtures of difluoromethane (HFC-32), 1,1,1,2-tetrafluoroethane (HFC-134a), and pentafluoroethane (HFC-125a) using SAFT-VR, J Phys Chem B, 102 (1998) 7632-7639.

[13] L. Sun, H. Zhao, C. McCabe, Phase Equilibria of Gas Condensates and Light Petroleum Fractions from the SAFT-VR Approach, Aiche J, 53 (2007) 720-731.

[14] C. McCabe, A. Galindo, A. Gil-Villegas, G. Jackson, Predicting the high-pressure phase equilibria of binary mixtures of perfluoro-n-alkanes plus n-alkanes using the SAFT-VR approach, J Phys Chem B, 102 (1998) 8060-8069.

[15] F.J. Blas, M.C. Dos Ramos, Theory of phase equilibria for model mixtures of n-alkanes, perfluoroalkanes and perfluoroalkylalkane diblock surfactants, Mol Phys, 105 (2007) 1319-1334.

[16] A. Baylaucq, G. Watson, T. Latitte, C.K. Zeberg-Mikkelsen, D. Bessieres, C. Boned, Volumetric and derivative properties under pressure for the system 1-propanol plus toluene: A discussion of PC-SAFT and SAFT-VR (vol 247, pg 121, 2006), Fluid Phase Equilibria, 253 (2007) 80-80.

[17] G.N.I. Clark, A. Galindo, G. Jackson, S. Rogers, A.N. Burgess, Modeling and understanding closed-loop liquid - Liquid immiscibility in aqueous solutions of poly(ethylene glycol) using the SAFT-VR approach with transferable parameters, Macromolecules, 41 (2008) 6582-6595.

[18] A. Valtz, A. Chapoy, C. Coquelet, P. Paricaud, D. Richon, Vapour-liquid equilibria in the carbon dioxide-water system, measurement and modelling from 278.2 to 318.2K, Fluid Phase Equilibria, 226 (2004) 333-344.

[19] G.N.I. Clark, A.J. Haslam, A. Galindo, G. Jackson, Developing optimal Wertheim-like models of water for use in Statistical Associating Fluid Theory (SAFT) and related approaches, Mol Phys, 104 (2006) 3561-3581.

[20] A. Galindo, A. Gil-Villegas, P.J. Whitehead, G. Jackson, A.N. Burgess, Prediction of phase equilibria for refrigerant mixtures of difluoromethane (HFC-32), 1,1,1,2-tetrafluoroethane (HFC-134a), and pentafluoroethane (HFC-125a) using SAFT-VR, J Phys Chem B, 102 (1998) 7632-7639.

[21] S. Swaminathan, D.P. Visco, Thermodynamic modeling of refrigerants using the statistical associating fluid theory with variable range. 2. Applications to binary mixtures, Ind. Eng. Chem. Res., 44 (2005) 4806-4814.

[22] C.M. Colina, A. Galindo, F.J. Blas, K.E. Gubbins, Phase behavior of carbon dioxide mixtures with n-alkanes and n-perfluoroalkanes, Fluid Phase Equilibria, 222 (2004) 77-85.

[23] M.C. dos Ramos, F.J. Blas, A. Galindo, Phase equilibria, excess properties, and Henry's constants of the water plus carbon dioxide binary mixturet, J. Phys. Chem. C, 111 (2007) 15924-15934.

[24] J. Gross, G. Sadowski, Application of the perturbed-chain SAFT equation of state to associating systems, Ind. Eng. Chem. Res., 41 (2002) 5510-5515.

[25] J. Rozmus, J.C. de Hemptinne, P. Mougin, Application of GC-PPC-SAFT EoS to amine mixtures with a predictive approach, Fluid Phase Equilibria, 303 (2011) 15-30.

[26] A. Galindo, A. Gil-Villegas, G. Jackson, A.N. Burgess, SAFT-VRE: Phase behavior of electrolyte solutions with the statistical associating fluid theory for potentials of variable range, J Phys Chem B, 103 (1999) 10272-10281.

[27] J.M.A. Schreckenberg, S. Dufal, A.J. Haslam, C.S. Adjiman, G. Jackson, A. Galindo, Modelling of the thermodynamic and solvation properties of electrolyte solutions with the statistical associating fluid theory for potentials of variable range, Mol Phys, 112 (2014) 2339-2364.

[28] Y. Liu, Z.B. Li, J.G. Mi, C.L. Zhong, Modeling of aqueous electrolyte solutions based on primitive and first-order mean spherical approximation, Ind. Eng. Chem. Res., 47 (2008) 1695-1701.

[29] H.G. Zhao, M.C. dos Ramos, C. McCabe, Development of an equation of state for electrolyte solutions by combining the statistical associating fluid theory and the mean spherical approximation for the nonprimitive model, J Chem Phys, 126 (2007).

[30] K. Paduszynski, U. Domanska, Thermodynamic Modeling of Ionic Liquid Systems: Development and Detailed Overview of Novel Methodology Based on the PC-SAFT, J Phys Chem B, 116 (2012) 5002-5018.

[31] P.M. Ndiaye, E. Franceschi, D. Oliveira, C. Dariva, F.W. Tavares, J.V. Oliveira, Phase behavior of soybean oil, castor oil and their fatty acid ethyl esters in carbon dioxide at high pressures, J Supercrit Fluid, 37 (2006) 29-37.

[32] C.R.I. Jessica D. Haley, Peter T. Cummings, EXAMINING THE AGGREGATION BEHAVIOR OF POLYMER GRAFTED NANOPARTICLES USING MOLECULAR SIMULATION AND THEORY, Journal of Chemical Physics (under review), (2015).

[33] Y. Peng, C. McCabe, Molecular simulation and theoretical modeling of polyhedral oligomeric silsesquioxanes, Mol Phys, 105 (2007) 261-272.

[34] A. Galindo, L.J. Florusse, C.J. Peters, Prediction of phase equilibria for binary systems of hydrogen chloride with ethane, propane and n-dodecane, Fluid Phase Equilibria, 160 (1999) 123-131.

[35] H.G. Zhao, P. Morgado, C. McCabe, A. Gil Villegas, Predicting the Phase Behavior of Nitrogen + n-Alkanes for Enhanced Oil Recovery from the SAFT-VR Approach: Examining the Effect of the Quadrupole Moment, J Phys Chem B, 110 (2006) 24083-24092.

[36] A. GilVillegas, A. Galindo, P.J. Whitehead, S.J. Mills, G. Jackson, A.N. Burgess, Statistical associating fluid theory for chain molecules with attractive potentials of

variable range, J Chem Phys, 106 (1997) 4168-4186.

[37] H.G. Zhao, C. McCabe, Phase behavior of dipolar fluids from a modified statistical associating fluid theory for potentials of variable range, J Chem Phys, 125 (2006).

[38] C. McCabe, A. Galindo, SAFT Associating Fluids and Fluid Mixtures, in: J.V. Sengers, A.R.H. Goodwin, C.J. Peters (Eds.) Applied Thermodynamics of Fluids Royal Society of Chemistry, Cambridge, 2010, pp. 215-279.

[39] S. Tamouza, J.P. Passarello, P. Tobaly, J.C. de Hemptinne, Group contribution method with SAFT EOS applied to vapor liquid equilibria of various hydrocarbon series, Fluid Phase Equilibria, 222 (2004) 67-76.

[40] A. Lymperiadis, C.S. Adjiman, A. Galindo, G. Jackson, A group contribution method for associating chain molecules based on the statistical associating fluid theory (SAFT-gamma), J Chem Phys, 127 (2007).

[41] Y. Peng, K.D. Goff, M.C. dos Ramos, C. McCabe, Developing a predictive group-contribution-based SAFT-VR equation of state, Fluid Phase Equilibria, 277 (2009) 131-144.

[42] J. Vijande, M.M. Pineiro, J.L. Legido, D. Bessieres, Group-Contribution Method for the Molecular Parameters of the PC-SAFT Equation of State Taking into Account the Proximity Effect. Application to Nonassociated Compounds, Ind. Eng. Chem. Res., 49 (2010) 9394-9406.

[43] A. Tihic, G.M. Kontogeorgis, N. von Solms, M.L. Michelsen, L. Constantinou, A Predictive Group-Contribution Simplified PC-SAFT Equation of State: Application to Polymer Systems, Ind. Eng. Chem. Res., 47 (2008) 5092-5101.

[44] K. Paduszynski, U. Domanska, Heterosegmented Perturbed-Chain Statistical Associating Fluid Theory as a Robust and Accurate Tool for Modeling of Various Alkanes. 1. Pure Fluids, Ind. Eng. Chem. Res., 51 (2012) 12967-12983.

[45] R. Enick, S. Klara, Effects of CO2 solubility in brine on the compositional simulation of CO2 floods, SPE reservoir engineering, 7 (1992) 253-258.

[46] R.H. Davies, in Chemical Thermodynamics in Industry: Models and Computation, Blackwell Scientific Publishers,Oxford, (1985).

[47] N.C. Scrivner, Some Problems in Electrolyte Solutions, presented at the American Institute of Chemical Engineers Annual Meeting,San Francisco, CA, (1984).

[48] M.R.a.N.C.S. J. F. Zemaitis Jr. D. M. Clark, Handbook of Aqueous Electrolyte Thermodynamics, Design Institute for Physical Property Data, American Institute of Chemical Engineers, New York, (1986).

[49] A. Anderko, P.M. Wang, M. Rafal, Electrolyte solutions: from thermodynamic and transport property models to the simulation of industrial processes, Fluid Phase Equilibria, 194 (2002) 123-142.

[50] G.M.F. Kontogeorgis, G. K., Thermodynamic Models for Industrial Applications: From Classical and Advanced Mixing Rules to Association Theories, (2010) 461-523.

[51] K.S. Pitzer, Thermodynamics of electrolytes. I. Theoretical basis and general equations, The Journal of Physical Chemistry, 77 (1973) 268-277.

[52] J.R. Loehe, M.D. Donohue, Recent advances in modeling thermodynamic properties of aqueous strong electrolyte systems, Aiche J, 43 (1997) 180-195.

[53] K.S. Pitzer, D.R. Schreiber, The Restricted Primitive Model for Ionic Fluids - Properties of the Vapor and the Critical Region, Mol Phys, 60 (1987) 1067-1078.

[54] H.L. Friedman, Electrolyte-Solutions at Equilibrium, Annual Review of Physical Chemistry, 32 (1981) 179-204.

[55] X.Y. Ji, S.P. Tan, H. Adidharma, M. Radosz, Statistical associating fluid theory coupled with restricted primitive model to represent aqueous strong electrolytes: Multiple-salt solutions, Ind. Eng. Chem. Res., 44 (2005) 7584-7590.

[56] M.S. Wertheim, Fluids with Highly Directional Attractive Forces .1. Statistical Thermodynamics, J. Stat. Phys., 35 (1984) 19-34.

[57] M.S. Wertheim, Fluids With Highly Directional Attractive Forces .2. Thermodynamic Perturbation-Theory And Integral-Equations, J. Stat. Phys., 35 (1984) 35-47.

[58] M.S. Wertheim, Fluids with Highly Directional Attractive Forces .3. Multiple Attraction Sites, J. Stat. Phys., 42 (1986) 459-476.

[59] M.S. Wertheim, Fluids with Highly Directional Attractive Forces .4. Equilibrium Polymerization, J. Stat. Phys., 42 (1986) 477-492.

[60] Y.H. Fu, S.I. Sandler, A Simplified Saft Equation of State for Associating Compounds and Mixtures, Ind. Eng. Chem. Res., 34 (1995) 1897-1909.

[61] W.G. Chapman, K.E. Gubbins, G. Jackson, M. Radosz, SAFT: Equation-of-state solution model for associating fluids, Fluid Phase Equilibria, 52 (1989) 31-38.

[62] C.H. Twu, L.L. Lee, K.E. Starling, Improved analytical representation of argon thermodynamic behavior, Fluid Phase Equilibria, 4 (1980) 35-44.

[63] R.L. Cotterman, B.J. Schwarz, J.M. Prausnitz, Molecular Thermodynamics for

Fluids at Low and High-Densities .1. Pure Fluids Containing Small or Large Molecules, Aiche J, 32 (1986) 1787-1798.

[64] J.K. Johnson, E.A. Muller, K.E. Gubbins, Equation of State for Lennard-Jones Chains, J Phys Chem-Us, 98 (1994) 6413-6419.

[65] J.K. Johnson, J.A. Zollweg, K.E. Gubbins, The Lennard-Jones equation of state revisited, Mol Phys, 78 (1993) 591-618.

[66] S.H. Huang, M. Radosz, Equation of state for small, large, polydisperse, and associating molecules: extension to fluid mixtures, Ind. Eng. Chem. Res., 30 (1991) 1994-2005.

[67] S.H. Huang, M. Radosz, Equation of state for small, large, polydisperse, and associating molecules, Ind. Eng. Chem. Res., 29 (1990) 2284-2294.

[68] S. S. Chen and A. Kreglewski, Ber. Bunsen. Phys. Chem, , 81,(1977,) 1048–1052.

[69] S.J. Chen, I.G. Economou, M. Radosz, Density-tuned polyolefin phase equilibria. 2. Multicomponent solutions of alternating poly(ethylene-propylene) in subcritical and supercritical olefins. Experiment and SAFT model, Macromolecules, 25 (1992) 4987-4995.

[70] C. Chen, M.A. Duran, M. Radosz, Phase equilibria in polymer solutions. Block-algebra, simultaneous flash algorithm coupled with SAFT equation of state, applied to single-stage supercritical antisolvent fractionation of polyethylene, Ind. Eng. Chem. Res., 32 (1993) 3123-3127.

[71] S.-J. Chen, I.G. Economou, M. Radosz, Phase behavior of LCST and UCST solutions of branchy copolymers: experiment and SAFT modelling, Fluid Phase Equilibria, 83 (1993) 391-398.

[72] M. Lora, M.A. McHugh, Phase behavior and modeling of the poly(methyl methacrylate)–CO2–methyl methacrylate system, Fluid Phase Equilibria, 157 (1999) 285-297.

[73] C. Pan, M. Radosz, Phase Behavior of Poly(ethylene-co-hexene-1) Solutions in Isobutane and Propane, Ind. Eng. Chem. Res., 38 (1999) 2842-2848.

[74] G. Jackson, W.G. Chapman, K.E. Gubbins, Phase-Equilibria of Associating Fluids - Spherical Molecules with Multiple Bonding Sites, Mol Phys, 65 (1988) 1-31.

[75] A. Galindo, P.J. Whitehead, G. Jackson, A.N. Burgess, Predicting the high-pressure phase equilibria of water plus n-alkanes using a simplified SAFT theory with transferable intermolecular interaction parameters, J Phys Chem-Us, 100 (1996) 6781-6792.

[76] N.F. Carnahan, K.E. Starling, Equation of State for Nonattracting Rigid Spheres, J

Chem Phys, 51 (1969) 635

[77] A. Galindo, P.J. Whitehead, G. Jackson, Predicting the High-Pressure Phase Equilibria of Water + n-Alkanes Using a Simplified SAFT Theory with Transferable Intermolecular Interaction Parameters, The Journal of Physical Chemistry, 100 (1996) 6781-6792.

[78] A. Galindo, P.J. Whitehead, G. Jackson, A.N. Burgess, Predicting the Phase Equilibria of Mixtures of Hydrogen Fluoride with Water, Difluoromethane (HFC-32), and 1,1,1,2-Tetrafluoroethane (HFC-134a) Using a Simplified SAFT Approach, The Journal of Physical Chemistry B, 101 (1997) 2082-2091.

[79] J.G. Andersen, N. Koak, T.W. de Loos, Influence of pressure on the LLLE in water+n-alkyl polyoxyethylene ether+n-alkane systems, Fluid Phase Equilibria, 163 (1999) 259-273.

[80] F.J. Blas, L.F. Vega, Prediction of Binary and Ternary Diagrams Using the Statistical Associating Fluid Theory (SAFT) Equation of State, Ind. Eng. Chem. Res., 37 (1998) 660-674.

[81] F. Llovell, C.J. Peters, L.F. Vega, Second-order thermodynamic derivative properties of selected mixtures by the soft-SAFT equation of state, Fluid Phase Equilibria, 248 (2006) 115-122.

[82] M.C. dos Ramos, F.J. Blas, Examination of the Excess Thermodynamic Properties of n-Alkane Binary Mixtures: A Molecular Approach, The Journal of Physical Chemistry B, 109 (2005) 12145-12153.

[83] F.J.B.a.L.F. Vega, Critical behavior and partial miscibility phenomena in binary mixtures of hydrocarbons by the statistical associating fluid theory, J. Chem. Phys, 109 (1998) 7405–7413.

[84] J.C. Pàmies, L.F. Vega, Vapor−Liquid Equilibria and Critical Behavior of Heavy n-Alkanes Using Transferable Parameters from the Soft-SAFT Equation of State, Ind. Eng. Chem. Res., 40 (2001) 2532-2543.

[85] F. Llovell, L.F. Vega, Phase equilibria, critical behavior and derivative properties of selected n-alkane/n-alkane and n-alkane/1-alkanol mixtures by the crossover soft-SAFT equation of state, The Journal of Supercritical Fluids, 41 (2007) 204-216.

[86] A.M.A. Dias, J.C. Pàmies, J.A.P. Coutinho, I.M. Marrucho, L.F. Vega, SAFT Modeling of the Solubility of Gases in Perfluoroalkanes, The Journal of Physical Chemistry B, 108 (2004) 1450-1457.

[87] A.M.A. Dias, C.M.B. Gonçalves, A.I. Caço, L.M.N.B.F. Santos, M.M. Piñeiro, L.F. Vega, J.A.P. Coutinho, I.M. Marrucho, Densities and Vapor Pressures of Highly

Fluorinated Compounds, Journal of Chemical & Engineering Data, 50 (2005) 1328-1333.

[88] A. Galindo, F.J. Blas, Theoretical Examination of the Global Fluid Phase Behavior and Critical Phenomena in Carbon Dioxide + n-Alkane Binary Mixtures, The Journal of Physical Chemistry B, 106 (2002) 4503-4515.

[89] C.M. Colina, L.F. Turrens, K.E. Gubbins, C. Olivera-Fuentes, L.F. Vega, Predictions of the Joule−Thomson Inversion Curve for the n-Alkane Series and Carbon Dioxide from the Soft-SAFT Equation of State†, Ind. Eng. Chem. Res., 41 (2002) 1069-1075.

[90] N. Pedrosa, J.C. Pàmies, J.A.P. Coutinho, I.M. Marrucho, L.F. Vega, Phase Equilibria of Ethylene Glycol Oligomers and Their Mixtures, Ind. Eng. Chem. Res., 44 (2005) 7027-7037.

[91] N. Mac Dowell, F. Llovell, N. Sun, J.P. Hallett, A. George, P.A. Hunt, T. Welton, B.A. Simmons, L.F. Vega, New Experimental Density Data and Soft-SAFT Models of Alkylimidazolium ([CnC1im]+) Chloride (Cl–), Methylsulfate ([MeSO4]−), and Dimethylphosphate ([Me2PO4]−) Based Ionic Liquids, The Journal of Physical Chemistry B, 118 (2014) 6206-6221.

[92] M.B. Oliveira, S.V.D. Freitas, F. Llovell, L.F. Vega, J.A.P. Coutinho, Development of simple and transferable molecular models for biodiesel production with the soft-SAFT equation of state, Chemical Engineering Research and Design, 92 (2014) 2898-2911.

[93] L.M.C. Pereira, M.B. Oliveira, F. Llovell, L.F. Vega, J.A.P. Coutinho, Assessing the N2O/CO2 high pressure separation using ionic liquids with the soft-SAFT EoS, The Journal of Supercritical Fluids, 92 (2014) 231-241.

[94] A. Galindo, L.A. Davies, A. Gil-Villegas, G. Jackson, The thermodynamics of mixtures and the corresponding mixing rules in the SAFT-VR approach for potentials of variable range, Mol Phys, 93 (1998) 241-252.

[95] C. McCabe, G. Jackson, SAFT-VR modelling of the phase equilibrium of long-chain n-alkanes, Physical Chemistry Chemical Physics, 1 (1999) 2057-2064.

[96] C. McCabe, A. Galindo, M.N. García-Lisbona, G. Jackson, Examining the Adsorption (Vapor−Liquid Equilibria) of Short-Chain Hydrocarbons in Low-Density Polyethylene with the SAFT-VR Approach, Ind. Eng. Chem. Res., 40 (2001) 3835-3842.

[97] L.M.B. Dias, E.J.M. Filipe, C. McCabe, J.C.G. Calado, Thermodynamics of Liquid (Xenon + Methane) Mixtures, The Journal of Physical Chemistry B, 108 (2004) 7377-7381.

[98] A. Galindo, A. Gil-Villegas, P.J. Whitehead, G. Jackson, A.N. Burgess, Prediction of Phase Equilibria for Refrigerant Mixtures of Difluoromethane (HFC-32), 1,1,1,2-Tetrafluoroethane (HFC-134a), and Pentafluoroethane (HFC-125a) Using SAFT-VR, The

Journal of Physical Chemistry B, 102 (1998) 7632-7639.

[99] P. Morgado, C. McCabe, E.J. M. Filipe, Modelling the phase behaviour and excess properties of alkane + perfluoroalkane binary mixtures with the SAFT–VR approach, Fluid Phase Equilibria, 228–229 (2005) 389-393.

[100] G. Watson, T. Lafitte, C.K. Zéberg-Mikkelsen, A. Baylaucq, D. Bessieres, C. Boned, Volumetric and derivative properties under pressure for the system 1-propanol + toluene: A discussion of PC-SAFT and SAFT-VR, Fluid Phase Equilibria, 247 (2006) 121-134.

[101] G.N.I. Clark, A. Galindo, G. Jackson, S. Rogers, A.N. Burgess, Modeling and Understanding Closed-Loop Liquid−Liquid Immiscibility in Aqueous Solutions of Poly(ethylene glycol) Using the SAFT-VR Approach with Transferable Parameters, Macromolecules, 41 (2008) 6582-6595.

[102] A. Valtz, A. Chapoy, C. Coquelet, P. Paricaud, D. Richon, Vapour–liquid equilibria in the carbon dioxide–water system, measurement and modelling from 278.2 to 318.2 K, Fluid Phase Equilibria, 226 (2004) 333-344.

[103] L. Sun, H. Zhao, C. McCabe, Predicting the phase equilibria of petroleum fluids with the SAFT-VR approach, Aiche J, 53 (2007) 720-731.

[104] P.-A. Artola, F.E. Pereira, C.S. Adjiman, A. Galindo, E.A. Müller, G. Jackson, A.J. Haslam, Understanding the fluid phase behaviour of crude oil: Asphaltene precipitation, Fluid Phase Equilibria, 306 (2011) 129-136.

[105] L. Sun, H. Zhao, S.B. Kiselev, C. McCabe, Application of SAFT–VRX to binary phase behaviour: alkanes, Fluid Phase Equilibria, 228–229 (2005) 275-282.

[106] F.J. Blas, A. Galindo, Study of the high pressure phase behaviour of CO2+n-alkane mixtures using the SAFT-VR approach with transferable parameters, Fluid Phase Equilibria, 194–197 (2002) 501-509.

[107] G. Sadowski, J. Gross, Perturbed-chain SAFT: An equation of state based on a perturbation theory for chain molecules, Ind. Eng. Chem. Res., 40 (2001) 1244-1260.

[108] J. Gross, G. Sadowski, Perturbed-Chain SAFT: An Equation of State Based on a Perturbation Theory for Chain Molecules, Ind. Eng. Chem. Res., 40 (2001) 1244-1260.

[109] F. Tumakaka, G. Sadowski, Application of the Perturbed-Chain SAFT equation of state to polar systems, Fluid Phase Equilibria, 217 (2004) 233-239.

[110] I.A. Kouskoumvekaki, N. von Solms, T. Lindvig, M.L. Michelsen, G.M. Kontogeorgis, Novel Method for Estimating Pure-Component Parameters for Polymers: Application to the PC-SAFT Equation of State, Ind. Eng. Chem. Res., 43 (2004) 2830-

2838.

[111] K. Paduszyński, U. Domańska, Thermodynamic Modeling of Ionic Liquid Systems: Development and Detailed Overview of Novel Methodology Based on the PC-SAFT, The Journal of Physical Chemistry B, 116 (2012) 5002-5018.

[112] T. Spyriouni, X. Krokidis, I.G. Economou, Thermodynamics of pharmaceuticals: Prediction of solubility in pure and mixed solvents with PC-SAFT, Fluid Phase Equilibria, 302 (2011) 331-337.

[113] F. Ruether, G. Sadowski, Modeling the solubility of pharmaceuticals in pure solvents and solvent mixtures for drug process design, Journal of Pharmaceutical Sciences, 98 (2009) 4205-4215.

[114] D.L. Gonzalez, F.M. Vargas, G.J. Hirasaki, W.G. Chapman, Modeling Study of CO2-Induced Asphaltene Precipitation†, Energ Fuel, 22 (2008) 757-762.

[115] I.A. Kouskoumvekaki, N. von Solms, M.L. Michelsen, G.M. Kontogeorgis, Application of the perturbed chain SAFT equation of state to complex polymer systems using simplified mixing rules, Fluid Phase Equilibria, 215 (2004) 71-78.

[116] I.A. Kouskoumvekaki, G.J.P. Krooshof, M.L. Michelsen, G.M. Kontogeorgis, Application of the Simplified PC-SAFT Equation of State to the Vapor−Liquid Equilibria of Binary and Ternary Mixtures of Polyamide 6 with Several Solvents, Ind. Eng. Chem. Res., 43 (2004) 826-834.

[117] S. Tamouza, J.P. Passarello, P. Tobaly, J.C. de Hemptinne, Application to binary mixtures of a group contribution SAFT EOS (GC-SAFT), Fluid Phase Equilibria, 228 (2005) 409-419.

[118] T.X.N. Thi, S. Tamouza, P. Tobaly, J.P. Passarello, J.C. de Hemptinne, Application of group contribution SAFT equation of state (GC-SAFT) to model phase behaviour of light and heavy esters, Fluid Phase Equilibria, 238 (2005) 254-261.

[119] D. NguyenHuynh, J.P. Passarello, P. Tobaly, J.C. de Hemptinne, Application of GC-SAFT EOS to polar systems using a segment approach, Fluid Phase Equilibria, 264 (2008) 62-75.

[120] A. Lymperiadis, C.S. Adjiman, G. Jackson, A. Galindo, A generalisation of the SAFT-gamma group contribution method for groups comprising multiple spherical segments, Fluid Phase Equilibria, 274 (2008) 85-104.

[121] V. Papaioannou, C.S. Adjiman, G. Jackson, A. Galindo, Simultaneous prediction of vapour-liquid and liquid-liquid equilibria (VLE and LLE) of aqueous mixtures with the SAFT-gamma group contribution approach, Fluid Phase Equilibria, 306 (2011) 82-96.

[122] C. McCabe, Y. Peng, K.D. Goff, M.C. dos Ramos, Developing a predictive group-contribution-based SAFT-VR equation of state, Fluid Phase Equilibria, 277 (2009) 131-144.

[123] Y. Peng, K.D. Goff, M.C. dos Ramos, C. McCabe, Predicting the Phase Behavior of Polymer Systems with the GC-SAFT-VR Approach, Ind. Eng. Chem. Res., 49 (2010) 1378-1394.

[124] M.C. dos Ramos, J.D. Haley, J.R. Westwood, C. McCabe, Extending the GC-SAFT-VR approach to associating functional groups: Alcohols, aldehydes, amines and carboxylic acids, Fluid Phase Equilibria, 306 (2011) 97-111.

[125] J. Vijande, M.M. Pineiro, J.L. Legido, Group-Contribution Method with Proximity Effect for PC-SAFT Molecular Parameters. 2. Application to Association Parameters: Primary Alcohols and Amines, Ind. Eng. Chem. Res., 53 (2014) 909-919.

[126] J. Gross, G. Sadowski, Application of perturbation theory to a hard-chain reference fluid: an equation of state for square-well chains, Fluid Phase Equilibria, 168 (2000) 183-199.

[127] D. NguyenHuynh, A. Falaix, J.P. Passarello, P. Tobaly, J.C. de Hemptinne, Predicting VLE of heavy esters and their mixtures using GC-SAFT, Fluid Phase Equilibria, 264 (2008) 184-200.

[128] D. NguyenHuynh, J.P. Passarello, J.C. de Hemptinne, P. Tobaly, Extension of polar GC-SAFT to systems containing some oxygenated compounds: Application to ethers, aldehydes and ketones, Fluid Phase Equilibria, 307 (2011) 142-159.

[129] D. Nguyen-Huynh, T.K.S. Tran, S. Tamouza, J.P. Passarello, P. Tobaly, J.C. de Hemptinne, Modeling Phase Equilibria of Asymmetric Mixtures Using a Group-Contribution SAFT (GC-SAFT) with a k(ij) Correlation Method Based on London's Theory. 2. Application to Binary Mixtures Containing Aromatic Hydrocarbons, n-Alkanes, CO2, N-2, and H2S, Ind. Eng. Chem. Res., 47 (2008) 8859-8868.

[130] T.K.S. Tran, D. NguyenHuynh, N. Ferrando, J.P. Passarello, J.C. de Hemptinne, P. Tobaly, Modeling VLE of H(2) + Hydrocarbon Mixtures Using a Group Contribution SAFT with a k(ij) Correlation Method Based on London's Theory, Energ Fuel, 23 (2009) 2658-2665.

[131] N.H. Dong, J.C. de Hemptinne, R. Lugo, J.P. Passarello, P. Tobaly, Modeling Liquid-Liquid and Liquid-Vapor Equilibria of Binary Systems Containing Water with an Alkane, an Aromatic Hydrocarbon, an Alcohol or a Gas (Methane, Ethane, CO2 or H2S), Using Group Contribution Polar Perturbed-Chain Statistical Associating Fluid Theory, Ind. Eng. Chem. Res., 50 (2011) 7467-7483.

[132] N. von Solms, M.L. Michelsen, G.M. Kontogeorgis, Computational and Physical

Performance of a Modified PC-SAFT Equation of State for Highly Asymmetric and Associating Mixtures, Ind. Eng. Chem. Res., 42 (2003) 1098-1105.

[133] A. Tihic, N. von Solms, M.L. Michelsen, G.M. Kontogeorgis, L. Constantinou, Analysis and applications of a group contribution sPC-SAFT equation of state, Fluid Phase Equilibria, 281 (2009) 60-69.

[134] A. Tihic, N. von Solms, M.L. Michelsen, G.M. Kontogeorgis, L. Constantinou, Application of sPC-SAFT and group contribution sPC-SAFT to polymer systems—Capabilities and limitations, Fluid Phase Equilibria, 281 (2009) 70-77.

[135] A. Gil Villegas, A. Galindo, P.J. Whitehead, S.J. Mills, G. Jackson, A.N. Burgess, Statistical associating fluid theory for chain molecules with attractive potentials of variable range, J Chem Phys, 106 (1997) 4168-4186.

[136] J.A. Barker, Henderso.D, Perturbation Theory and Equation of State for Fluids - Square-Well Potential, J Chem Phys, 47 (1967).

[137] J.A. Barker, Henderso.D, Perturbation Theory and Equation of State for Fluids .2. A Successful Theory of Liquids, J Chem Phys, 47 (1967).

[138] R.W. Zwanzig, High-temperature equation of state by a perturbation method. I. nonpolar gases, The Journal of Chemical Physics, 22 (1954) 1420--1426.

[139] D.H. JA Barker, Rev. Mod. Phys, 48 (1975).

[140] B.H. Patel, H. Docherty, S. Varga, A. Galindo, G.C. Maitland, Generalized equation of state for square-well potentials of variable range, Mol Phys, 103 (2005) 129-139.

[141] J.S. Rowlinson, Molecular Theory of Liquids and Liquid-Mixtures, Ber Bunsen Phys Chem, 85 (1981) 970-979.

[142] T. Boublik, Hard-Sphere Equation of State, J Chem Phys, 53 (1970).

[143] G.A. Mansoori, N.F. Carnahan, K.E. Starling, T.W. Leland, Equilibrium Thermodynamic Properties of Misture of Hard Spheres, J Chem Phys, 54 (1971) 1523.

[144] T.F. Anderson, J.M. Prausnitz, Application of Uniquac Equation to Calculation of Multicomponent Phase-Equilibria .1. Vapor-Liquid-Equilibria, Ind Eng Chem Proc Dd, 17 (1978) 552-561.

[145] A. Fredenslund, J. Gmehling, M.L. Michelsen, P. Rasmussen, J.M. Prausnitz, Computerized Design of Multicomponent Distillation-Columns Using Unifac Group Contribution Method for Calculation of Activity-Coefficients, Ind Eng Chem Proc Dd, 16 (1977) 450-462.

[146] M.K. Ikeda, L.A. Schaefer, Examining the effect of binary interaction parameters on VLE modelling using cubic equations of state, Fluid Phase Equilibria, 305 (2011) 233-237.

[147] W.G. Chapman, G. Jackson, K.E. Gubbins, Phase-Equilibria of Associating Fluids Chain Molecules With Multiple Bonding Sites, Mol Phys, 65 (1988) 1057-1079.

[148] S.P. Tan, H. Adidharma, M. Radosz, Recent advances and applications of statistical associating fluid theory, Ind Eng Chem Res, 47 (2008) 8063-8082.

[149] F.J. Blas, A. Galindo, Study of the high pressure phase behaviour of CO2+n-alkane mixtures using the SAFT-VR approach with transferable parameters, Fluid Phase Equilibria, 194 (2002) 501-509.

[150] A. Galindo, F.J. Blas, Theoretical examination of the global fluid phase behavior and critical phenomena in carbon dioxide plus n-alkane binary mixtures, J Phys Chem B, 106 (2002) 4503-4515.

[151] Design Institute for Physical Property Data (U.S.), Knovel (Firm), DIPPR Project 801, full version evaluated standard thermophysical property values, in, BYU DIPPR, Thermophysical Properties Laboratory, Provo, Utah, 2005.

[152] P. Passarello, Private communication.

[153] J. Sponer, J. Leszczynski, P. Hobza, Electronic properties, hydrogen bonding, stacking, and cation binding of DNA and RNA bases, Biopolymers, 61 (2001) 3-31.

[154] J.D. Hepworth, D.R. Waring, M.J. Waring, Royal Society of Chemistry (Great Britain), Aromatic chemistry, Royal Society of Chemistry, Cambridge, 2002.

[155] M. Sainsbury, Aromatic chemistry, Oxford University Press, Oxford ; New York, 1992.

[156] C. McCabe, A. Gil-Villegas, G. Jackson, F. del Rio, The thermodynamics of heteronuclear molecules formed from bonded square-well (BSW) segments using the SAFT-VR approach, Mol Phys, 97 (1999) 551-558.

[157] S. Kirkpatrick, C.D. Gelatt, M.P. Vecchi, Optimization by Simulated Annealing, Science, 220 (1983) 671-680.

[158] W.B. Dolan, P.T. Cummings, M.D. Levan, Process Optimization Via Simulated Annealing - Application to Network Design, Aiche J, 35 (1989) 725-736.

[159] C. McCabe, S.B. Kiselev, Application of crossover theory to the SAFT-VR equation of state: SAFT-VRX for pure fluids, Ind. Eng. Chem. Res., 43 (2004) 2839-2851.

[160] T. Lafitte, D. Bessieres, M.M. Pineiro, J.L. Daridon, Simultaneous estimation of phase behavior and second-derivative properties using the statistical associating fluid theory with variable range approach, J Chem Phys, 124 (2006).

[161] M. Goral, Vapor-Liquid-Equilibria in Nonpolar Mixtures .3. Binary-Mixtures of Alkylbenzenes and N-Alkanes at 313.15 K, Fluid Phase Equilibria, 102 (1994) 275-286.

[162] K.D. Kassmann, H. Knapp, Vapor-Liquid-Equilibria for Binary and Ternary Mixtures of Benzene, Toluene and Normal-Butyraldehyde, Ber Bunsen Phys Chem, 90 (1986) 452-458.

[163] A.M. Al-Ghamdi, V.N. Kabadi, High temperature VLE for the benzene-ethylbenzene system, J Chem Eng Data, 46 (2001) 1330-1332.

[164] Kesselma.Wd, Hollenba.Ge, A.L. Myers, A.E. Humphrey, Vapor-Liquid Equilibrium Data for Benzene-Alkylbenzene Systems, J Chem Eng Data, 13 (1968) 34.

[165] K. Kurihara, H. Hori, K. Kojima, Vapor-liquid equilibrium data for acetone plus methanol plus benzene, chloroform plus methanol plus benzene, and constituent binary systems at 101.3 kPa, J Chem Eng Data, 43 (1998) 264-268.

[166] J.B. Ott, K.N. Marsh, A.E. Richards, Excess-Enthalpies, Excess Gibbs Free-Energies, and Excess Volumes for (Di-Normal-Butyl Ether + Benzene) and Excess Gibbs Free-Energies and Excess Volumes for (Di-Normal-Butyl Ether + Tetrachloromethane) at 298.15-K and 308.15-K, J Chem Thermodyn, 13 (1981) 447-455.

[167] J. Linek, Wichterl.I, Polednov.J, Liquid-Vapor Equilibrium .53. Systems Benzene-Diisopropyl Ether, Diisopropyl Ether-Toluene, Diisopropyl Ether-Ethylbenzene, Benzene-Dipropyl Ether, Dipropyl Ether-Toluene and Dipropyl Ether-Ethylbenzene, Collect Czech Chem C, 37 (1972) 2820.

[168] I.A.E. Borisova, M.E.; Sokolov,N.M.; Mikhailov,V.A.; Evropin,V.A.; Gorbunov,A.I.;, Vapor-Liquid Equilibrium in the System Diethyl Ether - Tolene at 760 mm Hg, Deposited Doc. VINITI, (1982).

[169] S. Maken, J.J. Park, U. Bhardwaj, K.C. Singh, J.W. Park, S.D. Han, B.R. Deshwal, (Vapour plus liquid) equilibria of (1-butanol + benzene, or toluene, or o-, or m-, or p-xylene) at T=308.15 K, J Chem Thermodyn, 36 (2004) 309-315.

[170] C.B. Kretschmer, R. Wiebe, Liquid-Vapor Equilibrium of Ethanol-Toluene, J. Am. Chem. Soc., 71 (1949) 1793-1797.

[171] J. Fernandez, R. Garriga, I. Velasco, S. Otin, Thermodynamic properties of binary mixtures containing n-alkylamines - I. Isothermal vapour-liquid equilibrium and excess molar enthalpy of n-alkylamine plus toluene mixtures. Measurement and analysis in

terms of group contributions, Fluid Phase Equilibria, 152 (1998) 243-254.

[172] J. Fernandez, R. Garriga, I. Velasco, S. Otin, Thermodynamic properties of binary mixtures containing n-alkylamines II. Isothermal vapour-liquid equilibrium and excess molar enthalpy of n-alkylamine plus ethylbenzene mixtures. Measurement and analysis in terms of group contributions, Fluid Phase Equilibria, 163 (1999) 231-242.

[173] K.S. Pitzer, G. Mayorga, Thermodynamics of Electrolytes .2. Activity and Osmotic Coefficients for Strong Electrolytes with One or Both Ions Univalent, J Phys Chem-Us, 77 (1973) 2300-2308.

[174] K.S. Pitzer, G. Mayorga, Thermodynamics of Electrolytes. III. Activity and Osmotic Coefficients for 2-2 Electrolytes, J Solution Chem, 3 (1974) 539-546.

[175] C.-C. Chen, H. Britt, J. Boston, L. Evans, Local composition model for excess Gibbs energy of electrolyte systems. Part I: Single solvent, single completely dissociated electrolyte systems, Aiche J, 28 (1982) 588-596.

[176] R.A. Robinson, R.H. Wood, P.J. Reilly, Calculation of Excess Gibbs Energies and Activity Coefficients from Isopiestic Measurements on Mixtures of Lithium and Sodium Salts, J Chem Thermodyn, 3 (1971) 461.

[177] Wood, J. Phys. Chem., 73 (1969).

[178] Scatchar.G, R.M. Rush, J.S. Johnson, Osmotic and Activity Coefficients for Binary Mixtures of Sodium Chloride, Sodium Sulfate, Magnesium Sulfate, and Magnesium Chloride in Water at 25 Degrees .3. Treatment with Ions as Components, J Phys Chem-Us, 74 (1970) 3786.

[179] K.S. Pitzer, R.N. Roy, L.F. Silvester, Thermodynamics of Electrolytes .7. Sulfuric-Acid, J Am Chem Soc, 99 (1977) 4930-4936.

[180] K.S. Pitzer, Ionic Fluids, J Phys Chem-Us, 88 (1984) 2689-2697.

[181] K.S. Pitzer, Thermodynamics of Unsymmetrical Electrolyte Mixtures - Enthalpy and Heat-Capacity, J Phys Chem-Us, 87 (1983) 2360-2364.

[182] H.P. Meissner, C.L. Kusik, Activity-Coefficients of Strong Electrolytes in Multicomponent Aqueous-Solutions, Aiche J, 18 (1972) 294.

[183] H.P. Meissner, J.W. Tester, C.L. Kusik, Activity-Coefficients of Strong Electrolytes in Aqueous-Solution - Effect of Temperature, Aiche J, 18 (1972) 661.

[184] J.L. Cruz, H. Renon, New Thermodynamic Representation of Binary Electrolyte-Solutions Non-Ideality in Whole Range of Concentrations, Aiche J, 24 (1978) 817-830.

[185] C.C. Chen, H.I. Britt, J.F. Boston, L.B. Evans, Local Composition Model for Excess Gibbs Energy of Electrolyte Systems .1. Single Solvent, Single Completely Dissociated Electrolyte Systems, Aiche J, 28 (1982) 588-596.

[186] Y. Liu, A.H. Harvey, J.M. Prausnitz, Thermodynamics of Concentrated Electrolyte-Solutions, Chem Eng Commun, 77 (1989) 43-66.

[187] H.L. Friedman, Electrolyte solutions at equilibrium, Annual Review of Physical Chemistry, 32 (1981) 179-204.

[188] D. Ben-Yaakov, D. Andelman, R. Podgornik, Dielectric decrement as a source of ion-specific effects, J Chem Phys, 134 (2011).

[189] D. Henderson, ACS Symp. Ser., 47 (1983).

[190] D. Henderson, L. Blum, A. Tani, Equation of State of Ionic Fluids, Acs Sym Ser, 300 (1986) 281-296.

[191] G. Jin, M.D. Donohue, An Equation of State for Electrolyte-Solutions .1. Aqueous Systems Containing Strong Electrolytes, Ind. Eng. Chem. Res., 27 (1988) 1073-1084.

[192] G. Jin, M.D. Donohue, An Equation of State for Electrolyte-Solutions .2. Single Volatile Weak Electrolytes in Water, Ind. Eng. Chem. Res., 27 (1988) 1737-1743.

[193] G. Jin, M.D. Donohue, An Equation of State for Electrolyte-Solutions .3. Aqueous-Solutions Containing Multiple Salts, Ind. Eng. Chem. Res., 30 (1991) 240-248.

[194] P. Vimalchand, I. Celmins, M.D. Donohue, Vle Calculations for Mixtures Containing Multipolar Compounds Using the Perturbed Anisotropic Chain Theory, Aiche J, 32 (1986) 1735-1738.

[195] J. Percus, G. Yevick, Hard-core insertion in the many-body problem, Physical Review, 136 (1964) B290.

[196] J. Lebowitz, J. Percus, Mean spherical model for lattice gases with extended hard cores and continuum fluids, Physical Review, 144 (1966) 251.

[197] E. Waisman, J.L. Lebowitz, Mean spherical model integral equation for charged hard spheres I. Method of solution, The Journal of Chemical Physics, 56 (1972) 3086.

[198] E. Waisman, The radial distribution function for a fluid of hard spheres at high densities: Mean spherical integral equation approach, Mol Phys, 25 (1973) 45-48.

[199] M. Wertheim, Exact solution of the mean spherical model for fluids of hard spheres with permanent electric dipole moments, The Journal of Chemical Physics, 55 (1971) 4291.

[200] R. Palmer, J. Weeks, Exact solution of the mean spherical model for charged hard spheres in a uniform neutralizing background, The Journal of Chemical Physics, 58 (1973) 4171.

[201] S. Adelman, J. Deutch, Exact solution of the mean spherical model for simple polar mixtures, The Journal of Chemical Physics, 59 (1973) 3971.

[202] S. Adelman, J. Deutch, Exact solution of the mean spherical model for strong electrolytes in polar solvents, The Journal of Chemical Physics, 60 (1974) 3935.
[203] L. Blum, Solution of the mean spherical approximation for hard ions and dipoles of arbitrary size, J. Stat. Phys., 18 (1978) 451-474.

[204] L. Blum, D. Wei, Analytical solution of the mean spherical approximation for an arbitrary mixture of ions in a dipolar solvent, The Journal of Chemical physics, 87 (1987) 555.

[205] M. Golovko, I. Protsykevich, Analytic solution of the mean spherical approximation for ion-dipole model in a neutralizing background, J. Stat. Phys., 54 (1989) 707-733.

[206] L. Blum, Mean spherical model for asymmetric electrolytes: I. Method of solution, Mol Phys, 30 (1975) 1529-1535.

[207] L. Blum, Mean spherical model for a mixture of charged spheres and hard dipoles, Chemical Physics Letters, 26 (1974) 200-202.

[208] J.S. Hoye, G. Stell, Ionic Solution in a Molecular Polar-Solvent, J Chem Phys, 68 (1978) 4145-4150.

[209] C. McCabe, A. Galindo, SAFT associating fluids and fluid mixtures, Applied Thermodynamics of Fluids, (2010) 215-279.

[210] H. Zhao, M.C. dos Ramos, C. McCabe, Development of an equation of state for electrolyte solutions by combining the statistical associating fluid theory and the mean spherical approximation for the nonprimitive model, The Journal of Chemical physics, 126 (2007) 244503.

[211] W.G. Chapman, G. Jackson, K.E. Gubbins, Phase equilibria of associating fluids: Chain molecules with multiple bonding sites, Mol Phys, 65 (1988) 1057-1079.

[212] M. Wertheim, Fluids with highly directional attractive forces. II. Thermodynamic perturbation theory and integral equations, J. Stat. Phys., 35 (1984) 35-47.

[213] M. Wertheim, Fluids with highly directional attractive forces. I. Statistical thermodynamics, J. Stat. Phys., 35 (1984) 19-34.

[214] M. Wertheim, Fluids with highly directional attractive forces. IV. Equilibrium polymerization, J. Stat. Phys., 42 (1986) 477-492.

[215] M. Wertheim, Fluids with highly directional attractive forces. III. Multiple attraction sites, J. Stat. Phys., 42 (1986) 459-476.

[216] E.A. Muller, K.E. Gubbins, Molecular-based equations of state for associating fluids: A review of SAFT and related approaches, Ind. Eng. Chem. Res., 40 (2001) 2193-2211.

[217] I.G. Economou, Statistical associating fluid theory: A successful model for the calculation of thermodynamic and phase equilibrium properties of complex fluid mixtures, Ind Eng Chem Res, 41 (2002) 953-962.

[218] A. Galindo, A. Gil-Villegas, G. Jackson, A.N. Burgess, SAFT-VRE: Phase behavior of electrolyte solutions with the statistical associating fluid theory for potentials of variable range, The Journal of Physical Chemistry B, 103 (1999) 10272-10281.

[219] S.P. Tan, H. Adidharma, M. Radosz, Statistical associating fluid theory coupled with restricted primitive model to represent aqueous strong electrolytes, Ind. Eng. Chem. Res., 44 (2005) 4442-4452.

[220] B. Behzadi, B. Patel, A. Galindo, C. Ghotbi, Modeling electrolyte solutions with the SAFT-VR equation using Yukawa potentials and the mean-spherical approximation, Fluid phase equilibria, 236 (2005) 241-255.

[221] M. Uematsu, E.U. Franck, Static Dielectric-Constant of Water and Steam, J Phys Chem Ref Data, 9 (1980) 1291-1306.

[222] G.H.a.M. Hudson, J. C., Intermolecular forces between unlike molecules. A more complete form of the combining rules, Trans. Faraday Soc., 56 (1960) 761-766.

[223] X.Y. Ji, S.P. Tan, H. Adidharma, M. Radosz, Statistical associating fluid theory coupled with restrictive primitive model extended to bivalent ions. SAFT2: 2. Brine/seawater properties predicted, J Phys Chem B, 110 (2006) 16700-16706.

[224] L. Blum, Mean Spherical Model for Asymmetric Electrolytes .1. Method of Solution, Mol Phys, 30 (1975) 1529-1535.

[225] L. Blum, J.S. Hoye, Mean Spherical Model for Asymmetric Electrolytes .2. Thermodynamic Properties and Pair Correlation-Function, J Phys Chem-Us, 81 (1977) 1311-1317.

[226] L.F. Cameretti, G. Sadowski, J.M. Mollerup, Modeling of aqueous electrolyte solutions with perturbed-chain statistical associated fluid theory, Ind. Eng. Chem. Res., 44 (2005) 3355-3362.

[227] C. Held, L.F. Cameretti, G. Sadowski, Modeling aqueous electrolyte solutions: Part 1. Fully dissociated electrolytes, Fluid Phase Equilibria, 270 (2008) 87-96.

[228] C. Held, G. Sadowski, Modeling aqueous electrolyte solutions. Part 2. Weak electrolytes, Fluid Phase Equilibria, 279 (2009) 141-148.

[229] C. Held, A. Prinz, V. Wallmeyer, G. Sadowski, Measuring and modeling alcohol/salt systems, Chem Eng Sci, 68 (2012) 328-339.

[230] W.B. Liu, Y.G. Li, J.F. Lu, A new equation of state for real aqueous ionic fluids based on electrolyte perturbation theory, mean spherical approximation and statistical associating fluid theory, Fluid Phase Equilibria, 158 (1999) 595-606.

[231] C. Mavroyannis, Stephen, M. J., Dispersion forces, Mol Phys, 5 (1962) 629-638.

[232] Z. Liu, W. Wang, Y. Li, An equation of state for electrolyte solutions by a combination of low-density expansion of non-primitive mean spherical approximation and statistical associating fluid theory, Fluid phase equilibria, 227 (2005) 147-156.

[233] Z.P. Liu, Y.G. Li, J.F. Lu, Low-density expansion of the solution of mean spherical approximation for ion-dipole mixtures, J Phys Chem B, 106 (2002) 5266-5274.

[234] J.A. Myers, S.I. Sandler, R.H. Wood, An equation of state for electrolyte solutions covering wide ranges of temperature, pressure, and composition, Ind. Eng. Chem. Res., 41 (2002) 3282-3297.

[235] W. Furst, H. Renon, Representation of Excess Properties of Electrolyte-Solutions Using a New Equation of State, Aiche J, 39 (1993) 335-343.

[236] J. Rozmus, J.C. de Hemptinne, A. Galindo, S. Dufal, P. Mougin, Modeling of Strong Electrolytes with ePPC-SAFT up to High Temperatures, Ind. Eng. Chem. Res., 52 (2013) 9979-9994.

[237] E.G. Schmidt, U. , Properties of water and steam in SI-units, Springer Verlag; New York, (1982).

[238] S. Herzog, J. Gross, W. Arlt, Equation of state for aqueous electrolyte systems based on the semirestricted non-primitive mean spherical approximation, Fluid Phase Equilibria, 297 (2010) 23-33.

[239] M.V. Fedotova, S.E. Kruchinin, H.M.A. Rahman, R. Buchner, Features of ion hydration and association in aqueous rubidium fluoride solutions at ambient conditions, J Mol Liq, 159 (2011) 9-17.

[240] C.J. Fennell, A. Bizjak, V. Vlachy, K.A. Dill, S. Sarupria, S. Rajamani, S. Garde, Ion Pairing in Molecular Simulations of Aqueous Alkali Halide Solutions (vol 113, pg

6782, 2009), J Phys Chem B, 113 (2009) 14837-14838.

[241] T. Driesner, T.M. Seward, I.G. Tironi, Molecular dynamics simulation study of ionic hydration and ion association in dilute and 1 molal aqueous sodium chloride solutions from ambient to supercritical conditions, Geochim Cosmochim Ac, 62 (1998) 3095-3107.

[242] D. Wei, L. Blum, The mean spherical approximation for an arbitrary mixture of ions in a dipolar solvent: Approximate solution, pair correlation functions, and thermodynamics, The Journal of Chemical physics, 87 (1987) 2999.

[243] H. Zhao, Y. Ding, C. McCabe, Phase behavior of dipolar associating fluids from the SAFT-VR+D equation of state, J Chem Phys, 127 (2007).

[244] S.A. Clough, Y. Beers, G.P. Klein, L.S. Rothman, Dipole-Moment of Water from Stark Measurements of H2o, Hdo, and D2o, J Chem Phys, 59 (1973) 2254-2259.

[245] C.A. Coulson, Eisenber.D, Interactions of H2o Molecules in Ice .2. Interaction Energies of H2o Molecules in Ice, Proc R Soc Lon Ser-A, 291 (1966) 454.

[246] P.L. Silvestrelli, M. Parrinello, Water molecule dipole in the gas and in the liquid phase, Phys Rev Lett, 82 (1999) 3308-3311.

[247] Z. Rappoport, Chemical Rubber Company., CRC handbook of tables for organic compound identification, 3rd ed., CRC Press, Boca Raton, Fla., 1967.

[248] C. McCabe, S.B. Kiselev, A crossover SAFT-VR equation of state for pure fluids: preliminary results for light hydrocarbons, Fluid Phase Equilibria, 219 (2004) 3-9.

[249] P.C. Albright, J.V. Sengers, J.F. Nicoll, M. Leykoo, A Crossover Description for the Thermodynamic Properties of Fluids in the Critical Region, Int J Thermophys, 7 (1986) 75-85.

[250] H. Adidharma, M. Radosz, Prototype of an engineering equation of state for heterosegmented polymers, Ind. Eng. Chem. Res., 37 (1998) 4453-4462.

[251] R.D. Shannon, Revised Effective Ionic-Radii and Systematic Studies of Interatomic Distances in Halides and Chalcogenides, Acta Crystallogr A, 32 (1976) 751-767.

[252] Goldschmidt, Math. NatK1, 60 (1927) 1263.

[253] L. Pauling, The nature of the Chemical bond—1992, Journal of Chemical Education, 69 (1992) 519.

[254] R.D. Shannon, C.T. Prewitt, Revised Values of Effective Ionic Radii, Acta Crystall B-Stru, B 26 (1970) 1046.

[255] R. Shannon, Revised effective ionic radii and systematic studies of interatomic distances in halides and chalcogenides, Acta Crystallographica Section A: Crystal Physics, Diffraction, Theoretical and General Crystallography, 32 (1976) 751-767.

[256] B.S. Gourary, F.J. Adrian, Wave functions for electron-excess color centers in alkali halide crystals, Solid State Physics, 10 (1960) 127-247.

[257] M. Blander, Molten salt chemistry, Interscience Publishers, New York,, 1964.

[258] J. Mahler, I. Persson, A Study of the Hydration of the Alkali Metal Ions in Aqueous Solution, Inorg Chem, 51 (2012) 425-438.

[259] P.A. Bergstrom, J. Lindgren, O. Kristiansson, An Ir Study of the Hydration of Clo4-, No3-, I-, Br-, Cl-, and So42- Anions in Aqueous-Solution, J Phys Chem-Us, 95 (1991) 8575-8580.

[260] K. Levenberg, A Method for the Solution of Certain Non-Linear Problems in Least Squares, Quarterly of Applied Mathematics 2(1944) 164–168.

[261] S.Dufal, Ph.D. thesis, Imperial College London, (2013).

[262] C.C. Pye, W. Rudolph, R.A. Poirier, An ab initio investigation of lithium ion hydration, J Phys Chem-Us, 100 (1996) 601-605.

[263] Michael H. Abraham, János Liszi, E. Papp, Calculations on ionic solvation. Part 6, J. Chem. Soc., Faraday Trans. 1, 78 (1982) 197--211.

[264] A. Eiberweiser, R. Buchner, Ion-pair or ion-cloud relaxation? On the origin of small-amplitude low-frequency relaxations of weakly associating aqueous electrolytes, J Mol Liq, 176 (2012) 52-59.

[265] R.A. Robinson, R.H. Stokes, Electrolyte solutions : the measurement and interpretation of conductance, chemical potential, and diffusion in solutions of simple electrolytes, 2nd ed., Butterworths, London,, 1959.

[266] A. Gil-Villegas, A. Galindo, G. Jackson, A statistical associating fluid theory for electrolyte solutions (SAFT-VRE), Mol Phys, 99 (2001) 531-546.

[267] M. Paunovic, M. Schlesinger, Fundamentals of electrochemical deposition, 2nd ed., Wiley-Interscience, Hoboken, N.J., 2006.

[268] P.J.W. Debye, Polar molecules, Chemical Catalog Company, Inc, New York, 1929.

[269] J.B.a.R. Hasted, D. M. and Collie, C. H., Dielectric Properties of Aqueous Ionic Solutions. Parts I and II, The Journal of Chemical Physics, 16 (1948) 1-21.

[270] Y.Z. Wei, P. Chiang, S. Sridhar, Ion Size Effects on the Dynamic and Static Dielectric-Properties of Aqueous Alkali Solutions, J Chem Phys, 96 (1992) 4569-4573.

[271] Y.Z. Wei, S. Sridhar, Dielectric-Spectroscopy up to 20 Ghz of Licl/H2o Solutions, J Chem Phys, 92 (1990) 923-928.

[272] B. Maribo-Mogensen, G.M. Kontogeorgis, K. Thomsen, Modeling of Dielectric Properties of Aqueous Salt Solutions with an Equation of State, J Phys Chem B, 117 (2013) 10523-10533.

[273] D.G. Archer, Thermodynamic Properties of the Nacl+H2o System .2. Thermodynamic Properties of Nacl(Aq), Nacl.2h2o(Cr), and Phase-Equilibria, J Phys Chem Ref Data, 21 (1992) 793-829.

[274] E.M.W. C.C. Panichajakul, Thermodynamic Behavior of Electrolytes in Mixed Solvents, American Chemical Society, 155 (1976).

[275] R.N.R. B. Sen, J.J. Gibbons, D.A. Johnson, L.H. Adcock,, American Chemical Society, Thermodynamic Behavior of Electrolytes in Mixed Solvents. II, 177 (1979).

[276] R.M. Fuoss, Conductimetric Determination of Thermodynamic Pairing Constants for Symmetrical Electrolytes, P Natl Acad Sci USA, 77 (1980) 34-38.

[277] W.J. Hamer, Y.-C. Wu, Osmotic Coefficent and Mean Activity Coefficient of Uni-univalent Electrolytes in Water at 25 C, Journal of Physical Reference Data, (1972) 1047-1100.

[278] A. Niazi, N. Olszowy, B.D. Rabideau, A.E. Ismail, Measurement of enthalpy and free energy changes for dissolution in concentrated electrolyte media using molecular simulations, AIChE Annual Conference, (2014).

[279] A.F. Bo Sander, Peter Rasmussen, Calculation of vapour-liquid equilibria in mixed solvent/salt systems using an extended UNIQUAC equation, Chemical Engineering Science, 41 (1986) 1171-1183.

[280] E.A. Macedo, Per Skovborg, and Peter Rasmussen, "Calculation of phase equilibria for solutions of strong electrolytes in solvent—water mixtures.", Chemical Engineering Science, 45 (1990) 875-882.

[281] I. Kikic, Maurizio Fermeglia, and Peter Rasmussen, Unifac prediction of vapor—liquid equilibria in mixed solvent—salt systems, Chemical engineering science 46 (1991) 2775-2780.

[282] J. Li, Hans-Martin Polka, and Jürgen Gmehling, A gE model for single and mixed solvent electrolyte systems: 1. Model and results for strong electrolytes, Fluid Phase Equilibr, 94 (1994) 89-114.

[283] H. Zerres, and J. M. Prausnitz, Thermodynamics of phase equilibria in aqueous-organic systems with salt, AIChE journal 40 (1994) 676-691.

[284] Y. Liu, and Suphat Watanasiri, Representation of liquid-liquid equilibrium of mixed-solvent electrolyte systems using the extended electrolyte NRTL model, Fluid Phase Equilibr, 116 (1996) 193-200.

[285] W.e.a. Yan, Prediction of vapor–liquid equilibria in mixed-solvent electrolyte systems using the group contribution concept, Fluid Phase Equilibr, 162 (1999) 97-113.

[286] M.C. Iliuta, Kaj Thomsen, and Peter Rasmussen, Extended UNIQUAC model for correlation and prediction of vapour–liquid–solid equilibria in aqueous salt systems containing non-electrolytes. Part A. Methanol–water–salt systems, Chemical Engineering Science 55 (2000) 2673-2686.

[287] G.N.a.R. Lewis, Merle, The activity coefficient of strong electrolytes. 1, Journal of the American Chemical Society, 43 (1921) 1112-1154.

[288] B. Sander, A. Fredenslund, P. Rasmussen, Calculation of Vapor-Liquid-Equilibria in Mixed-Solvent Salt Systems Using an Extended Uniquac Equation, Chemical Engineering Science, 41 (1986) 1171-1183.

[289] L.L. Lee, Thermodynamic consistency and reference scale conversion in multisolvent electrolyte solutions, J Mol Liq, 87 (2000) 129-147.

[290] M.J.E.D. Cardoso, J.P. Oconnell, Activity-Coefficients in Mixed-Solvent Electrolyte-Solutions, Fluid Phase Equilibr, 33 (1987) 315-326.

[291] W.D. Yan, M. Topphoff, C. Rose, J. Gemhling, Prediction of vapor-liquid equilibria in mixed-solvent electrolyte systems using the group contribution concept, Fluid Phase Equilibr, 162 (1999) 97-113.

[292] E.A. Macedo, P. Skovborg, P. Rasmussen, Calculation of Phase-Equilibria for Solutions of Strong Electrolytes in Solvent Water Mixtures, Chemical Engineering Science, 45 (1990) 875-882.

[293] B.H. Patel, P. Paricaud, A. Galindo, G.C. Maitland, Prediction of the Salting-Out Effect of Strong Electrolytes on Water + Alkane Solutions, Ind Eng Chem Res, 42 (2003) 3809-3823.

[294] J. Gross, G. Sadowski, Perturbed-chain SAFT: An equation of state based on a perturbation theory for chain molecules, Industrial & Engineering Chemistry Research, 40 (2001) 1244-1260.

[295] G. Das, S. Hlushak, M.C. dos Ramos, C. McCabe, Predicting the thermodynamic properties and dielectric behavior of electrolyte solutions using the SAFT-VR+DE

equation of state, AIChE Journal, in press (2015).

[296] D.Q. Wei, L. Blum, The Mean Spherical Approximation for an Arbitrary Mixture of Ions in a Dipolar Solvent - Approximate Solution, Pair Correlation-Functions, and Thermodynamics, J Chem Phys, 87 (1987) 2999-3007.

[297] J.S. Rowlinson, F.L. Swinton, Liquids and Liquid Mixtures, 3rd ed., Butterworth Scientific, London, 1982.

[298] E.K. Karakatsani, G.M. Kontogeorgis, I.G. Economou, Evaluation of the truncated perturbed chain-polar statistical associating fluid theory for complex mixture fluid phase equilibria, Ind Eng Chem Res, 45 (2006) 6063-6074.

[299] E.K. Karakatsani, T. Spyriouni, I.G. Economou, Extended statistical associating fluid theory (SAFT) equations of state for dipolar fluids, Aiche J, 51 (2005) 2328-2342.

[300] L. Blum, Torruell.Aj, Invariant Expansion for 2-Body Correlations - Thermodynamic Functions, Scattering, and Ornstein-Zernike Equation, J Chem Phys, 56 (1972) 303.

[301] L. Blum, D.Q. Wei, Analytical Solution of the Mean Spherical Approximation for an Arbitrary Mixture of Ions in a Dipolar Solvent, J Chem Phys, 87 (1987) 555-565.

[302] C.G. Gray, K.E. Gubbins, Theory of molecular fluids. Volume 1, Fundamentals, Clarendon, Oxford, 1984.

[303] C.G. Gray, Y.S. Sainger, C.G. Joslin, P.T. Cummings, S. Goldman, Computer-Simulation of Dipolar Fluids - Dependence of the Dielectric-Constant on System Size - a Comparative-Study of Ewald Sum and Reaction Field Approaches, J Chem Phys, 85 (1986) 1502-1504.

[304] J.A. Barker, R.O. Watts, Monte-Carlo Studies of Dielectric Properties of Water-Like Models, Mol Phys, 26 (1973) 789-792.

[305] P.T. Cummings, I. Nezbeda, W.R. Smith, G. Morriss, Monte-Carlo Simulation Results for the Full Pair Correlation-Function of the Hard Dumbbell Fluid, Mol Phys, 43 (1981) 1471-1475.

[306] A. Gil-Villegas, G. Jackson, S.C. McGrother, Computer simulation of dipolar liquid crystals., J Mol Liq, 76 (1998) 171-181.

[307] A.L. Benavides, Y. Guevara, F. Delrio, Vapor-Liquid-Equilibrium of a Multipolar Square-Well Fluid .1. Effect of Multipolar Strengths, Physica A, 202 (1994) 420-437.

[308] M. Neumann, O. Steinhauser, G.S. Pawley, Consistent Calculation of the Static and Frequency-Dependent Dielectric-Constant in Computer-Simulations, Mol Phys, 52

(1984) 97-113.

[309] P.T. Cummings, H.D. Cochran, J.M. Simonson, R.E. Mesmer, S. Karaborni, Simulation of Supercritical Water and of Supercritical Aqueous-Solutions, J Chem Phys, 94 (1991) 5606-5621.

[310] A.V. Bandura, S.N. Lvov, D.D. Macdonald, Thermodynamics of ion solvation in dipolar solvent using Monte Carlo mean reaction field simulation, J Chem Soc Faraday T, 94 (1998) 1063-1072.

[311] D.M. Tsangaris, J.J. Depablo, Bond-Bias Simulation of Phase-Equilibria for Strongly Associating Fluids, J Chem Phys, 101 (1994) 1477-1489.

[312] D.P. Visco, D.A. Kofke, Modeling the Monte Carlo simulation of associating fluids, J Chem Phys, 110 (1999) 5493-5502.

[313] B. Chen, J.J. Potoff, J.I. Siepmann, Adiabatic nuclear and electronic sampling Monte Carlo simulations in the Gibbs ensemble: Application to polarizable force fields for water, J Phys Chem B, 104 (2000) 2378-2390.

[314] D.P. Visco, D.A. Kofke, A comparison of molecular-based models to determine vapor-liquid phase coexistence in hydrogen fluoride, Fluid Phase Equilibr, 158 (1999) 37-47.

[315] B. Chen, J.I. Siepmann, A novel Monte Carlo algorithm for simulating strongly associating fluids: Applications to water, hydrogen fluoride, and acetic acid, J Phys Chem B, 104 (2000) 8725-8734.

[316] B. Chen, J.I. Siepmann, Partitioning of alkane and alcohol solutes between water and (Dry or wet) 1-Octanol, Journal of the American Chemical Society, 122 (2000) 6464-6467.

[317] N.A. Busch, M.S. Wertheim, Y.C. Chiew, M.L. Yarmush, A Monte-Carlo Method for Simulating Associating Fluids, J Chem Phys, 101 (1994) 3147-3156.

[318] H. Docherty, A. Galindo, A study of Wertheim's thermodynamic perturbation theory (TPT1) for associating fluids with dispersive interactions: the importance of the association range, Mol Phys, 104 (2006) 3551-3560.

[319] S.J. Han, H.Q. Pan, Thermodynamics of the Sodium Bromide-Methanol-Water and Sodium Bromide-Ethanol-Water 2 Ternary-Systems by the Measurements of Electromotive-Force at 298.15-K, Fluid Phase Equilibr, 83 (1993) 261-270.

[320] M.C. Kroon, E.K. Karakatsani, I.G. Economou, G.J. Witkamp, C.J. Peters, Modeling of the carbon dioxide solubility in imidazolium-based ionic liquids with the tPC-PSAFT equation of state, J Phys Chem B, 110 (2006) 9262-9269.

[321] L.F. Vega, O. Vilaseca, F. Llovell, J.S. Andreu, Modeling ionic liquids and the solubility of gases in them: Recent advances and perspectives, Fluid Phase Equilibr, 294 (2010) 15-30.

[322] A.a.F. Johnson, WF, Salt effect in vapor-liquid equilibrium, part II, The Canadian Journal of Chemical Engineering, 38 (1960) 78--87.

[323] S. Ohe, Prediction of Salt Effect on Vapor—Liquid Equilibrium: A Method Based on Solvation II, (1976).

[324] R.a.A. Rousseau, DL and Schoenborn, EM, Salt effect in vapor-liquid equilibria: Correlation of alcohol-, water-, salt systems, Aiche J, 18 (1972) 825--829.

[325] R.a.B. Rousseau, JE, Vapor-liquid equilibrium for salt containing systems: Correlation of binary solvent data and prediction of behavior in multicomponent solvents, Aiche J, 24 (1978) 718--725.

[326] D.a.F. Jaques, WF, Prediction of vapor composition in isobaric vapor-liquid systems containing salts at saturation, DTIC Document, (1972).

[327] B. Mock, L.B. Evans, C.C. Chen, Thermodynamic Representation of Phase-Equilibria of Mixed-Solvent Electrolyte Systems, Aiche J, 32 (1986) 1655-1664.

[328] A. Kolker, J. dePablo, Thermodynamic modeling of vapor-liquid equilibria in mixed aqueous-organic systems with salts, Ind Eng Chem Res, 35 (1996) 234-240.

[329] A. Kolker, J. dePablo, Thermodynamic modeling of the solubility of salts in mixed aqueous-organic solvents, Ind Eng Chem Res, 35 (1996) 228-233.

[330] S. Dahl, E.A. Macedo, The Mhv2 Model - a Unifac-Based Equation of State Model for Vapor Liquid and Liquid Liquid Equilibria of Mixtures with Strong Electrolytes, Ind Eng Chem Res, 31 (1992) 1195-1201.

[331] C.a.S. Christensen, B and Fredenslund, AA and Rasmussen, P, Towards the extensionof UNIFAC to mixtures with electrolytes, Fluid Phase Equilibr, 13 (1983) 297--309.

[332] B.H. Patel, P. Paricaud, A. Galindo, G.C. Maitland, Prediction of the salting-out effect of strong electrolytes on water plus alkane solutions, Industrial & Engineering Chemistry Research, 42 (2003) 3809-3823.

[333] R.C. Reid, J.M. Prausnitz, B.E. Poling, The properties of gases and liquids, 4th ed., McGraw-Hill, New York, 1987.

[334] G. Das, Stepan and McCabe, Clare, Development of equation of state for mixed solvent electrolyte systems using statistical associating fluid theory along with mean

spherical approximation of non-primitive model, (2015).

[335] G.H. Das, Stepan; dos Ramos, M. Carolina and McCabe, Clare, Predicting the thermodynamic properties and dielectric behavior of electrolyte solutions using SAFT-VR+DE equation of state, Aiche Journal, under review (2015).

[336] J.K. Gregory, D.C. Clary, K. Liu, M.G. Brown, R.J. Saykally, The water dipole moment in water clusters, Science, 275 (1997) 814-817.

[337] G.M. Kontogeorgis, I. Tsivintzelis, N. von Solms, A. Grenner, D. Bogh, M. Frost, A. Knage-Rasmussen, I.G. Economou, Use of monomer fraction data in the parametrization of association theories, Fluid Phase Equilibr, 296 (2010) 219-229.

[338] G.M. Kontogeorgis, E.C. Voutsas, I.V. Yakoumis, D.P. Tassios, An equation of state for associating fluids, Industrial & Engineering Chemistry Research, 35 (1996) 4310-4318.

[339] C. Panayiotou, M. Pantoula, E. Stefanis, I. Tsivintzelis, I.G. Economou, Nonrandom hydrogen-bonding model of fluids and their mixtures. 1. Pure fluids, Industrial & Engineering Chemistry Research, 43 (2004) 6592-6606.

[340] R. Khare, A.K. Sum, S.K. Nath, J.J. de Pablo, Simulation of vapor-liquid phase equilibria of primary alcohols and alcohol-alkane mixtures, J Phys Chem B, 108 (2004) 10071-10076.

[341] M.N. Garcia-Lisbona, A. Galindo, G. Jackson, A.N. Burgess, An examination of the cloud curves of liquid-liquid immiscibility in aqueous solutions of alkyl polyoxyethylene surfactants using the SAFT-HS approach with transferable parameters, J Am Chem Soc, 120 (1998) 4191-4199.

[342] G. Akerlof, Dielectric constants of some organic solvent-water mixtures at various temperatures, J. Am. Chem. Soc. , 54.

[343] P.S. Albright, L.J. Gosting, Dielectric Constants of the Methanol-Water System from 5 to 55°1, J Am Chem Soc, 68 (1946) 1061-1063.

[344] M.S.H. Bader, K.A.M. Gasem, Determination of infinite dilution activity coefficients for organic-aqueous systems using a dilute vapor-liquid equilibrium method, Chem Eng Commun, 140 (1996) 41-72.

[345] K. Kurihara, T. Minoura, K. Takeda, K. Kojima, Isothermal Vapor-Liquid-Equilibria for Methanol Plus Ethanol Plus Water, Methanol Plus Water, and Ethanol Plus Water, J Chem Eng Data, 40 (1995) 679-684.

[346] M. Holz, H. Weingartner, H.G. Hertz, Nuclear Magnetic-Relaxation of Alkali-Halide Nuclei and Preferential Solvation in Methanol-Water Mixtures, J Chem Soc Farad T 1, 73 (1977) 71-83.

[347] E. Hawlicka, D. Swiatla-Wojcik, MD Simulation Studies of Selective Solvation in Methanol−Water Mixtures: An Effect of the Charge Density of a Solute, The Journal of Physical Chemistry A, 106 (2002) 1336-1345.

[348] A. Basili, P.R. Mussini, T. Mussini, S. Rondinini, B. Sala, A. Vertova, Transference numbers of alkali chlorides and characterization of salt bridges for use in methanol plus water mixed solvents, J Chem Eng Data, 44 (1999) 1002-1008.

[349] M.C. Hu, R.F. Cui, S.N. Li, Y.C. Jiang, S.P. Xia, Determination of activity coefficients for cesium chloride in methanol-water and ethanol-water mixed solvents by electromotive force measurements at 298.15 K, J Chem Eng Data, 52 (2007) 357-362.

[350] F. Hernandez-Luis, M.V. Vazquez, M.A. Esteso, Activity coefficients for NaF in methanol-water and ethanol-water mixtures at 25 degrees C., J Mol Liq, 108 (2003) 283-301.

[351] A. Basili, P.R. Mussini, T. Mussini, S. Rondinini, Thermodynamics of the cell: {NaxHg1-x vertical bar NaCl(m)vertical bar AgCl vertical bar Ag} in (methanol plus water) solvent mixtures, J Chem Thermodyn, 28 (1996) 923-933.

Appendix

Free energy contribution for electrostatic interaction A^{el} is determined using the MSA for mixtures of ions and dipoles developed by Blum and Wei and Golovko [204, 205, 242]. Within the MSA, the expression for the electrostatic free energy is given by

$$\frac{A^{el}}{Vk_bT} = \frac{E^{el}}{Vk_bT} - J - J' \tag{A.1}$$

where, V is a total volume of the solution, and E^{el}/Vk_bT is an internal energy per unit of volume

$$\frac{E^{el}}{Vk_bT} = \frac{1}{4\pi}\left\{\alpha_0^2 \sum_{k=1}^{2} \rho_k z_k N_k - 2\alpha_2\alpha_0\rho_n B^{10} - \frac{2\alpha_2^2\rho_n b_2}{\sigma_n^3}\right\} \tag{A.2}$$

with virial integral terms J and J' defined as [205],

$$J = \frac{1}{12\pi}\left\{\alpha_0^2 \sum_{k=1}^{2} \rho_k z_k N_k - 2\alpha_0\alpha_2\rho_n B^{10} - \frac{6\alpha_2^2\rho_n b_2}{\sigma_n^3}\right\} \tag{A.3}$$

$$J' = \frac{\pi}{3}\sum_i\sum_j \rho_i\rho_j\sigma_{ij}\left\{\sum_{nml}\frac{(-1)^l}{2l+1}\left[g_{ij}^{nml}\left(\sigma_{ij}\right)\right]^2 - \left[g_{ij}^{hs}\left(\sigma_{ij}\right)\right]^2\right\} \tag{A.4}$$

where α_0 and α_2 are the ion-ion coupling and dipole-dipole strength parameters, the quantities are defined as,

$$\alpha_0^2 = \frac{4\pi^2}{k_bT}\ ,\ \alpha_2^2 = \frac{4\pi\mu^2}{3k_bT} \tag{A.5}$$

where μ is the dipole moment of solvent species, k_b and T are the boltzman constant and temperature respectively.

$g_{ij}^{nml}(\sigma_{ij})$ is the contact values of the radial distribution function (RDF) invariant expansion coefficients, and $g_{ij}^{hs}(\sigma_{ij})$ is the hard-sphere contact value. The contact values of the invariant expansion coefficients of the radial distribution function of equation is given by,

$$g_{ij}^{hs}(\sigma_{ij}) = \frac{1}{1-\zeta_3} + \frac{\pi\sigma_i\sigma_j\zeta_2}{4(1-\zeta_3)^2\sigma_{ij}}$$

$$g_{ij}^{000}(\sigma_{ij}) = \frac{Q_{ij}^{'00}}{2\pi\sigma_{ij}} \tag{A.6}$$

$$g^{011}(\sigma_{in}) = \frac{\sqrt{3}Q_{in}^{'01}}{2\pi\sigma_{in}}$$

$$g_{nn}^{110}(\sigma_{nn}) = \frac{Q_{nn}^{'11} + \frac{2q'}{\rho_n\sigma_n^2}}{2\sqrt{3}\pi\sigma_n}$$

$$g_{nn}^{112}(\sigma_{nn}) = \frac{\sqrt{10}\left(Q_{nn}^{'11} - \frac{q'}{\rho_n\sigma_n^2}\right)}{2\sqrt{3}\pi\sigma_n} \tag{A.7}$$

where $\Delta = 1 - \frac{\pi}{6}\sum_{i=1}^{n}\rho_i\sigma_i^3$ and $\zeta_2 = \sum_{i=1}^{n}\rho_i\sigma_i^2$ with ρ_i and σ_i representing density and segment diameter of individual species in the solution. ρ_n and σ_n are the density and segment diameter of the dipolar solvent species present in the solution. The parameters B^{10} and b_2 corresponds to the ion-dipole and dipole-dipole interactions respectively, and are obtained from the solution of Ornstein-Zernike equation given by Wei and Blum. The

quantities β_6 , λ are related to dipolar strength parameters and expressions are given by,

$\beta_6 = 1 - \frac{1}{6} b_2$, $\beta_3 = 1 + \frac{1}{3} b_2$ and $\lambda = \frac{\beta_3}{\beta_6}$.

$q' = \frac{-b_2 (1-\lambda)(\lambda+3)}{(1+\lambda)^2}$, and $Q_{ij}^{'mn} = \left. \frac{\partial Q_{ij}^{mn}(r)}{\partial r} \right|_{r=\sigma_{ij}}$ are the contact values of the Baxter factorization function expansion coefficients,[204, 242] and are given by,

$$
\begin{aligned}
Q_{ij}^{'00} &= \frac{2\pi}{\Delta}\left(\sigma_{ij} + \frac{\pi \sigma_i \sigma_j \xi_2}{4\Delta} \right) - \frac{1}{2} D_i^F D_j^F \left(\frac{\rho_n \sigma_n^2 \upsilon_\eta^2}{D\beta_6^2 (\sigma_n + \lambda\sigma_i)(\sigma_n + \lambda\sigma_j)} + \frac{4\Gamma_i^s \Gamma_j^s}{DD_{ac}} \right) \\
Q_{in}^{'00} &= Q_{ni}^{'00} = \frac{2\pi}{\Delta}\left(\sigma_{in} + \frac{\pi \sigma_i \sigma_n \xi_2}{4\Delta} \right) \\
Q_{in}^{'01} &= -\frac{D_i^F}{D\beta_6}\left(\frac{\lambda \upsilon_\eta}{\sigma_n + \lambda\sigma_i} + 2\Gamma_i^s a_n^1 \right) \\
Q_{ni}^{'10} &= \frac{D_i^F}{D\beta_6}\left(\frac{\lambda \upsilon_\eta}{\sigma_n + \lambda\sigma_i} + 2\Gamma_i^s a_n^1 \right) \\
Q_{nn}^{'11} &= \frac{2\lambda}{D\rho_n \sigma_n^2}\left(\lambda + \frac{\rho_n \sigma_n^2 \Omega^{10} a_n^1}{2\beta_6^2} \right) + \frac{\sigma_n B^{10} a_n^1}{2\beta_6} - \frac{2}{\rho_n \sigma_n^2}
\end{aligned}
\tag{A.8}
$$

where Γ , B^{10} and b_2 are the parameters corresponding to ion-ion, ion-dipole and dipole-dipole interactions and obtained numerically solving following equations,

$$
\sum_{i=1}^{n-1} \rho_i \left(a_i^0 \right)^2 + \rho_n \left(\sigma_n^1 \right)^2 = \alpha_0^2 \tag{A.9}
$$

$$
-\sum_{i=1}^{n-1} \rho_i a_i^0 k_{ni}^{10} + a_n^1 \left(1 - \rho_n k_{nn}^{11} \right) = \alpha_0 \alpha_2 \tag{A.10}
$$

$$
\left(1 - \rho_n k_{nn}^{11} \right)^2 + \rho_n \sum_{i=1}^{n-1} \rho_i \left(k_{ni}^{10} \right)^2 = y_1^2 + \rho_n \alpha_2^2 \tag{A.11}
$$

In the above equation, K_{ni}^{10} and K_{nn}^{11} represents $K-matrix$ given in terms of the Baxter matrix $Q_{ij}^{mn}(r)$ is given by,

$$K_{ij}^{mn} = \int_{\lambda_{ji}}^{\sigma_{ij}} dr Q_{ij}^{mn}(r) \tag{A.12}$$

Additional to equations (A.9)-(A.10), compared to the equation (2.17) of Wei *et al*.[242], we calculate V_η from known Γ, B^{10} and b_2, by numerically solving the following equation,

$$B^{10} = \frac{\beta_6 V_\eta}{2} \sum_{i=1}^{n-1} \frac{\rho_i z_i^2}{(\sigma_n + \sigma_i \lambda)(1 + \Gamma\sigma_i + \Delta\Gamma_i)} \tag{A.13}$$

where, $\Delta\Gamma_i$ is given by equation (A2.5) and is proportional to V_η. Obtaining in this way makes our solution of the theory numerically consistent solution. Therefore, the numerical procedure consists of simultaneous solution of four equations (A.9)-(A.11) and (A.13) for four unknowns; Γ, B^{10}, b_2 and V_η.

The other parameters in expression (A.2)-(A.4) and (A.8) are expressed in terms of Γ, B^{10}, b_2 and V_η are given by [204, 242],

$$\Delta\Gamma_i = \frac{V_\eta \rho_n \sigma_n^2 \sigma_i^2 B^{10}}{8\beta_6(\sigma_n + \lambda\sigma_i)} \tag{A.14}$$

$$D_i^F = \frac{z_i \beta_6}{2(1 + \sigma_i \Gamma - \Delta\Gamma_i)}, \; m_i = \frac{V_\eta D_i^F}{\sigma_n + \lambda\sigma_i} \tag{A.15}$$

$$D = 1 + V_\eta^2 \rho_\eta \sigma_n^2 \sum_{i=1}^{n-1} \frac{\rho_i \sigma_i^2 \left(D_i^F\right)^2}{\left[2\beta_6(\sigma_n + \lambda\sigma_i)\right]^2} \;, \; D_{ac} = \sum_{i=1}^{n-1} \rho_i \left(D_i^F\right)^2$$

$$\Gamma_i^s = \frac{\left(1+\Gamma\sigma_i - \Delta\Gamma_i\right)D-1}{\sigma_i}, \Omega_{10} = V_\eta \sum_i^{n-1} \frac{\rho_i \sigma_i (D_i^F)^2}{\left[2\beta_6\left(\sigma_n + \lambda\sigma_i\right)\right]^2}$$

$$N_i = \frac{2D_i^F}{\beta_6\sigma_i}\left[1+\frac{V_\eta \rho_n \sigma_n^3 B^{10}\sigma_i}{24(\sigma_n+\lambda\sigma_i)}\right] - \frac{z_i}{\sigma_i}$$

$$a_i^0 = \frac{\beta_6 \Gamma_i^s D_i^F}{D_{ac}} \ , \ a_n^1 = \frac{D\beta_6}{2D_{ac}}\left[\frac{\sigma_n B^{10}}{2} + \frac{\Omega_{10}\lambda}{D\beta_6}\right]$$

$$-k_{ni}^{10} = \frac{\sigma_n^2 D_i^F}{2D\beta_6^2}\left[\frac{V_\eta}{\sigma+\lambda\sigma_i} + \frac{\Omega_{10}\Gamma_i^s}{D_{ac}}\right] + \frac{\sigma_n^3 B^{10} a_i^0}{12\beta_6}$$

$$1-\rho_n k_{nm}^{11} = \frac{1}{D\beta_6}\left[\lambda + \frac{\rho_n \sigma_n^2 \Omega_{10} a_n^1}{2\beta_6^2}\right] + \frac{\rho_n \sigma_n^3 B^{10} a_n^1}{12\beta_6}$$

The ionic excess chemical potentials is given by,

$$\beta\mu_i = \frac{z_i\left(\alpha_0^2 N_i - \alpha_0\alpha_2\rho_n m_i\right)}{4\pi}$$

The chemical potential of dipolar molecules is given by,

$$\beta\mu_n = \frac{\left(-\alpha_0\alpha_2 B_{10} - 2\alpha_2^2 b_2/\sigma_n^3\right)}{4\pi}$$

Since in the MSA, the excess Gibbs free energy equals the excess internal energy, the pressure is given by

$$\beta P = \frac{\beta(E-A)}{V}$$